Production, purification and structural characterisation of recombinant barley limit dextrinase and characterisation of its interaction with the endogenous limit dextrinase inhibitor

Vester-Christensen, Malene Bech

Publication date:
2010

Document Version
Publisher's PDF, also known as Version of record

Production, Purification and Structural Characterisation of Recombinant Barley Limit Dextrinase and Characterisation of its Interaction with the Endogenous Limit Dextrinase Inhibitor

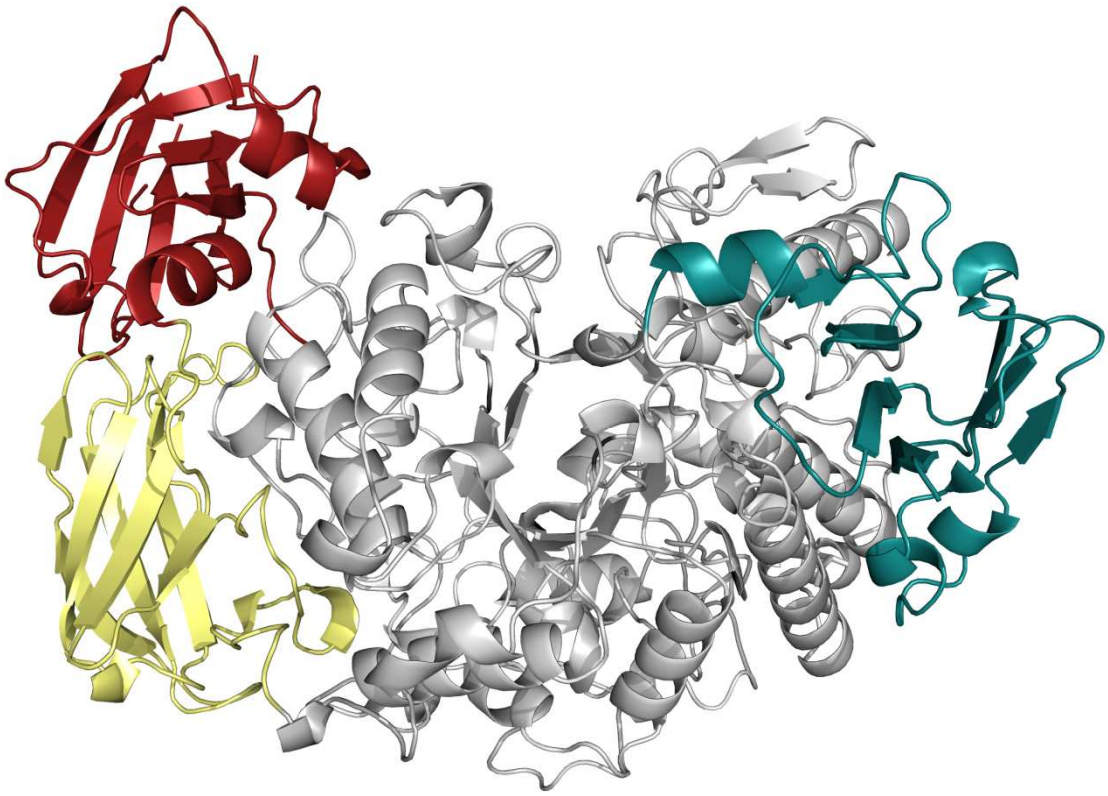

Malene Bech Vester-Christensen
Ph. D. Thesis
November 2009
Enzyme & Protein Chemistry
Department of Systems Biology
Technical University of Denmark

DTU

Enzyme and Protein Chemistry
Department of Systems Biology

Preface

This Ph.D. thesis represents the result of my Ph.D. study carried out at Enzyme and Protein Chemistry (EPC), Department of Systems Biology, Technical University of Denmark (DTU) in the period from February 2006 to September 2009.

This project was funded by the Technical University of Denmark an received support from the Danish Natural Science Research Council, the Centre for Advanced Food Studies, and the Carlsberg Foundation.

The work has resulted in the following publications (Appendix 7.6).

Vester-Christensen, M. B., Abou Hachem, M., Naested, H., and Svensson, B. (2009) Secretory expression of functional barley limit dextrinase by *Pichia pastoris* using high cell-density fermentation, *Protein Expr. Purif.*, doi: 10.1016/j.pep.2009.08.016. *In press*

Vester-Christensen, M. B., Abou Hachem, M., Svensson, B., and Henriksen, A. (2009) Crystal structure of barley limit dextrinase. A debranching enzyme involved in starch synthesis and breakdown, to be submitted to J. Biol. Chem.

Vester-Christensen, M. B., Jensen, J. M. Abou Hachem, M., Svensson, B., N-terminal mutations of the high-affinity barley limit dextrinase inhibitor suggests a mode of action different from that of α-amylase inhibitors from the same family, to be submitted to Biochemistry.

Kgs. Lyngby, November 2009

Malene Bech Vester-Christensen

Acknowledgements

During the period of the work and the writing of the thesis I have received help and advice from a number of people. I am in great dept to my primary supervisor from Enzyme and Protein Chemistry Group (EPC), DTU, Professor Birte Svensson for giving me the opportunity to carry out my Ph.D. study at EPC. I am grateful for her support and expert advice throughout the whole project. My second supervisor Associate Professor Maher Abou Hachem is greatly acknowledged for good and fruitful discussions, excellent technical help and support. His contribution to this thesis, however, has not only being as an excellent and inspirational scientific supervisor, but also as a very good and encouraging friend.

Professor Anette Henriksen, Protein Chemistry Group, Carlsberg Laboratory, who has been my third supervisor, is thanked for excellent technical help, as well as fruitful and stimulating discussion on the limit dextrinase structure.

I would like to thank Professor Rob Field, Martin Rejzek and Simone Deldola, Department of Biological Chemistry, John Innes Centre, Norwich Research Park, UK, for their support and help during my visit and for providing me with fluoride oligosaccharides for transglycosylation.

The collaborators at the Department of Biochemistry and Molecular Biology, University of Southern Denmark, Martin Zehl, Sabine Amon and Ole Nørregaard Jensen are thanked for the full-length mass spectrometry analysis of LDI.

All former and present members of the Enzyme and Protein Chemistry group are acknowledged for their help and discussions and for providing a good working environment, especially my friends Camilla Christiansen, Johanne M. Jensen, Karina Jansen, Eun Seong Seo, and Adiphol Dilokpimol. Hiroyuki Nakai and Martin J. Baumann are thanked for fruitful discussions on the transglycosylation activity of carbohydrases, Folmer Fredslund for discussions on crystallization and structural aspects, Birgit Bønsager for providing the cDNA clone of LDI and Johanne M. Jensen for her excellent work on LDI. I thank Henrik Næsted my friend and former supervisor for his support and advice during his time as my supervisor as well as after.

I would like to thank the EPC technicians, Karina Jansen, Morten Ejby Hansen, Susanne Blume and Birgit Andersen for their excellent assistance in the lab. Anne Blicher is acknowledged for performing amino acid analysis and N-terminal sequencing. From the Protein Chemistry Group, Carlsberg Laboratory, technician Anette Kure and Post doc Valerie Pye for technical assistance during crystallization setup and data collection.

Finally I would like to thank my friends and family, especially my loving husband Martin and my wonderful girls, Mathilde and Mille, for being supportive and extremely patient with me through this study.

Summary

Heterologous production of large multi domain proteins from higher plants is often cumbersome. Barley limit dextrinase (LD), a 98 kDa multi domain starch and α-limit dextrin debranching enzyme, plays a major role in starch mobilization during seed germination and is possibly involved in starch biosynthesis by trimming of intermediate branched α-glucan structures. Highly active barley LD is obtained by secretory expression during high cell-density fermentation of *Pichia pastoris*. The LD encoding gene fragment without signal peptide was subcloned in-frame with the *Saccharomyces cerevisiae* α-factor secretion signal of the *P. pastoris* vector pPIC9K under control of the alcohol oxidase 1 promoter. Optimization of a fed-batch fermentation procedure enabled efficient production of LD in a 5-L bioreactor, which combined with affinity chromatography on β-cyclodextrin-Sepharose followed by Hiload Superdex 200 gel filtration yielded 34 mg homogenous LD (84% recovery). The identity of the recombinant LD was verified by N-terminal sequencing and by mass spectrometric peptide mapping. A molecular mass of 98 kDa was estimated by SDS-PAGE in excellent agreement with the theoretical value of 97419 Da. Kinetic constants of LD catalysed pullulan hydrolysis were found to $K_{m,app}$ = 0.16 ± 0.02 mg/mL and $k_{cat,app}$ = 79 ± 10 s^{-1} by fitting the uncompetitive substrate inhibition Michealis-Menten equation, which reflects significant substrate inhibition and/or transglycosylation. The resulting catalytic coefficient, $k_{cat,app}/K_{m,app}$= 488 ± 23 mL/(mg·s) is 3.5 fold higher than for barley malt LD. Surface plasmon resonance (SPR) analysis showed α-, β-, and γ-cyclodextrin (CD) binding to LD with K_d of 27.2, 0.70, and 34.7 μM, respectively.

LD extracted from germinating barley seeds is found in a "bound", inactive form and a free, enzymatically active form. The inactive LD form was proposed to consist of a complex with the endogenous limit dextrinase inhibitor (LDI) and extraction under reducing conditions resulted in enzymatically fully active LD. The binding kinetics and energetics of LD with LDI wild-type and N-terminal extension or truncation variants of LDI produced in *P. pastoris*, were determined using SPR analysis. Fitting a 1:1 binding model to SPR data showed a high-affinity binding of $K_D = 40 \pm 3 \times 10^{-12}$ M with $k_{on} \sim 1 \times 10^6$ M^{-1} s^{-1} and $k_{off} \sim 5 \times 10^{-5}$ s^{-1} at pH 6.0, 150 NaCl and 25 °C. The dissociation rate k_{off} increased 10-fold by raising pH from the optimum pH 6.5 to 10, whereas k_{on} was maintained resulting in K_D being pH dependent. In contrast k_{off} and k_{on} varied only by factor of 2 at 75 mM – 1 M NaCl. Electrostatic forces thus did not contribute significantly to the LD/LDI stability. Favourable enthalpic and entropic contributions to complex formation were indicated by the van't Hoff parameters $\Delta H° = -27$ kJ/mol and $T\Delta S° = 30$ kJ/mol resulting in a binding free energy $\Delta G° = -57$ kJ/mol as calculated from K_D values in the temperature range 10–35 °C. The N-terminally extended or truncated LDI mutants changed K_D marginally, suggesting the wild-type LDI N-terminal sequence not to be critical for binding to LD.

The crystal structures of LD in complex with the competitive inhibitors α- and β-cyclodextrin have been refined at 2.5 Å and 2.1 Å, respectively. The enzyme is composed of four domains: an eight-stranded N-terminal domain, a putative carbohydrate binding module (CBM48), followed by the catalytic domain comprising a $(\beta/\alpha)_8$-like barrel lacking α-helix 5 and finally a C-terminal domain consisting of a two-sheet β-sandwich motif. The CDs are observed at the expected carbohydrate main-chain binding-site occupying the aglycone subsites +1 and +2. One glycerol molecule and

three water molecules mimic a glucose residue at subsite –1, thereby identifying residues involved in substrate binding. The spaciousness of Met^{440}, a uniquely positioned residue amongst α-1,6 acting enzymes, would clash with glucosyl residues at subsite –4.This steric hindrance is proposed to affect substrate specificity. A part of an extended loop between β5 and β6 of the catalytic $(\beta/\alpha)_8$-barrel (residues Asp^{513}–Asn^{520}) differs from microbial pullulanases in sequence and structure and seems to contribute both to the substrate specificity and to the observed higher affinity of LD towards α-CD compared to pullulanases. Novel insight onto the specificity determinants and possible role in starch biosynthesis is illuminated by this first structure of a plant limit dextrinase.

Dansk Resumé

Heterolog produktion af store multidomæne proteiner fra højere planter er ofte besværlig. Byg limit dextrinase (LD), er et 98 kDa stort multidomain stivelses og grænsedextrin afgreningsenzym, som spiller en vigtig rolle i stivelsesmobilisering under frøspiring og er muligvis også involveret i stivelse biosyntesen ved trimning af intermediære forgrenede α-glucan strukturer. Aktivet byg LD er blevet fremstillet ved sekretorisk ekspression i en høj celledensitets fermentering af *Pichia pastoris*. Det LD kodende genfragment uden signal peptid blev subklonet in-frame med *Saccharomyces cerevisiae* α-faktor sekretion signalet ind i *P. pastoris* ekspression vektoren, pPIC9K under kontrol af alkohol oxidase 1 promotoren. Optimering af en fed-batch fermentering procedure i en 5-L bioreaktor efterfulgt af affinitetskromatografi på β-cyclodextrin-Sepharose og gelfiltrering (Hiload Superdex 200) resulterede i 34 mg homogent LD (84% udbytte). Identiteten af det rekombinante LD blev påvist med N-terminal sekvensering og ved peptid massespektrometrisk. En molekylmasse på 98 kDa blev anslået ved SDS-PAGE og er i glimrende overensstemmelse med den teoretiske værdi på 97,419 kDa. Kinetiske konstanter for LD katalyseret pullulan hydrolyse blev bestemt til $K_{m,app}$ = 0,16 ± 0,02 mg/mL og $k_{cat,app}$ = 79 ± 10 s^{-1} ved anvendelse af Michealis-Menten ligningen for ikke-konkurrencedygtige substrat hæmning, hvilket afspejler en væsentlig substrat-hæmning og/eller transglycosylation. Den katalytiske koefficient, $k_{cat,app}/K_{m,app}$ = 488 ± 23 mL/(mg·s) er 3,5 gange højere end for LD isoleret fra byg malt. Surface plasmon resonans (SPR) analyse viste at α-, β-og γ-cyclodextrin (CD) bandt til LD med en K_d på hhv. 27,2, 0,70, og 34,7 mM.

LD isoleret fra spirende byg frø er fundet i en "bundet" inaktiv form, og en fri enzymatisk aktiv form. Den inaktive LD form blev foreslået til at bestå af et kompleks med den endogene limit dextrinase hæmmer (LDI) og isolering under reducerende forhold resulterede i enzymatisk fuldt aktivt LD. Bindings kinetik og energetik af LD med LDI vildtype og N-terminal forlængelede eller trunkerede varianter af LDI produceret i *P. pastoris*, blev bestemt ved hjælp af SPR analyse. Anvendelse af en 1:1-bindingsmodel til de generede SPR data viste en høj bindingsaffinitet med K_D = 40 ± 3 × 10^{-12} M og k_{on} ~ 1 × 10^6 M^{-1} s^{-1} og k_{off} ~ 5 × 10^{-5} s^{-1} ved pH 6,0, 150 mM NaCl og 25 °C. Ved at hæve pH-værdien fra den optimale pH-værdien, 6,5 til 10 steg dissociation hastigheden k_{off} 10 gange, mens k_{on} blev opretholdt, hvilket resulterede i en pH-afhængig K_D. I modsætning varierede k_{off} og k_{on} kun med en faktor 2 ved ændring af NaCl indholdet i bufferen fra 75 mM – 1 M. Elektrostatiske kræfter synes derfor ikke at bidrage væsentligt til LD/LDI stabiliteten. van't Hoff parametrene blev beregnet ud fra K_D værdierne i temperaturintervallet 10–35 °C. Favorable enthalpi- og entropi-værdier ($\Delta H°$ = – 27 kJ/mol og $T\Delta S°$ = 30 kJ/mol) indikerede at begge komponenter bidrog til kompleksdannelsen og resulterede i en bindings fri energi, $\Delta G°$ = – 57 kJ/mol. N-terminalt forlængede eller trunkerede LDI mutanter ledte kun til en marginal ændring af K_D, hvilket indikerer at den N-terminale sekvens af vildtype LDI ikke er afgørende for binding til LD.

Krystalstrukturerne af LD i kompleks med de kompetitive inhibitorer α- og β-CD er blevet forfinet til hhv. 2,5 Å og 2,1 Å. Enzymet består af fire domæner: Et otte-strenget N-terminale domæne; et formodet kulhydrat bindende modul (CBM48), efterfulgt af et katalytisk domæne bestående af en $(\beta/\alpha)_8$-lignende tønde som mangler α-helix 5 og endelig et C-terminal domæne bestående af et to-arket β-sandwich-motiv.

Cyclodextrinerne er observeret ved det forventede bindingssted for den primære kulhydrat kæde og okkuperer aglycon subsite +1 og +2. Et glycerol molekyle og tre vandmolekyler efterlignede en glukose rest ved subsite –1, og dermed identificerede aminosyre rester, der er involveret i substrat binding. Positionen af den rummelighed aminosyre rest Met^{440} i LD, som har en unik position blandt α-1,6 afgreningsenzymerne, vil kollidere med glucosyl rester ved subsite –4. Denne sterisk hindring foreslås at påvirke substrat specificiteten. En del af en udvidet loop mellem β5 og β6 af den katalytiske $(\beta/\alpha)_8$-tønde (aminosyre rester Asp^{513}–Asn^{520}) adskiller sig fra de mikrobielle pullulanaser i både sekvens og struktur og synes at bidrage til både den observerede substratspecificitet og den højere α-CD affinitet af LD i forhold til pullulanaserne. Ny indsigt i substrat specifikke afgørende faktorer og den mulige rolle i stivelse biosyntesen er belyst ved hjælp af denne første struktur af en plante limit dextrinase.

Abbreviations

AICc, Aikaike information criteria
AmpR, ampicillin resistance
AOX, alcohol oxidase
BaPUL, pullulanase from *Bacillus acidopullulyticus*
BCIP, bromo chloro indolyl phosphate
BsPUL, pullulanase from *Bacillus subtilis* str. 168
CBD, chitin binding domain
CBM, carbohydrate binding module
CD, cyclodextrin
CFHI, bifunctional corn Hageman factor inhibitor
CWW, cell wet weight
DNJ, 1-deoxynojirimycin
EDTA, ethylenediaminetetraacetic acid
ESI-MS, electrospray ionization - mass spectrometry
ESI-Q-TOF, electrospray ionization-quadrupole-time of flight
GA_3, gibberellic acid
GBD, glycogen binding domain
GH13_12, glycoside hydrolase family 13 subfamily 12
GH13_13, glycoside hydrolase family 13 subfamily 13
GH13_14, glycoside hydrolase family 13 subfamily 14
G1M, 4-*O*-α-D-glucopyranosylmoranoline
G2F, α-maltosyl fluoride
G3F, α-maltotriosyl fluoride
G4, maltotetraose
Glc, glucose
Gol, glycerol
HIS4, histidinol dehydrogenase
HTS, high-throughput screening
IEF, isoelectric focusing
IPTG, isopropyl β-D-1-thiogalactopyranoside
PaISO, isoamylase from *Pseudomonas amyloderamosa*
KanR, kanamycin resistance
KpPUL, pullulanase from *Klebsiella pneumoniae*
LC-MS, liquid chromatography-mass spectrometry
LD, limit dextrinase
LDI, limit dextrinase inhibitor
MALDI-TOF-MS, matrix assisted laser desorption ionisation time-of-flight mass spectrometry
MR, molecular replacement
MS, mass spectrometry
MeOH, methanol
NBT, nitroblue tetrazolium
PAC, prespotted anchorchip
PAGE, polyacrylamide gel-electrophoresis

PEG, polyethylene glycol
PPA, porcine pancreatic α-amylase
PVDF, polyvinylidene fluoride
RATI, ragi α-amylase/trypsin inhibitor
RU, response unit
SDS, sodium dodecyl sulfate
SPR, surface plasmon resonance
SS, sum of squared residuals
TBST, Tris-buffered saline Tween-20
TFA, trifluoroacetic acid
TLC, thin layer chromatography
TLS, translation/libration/screw
TMA, α-amylase from the larvae of *Tenebrio molito*

Content

1 Introduction

1.1 Carbohydrate-Active Enzymes and Clan-H

Carbohydrate-active enzymes are classified according to the CAZy classification (*1*), which divides the enzymes into four main classes based on the type of catalysed reaction: glycoside hydrolases (GH) (*2*), glycosyl transferases (GT) (*3*), polysaccharide lyases (PL) and carbohydrate esterases (CE) (*4*). In addition to the catalytically active classes of enzymes, a special class of non-catalytic carbohydrate binding modules (CBM) is defined (*5*). Within each main class the enzymes are grouped based on sequence similarities. Up to this date, 115 different GH families have been classified, which again are grouped into 14 clans (GH-A to GH-N) based on a common over-all protein fold and catalytic mechanism. GH13, 70 and 77 all belong to clan-H sharing the same catalytic domain containing a $(\beta/\alpha)_8$-barrel. The specificity in GH13 is diverse covering more than 20 different activities in three enzyme classes; transferases (EC 2.x.x.x), hydrolases (EC 3.x.x.x) and isomerases (EC 5.x.x.x) (*1*). Furthermore, GH13 has been divided into 35 subfamilies based on clustering, similarity search and phylogenetic methods (*6*). Enzymes belonging to GH13 utilize the retaining mechanism with the catalytic nucleophile/base being an aspartate and the catalytic proton donor being a glutamate, both identified experimentally (see section 1.21 for detailed description of the mechanism).

1.2 Limit Dextrinase (LD)

Starch, the most prominent carbohydrate in the human diet, the major carbohydrate reserve in cereal seeds and an important industrial raw material, occurs as compact supramolecular granules in barley grains and is composed of the polysaccharides amylose (Figure 1.1A), a linear α-1,4-glucan, and about 70% amylopectin (Figure 1.1B) (reviewed in (*7*)). In addition to a linear α-1,4-glucan structure, the amylopectin contains frequent α-1,6 glucosidic branches connecting shorter linear α-1,4 linked chains of varying length to the α-1,4-glucan main-chain (reviewed in (*7*)).

In barley, starch granules are stored in the seed endosperm that consists of dead tissue and the concerted action of different amylolytic enzymes is required for its breakdown to metabolisable oligosaccharides, maltose, and glucose (*8*) (Figure 1.2A). The germination of barley grain (Figure 1.2B) is initiated by an increase in temperature and the uptake of water, which induces the synthesis of the phytohormone gibberellic acid (GA_3) in the embryo. GA_3 diffuses to the aleurone layer where it induces *de novo* synthesis of limit dextrinase (LD), α-amylases (isoform 1 and 2) and α-glucosidase (*9*, *10*). The hydrolytic enzymes are then released to the starchy endosperm where they are involved in the mobilisation of storage starch, which provides energy to the growing plantlet. LD thus hydrolyses α-1,6-glucosidic bonds in α-limit dextrins derived from amylopectin, but has low activity towards amylopectin, present in the mature seed, itself (*11*); α-amylase hydrolyses α-1,4 glucans in an endo-fashion; β-amylase catalyses release of maltose from non-reducing ends of the substrates and is unable to pass α-1,6-

branch points; and the α-glucosidase primarily hydrolyses maltooligosaccharides to glucose (*8*) (Figure 1.2A).

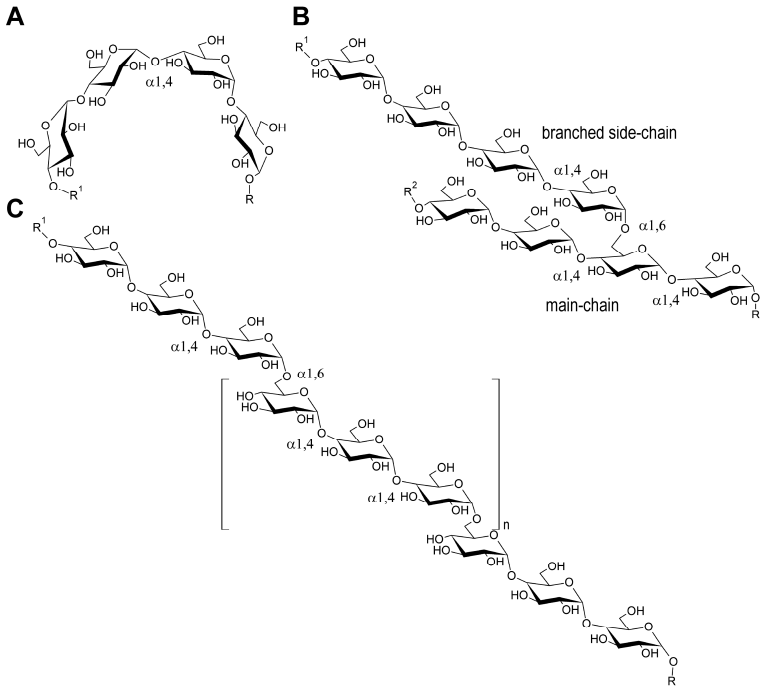

Figure 1.1. Representative structures of linear α-1,4 linked amylose (A), the α-1,4 branched α-1,6 linked amylopectin (B) and pullulan composed of α-1,6-linked maltotriose repeats (C). R indicates the reducing end of the polymers and R^1 indicates the non-reducing end of the polymers, amylose and pullulan, as well as the non-reducing end of the sugar side-chain of amylopectin. R^2 indicates the non-reducing end of the sugar main-chain of amylopectin. n is an integer indicating the number of maltotriose repeats in the pullulan.

LD (EC. 3.2.1.41, pullulanase) is indeed the sole debranching enzyme in seed starch mobilization (*8, 12*). In barley a single gene encodes LD, which is induced in the germinating seed by the GA_3 (*9, 12*). Transcripts of the LD gene can be detected in the aleurone layer already 12 h after the onset of germination, but LD activity does not increase until two days later and reaches a maximum at day 5 after onset of germination (*9, 13*). The level of LD activity in the starchy endosperm is low compared with the α-amylase activity. Furthermore, the release of LD from the aleurone layer to the endosperm appears to be slower than of α-amylase (*13*) and it was suggested therefore to occur as a consequence of cell wall degradation and not *via* a secretory pathway. The secretion of LD, however, has been a matter of debate since a putative leader sequence has been identified upstream the mature peptide, but was not predicted to be a signal peptide targeting to the ER (*9, 12*).

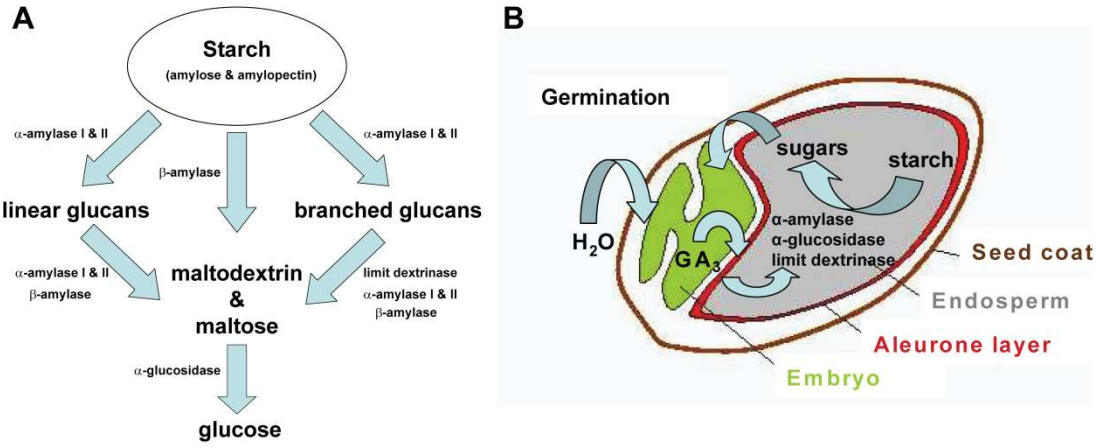

Figure 1.2. A. The role of α-amylase isoform I and II, β-amylase, limit dextrinase and α-glucosidase in degradation of amylase and amylopectin in cereal seed starchy endosperm. B. The germination of barley grain is initiated by an increase in temperature and the uptake of water, which induces the synthesis of the phytohormone gibberellic acid (GA_3) in the embryo. GA_3 diffuses to the aleurone layer where it induces *de novo* synthesis of limit dextrinase, α-amylases and α-glucosidase. The hydrolytic enzymes are then released to the starchy endosperm, where they are involved in the catabolism of the storage starch for support of the growing plantlet.

In addition to an important role in starch degradation in germinating seeds, LD is shown in maize (*14*) and *Arabidopsis* (*15*) to participate in the breakdown of transitory starch in leaves. Furthermore, LD is present in developing grains and suggested to play a role in starch biosynthesis (*9, 13, 16*). The hypothesis that the structure of amylopectin is the outcome of a balance between debranching and branching enzyme activities (*17, 18*) gets support both from maize deficient in pullulanase-type debranching enzyme (*i.e.* LD), having affected starch granule morphology (*14*) and from a *Arabidopsis* mutant deficient in three isoamylase isozymes and the single LD isozyme with abolished starch granule biosynthesis (*19*). It is therefore believed that successful synthesis of the amylopectin starch fraction in plants involves the action of two types of α-1,6 glycoside hydrolases, the isoamylases (EC 3.2.1.68) and the limit dextrinase (*20, 21*).

Besides the activity towards limit dextrins, LD also shows high activity towards pullulan, a linear polysaccharide composed of α-1,6-linked maltotriose repeats (*8, 11*) (Figure 1.1C). LD is thus classified together with pullulanases that are large multidomain enzymes that belong to either glycoside hydrolase family 13 subfamily 12 (GH13_12) (firmicutes), subfamily 13 (GH13_13) (bacteria and eukaryota) or subfamily 14 GH13_14) (bacteria), depending on their phylogenetic origin (*1, 6*). Pullulanase encoding genes are identified in plants and their gene products are referred to as LDs. The primary structures of plant LDs are highly conserved with sequence identities of 80–95% for the cereal homologous enzymes from barley, rice, maize and wheat, which are all monocots. The more phylogenic distant homologues from the dicots *e.g.* spinach and *Arabidopsis* share only 62% over-all sequence identity with barley LD (Figure 1.3). Comparison of the barley LD primary structure with that of the microbial pullulanases from *Bacillus subtilis* str. 168 (BsPUL), *Bacillus acidopullulyticus* (BaPUL) and *Klebsiella pneumoniae* (KpPUL) shows sequence identities ranging from 30 to 35% (blastp, default settings, BLOMSUM 62, gap opening and extension penalties of 11 and 1, respectively;

http://blast.ncbi.nlm.nih.gov/Blast.cgi). So far the vast majority of the characterized pullulanases are of microbial origin. The reason for lack of structural information on LD primarily stems from its low abundance and lack of efficient purification procedures for homogeneous plant proteins and efficient heterologous expression systems for plant LD. In the past recombinant production of LD from maize (*22*), spinach (*23*), and wheat (*24*) resulted in very poor yields, which emphasised the challenges of producing some plant proteins in *E. coli*. A similar situation was found for barley α-glucosidase (*25*), in which case, however, a breakthrough was obtained by high cell-density fermentation of the host *Pichia pastoris* resulting in good yields of very pure and five times more catalytically efficient α-glucosidase than the enzyme purified from malt (*26*).

The α-1,6 acting enzymes including pullulanases of bacterial and LD of plant origin (EC 3.2.1.41), isoamylases (EC 3.2.1.68), neopullulanases (EC 3.2.1.135), the latter having α-1,4 activity as the main activity, are all composed of similar domain organisation, although the number of domains can vary. An N-terminal part, which varies in length and can contain several independent structural domains including carbohydrate binding modules (CBMs) and is followed by the catalytic $(\beta/\alpha)_8$-barrel domain. A loop protruding from the $(\beta/\alpha)_8$-barrel between β-strand 2 and α-helix 2 is often referred to as Loop 2 (*27, 28*). Furthermore, a long loop is connecting β-strand 3 and α-helix 3 (by convention called B-domain (*27, 28*), despite the fact that it cannot be considered a structurally independent domain). The catalytic domain is followed by a C-terminal domain, with a two-sheets β-sandwich structural motif which was first described in TAKA-amylase A, an α-amylase produced by *Aspergillus oryzae* (*29*). LDs and isoamylases contain only one annotated CBM namely CBM48 (*30*), whereas the 3D structures of KpPUL and BaPUL (*31, 32*) reveal two carbohydrate binding modules, CBM41 and CBM48, situated N-terminally to the catalytic domain. Based on multiple sequence alignment of GH13 family members and the Pfam domain prediction (*27, 33*), LD is proposed to be composed of an N-terminal part including an uncharacterized part and a CBM48 module (*30*).

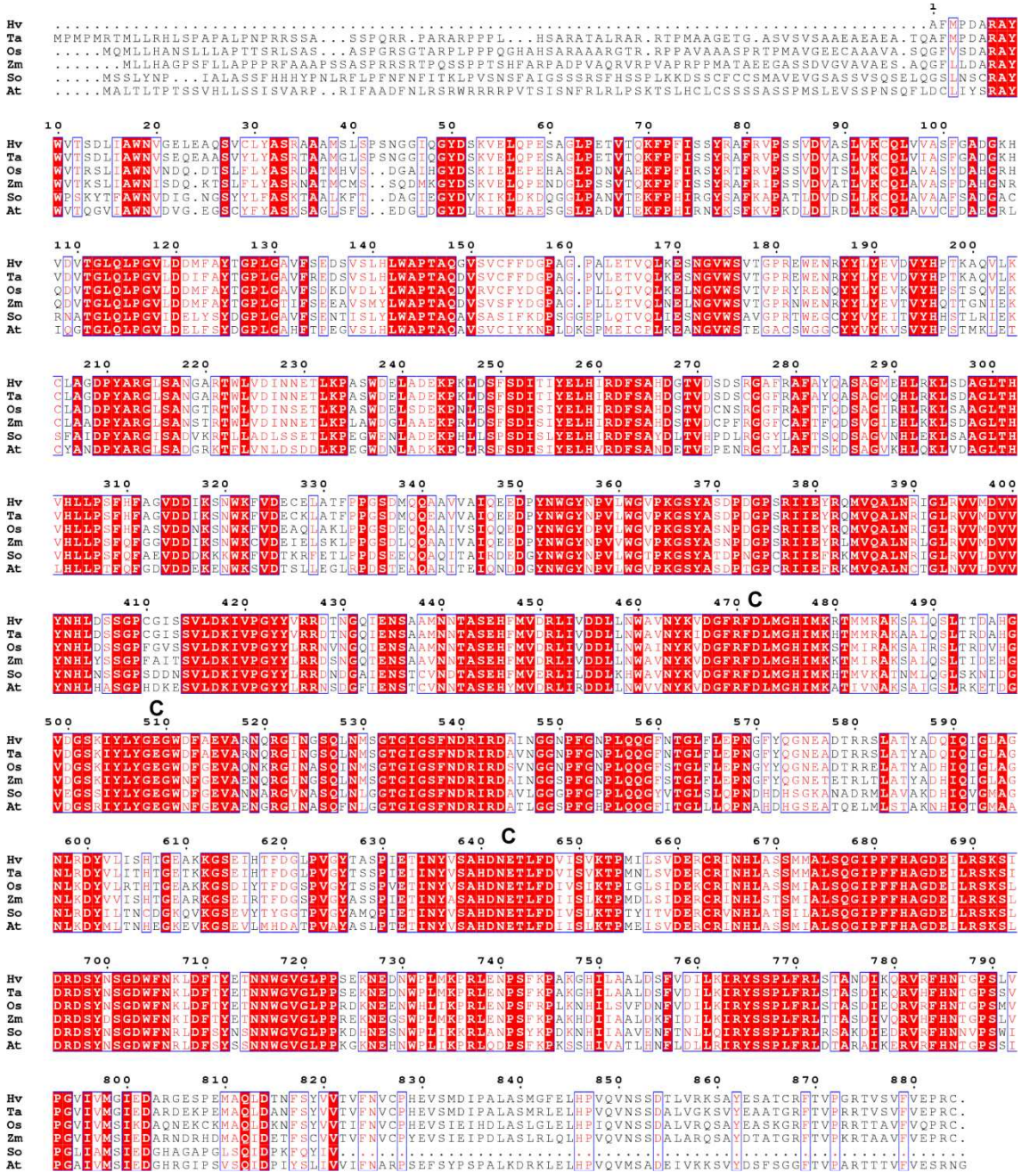

Figure 1.3. Sequence alignment of plant limit dextrinases The alignment rendering was done with the program ESPript *(34)*. C, indicates the three catalytic residues Asp473 (nucleophile), Glu510 (general acid/base, and Glu644 (third acid in the catalytic triad). Hv, *Hordeum vulgare*, acc.# AAD04189 expressed in *Pichia pastoris*; Ta, *Tritium aestivum*, acc.# ABL84490 ; Os, *Oryza sativa*, acc.# H0806H05; Zm, *Zea mays*, acc.# AAD11599; So, *Spinacia oleracea*, acc.# CAA58803; At, *Arabidopsis thaliana*, acc.# Q8GTR4. Identical residues in the alignment are marked with red boxes and white characters, similar residues are in red characters, while blue frame indicates similarity across groups.

1.2.1 Reaction Mechanism and Substrate Specificity of LD

LD catalysed hydrolysis of the α-1,6 glycosidic bond takes place *via* general acid catalysis, which requires a proton donor (Asp^{473}) and a nucleophile/base (Glu^{510}). Cleavage of the α-1,6 linkage results in retention of the configuration around the anomeric carbon *via* a double displacement mechanism, which is common for GH13 family members independent of the linkage being an α-1,4 or α-1,6 bond (*35*). The two-step reaction involves a nucleophilic attack from the deprotonated Asp^{473} forming a covalent β-glycosyl-enzyme intermediate and simultaneously a protonation of the leaving aglycone by Glu^{510}. The oxocarbonium ion-like transition state is believed to be stabilized by side-chains from several conserved amino acids in the active site, especially His^{404} and His^{641} (*12*, *35*, *36*). The deprotonated Glu^{510} acts as a base by activating the acceptor being either a water molecule or a primary hydroxyl group at C6 in a glucose residue in the intermediate, which results in the retention of the α-configuration in either a free reducing end (hydrolysis, Figure 1.4A) or a new α-1,6 glycosidic bond (transglycosylation, Figure 1.4B).

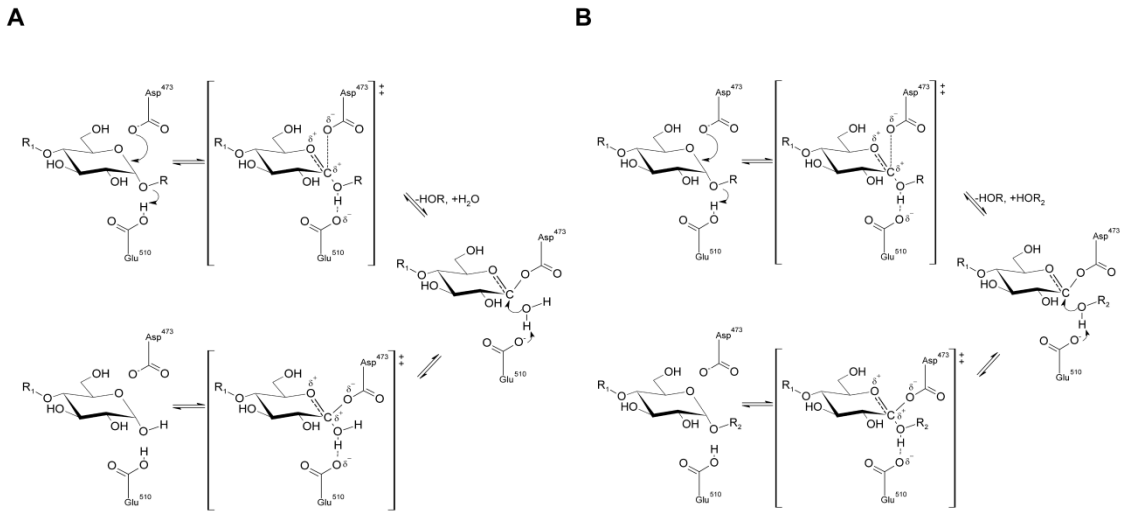

Figure 1.4 LD catalysed α-1,6 hydrolysis mechanism with retention of the α-configuration of either the reducing end (hydrolysis) (A) or in a new glucosidic bond (transglycosylation) (B). The distance between the nucleophile and the acid/base is typically 5.5 Å (*35*). R and R_1 indicate glucose residues at the reducing and non-reducing end, respectively, of the substrate. R_2 indicates the glucose residues of the incoming acceptor.

LD is specific for cleavage of α-1,6 bonds in branched dextrins and polymers with α-1,4 main-chain bonds which can be either linear like pullulan or branched like amylopectin and is classified as a starch debranching enzyme. The relative rates of LD and KpPUL hydrolysis of a range of starch derived oligosaccharides and polymers as well as pullulan is summarised in Table 1.1 and clearly shows a preference for the polymer derived oligosaccharides compared with polymeric substrates, in contrast to isoamylase (*37*, *38*). The optimum length of the main-chain is four glucose residues for both LD and KpPUL and for LD a 2-fold increase in hydrolysis rate is observed when the side-chain changes from α-maltosyl to α-maltotriosyl, which indicates that the optimum

length of side-chain for hydrolysis is three glucose residues (*11*). LD and KpPUL show no hydrolytic activity towards the di- and trisaccharides, isomaltose, panose and isopanose and neither are they capable of catalysing the hydrolysis of α-1,6 linkages between a single glucose residues attached to either linear or cyclic oligosaccharides (*11, 39, 40*).

Table 1.1. Relative rates of hydrolysis of various substrates by LD and KpPUL

Substrate	Relative rate[a]	Relative rate[b]	Relative rate[c]
	LD	LD	KpPUL
6^3-α-maltosylmaltotriose	-	13	49
6^3-α-maltosylmaltotetraose	-	123	169
6^3-α-maltotriosylmaltotriose	-	129	90
6^3-α-maltotriosylmaltotetraose	358	243	123
Nonasaccharide from pullulan	-	114	-
Pullulan	100	100	100
α-CD	-	12	-
Amylopectin β-limitdextrin	-	68	-
Amylopectin	-	<<1	-
Glycogen	-	0	-

[a] (*37*), [b] (*11*), [c] (*39*). [b] and [c] not necessarily determined at saturating conditions.

LD (*11*, *41-43*) as well as other debranching enzymes such as KpPUL and BaPUL *(44)*, the debranching enzyme TreX from *Sulfolobus solfataricus* P2 (*45*), and isoamylase from *Pseudomonas amyloderamosa* (PaISO) (*44*) have been shown to display transglycosylation activity in addition to their hydrolytic activity. The transglycosylation activity of LD can be used in the production of new materials for applications in *e.g.* prebiotics, synthesis of novel inhibitors or potentially drug delivery. Chemoenzymatic syntheses of oligosaccharides with specific structures are clearly competitive with conventional synthetic approaches, which are often inadequate in producing substantial quantities of the product, owing the time consumption and complex nature of the synthesis involving selective protection/deprotection and manipulation of the reactants. In addition to the clear advantage in producing novel compounds an investigation of the LD catalysed transglycosylation reactions using different lengths of linear donors and acceptors may also lead to a better understanding of the substrate specificity of LD.

1.3 Limit Dextrinase Inhibitor (LDI)

LD extracted from germinating barley seeds is found in a “bound”, inactive form and a free, enzymatically active form (*46*). The inactive LD form was proposed to consist of a complex with the endogenous limit dextrinase inhibitor (LDI) and extraction under reducing conditions resulted in enzymatically fully active LD (*46, 47*). After the onset of germination, the amount of the free LD increased with time coinciding with the disappearance of LDI (*46, 48*). Whether this disappearance is caused by reduction by thioredoxin *h* (*49*) or degradation by a proteases (*46*) is not known.

LDI belongs to the CM-protein family of small proteins (110–160 amino acids) found in chloroform/methanol extracts of flour, also referred to as the cereal-type

inhibitors (*50*). This group includes α-amylase and protease inhibitors active on enzymes from different species, and proposed to be part of the plant defence against pest and pathogens (*50*). Members of this family are monomers, dimers or tetramers (*51, 52*) and share the common fold; bifunctional inhibitor/lipid-transfer protein/seed storage 2S albumin (SCOP: Structural Classification of Proteins (*53*)), which features a helical bundle with a simple up-and-down topology. Despite a high sequence identity (up 98%) amongst family members, very high specificity was observed (*54*). The variation is mainly in the flexible loop between α-helix 3 and α-helix 4 and at the C-terminal, which makes the prediction of specific interactions between inhibitor and target enzyme very challenging in the absence of a complex structure (*54, 55*). Furthermore, the loop region around the catalytic site of a target enzyme also plays an important role in the interaction between the enzyme and inhibitor (*54*). Cereal-type inhibitors and their target enzymes form a 1:1 molar complex (*51, 55-60*), and the inhibition was found to be competitive using *p*-nitrophenyl α-D-maltoside as substrate, with K_i in the range of 11–57 nM, depending on inhibitor and α-amylase (*51, 56, 58*).

The N-terminal of RATI, α-amylase/trypsin bifunctional inhibitor from ragi is directly involved in the interaction with TMA, α-amylase from the larvae of *Tenebrio molitor*, as observed in the crystal structure of the complex. This interaction is primarily mediated by hydrogen bonding between the terminal amino group of Ser^{1} and the carboxyl groups of the catalytic residues in TMA (Asp^{185} and Asp^{287}), but also by hydrophobic interactions between Val^{2} (RATI) and Trp^{56}, Trp^{57} and Tyr^{60} in TMA are contributing (*59*).

LDI has 114 amino acids and the nine cysteines form 4 disulfide bonds, and leaving one free thiol group, possibly Cys^{59} (*61*). Two forms of LDI with p*I*-values of 6.7 and 7.2, respectively, were extracted and purified from mature barley seeds in very small amounts (*62*). The two forms have identical amino acid sequence and inhibitory activity, but differ in the post-translational modification, by either a glutathione or a cysteine forming a mixed disulfide bond with the free Cys^{59} (*61, 62*). To date only basic data on LDI and its interactions with LD have been reported (*57, 61, 62*). The stoichiometry of the complex between LD and LDI was characterized as a 1:1 molar ratio by mass spectrometry (*57*). In addition the binding between LD and LDI was reported to be strong although no quantitative data were available (*57, 62*). The three-dimensional structure of LDI has been modelled based on the structure of RATI, sharing 46% sequence identity with LDI (*61*). Based on this model, LDI is predicted to assume the same fold as other CM-proteins (*61*). Trypsin inhibitors of this family, share a common loop sequence believed to account for their trypsin inhibitory activity. LDI does not possess this activity presumably due to a sequence difference in this particular loop (*57*). It has been suggested that LDI binds to the active site of LD in a similar manner to RATI and TMA as seen in the crystal structure of the complex (*59*), and that the N-terminus of the LDI is critical in binding to LD (*61*). Especially Ser^{4} and Val^{5} from LDI were suggested to interact with LD and it has been believed that the three amino acids (TLE) preceding Ser^{4} are important for the specificity of LDI for LD and the lack of inhibitory activity towards α-amylases (*61*). LDI purified from barley seed displayed some variations in the length of the C-terminus, precluding an important role of the C-terminus of LDI in binding to LD (*57, 62*). LDI seems to be highly specific for LD as two different debranching enzymes of bacterial origin namely KpPUL and PaISO were virtually insensitive to LDI (*47*).

1.4 LD and LDI in Malting and Brewing

In addition to the roles in starch biosynthesis in the developing grains (*21*) and degradation in the germinating seed (*8*), LD is central in beer production by catalyzing oligosaccharide debranching during malting and mashing (*63*). In the brewing and distilling industries the degradation of starch into fermentable carbohydrate *i.e.* glucose, maltose, and maltotriose, is specifically important for reaching a high alcohol level (*64*). However, significant amounts of unfermentable branched dextrins present in beer is in part attributed to the presence of high levels of LDI in malt, which inhibits the activity of LD (*48, 65*). Thus by increasing the effectiveness of LD in the mashing process, a higher alcohol yield would be obtained during the fermentation process which would be advantageous for the brewing industry. Based on this one could infer that lowering the amount of LDI would lead to a higher alcohol yield, however, other data suggests that the presence of the heat stable LDI in the mash stabilizes the heat labile LD and protects it against inactivation (*66*). One could therefore argue that lowering the LDI levels will not necessarily lead to an increased LD activity in the mash, due to the heat inactivation of LD in the absent of LDI. This is further complicated due to cultivar variations in both heat stability and activity of LD (*67*).

1.5 Objectives of the Present Study

Despite the fact that LD has been studied since the fifties (*68*) insight is lacking both on the precise role of LD in the biosynthesis of amylopectin and on the molecular basis for substrate specificity in biological and industrial processes. Even though the LD/LDI system is of great importance in both academic and industrial contexts, details of their interactions remain elusive up to date, perhaps due to the challenges in purification of native proteins from their natural source. The general objective was to perform structure-function studies of barley limit dextrinase and characterize the interaction between LD and its endogenous inhibitor.

The specific goals were:

- To establish a system for recombinant expression of barley limit dextrinase, which will facilitate future investigation of structure-function relationships using site-directed mutagenesis and truncations guided by information of family GH13 domain architecture as retrieved from the CAZy-database (*1*).

- To examine the transglycosylation activity of LD using α-maltosyl or α-maltotriosyl fluorides as donor and a range of linear and cyclic dextrins as acceptor. In addition to obtaining novel oligosaccharide products using transglycosylation, the transglycosylation pattern of LD will also give information of the structure-function relationship of the enzyme with focus on the active site area.

- To establish a heterologous expression system for barley limit dextrinase inhibitor and to discern the kinetics and the energetics of complex formation between LD and LDI (LD/LDI), including an evaluation of the role of the N-terminal loop of LDI in the inhibitory activity and binding affinity to LD.

- To crystallize and determine the 3D structure of LD and the LD/LDI complex.

2 Experimental Procedures

2.1 Construct, Expression and Purification

2.1.1 Limit Dextrinase

2.1.1.1 Construction of E. coli *LD Expression Plasmid*

An LD cDNA (GenBank accession No. **AF022725**) (*12*) cloned in the pET11a expression vector was provided from an in-house collection (*41*). Sequencing showed that the clone contained three mutations compared with the published sequence (*12*). These mutations were corrected using Quikchange Multi site-directed mutagenesis kit (Stratagene, La Jolla, CA) and the primers MVC1, MVC3, MVC5 (Table 2.1). The corrections were performed as recommended by the manufacturer (Stratagene). *E. coli* XL10-Gold (Stratagene) was transformed with the resulting pET11a/LD plasmid. The isolated plasmid was sequenced to confirm the back mutations to the wild-type LD sequence. The construct was subsequently transformed into Rosetta(DE3)™ (Novagen, Madison, WI) by electroporation for *E. coli* expression. This strain contains an extra plasmid harbouring the genes encoding the tRNA for the seven rare codons (AUA, AGG, AGA, CUA, CCC, CGG, and GGA).

Table 2.1. Primers used for construction of *E. coli* LD expression plasmids

Primers for correction of pET11/LD clone	
Name	Sequence
MVC1	5´-CCGGAAACCGTG*ACT*CAGAAGTTCCCTTTCATCAGC-3´
MVC3	5´-GCTGGTGACCCTTAT*GCT*AGAAGCCTTTCTGC-3´
MVC5	5´-GGGTACTATGTTAGAAGGGA*TAC*TAATGGCCAGATTGAG-3´

The triplet changed are indicated in italic.

2.1.1.2 Pilot Scale Expression in E. coli

LB medium (100 mL) containing 100 µg/mL ampicillin and 34 µg/mL chloramphenicol were inoculated with a culture grown overnight to a starting OD_{600} of 0.1. Untransformed Rosetta(DE3) strain served as negative control for expression. The cultures were induced at OD_{600} ~ 0.6 with isopropyl β-D-1-thiogalactopyranoside (IPTG) to a final concentration of 1 mM and the temperature was lowered to 20 °C. Samples (1 mL) were taken throughout the induction period and were immediately centrifuged at 13,000*g* for 2 min. Supernatants and pellets were stored on ice until SDS-PAGE and immunoblot analysis. The pellets were dissolved by adding 2 × SDS-loading buffer (50 µL) and aliquots of the supernatants were mix with the appropriate amount of SDS-loading buffer. The SDS-PAGE, Coomassie staining and immunoblotting were performed as described in section 2.5.2.

2.1.1.3 Construction of P. pastoris *LD Expression Plasmid*

The pET11a/LD plasmid was used as template in PCR with forward primer MVC8 and reverse primer MVC14 (Table 2.2). The PCR involved preheating at 94 °C (2 min), 30 cycles at 94 °C (15 s), 55 °C (30 s), and 72 °C (3 min), followed by a final elongation (7 min). The resulting PCR product (2678 bp) encoding the mature LD lacking the putative leader sequence (amino acid residues 22–905 according to

accession No, **AAD04189**, NCBI Protein database) with flanking NotI restriction sites introduced by the primers (in bold) was digested, gel-purified and cloned into the NotI site of the pPIC9K vector (Invitrogen, Carlsbad, CA) to obtain in-frame cloning with the α-mating factor secretion signal from *Saccharomyces cerevisiae* (Figure 2.1A).*E. coli*, XL10-Gold (Stratagene) was transformed with the resulting pPICK9/LD (Figure 2.1B) and isolated plasmids from single colony transformants, selected on LB-agar plates containing 100 µg/mL ampicillin, were analyzed for correct orientation of the inserted gene using the XbaI restriction site present in both vector and insert. The sequence of the final construct was verified by sequencing using forward primers and reverse primers covering the LD mature protein encoding region (Table 2.2.). Small scale plasmid preparation, restriction enzyme digestion, ligation, and transformation followed standard molecular biology protocols (*69*).

Table 2.2. Primers used for construction of *P. pastoris* LD expression plasmids and sequencing

Primers for *P. pastoris* construct	
Name	Sequence
MVC8 (forw.)	5´-AA**GCGGCCGC**TGCGTTCATGCCGGA-3´
MVC14 (rev.)	5´-AA**GCGGCCGC**TTAACACCGAGGTTCGACAAAGACT-3´
Primers for LD sequencing in pPIC9K	
Name	Sequence
α-factor (forw.)	5´-TACTATTGCCAGCATTGCTGC-3´,
PLD001 (forw.)	5´-TGCAATTACCCGGCGTGCTG-3´
PLD003 (forw.)	5´-GAATATCGTCAGATGGTCCA-3´
PLD005 (forw.)	5´-TGATGTTATCAGTGTGAAGA-3´
PLD002 (rev.)	5´-CGGTTTTCCCACTCTCTTGG-3
PLD004 (rev.)	5´-TTAACCTATCAACCATGAAA-3´
PLD006 (rev.)	5´-AACACCCCAATTGTTTGTTT-3´
3AOX1 (rev.)	5´-GCAAATGGCATTCTGACATCC-3´

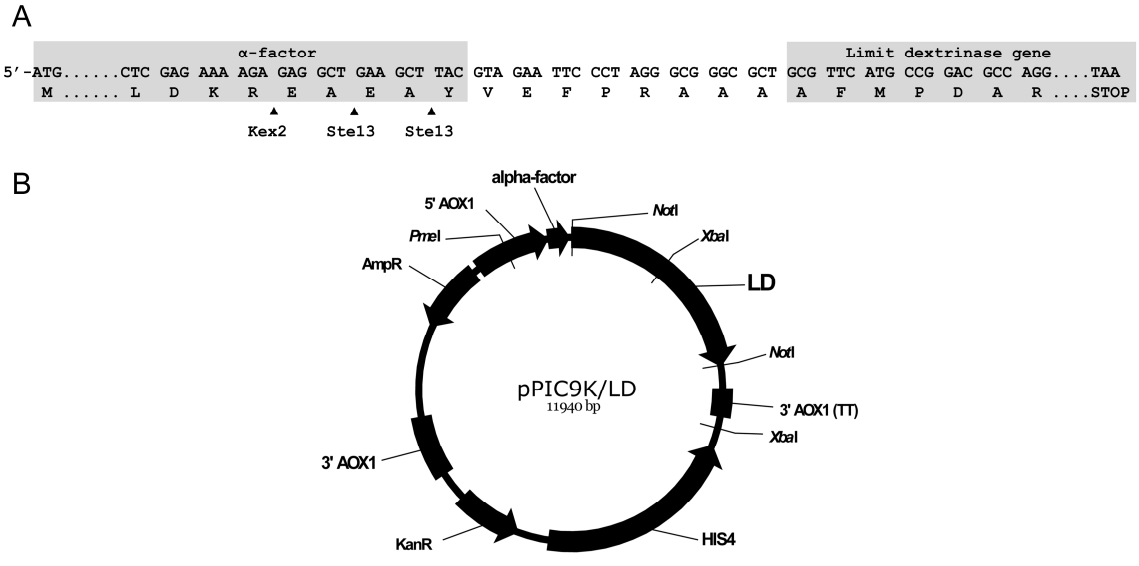

Figure 2.1. Design of the pPIC9K/LD plasmid. (A) Schematic representation of the construction of LD gene cloned in-frame with α-factor secretion signal. The linker between the α-factor and the LD gene is a part of the multiple cloning site. (B) The LD encoding expression plasmid used for *P. pastoris* transformation (*70*).

2.1.1.4 Transformation of P. pastoris *and Selection for Expression and LD Secretion*

Prior to transformation, pPICK9K/LD (20 μg) was linearized with PmeI followed by purification (Strataclean; Stratagene), precipitation, and redissolving in sterile Milli-Q water. Electrocompetent *P. pastoris* strain GS115 (Invitrogen) cells were transformed with the linearized plasmid by electroporation using a Micropulser (Bio-Rad, Hercules, CA). Transformants were isolated by prototrophic growth on minimal medium lacking histidine and supplemented with 1% sorbitol (RDB plates: 1 M sorbitol, 2% (w/v) dextrose, 1.34% (w/v) yeast nitrogen base without amino acids (YNB), 1.64 μM biotin, 270 μM L-glutamic acid, 335 μM L-methionine, 342 μM L-lysine, 381 μM L-leucine, 381 μM L-isoleucine) (*71*). Plates were incubated at 30 °C for 2–4 days.

Transformants secreting LD were selected by colony blotting using antibodies against LD from barley malt (*72*). Single colonies of His^+ transformants were picked from the initial RDB plates, transferred to YPD plates, grown for two days and then replicated to nitrocellulose membranes (Hybond ECL, 0.45 μm, Amersham Biosciences, Freiburg Germany) placed on minimal medium plates containing 0.5% (v/v) methanol (MM plates: 1.34% (w/v) YNB, 1.64 μM biotin, 0.5% (v/v) methanol) followed by incubation at 30 °C for two days. Secreted LD was detected by immunoblotting using anti-LD primary antibody (*72*), and goat anti-rabbit alkaline phosphatase conjugated secondary antibody (Dako, Glostrup, Denmark). The membrane was rinsed with Milli-Q water to remove cells before blocking in Tris-buffered saline Tween-20 (TBST) with BSA (25 mM Tris-HCl pH 7.5, 150 mM NaCl, 0.2% (v/v) Tween 20, 1% (w/v) BSA) for 30 min. The primary antibody was diluted 1:3000 in TBST and the antigen-antibody interaction was carried out at room temperature for 30 min. The membrane was washed (3 × 10 min) with TBST before probing with secondary antibody diluted 1:2000 in TBST (30 min). After washing (3 × 10 min) with TBST the immunoblot was developed using nitroblue tetrazolium (NBT)/5-bromo-4-chloro-3-indolyl phosphate (BCIP) colorimetric method (100 mM Tris-HCl pH 9.5, 100 mM NaCl, 5 mM $MgCl_2$, 0.33 mg/mL NBT, 0.17 mg/mL BCIP) and the reaction was stopped by change to Milli-Q water. LD from barley malt served as positive and *P. pastoris* strain GS115 transformed with the empty vector pPIC9K as negative control.

2.1.1.5 Pilot Scale Expression and High Cell-Density Fermentation of P. pastoris

Twelve His^+ transformants selected by colony immunoblotting were tested for expression in 50 mL culture using buffered complex medium following the supplier's guidelines for Mut^+ phenotype (*71*). LD activity was monitored after 96 h using the Limit-Dextrizyme assay (see section 2.2.1; Megazyme, Bray, Ireland). The culture medium was changed by adding 60 volumes of 100 mM Na acetate pH 5.5 followed by 10-fold concentration (Centricon, 30 kDa cut-off; Millipore, Cork, Ireland) prior to testing. Due to low LD activity in shake flask cultures, a 5 h assay reaction time was applied to ensure detection of secretory expression of active LD. The effect of induction temperature was analyzed by comparing LD activity in cell-free extract of cultures grown in minimal medium at either 30 or 22 °C for 72 h. The transformant selected for large scale bioreactor production was shown to secrete LD activity in minimal medium after induction at 22 °C for 72 h.

The bioreactor fermentation has three stages; i) a glycerol batch phase generating biomass; ii) a glycerol feed phase, with glycerol being delivered at growth limiting rate

for continued biomass generation and derepression of the alcohol oxidase promoter AOX1; and iii) a methanol feed phase for induction of expression with increasing methanol feed to a maximum level at 11 g/(L·h). Methanol induction was maintained for 89 h. The fermentation procedure guidelines for methanol feeding of the Mut^+ phenotype (*73*) were optimized and the fermentation was carried out in a 5-L Biostat B (B. Braun Biotech International, Melsungen, Germany) bioreactor equipped with an additional feed pump, gas mixer, dissolved oxygen tension polarographic electrode, and water cooler (*73*, *74*). The 2 L starting basal salt medium containing PMT1 (*74*) trace salts was inoculated with 150 mL culture (OD_{600} = 16) propagated overnight at 30 °C in buffered complex medium (BMGY: 1% (w/v) yeast extract, 2% (w/v) peptone, 0.1 M KH_2PO_4 pH 6.0, 1.34% (w/v) YNB, 1.64 μM biotin, 1% (v/v) glycerol) (*71*). The temperature was maintained at 29 °C by water cooling during glycerol batch and fed-batch phases. Prior to induction, the temperature was decreased to 22 °C and kept throughout the methanol feed phase. Solutions of 50% (w/v) glycerol and 100% methanol both containing PTM1 trace salts were used as carbon source during glycerol feed phase and methanol feed phase, respectively. Continuous addition of 28% aqueous ammonia served to maintain the pH at 5.5 and as a nitrogen source.

2.1.1.6 Purification of LD

Cells were harvested after five days of fermentation (centrifugation, 12,000*g*, 4 °C, 30 min), and the supernatant (2.5 L) was kept at 4 °C after adding sodium azide (final concentration 0.02% (w/v)). LD was purified by a two-step procedure involving affinity chromatography using β-cyclodextrin (β-CD) conjugated to Sepharose followed by gel filtration (Hiload Superdex 200 26/60, GE Healthcare, Uppsala, Sweden). The culture supernatant was split in two and ammonium sulphate was added to a final concentration of 1 M to secure binding of LD to β-CD-Sepharose (*72*), followed by centrifugation (12,000*g*, 4°C, 30 min) and filtration (0.45 μm, GE Water & Process Technologies, Trevose, PA), and pumped (30 mL/h) onto β-CD-Sepharose (20 mL bed volume in XK 16/10 column; GE Healthcare) equilibrated in 10 mM Na acetate pH 5.5, 500 mM NaCl, 5 mM $CaCl_2$. After wash with equilibration buffer (four column volumes; 60 mL/h), bound LD was eluted with 10 mM Na acetate pH 5.5, 5 mM $CaCl_2$, 7 mM β-CD at the same flow rate. Fractions (960 μL) were collected in tubes containing 40 μL 1 M Hepes/NaOH pH 7.0, 125 mM $CaCl_2$, 0.125% Triton X-100 and aliquots were analyzed by SDS-PAGE. Fractions with LD activity (see section 2.2.1 for assay) were pooled and concentrated to 18 mL (Centricon; 30 kDa cut-off, Millipore) after 2 mL were removed and dialyzed (Spectra/por dialysis membrane cut-off 12–14 kDa; Spectrum Laboratories, Rancho Dominguez, CA) 2 × 12 h against 2 × 3 L 50 mM Mes/NaOH pH 6.6, 250 mM NaCl and assayed for activity. Subsequently 4 × 4 mL portions from the concentrated β-CD pool (approximately 2.5 mg/mL LD) were applied on a Hiload Superdex 200 26/60 column (GE Healthcare) equilibrated with 50 mM Mes/NaOH pH 6.6, 250 mM NaCl and eluted (30 mL/h) with the same buffer. Collected fractions (4 mL) were analyzed by SDS-PAGE and LD containing fractions were pooled, concentrated (Centricon, 30 kDa cut-off; Millipore), assayed for activity, and stored at 4 °C. An ÄKTAexplorer (GE Healthcare) interfaced by UNICORN 5.0 control software (GE Healthcare) was used for both chromatographic procedures.

2.1.2 Limit Dextrinase Inhibitor

2.1.2.1 Cloning of LDI

A cDNA clone of LDI was provided by Birgit Bønsager, who had performed the cloning as follows. Husk from frozen barley seeds (cultivar Morex) was removed and milling of the seed was carried out in a mortar cooled in liquid nitrogen. RNA was extracted using RNeasy Plant Mini kit (Qiagen, Düsseldorf, Germany) and RT-PCR was carried out using One-Step RT-PCR Kit (Qiagen) and the primers LDI F and LDI R (Table 2.3). The cDNA was subsequently cloned in to the pCR 2.1-TOPO vector (Invitrogen) using the NdeI and BamHI sites (in bold) and the construct (pCR 2.1-TOPO /LDI) was transformed into *E.* coli TOP10 competent cells (Invitrogen).

Table 2.3. Primers used for cloning and mutagenesis of LDI and construction of LDI expression plasmids. Restriction sites are marked as bold in the primer

Primers for cloning of LDI	
Name	Sequence
LDI F (forw.)	5'-GAGAGA**CATATG**ACCCTGGAGAGCGTCAAGGACG-3'
LDI R (rev.)	5'-**GGATCC**CCTTATCCCGGCTCCTGGACGGACGA-3'
Primers for Intein-LDI construct	
Name	Sequence
MVC11 (forw.)	5'-AAAAAAA**GCTCTTC**TAACACCCTGGAGAGCGTCAAGGAC-3'
MVC12 (rev.)	5'-AA**GGATCC**TCATCCCGGCTCCTGAACGGA-3'
Primers for His-LDI	
Name	Sequence
MVC21 (forw.)	5'-AAAAAAAAA**GAATTC***CATCATCATCATCATCATCAT*CTTGTTCCACGTGG TTCTACCCTGGA-3'
MVC22 (rev.)	5'-TGATTAACT**GGTACC**TTATCCCGGCTCCTG-3'
Primers for *P. Pastoris* construct (EF-LDI-His)	
Name	Sequence
MVC23 (forw.)	5'-AAAAAAAAA**GAATTC**ACCCTGGAGAGCG-3'
MVC20 (rev.)	5'-TGATTAACT**GGTACC**TTA*ATGATGATGATGATGATG*TCCCGGCTCCTG-3'
Primers for deletion of EF (wt-LDI-His)	
Name	Sequence
MVC24 (forw.)	5'-GAGAAAAGAGAGGCTGAAGCTACCCTGGAGAGCGTCAAGGACGA-3'
MVC25 (rev.)	5'- TCGTCCTTGACGCTCTCCAGGGTAGCTTCAGCCTCTCTTTTCTC-3'
Primers for deletion of TLESV (ΔV^5LDI-His)	
Name	Sequence
MVC28 (forw.)	5'-GAGAAAAGAGAGGCTGAAGCTAAGGACGAGTGCCAACCAGGGGT-3'
MVC29 (rev.)	5'-ACCCCTGGTTGGCACTCGTCCTTAGCTTCAGCCTCTCTTTTCTC-3'

The cDNA corresponding to amino acid residues 25–138 (accession No, **ABB88573**, NCBI Protein database), encoding a protein sequence identical to the previously published (*61, 75*), was used as template for PCR amplification with the appropriate primer pairs (Table 2.3).

2.1.2.2 Cloning, Expression and Purification of the Intein-LDI Construct

The intein-LDI construct was amplified using the primer pair MVC11 and MVC12 (Table 2.3). The restriction sites SapI and BamHI were used for cloning the fragment

in-frame with the chitin binding domain (CBD) from *Bacillus circulans* and the *Ssp* DnaB intein from the cyanobacterium *Synecchocystis* sp PCC6803 of the *E. coli* expression plasmid, pTWIN1 (New England Biolabs, Ipswich, MA). Purification of the expressed gene product by auto cleavage on a chitin bead column by decreasing the pH and increasing the temperature will result in wild-type N-terminal sequence of LDI. The ligated plasmid pTWIN/LDI was subsequently transformed into the *E. coli* cloning strain DH5α, before transformation into the expression strain Rosetta-gami™2(DE3) (Novagen). This strain contains an extra plasmid harbouring the genes encoding the tRNA for the seven rare codons (AUA, AGG, AGA, CUA, CCC, CGG, and GGA) as well as mutations in both the thioredoxin reductase (*trxB*) and glutathione reductase (*gor*) genes, resulting in enhanced disulfide bond formation in the cytoplasm and improved protein folding *in vivo*. Small scale plasmid preparation, restriction enzyme digestion, ligation, and transformation followed standard molecular biology protocols (*69*).

A preculture of LB containing 100 µg/mL ampicillin, 34 µg/mL chloramphenicol, 12.5 µg/mL tetracycline was inoculated with a single colony and propagated at 37 °C overnight. Fresh LB medium (400 mL) including 100 µg/mL ampicillin, 34 µg/mL chloramphenicol, 12.5 µg/mL tetracycline was inoculated with the overnight culture to a start OD_{600} of approximate 0.08 and grown at 37 °C until mid log phase (OD_{600} ~ 0.5). The cells were divided into two flasks (200 mL) and induced by addition of IPTG (final concentration 0.3 mM). The two cultures were incubated at 15 °C and 37 °C for 19 h and 2h, respectively. The cells were harvested by centrifugation (5,000*g*, 4 °C, 10 min) and the pellets were stored at –20 °C until use. The cells were resuspended in buffer B1 (100 mM Tris pH 8.5, 0.5 M NaCl, 1 mM EDTA), lysed by sonication followed by centrifugation (19,000*g*, 4 °C, 30 min). The clarified cell extract was loaded (30 mL/h) on a chitin bead column (column volume = 4 mL) (New England Biolabs) equilibrated with 40 mL B1 (60 mL/h) and subsequently washed with 48 mL B1 (120 mL/h). The auto cleavage of the intein was facilitated by washing the column with 48 mL B2 (20 mM Hepes/NaOH pH 7.0, 0.5 M NaCl, 1 mM EDTA) until pH of the eluate was ~ 7.0. The column flow was stopped and the cleavage reaction was left overnight at 23 °C. The cleavage protein (LDI) was eluted with 12 mL B2 (60 mL/h) in 0.5 mL fractions, which were analysed by SDS. Fractions were pooled three and three and concentrated 20-fold before analysing for LD inhibition activity. An ÄKTAexplorer (GE Healthcare) interfaced by UNICORN 5.0 control software (GE Healthcare) was used for the chromatographic procedures.

2.1.2.3 Cloning, Expression and Purification of **P. pastoris** *His-LDI Construct*

The pCR 2.1-TOPO/LDI construct (section 2.1.2.1) was used as template for PCR amplification of a *P. pastoris* His-LDI expression construct with forward primer MVC21 and reverse primer MVC22 (Table 2.3.) A thrombin (underlined in primer) cleavable N-terminal hexa-histidine tag (in italic) was introduced with the forward primer MVC21. Cleavage of the expressed gene product with thrombin will result in an N-terminal addition of two extra amino acids, glycine and serine (in bold) (**GS**TLESVKDECQ). The amplified product was cloned in-frame with the *Saccharomyces cerevisiae* α-factor secretion signal of the *P. pastoris* vector pPICZα A using the EcoRI and KpnI sites (marked in bold in the primer). The plasmids harbouring the above constructs were linearized with PmeI and transformed into *P. pastoris* strain

X33 by electroporation and selected on YPDS plates supplemented with 100 µg/mL zeocin (Invitrogen). Small scale plasmid preparation, restriction enzyme digestion, ligation, and transformation followed standard molecular biology protocols (*69*). Five selected clones were tested for heterologous expression of LDI in 50 mL culture flasks according to the EasySelect™ *Pichia* Expression Kit (Invitrogen) (*71*). Precultures of YPD (1% (w/v) yeast extract, 2% (w/v) peptone, 2% (w/v) glucose) of the selected clones were inoculated with a single colony and incubated overnight at 30 °C. 1 mL of the precultures were used for inoculating 50 mL of freshly prepared BMGY (1% (w/v) yeast extract, 2% (w/v) peptone, 0.1 M KH_2PO_4 pH 6.0, 1.34% (w/v) YNB, 1.64 µM biotin, 1% (v/v) glycerol), which were incubated overnight at 30 °C. The cells were induced by changing the growth medium to buffered methanol-complex medium (BMMY: 1% (w/v) yeast extract, 2% (w/v) peptone, 0.1 M KH_2PO_4 pH 6.0, 1.34% (w/v) YNB, 1.64 µM biotin, 0.5% (v/v) methanol). The cells were harvested by centrifugation (1,500*g*, 20 °C, 5 min) and resuspended in BMMY (50 mL) to give an OD_{600} ~ 5. The cultures were incubated at 17 °C for 72 h. Methanol (final concentration 0.5 % (v/v)) was added every 24 h for continous induction and supply of carbon source. 1 mL samples were taken every 24 h and analysed by SDS-PAGE for LDI expression and secretion. Cells were harvested by centrifugation (12,000*g*, 4 °C, 30 min). Based on the SDS-PAGE result two clones were selected for purification. Imidazole and NaCl were added to the culture supernatant to 10 mM and 500 mM, respectively, and pH was adjusted to 7.4 by addition of K_2HPO_4(s), followed by centrifugation (12,000*g*, 4 °C, 30 min) and filtration (0.45 µm) before application onto the 1 mL HisTrap HP column (GE Healthcare) (40 mL/h) equilibrated with 20 mM Na phosphate, pH 7.4, 10 mM imidazole, 500 mM NaCl. The column was washed with equilibration buffer (60 mL/h) until a stable A_{280} signal was reached, and a linear imidazole gradient by mixing the equilibration buffer with 20 mM Na phosphate pH 7.4, 500 mM imidazole, 500 mM NaCl (0–100%, 20 mL, 60 mL/h) was applied. Fractions (1 mL) were collected and analyzed by SDS-PAGE. An ÄKTAexplorer (GE Healthcare) interfaced by UNICORN 5.0 control software (GE Healthcare) was used for the chromatographic procedures.

LD inhibition was assayed by measuring residual LD activity after LDI addition (20 µL of culture supernatant concentrated 10-fold) using Limit-Dextrizyme tablets as substrate in 0.1 M sodium acetate buffer pH 5.5, 0.005% Triton X-100 (see section 2.2.1. for detailed assay description). The concentration of LDI was estimated from the band on a SDS-PAGE gel, resulting in an estimated ratio of LDI:LD in the reaction mixture to 1000:1.

2.1.2.4 Cloning and Site-Directed Mutagenesis of LDI-His

The pCR 2.1-TOPO/LDI construct (section 2.1.2.1) was used as template for PCR amplification of a *P. pastoris* LDI-His expression construct with forward primer MVC23 and reverse primer MVC20 (Table 2.3.) A hot start PCR protocol at 94 °C (3 min), 3 cycles at 94 °C (30 s), 50 °C (30 s), and 72 °C (45 s), followed by 22 cycles at 94 °C (30 s), 58 °C (30 s), and 72 °C (45 s) and a final elongation (7 min) was used. The resulting PCR product comprising the LDI gene and nucleotides encoding a C-terminal hexa-histidine tag (in italic, Table 2.3) was cloned in-frame with the *Saccharomyces cerevisiae* α-factor secretion signal of the *P. pastoris* vector pPICZα A using the EcoRI and KpnI sites (in bold, Table 2.3). This cloning procedure results in the additional amino acids glutamate and phenylalanine at the N-terminus (**EF**TLESVKDECQ) of the

gene product denoted as EF-LDI. The addition of EF was a consequence of using the EcoRI restriction site. Deletion of these two amino acid residues was done by site-directed mutagenesis using QuikChange® Lightning Site-Directed Mutagenesis Kit (Stratagene) and forward primer MVC24 and reverse primer MVC25 (Table 2.3). Expression of this clone results in a native N-terminus (TLESVKDECQ) denoted as wt-LDI. An N-terminal deletion of the TLESV was also constructed using QuikChange® Lightning Site-Directed Mutagenesis Kit and the following primer pair MVC28 and MVC29 (Table 2.3). This N-terminally truncated mutant, with the expected N-terminal sequence KDECQ, was denoted ΔV^5LDI (Figure 2.2). All the above mentioned N-terminal sequences assume correct processing at the second Ste13 protease cleavage site of the *Saccharomyces cerevisiae* α-factor secretion signal of the *P. pastoris* vector pPICZαA expression vector (*71*). Small scale plasmid preparation, restriction enzyme digestion, ligation, and transformation followed standard molecular biology protocols (*69*).

	wt-LDI	TLESVKDECQ
	EF-LDI	EFTLESVKDECQ
	ΔE^3LDI	SVKDECQ
Expected	ΔV^5LDI	KDECQ
Actual	ΔV^5LDI	EAEAKDECQ

Figure 2.2. N-terminal sequence of wild-type and mutant LDI. The actual sequence of mutant ΔV^5LDI differed for the expected due to the addition of four amino acid residues originating from the expression plasmid (see Result, section 3.2.3 for further description).

2.1.2.5 Expression and Purification of LDI-His and LDI-His-mutants

The plasmids harbouring the above constructs were linearized with PmeI and transformed into *P. pastoris* strain X33 by electroporation and selected on YPDS plates supplemented with 100 µg/mL zeocin (Invitrogen). Six selected clones from each construct transformation were tested for heterologous expression of LDI in 100 mL culture flasks according to the EasySelect™ *Pichia* Expression Kit (Invitrogen) (*71*). The cultures were induced after 24 h growth in BMGY (*71*) at 30 °C by transferring to BMMY (*71*) at 17 °C. Cells were harvested by centrifugation (12,000*g*, 4 °C, 30 min) after 72 h methanol induction. The production of active recombinant LDI was verified by SDS-PAGE and LD inhibition ([LD]=10 nM) was assayed by measuring residual LD activity after LDI addition (30 µL of culture supematant) using Limit-Dextrizyme tablets as substrate in 0.1 M sodium acetate buffer pH 5.5, 0.005% Triton X-100 (see section 2.2.1 for detailed assay description). To achieve a high level of active LDI, selected clones (EF-LDI and wt-LDI) were cultured in a 5-L Biostat B (B. Braun Biotech International) (see section 2.1.1.5). Cells (OD_{600} = 22) from a shake flask culture (300 mL) grown overnight at 30 °C in BMGY were harvested by centrifugation (1,500*g*, 20 °C, 5 min), resuspended in fresh BMGY (80 mL) and used for inoculation of the starting basal salt medium (3 L) containing PMT1 trace salts (*74*). The temperature was maintained at 28 °C by water cooling during the glycerol batch (~20 h) and fed-batch (30 mL/h 50% (w/v) glycerol; ~7 h) phases. Prior to induction, the temperature was decreased to 17 °C, and kept throughout the methanol feed phase (22–28 h). The methanol flow was successively increased from 1 g/(L·h) to reach the maximum of 11 g/(L·h) after 8 h. Addition of 28% aqueous ammonia served to maintain pH 5.5 and as a nitrogen source.

Cells were harvested by centrifugation (12,000*g*, 4 °C, 30 min); the supernatant (3.2 L) was supplemented with sodium azide to 0.02% (w/v) and kept at 4 °C. EF-LDI and wt-LDI were purified by a two-step procedure involving of affinity chromatography (5 mL HisTrap HP column; GE Healthcare) followed by anion exchange chromatography (MonoQ (10/100 GL) column; GE Healthcare). An ÄKTAexplorer chromatograph (GE Healthcare) interfaced by UNICORN 5.0 control software was used for the chromatographic purifications. Imidazole and NaCl were added to the culture supernatant to 10 mM and 500 mM, respectively, and pH was adjusted to 7.4 by addition of K_2HPO_4(s), followed by centrifugation (12,000*g*, 4 °C, 30 min) and filtration (0.45 µm) before application (120 mL/h) onto the HisTrap HP column equilibrated with 20 mM Na phosphate, pH 7.4, 10 mM imidazole, 500 mM NaCl. After washing with equilibration buffer (60 mL/h) until a stable A_{280} signal was reached, bound LDI was eluted (60 mL/h) by a two-step linear imidazole gradient by mixing the equilibration buffer with 20 mM Na phosphate pH 7.4, 500 mM imidazole, 500 mM NaCl (0–10%, 10 mL; 10–100%, 300 mL). Fractions (5 mL) were collected and analyzed by SDS-PAGE. LDI containing fractions were collected in two pools (2 × 50 mL), concentrated (Centricon; 3 kDa cut-off, Millipore) to 2 × 15 mL, and each was dialyzed (Spectra/por dialysis membrane (cut-off 6–8 kDa; Spectrum Laboratories) against 2 × 5 L 5 mM Bicine/NaOH pH 8.5 and 1 × 5 L 10 mM Bicine/NaOH pH 8.5. The dialyzed samples were centrifuged (12,000g, 4 °C, 30 min) and the supernatants (2 × 15 mL) were loaded onto a MonoQ 10/100 GL column and washed (150 mL/h; 150 mL) with the above buffer. Protein was eluted by a five-step linear salt and pH gradient with the elution buffers A: 10 mM Bicine/NaOH pH 8.5 and B: 10 mM Hepes/NaOH, pH 7.0, 250 mM NaCl (0–12.5%, 24 mL; 12.5–25%, 160 mL; 25–30%, 8 mL; 30–38%, 15 mL; 38–100%, 80 mL). Collected fractions (4 mL) were analyzed by SDS-PAGE and LDI containing fractions eluted in one peak were pooled, concentrated and buffer-changed to 10 mM Bicine/NaOH pH 8.5, 100 mM NaCl (Centricon, 3 kDa cut-off; Millipore).

The ΔV^5LDI mutant was produced as described above for the clone selection in a 500 mL shake flask culture with 48 h induction. Adjusted culture supernatant (pH 7.4, 10 mM imidazole, 500 mM NaCl) was loaded onto a 1 mL HisTrap HP column and eluted as above. The buffer was exchanged (10 mM Bicine/NaOH pH 8.5) using Microcon (3 kDa cut-off; Millipore) and the SDS-PAGE electrophoretically homogenous ΔV^5LDI (770 µg/mL) pool was used for SPR analysis.

2.2 Enzyme Activity and Inhibition

2.2.1 LD Hydrolytic Activity

LD activity during pilot expression, fermentation, and purification was assayed with Limit-Dextrizyme tablets (Megazyme) in 0.1 M Na acetate pH 5.5, 0.005% Triton X-100. LD (5–10 nM) diluted in assay buffer (0.5 mL) was preheated (5 min) on a 40 °C water bath before adding the Azurine-crosslinked-pullulan substrate tablet. The reaction was stopped after 10 min by adding 5 mL 1% (w/v) Tris and vigorously whirl-mixing. After 10 min incubation at R.T., the tubes were whirl-mixed and 2 mL were transferred to eppendorf tubes and centrifuged (14,000*g*, 10 min). The absorbance of the supernatant was measured at 590 nm. One activity unit is defined as the amount of

enzyme that releases one micromole of glucose reducing-sugar equivalents per min from pullulan under the defined assay conditions (*76*).

Kinetic constants of LD were determined from initial rates of hydrolysis at 12 different concentrations (0.02–1 mg/mL) of pullulan (Megazyme) by 3.6 nM LD in 20 mM Na acetate pH 5.5, 5 mM $CaCl_2$, 0.005% Triton X-100 (starting assay volume: 1.1 mL) at 37 °C. Aliquots (200 µL) were removed at 3 min intervals during 0–15 min, stopped by mixing with 500 µL freshly prepared developing buffer (0.4 M Na carbonate pH 10.7, 2.5 mM $CuSO_4$, 2.5 mM 4,4'-dicarboxy-1,2'-biquinoline, 6 mM L-serine) and 300 µL Milli-Q water (*77*) and the absorbance was measured after 30 min at 80 °C in microtiter plates (300 µL, in duplicates) at A_{540}. The release of reducing sugar was quantified using a maltose standard curve. V_{max} and K_m were determined by fitting either the Michaelis-Menten equation (eq. 2.1) or the equation for uncompetitive substrate inhibition (eq. 2.2) to the initial rates. $K_{i,s}$ is the dissociation constant for the inhibitory [substrate-enzyme]-substrate ternary complex.

(eq. 2.1) $$V = \frac{V_{max}}{1 + \frac{K_m}{[S]}}$$

(eq. 2.2) $$V_{i,sub} = \frac{V_{max}}{1 + \frac{K_m}{[S]} + \frac{[S]}{K_{i,s}}}$$

The fitting and plotting were performed using the Enzyme Kinetics Module 1.0 of the program Sigmaplot 9.01 (Systat Software, Chicago, IL).

2.2.2 LD Inhibition

wt-LDI (0.1–0.2 µM, 300 µL; 10 mM Bicine/NaOH pH 8.5, 0.1 M NaCl) was preincubated with LD (52 nM, 1200 µL; 100 mM Na acetate buffer pH 5.5, 5 mM $CaCl_2$, 0.005% Triton X-100) for 15 min at 25 °C. From the preincubation mixture 110 µL was added to 990 µL pullulan (Megazyme) at 8 different concentrations (0.025–0.3 mg/mL) in 100 mM Na acetate buffer pH 5.5, 5 mM $CaCl_2$, 0.005% Triton X-100 at 37 °C. The final concentrations of LDI and LD in the reaction mixture were 2 or 4 nM and 4.2 nM, respectively. The assay and detection of the hydrolysis product were performed as described in section 2.2.1. The LDI inhibition constant, K_i of LD was determined from initial rates of pullulan hydrolysis with or without the inhibitor present. K_i was determined by fitting the model for tight competitive inhibition (eq. 2.3) to the data using the Enzyme Kinetics Module 1.0 of the program Sigmaplot 9.01 (Systat Software). K_{app} is the apparent inhibition constant when dissociation of the enzyme-inhibitor complex is affected by substrate addition.

(eq. 2.3) $$v_i = \left(\frac{v_0}{2 \cdot [E]}\right) \cdot \left(([E] - [I] - K_{app}) - \sqrt{([E] - [I] - K_{app})^2 + 4 \cdot [E] \cdot K_{app}} \right),$$

where $$K_{app} = K_i \cdot \left(1 + \frac{[S]}{K_m}\right)$$

To determine the molar ratio for 100% inhibition, pullulan and LD concentrations were kept constant in the assay at 0.17 mg/mL and 4 nM, respectively, and the final LDI concentrations were varied between zero and 20 nM in the assay corresponding to LDI:LD molar ratios between zero and 5. The assay was carried out as above.

2.3 Transglycosylation

The transglycosylation catalysed by LD (18–38 nM) was analysed by using 20–40 mM α-maltosyl fluoride (G2F) or α-maltotriosyl fluoride (G3F) (a gift from Rob Field, Norwich, UK) as donors and 8–200 mM of different linear (maltose, maltotriose, maltotetraose, and maltohexaose) and cyclic oligosaccharides (α-cyclodextrin, β-cyclodextrin, and 6-*O*-α-maltosyl β-cyclodextrin) as acceptors. In addition to the linear and cyclic oligosaccharides, the known glycoside hydrolase inhibitors, 4-*O*-α-D-glucopyranosylmoranoline (G1M) (*78*) and acarbose (*79*) were also used as acceptors. The reaction was carried out in 50 mM Na acetate pH 5.5 at 40 °C. Samples were taken at different time points (0–240 min) and the reaction was terminated by addition of 1/10 volume of 1 M NaOH. The reaction was followed by thin-layer chromatography (TLC) by spotting diluted (1–4 times) samples onto a 8×12 cm TLC plate (TLC silica gel 60 F_{254}; Merck, Germany) and the plate was repeatedly irrigated (2–3 times) with a solvent mixture of acetonitrile: ethyl acetate: iso-propanol: water (85:20:50:70, by volume) at 25 °C. The carbohydrates on the TLC were detected by dipping the dried plate into a solution containing 2% (w/v) orcinol, 83% (v/v) ethanol and 11% (v/v) sulphuric acid followed by heating with a heat gun until the sugars appeared as pink-violet spots. Selected samples were also analysed by mass spectrometry (MS) to verify the correct mass of the transglycosylation products formed. The MS analysis was carried out by Dr. Gerhard Saalbach, JIC Proteomics Facility, Department of Biological Chemistry, John Innes Centre, UK. Samples were diluted in TFA before spotted on a prespotted anchorchip (PAC) plate (Bruker Daltonics, Bremen, Germany) containing pre-spotted matrix CHCA (α-cyano-4-hydroxycinnamic acid).

2.4 Surface Plasmon Resonance

2.4.1 Cyclodextrin Affinity

Affinity of LD for α-, β- and γ-cyclodextrin (CD) was determined using surface plasmon resonance (SPR) (BIAcore® T100; GE Healthcare). LD was immobilized using 100 μg/mL LD in 5 mM Na acetate buffer pH 4, 1 mM β-CD on a CM5 sensor chip (GE Healthcare) using random amine coupling (2800–3200 response units, RU). Sensorgrams (RU *vs*. time) of the binding of α-, β- and γ-CD in the range of 2.5–160 μM (17 concentrations), 0.125–40 μM (14 concentrations), and 4–160 μM (16 concentrations), respectively, were obtained at 25 °C using 3 min association and 2 min dissociation. CDs were dissolved in 20 mM Na acetate pH 5.5, 100 mM NaCl, 0.005% surfactant P-20, which was also used as running buffer. K_d was calculated by steady-state affinity fitting (BIAcore evaluation software 1.1, GE Healthcare) to the

equilibrium response R of CD at a given concentration after subtracting the reference flow cell signal; R_{max} is the response at saturation of the ligand on the chip.

(eq. 2.4) $$R = \frac{R_{max} \cdot [CD]}{[CD] + K_d}$$

2.4.2 LD/LDI Interaction

The LD/LDI interaction was analyzed by SPR using a BIAcore® T100 instrument (GE Healthcare). Immobilization of the different LDI forms on the sensor surface of a BIAcore CM5 sensor chip was performed following a standard amine coupling procedure according to the manufacturer's protocol using 10 µg/mL LDI in 5 mM Na acetate buffer pH 4 resulting in immobilization levels of 200–400 response units (RU) in sample cells, while reference cells were first activated, and then inactivated in the same procedure to be used as reference. Sensorgrams (RU *vs.* time) of LD (0.1–80 nM) binding using 4 and 15 min association and dissociation times, respectively, were recorded. Regeneration was performed by 2 injections of 10 mM glycine/HCl pH 1.5 for 60 s at 30 µL/min. The standard condition for determining binding kinetics was at 25 °C at a flow rate of 30 µL/min using seven LD concentrations (0.1–4 nM) in the running buffer 10 mM Mes/NaOH pH 6.0, 150 mM NaCl, 0.005% P-20 surfactant: Two to three start-up cycles were used before the first analysis cycle to ensure a stable response in the analysis. In order to evaluate possible contribution of mass transfer limitations, binding kinetics of the LD/LDI interaction at 25 °C were analyzed at two different flow rates, 30 µL/min 60 µL/min.

The effect of ionic strength on the binding kinetics was probed using an identical set up as above, but varying the NaCl concentration (0 mM, 75 mM, 150 mM, 300 mM, and 1000 mM) in the running buffer and similarly the effect of pH was assessed by varying the pH of the running buffer (pH 5.0–5.5, 10 mM Na acetate buffer; pH 6.0–6.5, 10 mM Mes/NaOH; pH 7.0–7.5 10 mM Hepes/NaOH; pH 8.0–9.0, 10 mM Bicine/NaOH; pH 9.5–10.0, glycine/NaOH). Temperature dependence was determined at nine temperatures in the range 10–45 °C with standard running buffer (10 mM Mes/NaOH pH 6.0, 150 mM NaCl, 0.005% P-20 surfactant) and five LD concentrations (0.4–8 nM). Two independent sets of data were collected for all conditions, and all concentrations were analyzed in duplicates within each data set, except for 0.4 nM LD, which was run four times and functioned as a control for evaluating the effect of time on the response level during the time course of the experiment. Sensorgrams collected from sample cells were subtracted from reference cell sensorgrams (no ligand immobilized) to account for refractive index changes due to minor solvent differences and for possible nonspecific LD binding to the reference cell surface. In addition, the reference cell subtracted sensorgrams were corrected by subtraction of averaged blank sensograms (buffer injected) to account for drift specific for the sample cell. Double corrected sensorgrams from the different binding experiments were analyzed using BIAcore T100 Evaluation Software version 1.1. A 1:1 binding model (eq. 2.5) (*80*) which also accounts for possible mass-transport limitations was fitted globally using non-linear regression to sensorgrams generated for each set of ligand concentrations to

determine the association rate constant, k_{on} (L/(mol·s)), the dissociation rate constant, k_{off} (s^{-1}).

$$\text{(eq. 2.5)} \qquad LD_0 \xrightarrow{k_t} LD + LDI \underset{k_{off}}{\overset{k_{on}}{\rightleftharpoons}} LD/LDI$$

Where LD_0 and LD are the concentrations of LD in the bulk and at the chip surface, respectively, and k_t is the mass transfer rate constant (RU M^{-1} m s^{-1}). The quality of the fits was judged by the residuals plots.

The equilibrium dissociation constant K_D (M) is also determined in this procedure from the ratio of the rate constants (eq. 2.6).

$$\text{(eq. 2.6)} \qquad K_D = k_{off}/k_{on}$$

The van't Hoff thermodynamic parameters at 25 °C and standard conditions were calculated from both non-linear (eq. 2.7) and linear van't Hoff (eq. 2.8) equations using kinetic data of the temperature dependence between 10–35 °C.

$$\text{(eq. 2.7)} \qquad \mathrm{RT}\ln K_D = \Delta H^\circ_{T_0} - T\Delta S^\circ_{T_0} + \Delta C^\circ_p (T - T_0) - T\Delta C^\circ_p \ln\left(\frac{T}{T_0}\right)$$

$$\text{(eq. 2.8)} \qquad \Delta G^\circ = \mathrm{RT}\ln K_D\,,\ \Delta G^\circ = \Delta H^\circ - T\Delta S^\circ$$

Where $\Delta G°$ is the standard free energy change, $\Delta H°$ and $\Delta S°$ are the standard enthalpy and entropy change, respectively. T is the absolute temperature (K), T_0 is the reference temperature (298.15 K for standard conditions), $\Delta Cp°$ is heat capacity change under standard conditions, R = 8.314 j/(K·mol) is the gas constant and K_D is the equilibrium dissociation constant (eq. 2.6).

2.5 Protein Characterization

2.5.1 Protein Assays

LD and LDI concentration was either quantified by Bradford Coomassie Plus kit (Pierce, Rockford, IL) with BSA as standard or spectrophotometrically at 280 nm using a molar extinction coefficient of 1.52 ×10^5 M^{-1}·cm^{-1} and 3.9 × 10^3 M^{-1} cm^{-1}, for LD and LDI, respectively, as determined on the basis of LD or LDI concentration calculated by aid of amino acid analysis.

2.5.2 SDS-PAGE, Isoelectric Focusing, and Immunoblotting

Protein purity was assessed by SDS-PAGE using NuPAGE® Novex Bis-Tris 4–12% gels (Invitrogen) in 1% Mes buffered polyacrylamide minigel Novex system with reducing agent added in the sample preparation and anti-oxidant in the buffer

system according to the manufacturers' recommendations and Coomassie Brilliant Blue G-250 staining (*81*).

Isoelectric focusing (IEF) was performed using the PhastSystem (Pharmacia, Sweden), pH 4–6 PhastGels (GE Healthcare) with low pI calibration kit (GE Healthcare, Buckinghamshire, UK) and Silver Kit staining (Pharmacia, Uppsala, Sweden).

Western blotting on polyvinylidene fluoride (PVDF) membranes (0.22 µm pore size) for N-terminal sequencing of impure samples was carried out using the Novex gel system with the XCell SureLock Mini-Cell according to the supplier's manual (Invitrogen). The Coomassie stained proteins of interest were excised from the membranes and the N-terminal sequence was determined using N-terminal Edman degradation (section 2.5.3).

Immunoblotting was carried out using the Novex gel system with the XCell SureLock Mini-Cell according to the supplier's manual (Invitrogen). LD was detected using polyclonal rabbit antibody raised against LD purified from barley malt (*72*) in combination with goat anti-rabbit alkaline phosphatase conjugated antibody (Dako). Unspecific binding of the antibodies to the membrane was prevented by blocking in TBST with BSA (25 mM Tris-HCl pH 7.5, 150 mM NaCl, 0.2% (v/v) Tween 20, 1% BSA) for 30 min. The primary antibody was diluted 1:3000 in TBST and the antigen-antibody interaction was carried out at room temperature for 30 min. The membrane was washed (3 × 10 min) with TBST before probing with secondary antibody diluted 1:2000 in TBST (30 min). After washing (3 × 10 min) with TBST the immunoblot was developed using NBT/BCIP colorimetric method (100 mM Tris-HCl pH 9.5, 100 mM NaCl, 5 mM $MgCl_2$, 0.33 mg/mL NBT, 0.17 mg/mL BCIP) and the reaction was stopped by change to Milli-Q water. LD purified from barley malt served as positive control.

2.5.3 Mass Spectrometry, Liquid Chromatography-Mass Spectrometry, Amino Acid Analysis, and N-Terminal Protein Sequencing

In-gel trypsin digestion of spots cut out from protein bands of SDS-PAGE gels and micropurification on Poros 20 R2 home-made nanocolumns (Perseptive Biosystems, Framingham, MA) were done as described (*82*). Peptides were eluted with 1 µL matrix solution (5 g/L α-cyano-hydroxycinnamic acid in 70% (v/v) CH_3CN and 0.1% (w/v) trifluoroacetate) directly onto the MALDI target and analyzed using an Ultraflex II MALDI-TOF-TOF mass spectrometer (Bruker-Daltonics) in positive ion reflector mode. Spectra were analyzed using FlexAnalysis software (Bruker-Daltonics) and calibrated by trypsin autolysis products (m/z 842.51 and m/z 2211.10). Peptide mass data were searched against the NCBI non-redundant database using Biotools software (Bruker Daltonics) and the Mascot server (http://www.matrixscience.com).

Full length mass spectrometry analysis of LDI using liquid chromatography-mass spectrometry (LC-MS) was performed as by Dr. Martin Zehls and Dr. Sabina Amon, Department of Biochemistry and Molecular Biology, University of Southern Denmark, Denmark as follows. Aliquots of the samples were diluted to 100 µL (final concentration 2.5 µM) with either 0.1% trifluoroacetic acid (TFA) (1^{st} runs) or 5% formic acid (2^{nd} runs). The proteins were desalted on-line to electrospray ionization-

mass spectrometry (ESI-MS) as described earlier (*83*). Briefly, the proteins were loaded onto a custom-made small-scale reversed-phase trap column and desalted for 3 min with 0.05% TFA at a flow rate of 200 µL/min. Elution and ESI were performed with 70% acetonitrile containing 0.05% TFA at a flow rate of 50 µL/min. Mass spectra were recorded with an ESI-Q-TOF mass spectrometer (Synapt HDMS, Waters, Milford, MA) in positive ion mode. Source parameters were as follows: capillary voltage: 3500 V, sample cone voltage: 50 V (1^{st} runs) or 40 V (2^{nd} runs), source temperature: 80 °C (1^{st} runs) or 100 °C (2^{nd} runs), desolvation gas temperature: 150 °C (1^{st} runs) or 300 °C (2^{nd} runs), and desolvation gas flow: 300-500 L/h (N_2). The mass spectrometer was operated in V-mode and calibrated with sodium iodide cluster ions. The mass spectra were processed with the MassLynx V4.0 SP2 software (Waters, Milford, MA). The accumulated mass spectra of the proteins were smoothed using the Savitzky-Golay algorithm and deconvoluted using the MaxEnt 1 algorithm. The deconvolution parameters were adjusted to yield optimal matching of the synthesized m/z spectrum (the mock spectrum) and the experimental m/z spectrum.

Amino acid analysis was performed after 24 h hydrolysis as described (*84*). Protein sequencing was carried out by automated N-terminal Edman degradation in a Procise 494 sequenator according to the manufacturer's recommendations (Applied Biosystems Foster City, CA). Highly pure Milli-Q water (18 MΩ) was used throughout.

2.6 Sequence Alignment and LDI Model Prediction

Multiple sequence alignment of plant limit dextrinase from barley, acc.# AAD04189, wheat, acc.# ABL84490, rice, acc.# H0806H05, maize, acc.# AAD11599, spinach, acc.# CAA58803 and Arabidopsis acc.# Q8GTR4was carried out using ClustalW2 (http://www.ebi.ac.uk/Tools/clustalw2/index.html) with default settings, gap opening and extension penalties of 10 and 0.2, respectively.

Multiple sequence alignment of the five most studied inhibitors LDI, RATI, CHFI (bifunctional corn Hageman factor inhibitor), the dimeric and the monomeric wheat inhibitors 0.19 and 0.28, respectively, was carried out using the ClustalW2 server. The pairwise alignment algorithms EMBOSS Needle was used for global alignment of LDI with RATI, CHFI, 0.19 and 0.28. RATI, was used as template for LDI homology modelling using the default parameters of the HHpred server (Homology detection & structure prediction by HMM-HMM comparison, http://toolkit.tuebingen.mpg.de/hhpred#) and the RATI structure (PDB code: 1B1U) as template. Structural visualization and comparison were made in PyMOL1.1 (*85*). The quality of the obtained LDI model was analyzed using the ProQ - protein quality prediction server (http://www.sbc.su.se/~bjornw/ProQ/ProQ.cgi) (*86*).

2.7 Crystallization and 3D Structure Determination

2.7.1 LD/LDI Complex Formation and Crystallization

LD (1.7 mL, 4.2 mg/mL) was mixed with LDI (0.8 mL, 6.4 mg/mL) resulting in a 2:1 molar ratio of LD:LDI. The purity of the LDI solution was only 95% as judged by

SDS-PAGE due to a smear at higher molecular mass. The protein mixture was incubated at room temperature for 30 min, centrifuged (12,000*g*, 4 °C, 15 min), loaded onto on a Hiload Superdex 200 26/60 column (GE Healthcare) equilibrated with 50 mM Mes/NaOH pH 6.6, 250 mM NaCl and eluted (60 mL/h) with the same buffer. Collected fractions (2 mL) corresponding to the peak on the chromatogram were pooled (total of 22 mL) and concentrated (Centricon, 30 kDa cut-off; Millipore) to 1 mL, which corresponded to 7 mg/mL of LD loaded on the column. Purified LD/LDI complex (600 µL) was send to the Centre for high-throughput structural biology, Hauptman Woodward Medical Research Institute, Buffalo, USA, for crystal-growth screening experiments in 1536-well microassay plates by mixing 0.2 µL protein solution with 0.2 µL crystallization agent. The crystallization method used in the high-throughput screening (HTS) system was microbatch-under-oil. In addition crystallization using hanging-drop, vapor-diffusion method was explored with Crystal Screen™ and Crystal Screen™ 2, and PEG/Ion™ Screen (Hampton Research, Aliso Viejo, CA) at 22 °C. The solution of crystallization drop was prepared on coverslips by mixing 2 µL LD/LDI solution with 2 µL of reservoir solution. The droplets were equilibrated against 0.5 mL of reservoir solution. Based on the result from the HTS of the crystallization condition, microbatch-under-oil screens were set up at 22 °C around the condition identified in the HTS by mixing 1 µL LD/LDI solution with 1 µL crystallization agent under 300 µL mineral oil (Sigma-Aldrich, Seelze, Germany) in a microtiter plate. Crystallization at the same condition was also investigated using the hanging-drop, vapor-diffusion method by mixing 1 µL LD/LDI solution with 2 µL of reservoir solution. The droplets were equilibrated against 1 mL of reservoir solution at 22 °C.

2.7.2 Crystallization and Data Collection of LD

LD was produced and purified as described in section 2.1.1.5. and 2.1.1.6 and concentrated to a final concentration of 9 mg/mL for the initial crystallization screens (*70*). Initially, crystallization using the hanging-drop, vapor-diffusion method was explored with Crystal Screen™, Crystal Screen™ 2, and PEG/Ion™ Screen (Hampton Research) at 22 °C. The LD solution contained β-CD, mixed in a 1:10 molar ratio. Crystals obtained from different condition in the PEG/Ion Screen all showed the same crystal morphology, *i.e.*, bundles of very thin needles. These were used for micro-seeding in later screens.

Prior to crystallization, LD (20 mg/mL; 50 mM MES, pH 6.6, 250 mM NaCl) was incubated on ice with α- or β-CD in 6-fold molar excess giving a final LD concentration of 13.3 mg/mL. The crystallization drop was placed on cover slips by mixing 1.5 µL LD-CD solution with 1 or 2 µL of reservoir solution. Additive Screen I–III (Hampton Research) was used to optimize crystallization conditions. Based on the additive screen cysteine (0.2 µL, 0.1 M) was added to the drop to a final concentration of 5–7 mM. LD:β-CD co-crystals were obtained by either using a reservoir solution containing 22% (w/v) PEG 3350, 5% (v/v) glycerol, 0.3 M NaI and streak seeding the drops, or by using a reservoir solution of 30% (w/v) PEG 3350, 10% (v/v) glycerol, 0.3 M NaI without seeding. LD:α-CD co-crystals were obtained using a reservoir solution of 30% (w/v) PEG 3350, 0.3 M NaI without seeding. In all cases, crystals appeared within one week. LD:β-CD crystals grown in 22% (w/v) PEG, 0.3 M NaI and 5% (v/v) glycerol were cryo-protected using a 1:1 mix of reservoir solution and PEG 400. LD:α-CD crystals

were cryo-protected using a 1:1 mix of reservoir solution and 30% (w/v) PEG 3350, 10% (v/v) glycerol, 0.3 M NaI. All crystals used for data collection were mounted on Mesh Litholoops (loop size 0.2 mm and mesh size 40 µm; Molecular Dimensions, Newmarket, UK) and flash-frozen in a steam of nitrogen. Crystal mounting in conventional cryo-loops gave rise to excessive mosaicity in the diffraction data.

X-ray diffraction data of LD:β-CD crystals were collected at the ESRF, Grenoble, France, on the micro focus beamline ID23-2 at a wavelength of 0.873 Å. X-ray diffraction data of LD:α-CD were collected at MAX-lab II, Lund University, Sweden at beamline I911-5 at a wavelength 0.910 Å.

2.7.3 Phasing, Model Building, Refinement and Structual Analysis

The data were integrated in Mosflm (*87*) scaled using the program Scala from the CCP4i Suite (*88, 89*), and the resultant structure factors were used for molecular replacement using Phaser (*90*) based on residues 177–1070 of KpPUL (PDB code: 2FGZ). The initial LD:β-CD model was build using Phenix.autobuild (*91*) from the molecular replacement (MR) phases and included 95% of the LD amino acid residues. Several rounds of model building and refinement were needed for both LD:β-CD and LD:α-CD using Phenix.refine (*91*) with simulated annealing and translation/libration/screw (TLS) refinement (15 segments) activated (*92*) and COOT 0.5.2 (*93*) for molecular visualization, validation and rebuilding. The LD:β-CD structure was used as model for MR to solve the structure of LD:α-CD. In addition to the COOT validation functions, final analysis of model geometry optimization were done in PROCHECK (*94*) and Molprobity (*95*). The structure of LD was compared with KpPUL, (apo, PDB code: 2FGZ; G4, 2FHF), BsPUL (2E8Y) and BaPUL (2WAN), as well as isoamylase from *Pseudomonas amyloderamosa* (PaISO) (1BF2) and *E. coli* glycogen branching enzyme (1M7X) using the program Pymol 1.1 (*85*) which was also used for generating the structural figures. The protein secondary structure motifs were obtained from PDBsum which are computed using PROMOTIF v.3.0 (*96*). The final round of phenix.refine included all reflections, while all other refinement rounds had 5% randomly chosen reflections kept aside as test set.

3 Results

3.1 Production, Purification and Characterization of Recombinant LD

3.1.1 Pilot Scale Expression in *E. coli*

Expression of the LD using the intracellular expression system *E. coli* Rosetta(DE3) and the pET11a/LD construct was analysed by SDS-PAGE. The Coomassie stained gel showed no significant difference in expression pattern between the induced untransformed strain and that harbouring the pET11a/LD plasmid during the three hours of induction. Furthermore, immunoblotting of the same samples did not reveal any bands at the expected size confirming that the expression of full-length LD in *E. coli* was unsuccessful. However, bands with lower molecular size were detected, which may be either degradation products or results of premature termination of the translation (data not shown).

3.1.2 Cloning and Selection of LD Secreting *P. pastoris* Transformants

The gene fragment encoding LD without the previously proposed putative transit peptide (*12*) was cloned downstream of the *P. pastoris* AOX1 promoter in pPIC9K in-frame with the N-terminal α-factor secretion signal to achieve secretion of recombinant LD by *P. pastoris*. The cloning resulted in an N-terminal tripeptide (ATQ) deletion of mature LD compared to the earlier published gene sequence (*97*). The same triptide sequence was lacking in approximately 50% of the LD molecules purified from germinating seeds (*72*) and in the gene sequence determined by others (*9*). The linearized construct (Figure 2.1B) was inserted into the genome by homologous recombination resulting in stable integration as judged from the maintained *P. pastoris* GS115 Mut^+ His^+ phenotype. Successful secretory expression was documented by strong colony immunoblotting response for 20 transformants out of 50 randomly selected and significant variation in production level was judged from intensity differences (data not shown). This corroborated the variations in LD activity (2.4–36.8 mU/mL) observed in a pilot scale secretory expression of the selected transformants. No LD activity was produced by strain GS115 transformed with empty pPIC9K and based on the results one transformant, LD26, was selected for further analysis. Remarkably, after 72 h induction no measurable LD activity was detected in minimal medium at 30 °C from LD26, whereas induction at 22°C for 72 h gave a 10-fold activity increase compared to the highest activity measured after 96 h induction at 30 °C.

3.1.3 Fermentation and Secretory Expression in 5-L Bioreactor

Very low LD yields in shake flask cultures motivated implementation of fed-batch high cell-density fermentation. Cell wet weight (CWW) and LD activity were monitored throughout the different stages of this fermentation. The initial batch phase (30 h) resulted in CWW of 114 mg/mL. The culture was then switched to fed-batch mode with 15 g/(L·h) glycerol feed for 6 h leading to CWW of 164 mg/mL. This was followed by initiation of induction by a methanol feed of 1 g/(L·h) for 2 h to allow adaptation to methanol metabolism. The methanol flow was successively increased to

reach the maximum of 11 g/(L·h) after 12 h. LD activity in the medium and CWW increased with time (Figure 3.1). The culture was terminated at 125 h (89 h induction) as the reactor headspace became limiting. The CWW was 315 g/L and the 2.5 L cell-free supernatant contained about 16 mg/L active LD as calculated from the specific activity of purified recombinant LD.

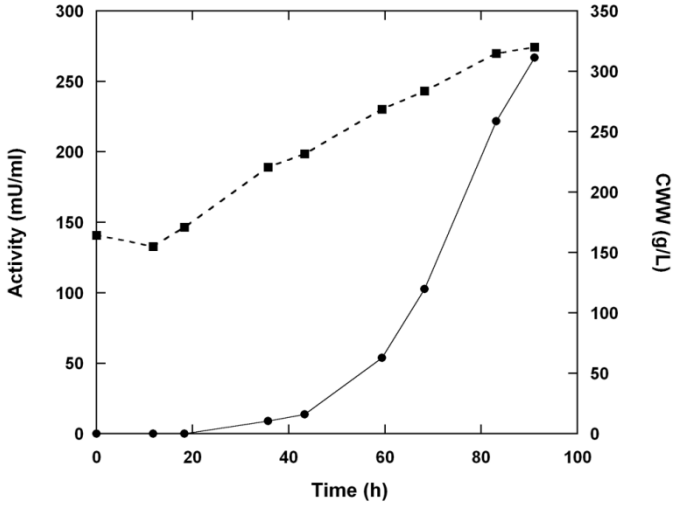

Figure 3.1. Progress of secreted LD activity (●) and CWW (cell wet weight) (■) during fermentation from the start of the methanol induction (*70*).

3.1.4 Purification and Characterization

LD purification was monitored by activity assay and SDS-PAGE (Table 3.1; Figure 3.2A). Less than 1% of the total activity in the culture supernatant appeared in the flow-through after application to β-CD-Sepharose in 1 M ammonium sulphate and the affinity chromatography resulted in high yield of very pure LD (Figure 3.2A, lane 2). Precipitation of eluted LD observed in preliminary experiments was prevented by immediate adjustment of the eluate to pH 6.7 (see section 2.1.1.6). Gel filtration further increased the LD purity and removed β-CD (Table 3.1; Figure 3.2A, lane 3). A minor peak eluted prior the main LD peak with an elution time (in column volumes) corresponding to dimerized LD. SDS-PAGE analysis showed that the peak indeed contained LD as the sole protein. Immunoblotting of pooled LD-containing fractions showed a predominant band corresponding to an apparent molecular weight of 98 kDa (Figure 3.2B, lane 2) in excellent agreement with both the theoretical value of 97419 Da and the migration of barley malt LD (Figure 3.2B, lane 1). A trace component of slightly lower molecular weight visible in SDS-PAGE possibly represented a cleavage product of secreted LD. The purification procedure resulted in 34 mg recombinant LD with specific activity of 14.2 U/mg corresponding to 11-fold purification and 84% recovery from the culture supernatant (Table 3.1).

Table 3.1. Purification of LD from 2.5 L *P. pastoris* culture supernatant (*70*)

	Total protein (mg)	Total activity (U)	Recovery (%)	Specific activity (U/mg)	Purification (fold)
Supernatant	456.9	573.3	100.0	1.3	1.0
β-CD-Sepharose	82.7	551.7	96.2	6.7	5.2
Sephadex G200	33.6	477.3	83.3	14.2	11.0

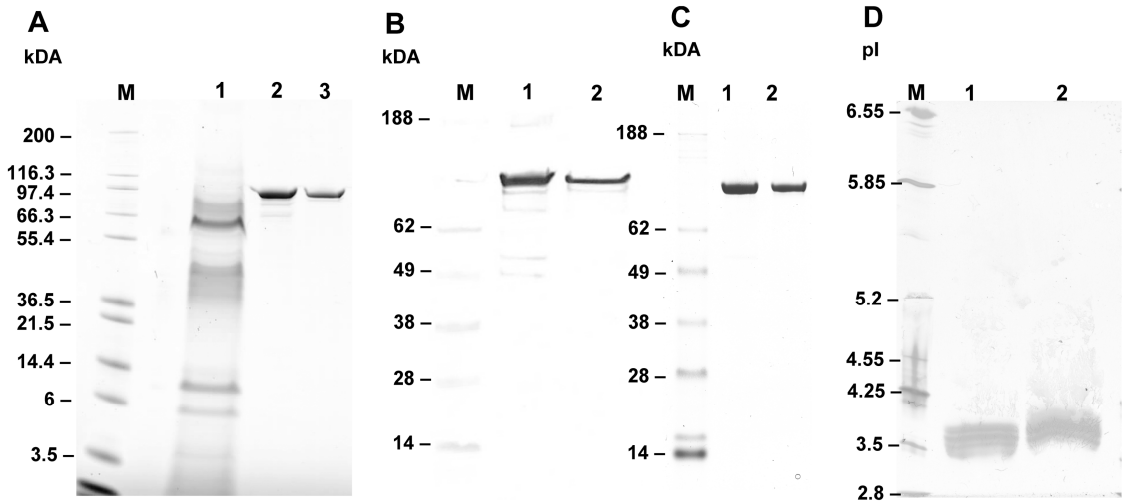

Figure 3.2. (A) Coomassie stained SDS-PAGE. Lane 1, culture supernatant (~3.5 µg total protein); lane 2, pool of β-CD-Sepharose eluate (~2.5 µg total protein); lane 3, pool of Hiload Superdex 200 eluate (~0.8 µg total protein). (B) Immunoblotting using barley LD specific antibody. Lane 1, LD purified from barley malt (~70 ng); lane 2, purified recombinant LD (~40 ng). (C) Coomassie stained SDS-PAGE. Lane 1, LD purified from barley malt (~1 µg); lane 2, purified recombinant LD (~1 µg). (D) Isoelectric focusing of LD (pH 4–6 PhastGels). Lane 1, LD purified from barley malt (~0.8 µg); lane 2, purified recombinant LD (~0.8 µg) (*70*).

The identity of recombinant LD was verified by peptide mapping using MALDI-TOF-MS (data not shown). A search against the NCBI non-redundant database resulted in mono-isotopic mass peaks with 27% sequence coverage of the LD protein sequence. Tryptic peptides comprising the four putative N-glycosylated positions were not identified, owing to size incompatibility with the present mass spectrometric analysis for two of them. However, the migration of LD in SDS-PAGE analysis as a single sharp band corresponding to the expected molecular mass is not supportive of significant glycosylation. Three different processed forms of LD can be predicted depending on the protease cleavage site, Kex2 or any of the two Ste13 sites, used (Figure 2.1A). Using the NotI site for the cloning will therefore normally, in the processed protein, result in a 9–13 amino acids N-terminal extension that originates from the expression plasmid (Figure 2.1A). N-terminal sequencing of LD revealed an alternative processed form of the secreted enzyme (AAFMPDAR, Figure 2.1A) presumably due to cleavage by one or more proteases produced by *P. pastoris*.

Isoelectric focusing of the recombinant LD and LD purified from barley malt showed a similar migration pattern with pI of ≈ 4.1 (Figure 3.2D). A number of closely migrating bands appear in a broader smeared zone indicating slight charge heterogeneity in both enzyme preparations, which was not further investigated.

3.1.5 LD Activity

Fitting the Michaelis-Menten equation (eq. 2.1) to initial rates of LD catalysed hydrolysis of pullulan revealed deviation of the hyperbolic fit from experimental data, in particular at substrate concentrations above 0.2 mg/mL (Figure 3.3, dashed line). Noticeably, however, fitting the Michaelis-Menten expression for uncompetitive substrate inhibition (eq. 2.2) matched the data very clearly (Figure 3.3, solid line). This is supported using standard statistical tools for model selection such as the corrected Akaike information criterion (AICc) (*98*) and the sum of squared residuals (SS) (tools included in the Sigmaplot 9.01 software). The Michaelis-Menten expression for uncompetitive substrate inhibition yields an AICc = –43.4 and SS = 8.3, while the regular Michaelis-Menten equation has values of AICc = –14.3 and SS = 20.1. Such deviation from the Michaelis-Menten model observed for other glycoside hydrolases, has previously been attributed to an increased transglycosylation rate at higher substrate concentrations rather than to substrate inhibition (*99, 100*). For LD this is in agreement with the K_m value for pullulan being significantly higher when fitting the equation for uncompetitive substrate inhibition as compared to fitting the regular Michaelis-Menten equation (Table 3.2).

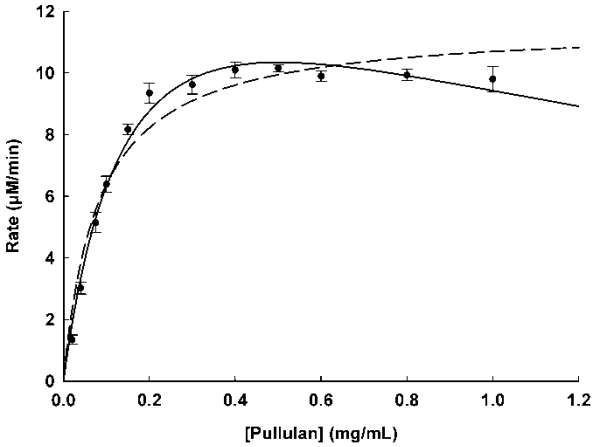

Figure 3.3. Apparent initial rate of release of reducing sugar as a function of pullulan concentration. Solid line, fit of Michaelis-Menten expression with uncompetitive substrate inhibition. Dashed line, classical Michaelis-Menten plot. Error bars indicate SD for triplicate measurements (*70*).

Table 3.2. Apparent kinetic constants of LD on pullulan obtained by nonlinear least-squares curve fitting[a]

Classical Michaelis-Menten			Uncompetitive substrate inhibition			
$K_{m,app}$ mg/mL	$k_{cat,app}$ s^{-1}	$(k_{cat}/K_m)_{,app}$ mL/(mg·s)	$K_{m,app}$ mg/mL	$k_{cat,app}$ s^{-1}	$K_{i,s,app}$ mg/mL	$(k_{cat}/K_m)_{,app}$ mL/(mg·s)
0.081 ± 0.003	61 ± 13	753	0.16 ± 0.02	78 ± 10	1.5 ± 0.4	488

[a]Values are based on independent triplicate measurements (*70*)

3.1.6 Transglycosylation

3.1.6.1 Linear Acceptors

α-Maltosyl fluoride (G2F) was used as donor in the initial reactions and a range of oligosaccharides from maltose to maltohexaose (G2–G6) were used as acceptors. Using maltose as acceptor the conversion rate of the maltosyl fluoride to the acceptor was high indicated by a fast decrease in the amount of G2F. The subsequent hydrolysis of the formed product seems to be relatively slower indicated by the accumulation of product (data not shown). Furthermore, the products formed from the initial transglycosylation also act as acceptors resulting in a polymerization of maltose with up to eight maltose α-1,6 repeats, which were identified by MALDI-tof MS (Appendix 7.1.1). The conversion rate of maltosyl fluoride to longer linear oligosaccharide (G3–G6) showed to be slower (data not shown) and the subsequent hydrolysis of the formed product relatively faster resulting in only minor product accumulation and an increase in maltose concentration. The relative hydrolysis and transglycosylation rates using maltotetraose as acceptor and maltotriosyl fluoride (G3F) and G2F, respectively, as donors were compared by TLC analysis (ratio donor:acceptor, 1:2, 20 mM:40 mM). The conversion rate of G3F was slower compared with G2F and the subsequent hydrolysis much faster (Figure 3.4).

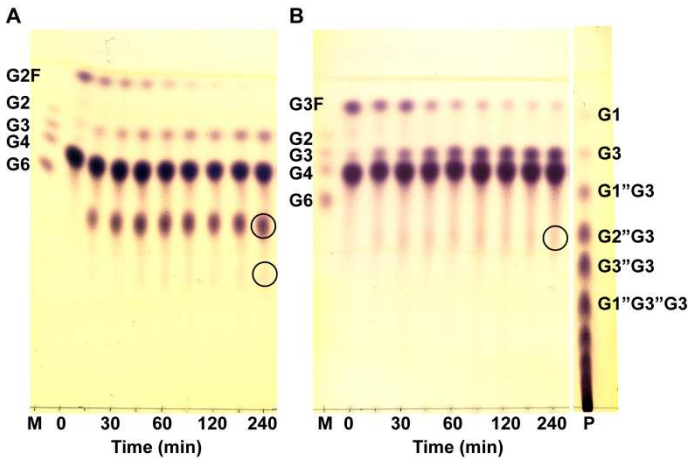

Figure 3.4. Comparison of the transglycosylation reaction using either maltosyl fluoride (A) or maltotriosyl fluoride (B) as donor and maltotetraose as acceptor. Donor:acceptor ratio 1:2 (20 mM: 40 mM). Transglycosylation products are indicated encircled.

Acarbose, a known α-amylase inhibitor (*79*) and 4-*O*-α-D-glucopyranosylmoranoline (G1M) (*78*), which has been shown to inhibit both barley α-glucosidase and β-amylase *in vitro* in the micro molar range (*Martin Rejzek, personal communication*) were used as acceptors in initial transglycosylation reaction with α-maltosyl fluoride as donor in order to produce new inhibitors. G1M has also been shown in preliminary inhibition studies of small synthetic and natural products to have inhibitory activity towards LD in the mM range (data not shown), which may indicate binding in the active site. Approximately 40% inhibition of LD (7.5 nM) in the presence of G1M (1 mM) was measured (data not shown). By comparison, more than 90% inhibition of LD by β-CD (100 µM) was observed under the same reaction conditions. The ratio donor to acceptor was 2:1 (20 mM:10 mM) for G2F:acarbose and 2.6:1 (20 mM: 7.7 mM) for G2F:G1M, which resulted primarily in polymerisation of maltose. MS data, however, revealed formation of transglycosylation products with the unique

molecular masses of single and double maltose substitutions of both acceptors (Appendix 7.1.2 and 7.1.3.).

3.1.6.2 Cyclic Acceptors

Using α- and β-CD which are known inhibitors of LD as acceptors multiple substitutions presumably of the ring were observed both by TLC and MS. These experiments were carried out with a large excess of the donor (ratio donor:acceptor, 4:1; 40 mM:10 mM) in the reaction mixture and additional maltosyl fluoride was added to the reaction at different time points. The constant level of maltose, originating from the fluoride solution, and the clear decrease in α-CD indicates that the product formed from the conversion of maltosyl fluoride to α-CD was not hydrolysed (Figure 3.5A), and under these reaction conditions 6 substitution products were detected by MS (Appendix 7.1.4).

Despite a 4-fold excess of donor no products from maltose polymerisation were observed, indicating that the CD's are much better acceptors than maltose for the transglycosylation. This conforms with the high affinity of LD towards the CD's (see section 3.1.7). The transglycosylation of maltosyl β-CD seems to be slightly faster than the α-CD. The subsequent hydrolysis of the product seems to be even faster than the transglycosylation resulting in only a minor accumulation of the transglycosylation product (Figure 3.5B). The same result was observed when using β-CD as acceptor.

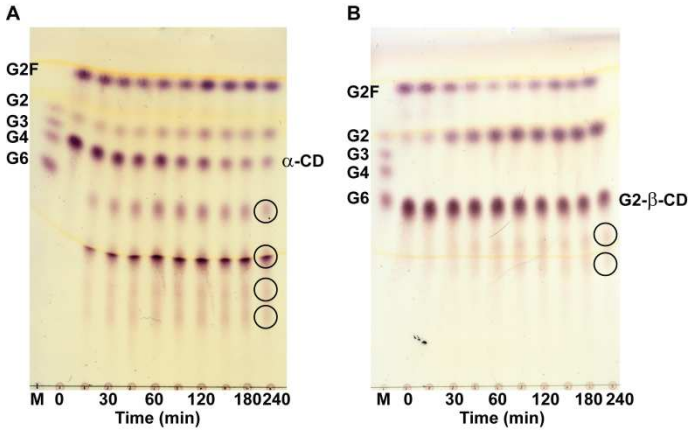

Figure 3.5. Comparison of the transglycosylation reaction using maltosyl fluoride as donor and either α-cyclodextrin (A) or (B) maltosyl β-cyclodextrin as acceptor. Donor:acceptor ratio 4:1 (40 mM:10 mM). Transglycosylation products are indicated with circles.

3.1.7 Cyclodextrin Affinity

The previously reported binding of cyclodextrins to debranching enzymes (*101*) is here confirmed and analyzed for the recombinant LD by SPR analysis. The approximately 100-fold difference in molecular weight between the chip-immobilized LD and the three CD analytes poises high demands on sensitivity. The developed experimental set up, however, resulted in highly reproducible sensorgrams for all three CDs with R_{max} values of 16–25 RU. Fitting of a one binding site model to the SPR data

of β-CD (Figure 3.6) revealed a submicromolar K_d, whereas α- and γ-CD had 40–50 times weaker affinity (Table 3.3).

Table 3.3. LD affinity towards cyclodextrins determined by SPR[a]

Analyte	K_d (μM)	Relative K_d*
α-CD	27.2 ± 0.9	39
β-CD	0.7 ± 0.1	1
γ-CD	34.7 ± 0.2	50

[a]Measurements were performed at 25 °C in 20 mM Na acetate pH 5.5, 100 mM NaCl, 0.005% P-20. K_d is based on independent duplicate runs, each run having three data points at each concentration. *K_d values normalized to β-CD. (*70*)

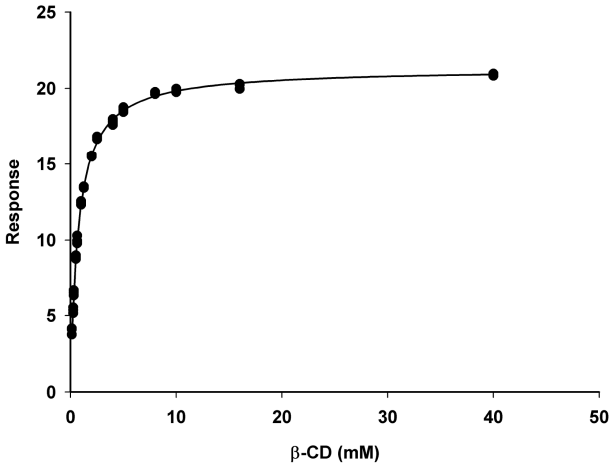

Figure 3.6. Fitting of a one binding site model to the SPR data of β-CD (*70*).

3.2 Production and Purification of Recombinant LDI

3.2.1 Expression and Purification of the Intein-LDI Construct

The gene fragment encoding CBD-intein-LDI (37.9 kDa) was expressed at both 15 °C and 37 °C in Rosetta-gami(DE3), however, the yield at both 37 °C (Figure 3.7) and 15 °C were very low (data not shown).

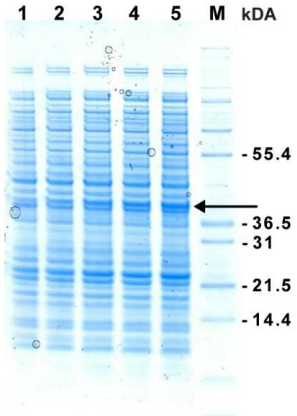

Figure 3.7. Coomassie stained SDS-PAGE of the CBD-intein-LDI expression in *E. coli* Rosetta-gami(DE3) at 37 °C. Lane 1, induction start; lane 2 30 min; lane 3–5, 1, 1.5 and 2 h induction, respectively. Expected size of the produced product is 37.9 kDa.

Purification of the fusion protein using the chitin column showed to be very efficient, indicated by the absence of the band corresponding to the expressed CBD-intein-LDI construct in SDS-PAGE analysis of the flow-through. The LDI was cleaved efficiently from the CBD-intein part by decreasing the pH and increasing the temperature. LDI eluted within the first three fractions and the 20-fold concentrated LDI pool was tested for LD inhibition activity. Based on an estimation of the LDI concentration from the SDS-PAGE the LDI:LD ratio in the Limit-Dextrizyme assay was 30:1. Despite the large excess of the inhibitor no inhibition of LD was observed.

3.2.2 Expression and Purification of *P. pastoris* His-LDI Construct

The five selected *P. pastoris* clones having a chromosomal integrated copy of the LDI-gene in-frame with the nucleotide sequence of a thrombin cleavable N-terminal His-tag were expressed at 17 °C. All five selected clones expressed and secreted a product with approximately the expected size of LDI (14.3 kDa) as judge by SDS-PAGE (Figure 3.8A). The products from two clones (clone 1 and 4) were selected for purification on His-Trap column as previously described (section 2.1.2.3). SDS-PAGE analysis of the flow-through from the loading of the samples and the column wash revealed that the protein was not binding to the column (Figure 3.8B). A sample from the flow-through blotted onto a PVDF membrane and N-terminally sequenced, was found to lack the N-terminal His-tag, presumably due to proteolytic activity by proteases produced by *P. pastoris* during fermentation. Two different N-terminal sequences were identified in the sample, one identical to the expected sequence resulting from cleavage by thrombin (resulting N-terminus; **GS**TLESVKDECQ) and one identical to the N-terminus of the Ragi α-amylase/trypsin inhibitor, RATI (SVKDECQ) (*102*). The LD inhibitory activity of LDI in the culture supernatant was analysed with a 1000-fold excess of LDI resulting in 100% inhibition of LD.

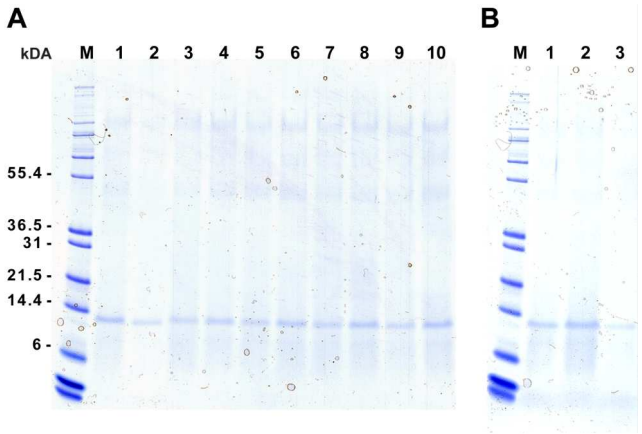

Figure 3.8. (A) Coomassie stained SDS-PAGE of the His-LDI expression in *P. pastoris* at 17 °C. Samples from each clone after 48 h and 72 h (harvest) induction. Lane 1–2, clone 1; lane 3–4, clone 4; lane 5–6, clone 7; lane 7–8, clone 11; lane 9–10, clone 12. (B) His-Trap purification of clone 1. Lane 1, clarified cell extract; lane 2, flow-though; lane 3, column wash.

3.2.3 Expression and Purification of LDI-His and LDI-His-mutants

The pilot expression of both EF-LDI and wt-LDI showed only minor variation in expression and inhibitory levels of the selected tested clones. Based on these results one of each clone (EF-LDI and wt-LDI) was selected for use in fed-batch high cell-density fermentation, which ensured reasonably high yields (~ 6 mg LDI pr L cell free extract) of inhibitory active LDI visualized by SDS-PAGE. The amount of LDI increased in the medium during the methanol phase despite a small decrease in the CWW towards the end of the fermentation. The EF-LDI and wt-LDI cultures were terminated after 22 h and 28 h induction with a CWW of 170 g/L and 120 g/L, respectively. The fermentations resulted in 3.2 L cell-free supernatant containing either EF-LDI or wt-LDI. Elution of both EF-LDI and wt-LDI from the HisTrap column gave two overlapping protein fraction peaks. SDS-PAGE analysis showed that the first eluted peak in addition to full-length LDI contained lower molecular mass fragments of LDI. Fractions were combined in two pools based on their purity judged from SDS-PAGE and purified by anion exchange chromatography. The anion exchange chromatography of EF-LDI resulted in several peaks with the EF-LDI eluting in one of them. Proteolytic activity in the fermentation medium, resulted in partial formation of a truncated version of the EF-LDI that lacks the N-terminal tripeptide (TLE) as compared to the wt-LDI sequence (ΔE^3LDI). The N-terminus of this construct was identical to the RATI (*102*). Since this truncated version has great relevance in elucidating the role of the N-terminal sequence in the LD/LDI interaction it was subjected to further analysis. Anion exchange chromatography purification of wt-LDI (pool 2 from HisTrap elution, Figure 3.9B; lane 1) also resulted in several peaks, however, the purification resulted in highly pure LDI with the expected native N-terminus (TLE) (Figure 3.9C, lane 1–5). Pool number 4 (Figure 3.9C, lane 4) was used for further analysis. Wt-LDI (Figure 3.9C, lane 7) was used for crystallization of the LD/LDI complex (section 2.7.1 and 3.4.1).

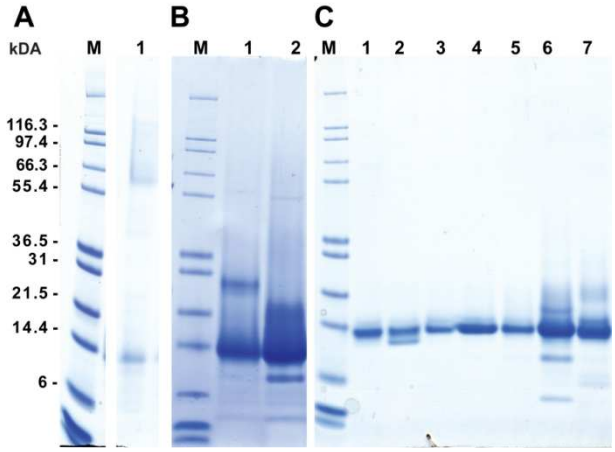

Figure 3.9. Coomassie stained SDS-PAGE of the purification of wt-LDI (A) Lane 1, culture supernatant. (B) Concentrated pools from HisTrap elution. Lane 1, pool 2; lane 2 pool 1. (C) Concentrated pools from anion exchange chromatography. Lane 1-6. Fraction from the anion exchange chromatography (of His Trap pool 2) of wt-LDI were pooled according to the peaks of the chromatogram; lane 7, pool from anion exchange chromatography of HisTrap pool 1. Expected size of the produced product is 13.5 kDa.

N-terminal sequencing of the constructed N-terminal truncated ΔV^5LDI showed that the Kex2 protease cleavage site was used in the processing instead of the Ste13 site

yielding an N-terminal sequence of EAEAKDECQ, with EAEA originating from the α-factor secretion signal (Figure 2.2).

LC-MS was performed on wt- and ΔE^3LDI under nonreducing conditions (Appendix 7.2). Unfortunately for unknown reasons the analysis of wt-LDI was unsuccessful. LC-MS analysis of ΔE^3LDI, however, revealed that the ΔE^3LDI pool used for SPR analysis was glutathionylated. The presents of several peaks indicated that the pool was not entirely pure, however the difference in the major peaks was due to cleavage of histidine residues from the hexa-histidine tag which should not affect the overall structure or function of LDI.

3.3 Characterization of the LD/LDI Interaction

3.3.1 Inhibition Kinetics

LDI inhibition of LD was analysed using pullulan as substrate. A K_i value of 1.7 nM ± 0.1 was determined by fitting the model for tight competitive inhibition (eq. 2.3) to the data (Figure 3.10A). The relatively high standard deviation observed for the 4 nM LDI inhibition data, is due to a very low residual LD activity. Fifty percent (50%) inhibition was reached at an approximate 1:1 molar ratio (1.1:1, 4.4 nM:4 nM) of LDI:LD and more than 90% inhibition was obtained at a 2:1 ratio (Figure 3.10B). At a 4-fold molar excess of LDI (LDI:LD = 5:1) 100% inhibition of LD was observed.

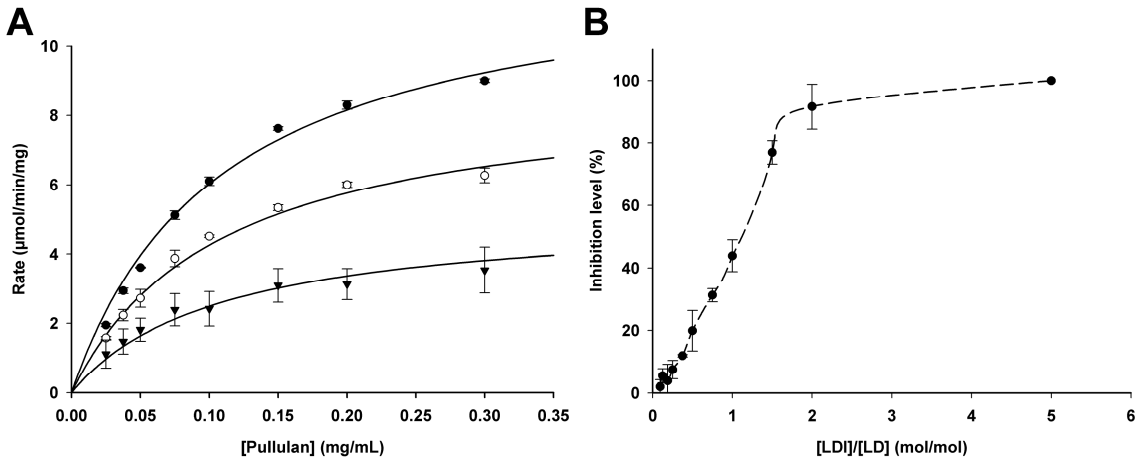

Figure 3.10. Inhibition of LD by wt-LDI. (A) Fit of Michaelis-Menten expression for tight competitive inhibition. No inhibitor (●), 2 nM LDI (○), 4 nM LDI (▼). Error bars indicate SD for duplicate measurements. (B) wt-LDI inhibition level (%) *vs.* LDI:LD (molar ratio), the curve is drawn though the experimental points. Error bars indicate SD for triplicate measurements.

3.3.2 Kinetics and Thermodynamics of LD/wt-LDI and LD/LDI Mutant Interactions

The set up used offers a two-fold advantage 1) enhanced signal by immobilizing the 10-fold smaller LDI as compared to LD, 2) signal robustness and longer life of the chip as LDI exhibits significantly better thermostability than LD, and thus can withstand repeated cycles of relatively harsh regeneration (pH 1.5). Indeed, the signal recovery after 27 cycles was 73 %. Relatively low immobilization levels were used to minimize possible mass transfer limitation and the essentially the same kinetics rate constants were obtained at flow rates of 30 μL/min and 60 μL/min, in addition the mass transfer constant, k_t in all runs was > 10^9 indicating that the kinetics of binding are largely unaffected by mass-transport from the bulk to the chip surface at these conditions. The signal magnitude did not permit injecting much lower LD concentrations than 0.1 nM (app. 2.5 K_D) which resulted in app. 4–5 RU response, thus determining the lowest concentration and an 80 fold higher concentration was the upper limit as using higher concentration resulted in significant deviation of the fit quality from the simple 1:1 model. This was possibly due to chip heterogeneity as less accessible sites or sites with decreased affinity due conformational changes that are detected after the saturation of natural high affinity sites. Finally the specificity of the binding is also attested with less than 5% of non-specific interactions with the reference cell.

A 1:1 binding model was fitted globally to the sensograms for each set of ligand concentrations to determine the rate constants k_{on} and k_{off}. Representative data and fits with LD concentration range 0.1–4 nM at standard conditions (Figure 3.11A) and at suboptimum conditions (10 mM Bicine/NaOH pH 10.0, 150 mM NaCl, 0.005% surfactant P-20, 25 °C) (Figure 3.11C). The figure clearly shows that excellent fits are obtained by the 1:1 model at standard conditions with no systematic deviations of the residuals which do not exceed 5%. The very high affinity binding evidently derives from a very slow k_{off} and a standard k_{on} value (*103, 104*). The quality of the fit is slightly worse for the pH 10 condition, but it is still very reasonable, and the deviations at the transition between the association and the dissociation phases may be caused by aggregation of the LD at the surface of the chip at this pH.

The effect of ionic strength on the LD/LDI-interaction was measured at zero to 1 M NaCl (Table 3.4). No binding was detected, however, when omitting salt from the running buffer despite an increase in the used LD concentration (1–80 nM) and changes in affinity in the concentration range 75 mM –1 M using LD of 0.1–4 nM predominantly resulted from increase in the k_{on}, that reached a maximum value at 300 mM NaCl corresponding also to optimal binding with K_D of 27.2 ± 1.3 pM.

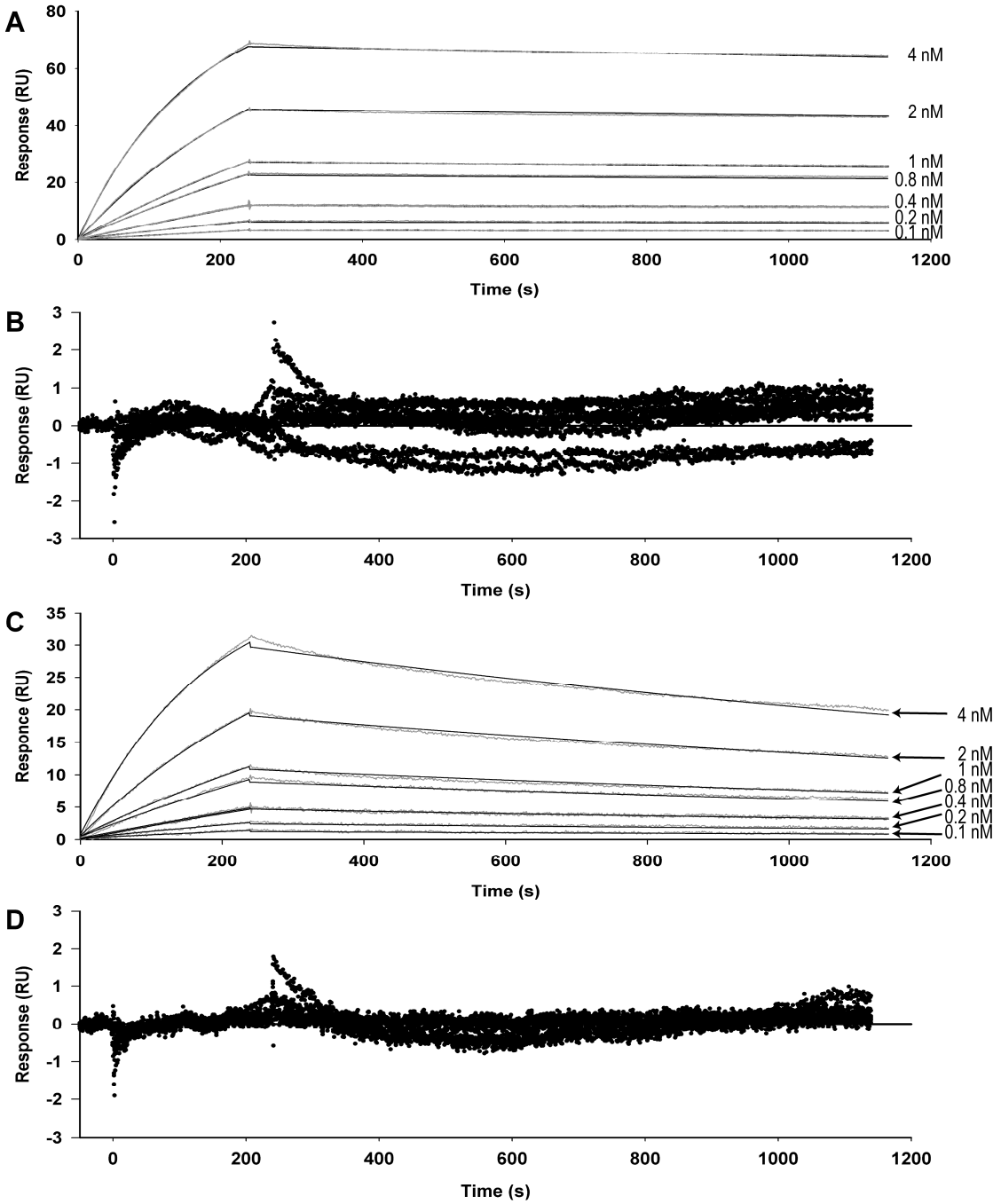

Figure 3.11. Representative fits of a 1:1 binding model (gray line) to the SPR data (black line) and residuals. The LD concentration range is 0.1–4 nM. (A) Binding data at standard conditions, 10 mM Mes/NaOH pH 6.0, 150 mM NaCl, 0.005% surfactant P-20, 25 °C and (B) the corresponding residuals. (C) Binding data at suboptimum conditions, 10 mM Bicine/NaOH pH 10.0, 150 mM NaCl, 0.005% surfactant P-20, 25 °C and (D) the corresponding residuals.

Table 3.4. Effect of ionic strength on the kinetics of binding of LD to LDI[a]

NaCl (mM)	$k_{on} \times 10^5$ (M^{-1} s^{-1})	$k_{off} \times 10^{-5}$ (s^{-1})	K_D (pM)
0	No binding detected		
75	9.0 ± 0.0	3.4 ± 1.5	37.3 ± 17.0
150	15.4 ± 0.2	6.4 ± 0.2	42.0 ± 2.0
300	17.3 ± 0.3	4.7 ± 0.1	27.2 ± 1.3
1000	9.4 ± 0.1	7.0 ± 0.1	74.1 ± 1.0

[a]Measurements were performed at 25 °C in 10 mM Mes/NaOH pH 6.0, 0.005% P-20. Seven LD concentrations in the range of 0.1–4 nM and 1–80 nM were used for 75–1000 mM and 0 mM NaCl, respectively. K_D is based on independent duplicate runs.

The pH dependence of the LD/LDI complex formation was analyzed in the range pH 5.0–10.0 (Table 3.5). A three-fold increase in k_{on} was observed from pH 5.0 to pH 6.5 followed by a slight decrease up to pH 10.0. The effect of pH on k_{off} was much more important. k_{off} thus decreased 5-fold from pH 5.0 to reach a minimum at pH 6.5 and then increased approximately 10-fold from pH 6.5 to 10.0. The combination of a high k_{on} and low k_{off} resulted in lowest K_D (highest affinity) of 27.2 ± 0.2 pM at pH 6.5. The optimum pH of the interaction is in good agreement with the physiological slightly acidic to neutral pH prevalent in the endosperm which is shown to acidify during germination (*105*, *106*), and the increase in K_D of 12–15 fold at both lower and higher pH values showed that K_D was dependent on pH.

Table 3.5. pH dependence of the kinetics of binding of LD to LDI[a]

pH	$k_{on} \times 10^5$ (M^{-1} s^{-1})	$k_{off} \times 10^{-5}$ (s^{-1})	K_D (pM)
5.0	6.1 ± 0.6	25.9 ± 3.2	425 ± 119
5.5	9.7 ± 0.1	8.6 ± 0.1	89.3 ± 0.1
6.0	14.2 ± 0.4	5.3 ± 0.1	37.3 ± 1.9
6.5	18.6 ± 0.2	5.1 ± 0.0	27.5 ± 0.2
7.0	18.1 ± 1.6	6.2 ± 0.2	34.5 ± 1.8
7.5	16.4 ± 0.0	8.1 ± 0.3	49.3 ± 1.7
8.0	16.7 ± 0.1	12.3 ± 0.0	73.8 ± 0.4
8.5	16.0 ± 0.1	21.8 ± 0.1	136.2 ± 2.2
9.0	12.4 ± 1.1	27.0 ± 0.5	219.2 ± 22.6
9.5	13.8 ± 0.3	31.3 ± 1.8	227.3 ± 18.0
10.0	14.5 ± 1.7	49.9 ± 4.4	345.1 ± 9.0

[a]Measurements were performed at 25 °C in appropriate buffers (see Material & Methods), added 150 mM NaCl and 0.005% P-20. Seven LD concentrations (0.1–4 nM) were used. K_D is based on independent duplicate runs.

The temperature dependence of the LD/LDI binding kinetics was determined using SPR at 9 different temperatures in the range 10–45 °C and five LD concentrations (0.4–8 nM) (Table 3.6). The affinity was found to be more favourable at low temperature as shown by a 6.5-fold lower K_D when the temperature was lowered from 45 to 10 °C which stemmed from mainly a 16-fold increase in k_{off} at 45 °C. However, the large change in k_{off} at temperatures above 35 °C may not only reflect the real dissociation rate of the complex, but could also be influenced by conformational changes of both proteins at higher temperature. The approximately 2-fold discrepancy between K_D at standard conditions (25 °C) determined in the temperature dependency analysis and the K_D determined in the ionic strength (Table 3.4) and pH dependency analysis (Table 3.5)

is primarily due to an approximately 2-fold lower k_{on}. This may be caused by a small variation in the LD concentration due to an altered sample preparation procedure.

Table 3.6. Temperature dependence of LD/LDI interaction[a]

Temp. (°C)	$k_{on} \times 10^5$ (M^{-1} s^{-1})	$k_{off} \times 10^{-5}$ (s^{-1})	K_D (pM)
10	5.6 ± 0.0	4.9 ± 0.3	88.0 ± 6.0
15	6.5 ± 0.0	5.7 ± 0.2	88.2 ± 3.1
20	7.6 ± 0.0	6.6 ± 0.2	86.2 ± 2.1
25	8.8 ± 0.1	8.3 ± 0.1	94.5 ± 0.5
30	10.1 ± 0.1	11.5 ± 0.2	114.5 ± 3.0
35	11.2 ± 0.0	19.7 ± 0.0	176.7 ± 0.4
37	11.6 ± 0.1	26.1 ± 0.3	225.1 ± 0.2
40	12.5 ± 0.1	39.6 ± 0.3	317.1 ± 3.6
45	13.9 ± 1.7	79.9 ± 5.1	580.5 ± 106.8

[a]Measurements were performed at different temperature in 10 mM Mes/NaOH pH 6.0, 150 mM NaCl, 0.005% P-20. Five LD concentrations (0.4–8 nM) were used. K_D is based on independent duplicate runs.

Despite the variation in K_D the energetics of the interaction at the reference temperature T = 298.15 K were extrapolated using the van't Hoff equation, which describes the correlation between temperature and the natural logarithm of the binding constant (K_D), and thereby allowing calculation of the of the interaction using either the non-linear (eq. 2.7) or the linear van't Hoff equation (eq. 2.8) (BIAcore T100 Evaluation Software version 1.1). In order to diminish the influence of conformational change and/or instability of the proteins at higher temperature the energetic of the interaction were calculated based on data measured from 10–35 °C. The standard thermodynamic parameters were calculated by applying both the non-linear (eq. 2.7) and the linear van't Hoff equation (eq. 2.8) and using the reference temperature T_0 of 25 °C (298.15 K). The use of the non-linear van't Hoff equation was justified by the curvature of the data over the measured range (Figure 3.12A). Binding of LD to LDI was driven by a large favorable free energy change, $\Delta G° = –57$ kJ/mol, and resulted in a significant decrease in heat capacity ($\Delta Cp° = –3.2$ kJ/(K·mol). The binding was moreover characterized by a substantial favorable change in entropy ($T\Delta S° = 30$ kJ/mol) mounting to approximately 53% of the total free energy of binding and an enthalpic contribution, $\Delta H°$ of –27 kJ/mol. Applying the linear van't Hoff equation changed the calculated contribution of the enthalpic and entropic components to the total free energy of binding ($\Delta G° = –57$ kJ/mol). The calculated contribution from the change in entropy was even more favorable ($T\Delta S° = 39$ kJ/mol), whereas the enthalpic contribution ($\Delta H° = –18$ kJ/mol) decreased from 47% to 31% of $\Delta G°$ (Figure 3.12B).

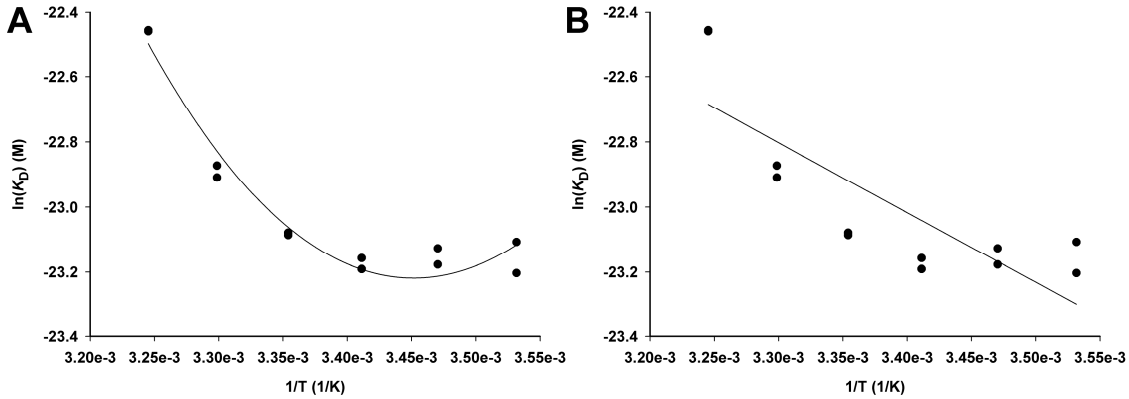

Figure 3.12. van't Hoff plots of the fitting of the non-linear (A) or linear (B) function to the data.

Analysis of the N-terminal LDI mutants revealed that the variation in the LDI N-terminal sequence seemed not to influence the overall interaction between LD and LDI, as indicated by similar K_D values found for both longer and truncated versions of LDI (Table 3.7). k_{on} for the truncated mutants was slightly lower whereas k_{off} for EF-LDI was slightly higher.

Table 3.7. Effect of N-terminal sequence on the binding of LDI to LD[a]

Inhibitor	$k_{on} \times 10^5$ (M/s)	$k_{off} \times 10^{-5}$ (s^{-1})	K_D (pM)
wt-LDI	14.8 ± 0.1	5.9 ± 0.7	40 ± 3
ΔV^5LDI	10.0 ± 0.0	5.7 ± 0.2	55 ± 2
ΔE^3LDI	9.1 ± 0.1	6.6 ± 0.1	72 ± 3
EF-LDI	13.5	11.3	84*

[a]Measurements were performed at 25 °C in 10 mM Mes/NaOH pH 6.0, 150 mM NaCl, 0.005% P-20. Seven LD concentrations in the range 0.1–8 nM were used. K_D is based on independent triplicate runs. *Based on a single run.

3.3.3 Sequence Alignment and LDI Modelling

Multiple sequence alignment of the five most studied inhibitors of this protein family LDI, RATI, CHFI, and the dimeric and monomeric wheat inhibitors 0.19 and 0.28 (Figure 3.13A) showed that most sequence dissimilarity among these family members occurred in the loop regions and in particular in loop 3 (L3) between α-helix 3 and α-helix 4 and as well as at the C-terminal (see below for further description). Pairwise alignment of LDI with RATI, CHFI, 0.19 and 0.28 showed sequence identities (similarities) of 48.4% (57.8%), 46.9% (53.1%), 25.8% (37.1%) and 21.7% (34.1%), respectively. Based on the high identity and similarity between LDI and RATI, the latter was used as template in homology modelling of LDI.

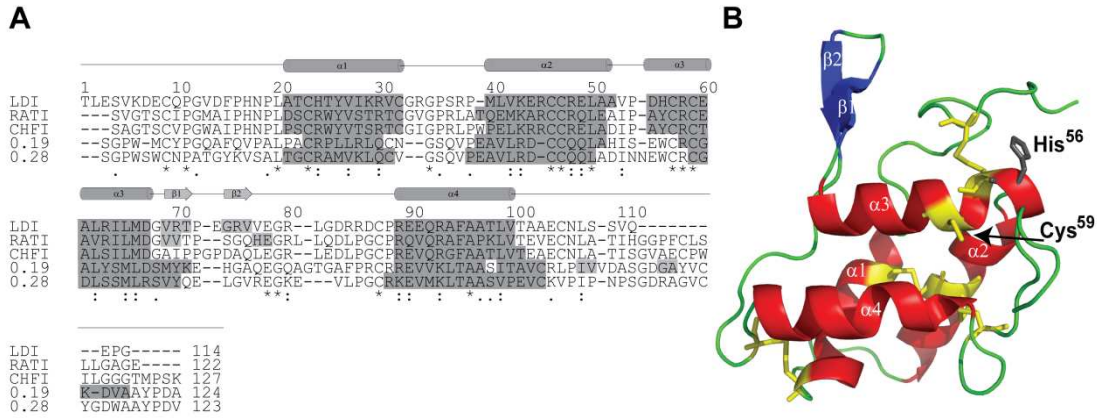

Figure 3.13 (A) Result of ClustalW2 multiple sequence alignment of the five most studied inhibitors LDI, RATI, CHFI, the dimeric and the monomeric wheat inhibitors 0.19 and 0.28, respectively. The top line display the secondary structure of LDI with α-helices shown as dark gray cylinders and β-strands as light gray arrows. The secondary structure is also indicated in the alignment for all the proteins; α-helices, dark gray shading and β-strands, light gray shading. (B) Homology model of LDI showing a helical bundle with a simple up-and-down topology. The α-helices and β-strands are shown in red and blue, respectively. The 4 disulfide bonds and Cys^{59} are shown as yellow sticks and His^{56} is coloured gray.

The quality of the obtained LDI model was getting a predicted LGscore of 2.035 placing it in the category of "fairly good models" (*107*). The structure (Figure 3.13B) displays the typical globular four-helix motif in a simple up-and-down manner as well as two short anti-parallel β-strands (residues Val^{69}–Thr^{71} and Gly^{74}–Val^{79}). The four helices (α1–α4) are linked by loop segments L1 (residues Gly^{33}–Pro^{39}), L2 (residues Val^{53}–Pro^{54}), L3 (residues Gly^{68}–Pro^{88}). The L3 loop between α-helix 3 and α-helix 4, may be very flexible thus for 0.19 no electron density was observed for residues Gly^{69}–Thr^{77} probably due to high flexibility in this segment (*108*). The last loop L4 including the C-terminus (Thr^{101}–Gly^{114}) follows α-helix 4, and is much shorter (8–13 residues) in the LDI structure compared with the structures of RATI, CHFI, and the wheat 0.19 and 0.28 inhibitors. Eight of the nine cysteine residues in LDI form disulfide bonds occurring in the pairs Cys^{9}–Cys^{57}, Cys^{23}–Cys^{46}, Cys^{32}–Cys^{87}, and Cys^{47}–Cys^{105}, resulting in a free Cys^{59}, as proposed by others (*61*). The N-terminal segment of the template structure (RATI) has been shown to be flexible (*102*) resulting in an unstructured N-terminus in the LDI model that lacks residues 1–3 (TLE). The structural arrangement surrounding Arg^{58} is conserved among members of the family. The non-polar part of the arginine side chain contributes to the hydrophobic core of the protein and the guanidinium group makes hydrogen bonds to the main chain carbonyl oxygens of Leu^{50} and Val^{53} in α-helix 2 and L2, respectively. Furthermore, the hydrogen bonding pattern of Arg^{58} is observed between Nη1 and the main chain carbonyl oxygen of Ser^{108}, together with Oδ1 and Oδ2 of Asp^{55} and finally between Nη2 (Arg^{58}) and the main-chain carbonyl oxygen of Val^{53} and Oδ1 of Asp^{55}. A similar hydrogen pattern is present in the crystal structures of RATI, CHFI and 0.19. No density were found in the electron density map for the residues Leu^{118}–Glu^{122} of RATI in complex with TMA (*59*) and residues Tyr^{120}–Val^{123} of 0.28 in complex with TMA (*55*), suggesting that the C-terminus is very flexible.

3.4 Crystallization and 3D Structure Determination

3.4.1 LD/LDI Complex Formation and Crystallization

The high affinity of LD towards LDI ensured an efficient purification of the LD/LDI complex using gel filtration at the chosen condition, with the complex eluting approximately 5% (in column volume) earlier than LD alone (Figure 3.14A). SDS-PAGE analysis (Appendix 7.2.) of the eluted fraction verified the co-exiting of both LD and LDI in the major peak. The symmetric shape of the peak indicates that the majority of LD is in complex with LDI. Excess of LDI in the reaction mixture eluted as a single peak much later. The minor peak eluting prior the LD/LDI complex has been shown by SDS-PAGE analysis to contain LD, which is suggested to have dimerized. The elution time for this peak is also approximately 5% (in column volume) earlier indicating that LDI interacts with the presumed dimer of LD.

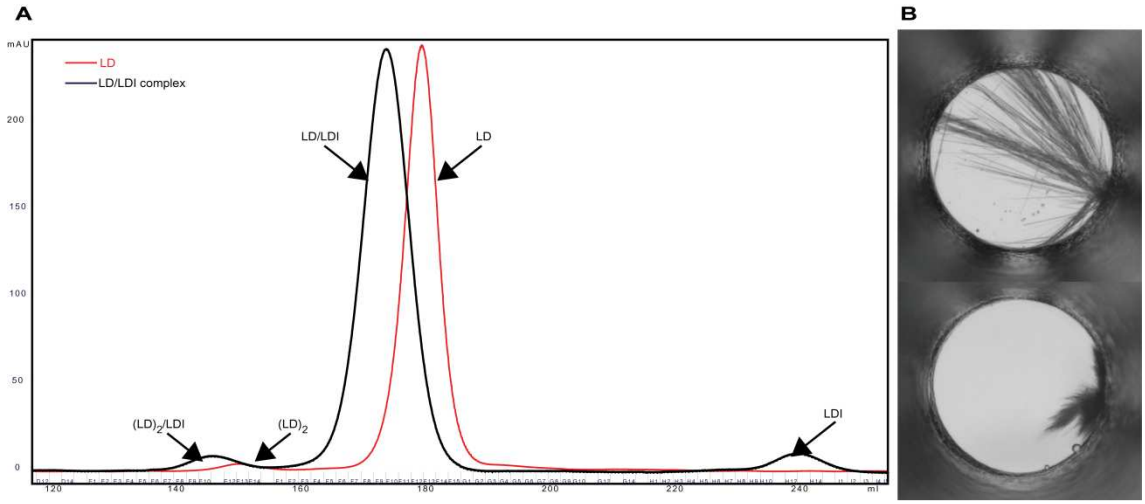

Figure 3.14. (A) Overlay of obtained chromatograms from purification of LD (red line) and LD/LDI complex (black line) in two separate run on Hiload Superdex 200 26/60 column. Y-axis: A_{280} (mAU), X-axis: mL. (B) High-throughput crystallization result one week after setup. Crystallization conditions: Top, $(NH_4)_2SO_4$ 1.14 M, CAPS 0.1 M, pH 10; bottom, $Na_2S_2O_3$ 0.94 M, CAPS 0.1 M, pH 10.

Crystals were obtained from the high-throughput screening of the crystallization condition after 1–4 weeks, and nine of these conditions were selected for scale-up experiments in both microbatch-under-oil and hanging drops vapour diffusion. Both the HTS selected conditions and the commercial available screens failed to produce crystals within three month.

3.4.2 Crystallization, Structure Determination and Model Quality of LD

LD expression and purification was according to previously described methods in section 2.1.1.5 and 2.1.1.6 (*70*) and showed a single band in SDS-PAGE. While the initial crystallization trials failed to produce crystals within the first three month, the PEG/Ion Screen ultimately resulted in protein crystals within a year. LD was found to crystallize under several different conditions, which all contained either iodine or thiocyanate in the crystallization buffer. The crystal morphology was not dependent on

protein or precipitant concentration. Crystals were bundles of very thin needles. However, addition of cysteine resulted in thicker separate, single crystal needles. Crystals obtained from seeded drops were very homogenous (Figure 3.15A) and measured 0.002 × 0.002 × 0.006 mm^3. While crystals obtained without seeding were slightly bigger and of highly variable crystal quality (Figure 3.15B). The seeded needles diffracted to 2.6 Å and belonged to space group $P2_12_12_1$, with one molecule in the unit cell and cell dimensions of a = 85.0 Å, b = 93.8 Å and c = 114.7 Å. The non-seeded crystals of LD:β-CD and LD:α-CD were of space group *C*2 and diffracted to 2.1 Å and 2.5 Å, respectively, with one molecule in the unit cell and a solvent contents of 43.7% (LD:β-CD) and 47.2% (LD:α-CD). Cell dimensions are included in Table 3.8, which summarizes data collection statistics.

The final structures show overall good electron density. However, the first two amino acids and residues 22–28, 40–49, and 102–109 in the N-domain had low level or no sigmaA weighted $2F_o$-F_c electron density and have not been included in the models. In addition to the three loops in the N-domain, the 806–810 loop in the C-domain had less than 1σ $2F_o$-F_c electron density for both side and main-chain. Two calcium ions, iodide (9 in the LD:α-CD structure and 5 in the LD:β-CD structure), glycerol (one in the LD:α-CD structure and 7 in the LD:β-CD structure) and water molecules (223 in the LD:α-CD structure and 604 in the LD:β-CD structure) are modelled and the resulting R_{cryst} and R_{free} values from the refinement are 16.3 % and 20.0 % for the LD:β-CD structure and 17.7 % and 22.6 % for the LD:α-CD structure, respectively.

R_{cryst} values dropped to 15.7% and 17.3%, respectively in the final refinement cycle, which included all reflections. The LD moieties of the two cyclodextrin complexes are virtually identical with an r.m.s.d. of 0.7 Å for all C^{α} atoms. Due to the higher resolution of the LD:β-CD, this complex is used to describe the overall structure.

The geometry of the models is good with approximately 89% of the residues in the most favoured region of the Ramachandran plot and only one residue (Phe^{566}) in a disallowed region. Phe^{566} is in a turn in the loop between β-strand 6 and α-helix 6 of the $(\beta/\alpha)_8$-barrel. The unfavourable φ and ψ angles in this tight turn could be caused by the bi-dentate salt bridge between the adjacent Glu^{568} and Arg^{875}, and the multiple hydrogen bonds emanating from Gln^{559}: Gln^{559} Nε2 - Glu^{568} O, Gln^{559} Nε2 - Thr^{563} O, Gln^{559} Oε1 - Gln^{574} Nε2 and Gln^{559} Oε1 - Asn^{570} N. In addition, the aliphatic part of the Arg^{581} side-chain contributes to hydrophobic interactions with the side-chain of Phe^{566}. Three residues Ala^{439}, Ala^{515} and Asn^{643} were found in the generously allowed region of the Ramachandran plot. Ala^{439} is in the center of a loop located in between two α-helices (α-helix 19 and 20, Figure 3.16B) in the B-domain part of the catalytic domain (*27*). The β-turn in the loop is sustained by the hydrogen bond between the main-chain nitrogen of Ala^{439} and the main-chain carbonyl oxygen of Asn^{436}. Ala^{515} is placed just borderline to an additional allowed region in the φ/ψ plot. The Ala^{515} is placed in the loop region, which also contains the general acid, Glu^{510} and Trp^{512} (subsite +2, see below for detailed description). The exact position of this loop exposes Phe^{514} towards subsite +2. It is influenced by hydrogen bonds between Asp^{513} Oδ1 - Asn^{525} Nδ2, Asp^{513} Oδ2 - Ala N, Glu^{516} Oε1 - Ser^{437} Oγ, Glu^{516} Oε2 - Asn^{442} Nδd and the salt bridge Glu^{516} Oε2 - Arg^{427} Nη1. The strained φ and ψ angles of Asn^{643}, which is positioned next to the third acid in the catalytic site, is a product of an Asn^{643} N - Arg^{697} O hydrogen bond but also the direct interactions of the side-chain with the β-CD glucose ring in subsite +1 could have an effect.

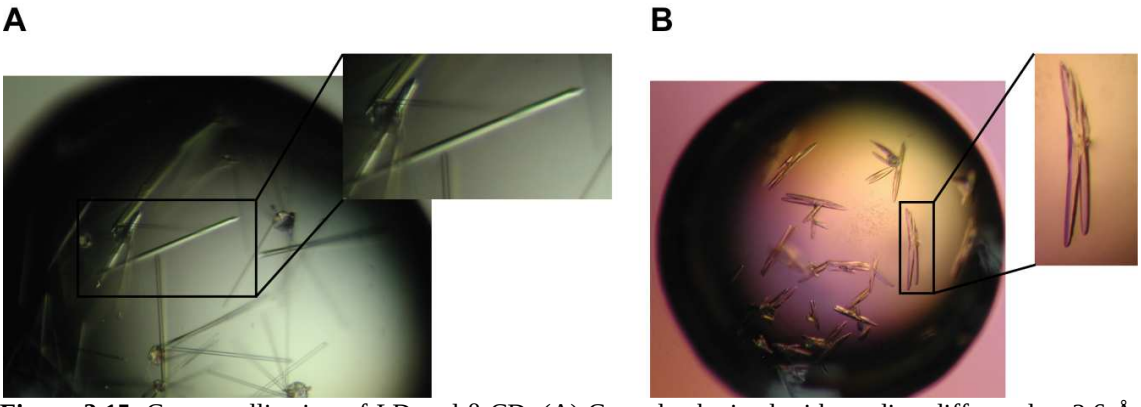

Figure 3.15. Co-crystallization of LD and β-CD. (A) Crystals obtained with seeding diffracted to 2.6 Å and belonged to space group $P2_12_12_1$. (B) Crystals obtained without seeding diffracted to 2.1 Å and belonged to space group *C*2. For crystallization condition see section 2.7.2.

Table 3.8. Data collection and refinement statistics

	HvLD·β-CD	HvLD·α-CD
Data collection		
Space group	*C*2	*C*2
Cell dimensions		
a, *b*, *c* (Å)	175.0, 82.4, 59.4	174.8, 85.6, 61.1
α, β, γ (°)	90.0, 96.1, 90.0	90.0, 96.8, 90.0
Molecules/asymmetric unit	1	1
Wavelength	0.873	0.910
Resolution (Å)	41.2–2.10	33.5–2.50
R_{sym} **(%)**	12.8 (45.8)[a]	9.3 (42.6)
Mean(*I*)/*σ*(mean(*I*))	11.4 (4.2)[a]	13.1 (2.3)
Completeness (%)	99.6 (99.2)[a]	97.0 (87)
Unique reflections	47764 (7091)[a]	12135 (3528)
Redundancy	4.3 (4.3)[a]	3.7 (3.1)
Wilson B-factor[b] (Å^2)	15.6	50.1
Refinement		
Resolution (Å)	41.2–2.10	33.5–2.5
Used reflections	48242	30653
R_{cryst}/R_{free} (%)	16.4/20.4	17.7/22.6
Final R_{cryst}	15.7	17.3
No. protein atoms	6709	6714
No. calcium ions	2	2
No. iodine	5	9
No. of glycerol	7	1
No. of cyclodextrin	1	1
No. of waters	604	223
Mean *B*-factor (Å^2)	12.2	35.1
R.m.s.d. values from ideal		
Bond lengths (Å)	0.003	0.003
Bond angels (°)	0.742	0.658
Ramachandran plot[c]		
Most favorable (%)	89.0	88.4
Additional allowed (%)	10.5	11.2
Generously allowed (%)	0.4	0.3
Disallowed (%)	0.1	0.1

[a]Highest resolution bin. [b]From Truncate (*88*). [c]Calculated with Procheck (*94*).

3.4.3 Overall Structure

The final model of HvLD in complex with β-CD is shown in Figure 3.16. The domain boarders, indicated by sequence alignment with structurally related proteins (*27*), are slightly displaced relative to those seen from the HvLD structure. The structure comprises four structural domains; the N-domain (reidues 3–124) of unknown function, a carbohydrate binding module (125–230) assigned to CBM48 of which a few members

have been demonstrated to bind to glycogen (*30*), the catalytic domain (231–774), and the C-domain (775–885) of unknown function. The N-domain consists of 8 strands (b1–b8) arranged primarily in an anti-parallel fashion and 4 α-helices (a1–a4), whereas the CBM48 consists of 9 strands (b9–b17) and 2 α-helices (a5–a6) (Figure 3.16B). The catalytic domain contains 33 α-helices and 12 β-strands. The core of the domain forms a $(\beta/\alpha)_8$-like barrel (Table 3.9), which resembles the corresponding barrel in α-amylases (*29, 109*) except the LD barrel has no helix α5. Instead, a loop between β5 and β6 holds Trp^{512} and embed subsite +2. As observed in the KpPUL structure (*31*) and previously described as Loop 2 (*27, 31, 110*), a long loop protrudes from the barrel scaffold following the second β-strand. Loop 2 includes Tyr^{357} and is part of the active site at subsite –1 (see below for detailed description of the active site). The B-domain is a part of the active site cleft accommodating the side-chain of branched oligosaccharides as identified by superimposition of the LD and the KpPUL:maltotetraose (G4) complex. Finally, the C-domain comprises a β-sandwich structure, in which each of the two sheets in the sandwich contains 4 β-strands flanked by short stretches of α-helices (4 in total).

Two Ca^{2+} sites were found in the structures of LD in complex with α-CD and β-CD (Figure 3.17). The first site is located in Loop 2 close to subsite –1 and Tyr^{357}. This Ca^{2+} site is identical to one of the five Ca^{2+} binding sites identified in KpPUL (*31*). The Ca^{2+} site has pentagonal bipyramidal geometry, with Ca^{2+} ligated by the side-chains oxygen atoms of Asp^{351} (Oδ1) and Asn^{701} (Oδ1), the main-chain carbonyl oxygens of Gln^{348} and Tyr^{353} and three, water molecules (Figure 3.17A). The average Ca^{2+}-O distance is 2.6 Å. The second LD Ca^{2+} site has an octahedral geometry. The Ca^{2+} ligands are the side-chain oxygen of Ser^{297} Oγ, the main-chain carbonyl groups of Gly^{393}, Leu^{301} and Ser^{297} and two water molecules. This site is located in the catalytic domain and connects the loops extending from the C-terminal ends of β-strand 2 and 3 (Figure 3.17B). The average Ca^{2+}-O distance is 2.7 Å. One negatively charged residue contributes to metal binding in site 1, while no negative charge contributes to metal binding in site 2.

Table 3.9. Secondary structure elements of the $(\beta/\alpha)_8$ barrel

Structure element of the (β/α)-barrel	Sequence
β1 (b18)	256-TIYEL-259
α1 (a13)	288-AGMEHLRKLSDA-299
β2 (b19)	303-HVHL-306
α2 (a18)	377-SRIIEYRQMVQALNR-391
β3 (b22)	395-RVVMDV-400
α3 (a20)	448-FMVDRLIVDDLLNWAVN-464
β4 (b23)	469-GFRF-472
α4 (a22)	480-KRTMMRAKSLQ-491
β5 (b24)	506-YLYG-509
α5	absent in structure
β6 (b25)	537-GSFN-540
α6 (a27)	577-EADTRRSLATYADQIQIGL-595
β7 (b28)	634-TIN-636
α7 (a30)	660-VDERCRINHLASMMAL-675
β8 (b29)	680-IPFFH-684
α8 (a37)	748-KGHILAALDSFVDILKIR-765

Numbers in parenthesis refers to the position of the structural elements in the topology diagram in Figure 3.16B.

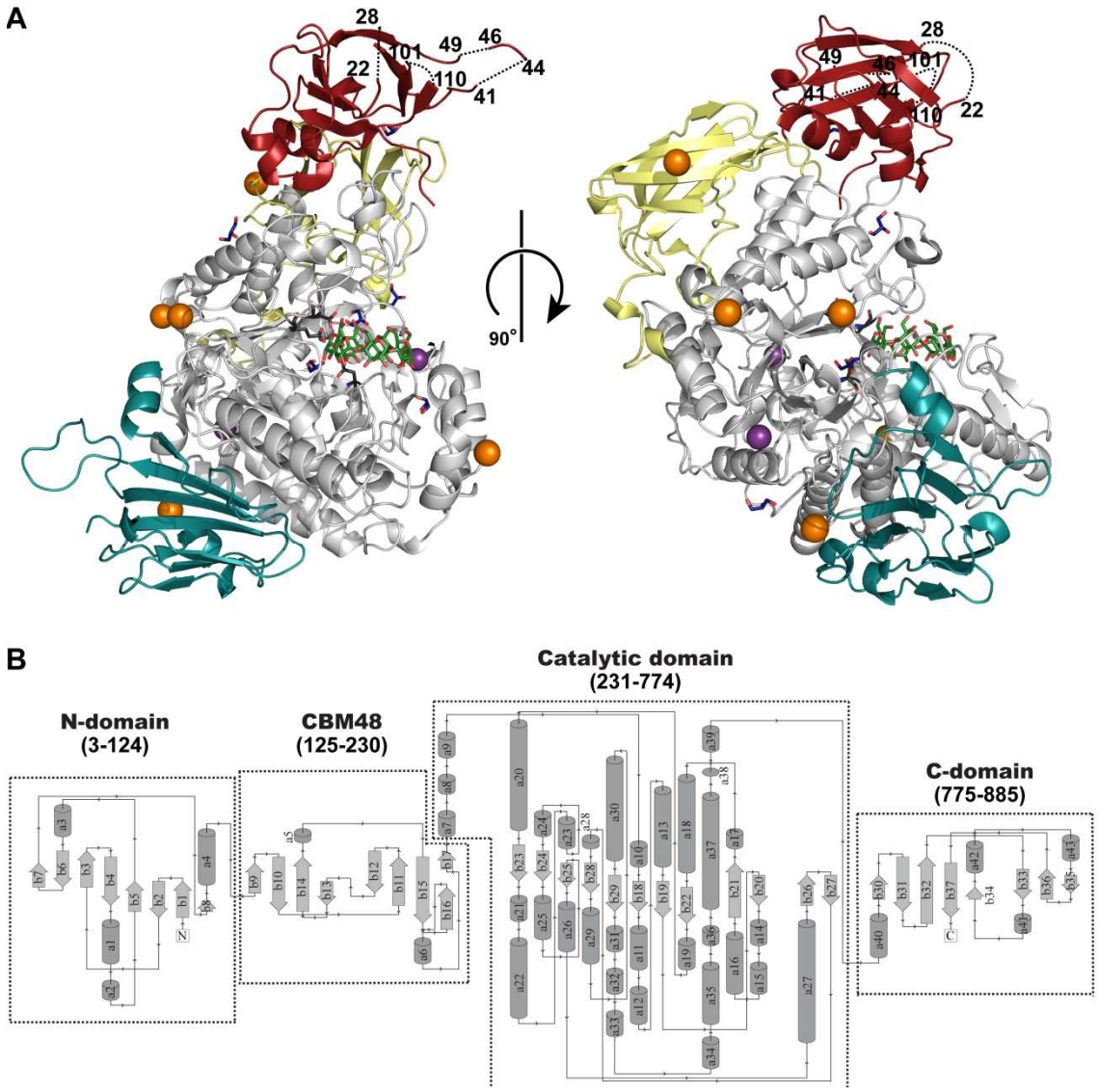

Figure 3.16. (A) overall structure of LD:β-CD and the same structure rotated 90°. N-domain in red, CBM48 in yellow, catalytic domain in light gray and C-domain in light cyan. Ca^{2+} in purple, I^{+} in orange, glycerol in blue and β-CD in green. The catalytic residues, Asp^{473}, Glu^{510}, and Asp^{642} are shown in dark gray. (B) topology diagram of LD. α-helices are shown as cylinders in dark gray and labelled a and β-strands are shown as arrows in light gray and labelled b.

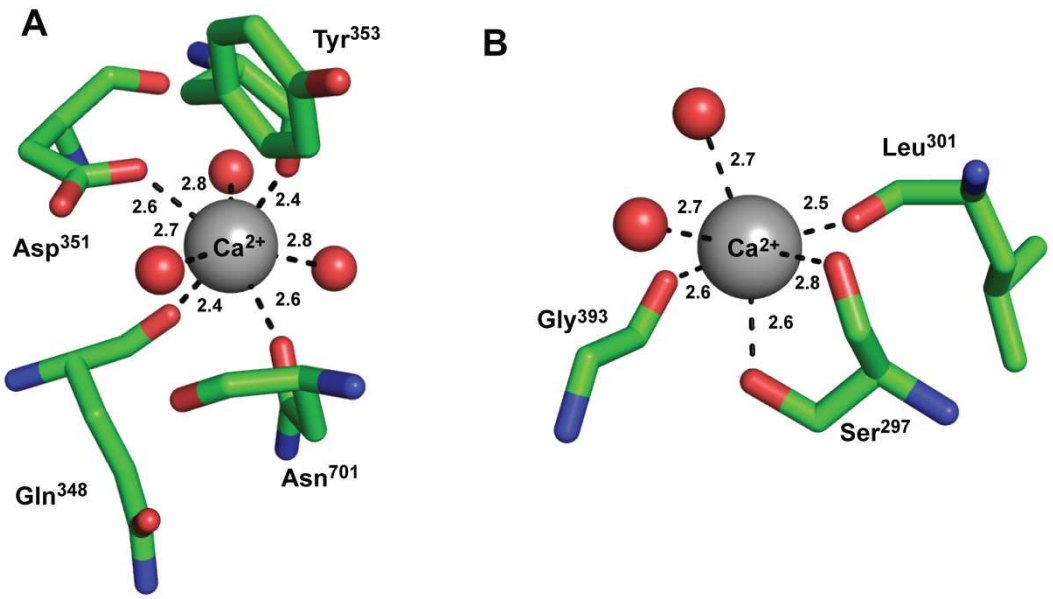

Figure 3.17. The models around the two calcium sites. A, the first Ca^{2+} site (Ca1) has a pentagonal bipyramidal geometry. B, the second LD Ca^{2+} site (Ca2) displays an octahedral geometry. The calcium ion is shown in gray, water molecules in red and ligand side-chains in green with residue numbers in dark gray. Polar interactions are shown with dashed lines and the distance between the calcium ion and the ligand atom is shown.

3.4.4 Active site of LD and Binding of Cylodextrins

The active site is defined by the positions of the catalytic residues, *i.e.* the catalytic nucleophile Asp^{473}, the general acid/base catalyst Glu^{510} and the third catalytic site acid, Asp^{642}, as determined by sequence alignment (*12*, *28*) (Figure 3.16). The α- and β-CDs are bound at this site (Figure 3.18B). Designation of the substrate-binding subsite numbering is in accord with previously introduced definitions (*31*, *111*). Subsites at the reducing end of the substrate are numbered with positive numbers starting from the point of hydrolysis, and subsites at the non-reducing end have negative numbers (*111*). The active site of LD is composed of two binding sites; the first (the branch binding side) being defined by subsites –1 through –2 and the second site (the main-chain site) is defined by subsite +2 through 0' (Figure 3.18A). Due to different structural restraints imposed by the ring of α- and β-CD, they bind differently to LD (Figure 3.18B).

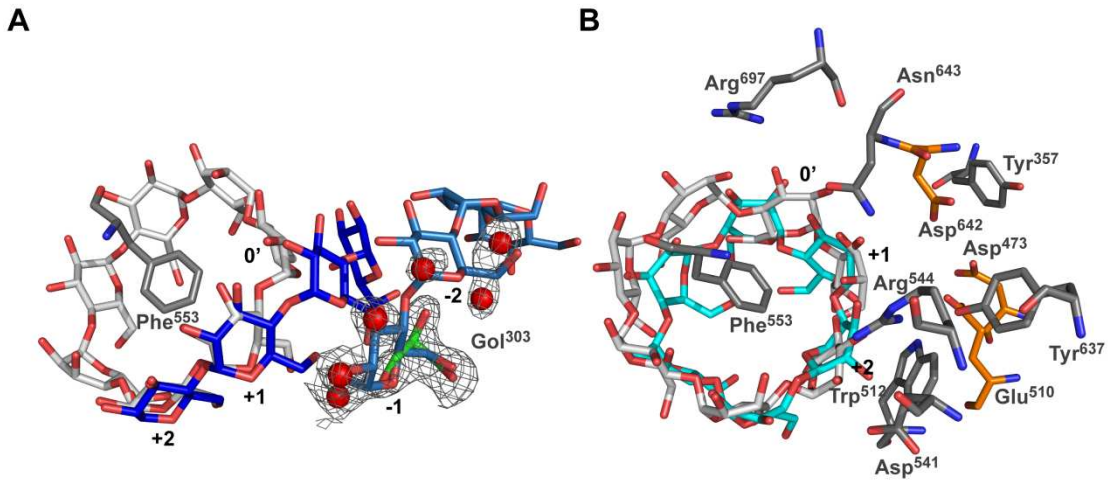

Figure 3.18. Superimposition of LD:β-CD onto pullulanase:maltotetraose (G4) complex. β-CD is coloured in light gray, LD Phe^{553} in dark gray, glycerol 303 in green, and water molecules in the active site of LD in red. The glycerol and water $2F_o–F_c$ maps at 1.0σ are shown as gray mesh. The G4 molecules of the pullulanase:G4 complex are drawn in blue (representing the sugar main-chain) and light blue (representing the branched sugar chain). B, Superimposition of LD:β-CD on LD:α-CD complex. β-CD and α-CD are colored in light gray and cyan, respectively, LD active site residues in dark gray. The catalytic residues, Asp^{473}, Glu^{510}, and Asp^{642} are shown in orange. The subsite numbers and residue numbers are black and gray, respectively.

Several amino acid residues of LD are involved in interactions with β-CD (Figure 3.19 and Figure 3.20), which has the strongest affinity towards LD of the two (β-CD: K_d = 0.7 µM, α-CD: K_d = 27.2 µM, section 3.1.7) (*70*). The majority of β-CD-protein interactions occur at subsite +2. Asp^{541} Oδ2 is in hydrogen bond contact with Glc O2, Arg^{544} Nη2 interacts with Glc O2, and Nη1 interacts with Glc O3. The position of Arg^{544} is further stabilized by a hydrogen bond between Nη1 of Arg^{544} and the hydroxyl group of Tyr^{637}. Finally, the indole ring of Trp^{512} stacks with the Glc at subsite +2. The Nε1 of Trp^{512} interacts with the general acid/base Glu^{510} Oε2, which stabilizes the position of this pivotal residue. At subsite +1, Asn^{643} Nδ2 interacts with O3 of Glc. Furthermore, Asn^{643} Oδ1 interacts *via* a water molecule with O2 and O3 of Glc at subsite 0' (Fig. 3B; Fig. 4). In addition, van der Waals interactions between Arg^{697} and Glc at subsite 0' are observed. Binding at this site could be stabilized by water mediated contacts to Arg^{697} O and Asp^{698} Oδ1. Finally, the aromatic ring of Phe^{553} is immersed in the central cavity of the β-CD molecule with van der Waals interactions or possibly weak aromatic hydrogen bonds (C(-H)..O distance = 3.3 Å–3.9 Å) to O4 of several Glc subunits of the β-CD molecule (Figure 3.20). The Phe^{553} Cζ is situated in the plane defined by the β-CD Glc residues, with an approximate inclination between this plane and the plane of the Phe^{553} aromatic ring of 20°. Furthermore, the main-chain carbonyl oxygen of Phe^{553} interacts *via* a water molecule with O3 of Glc of β-CD opposite subsite –1. By comparing the α-CD and the β-CD complexes it is suggested that the 40-fold weaker binding of α-CD to LD (*70*) may be caused by the lack of interaction between Arg^{697} and two Glc residues both directly or *via* water mediated contact (Figure 3.18B), the lack of an interaction between Nδ2 of Asn^{643} and an O3 as well as the missing interaction between Oδ1 and an O3 atom at subsite +1, the absence of the hydrogen bond between Asn^{551} and the glucose residue of β-CD at subsite +4 and a less favorable interaction with Phe^{553}. The α-CD plane is ~1 Å below the Phe^{553} Cζ atom and

the inclination between the aromatic ring plane and the α-CD Glc residues is close to 45°, which might give rise to loss of the hydrogen bond character of the interaction. Both CDs have some less well-defined Glc residues (subsites 0' and –1') with weighted $2F_o–F_c$ less than 1.0σ, and despite the fact that these are within interaction range of LD (Fig. 3C) they cannot be major contributors to binding energy.

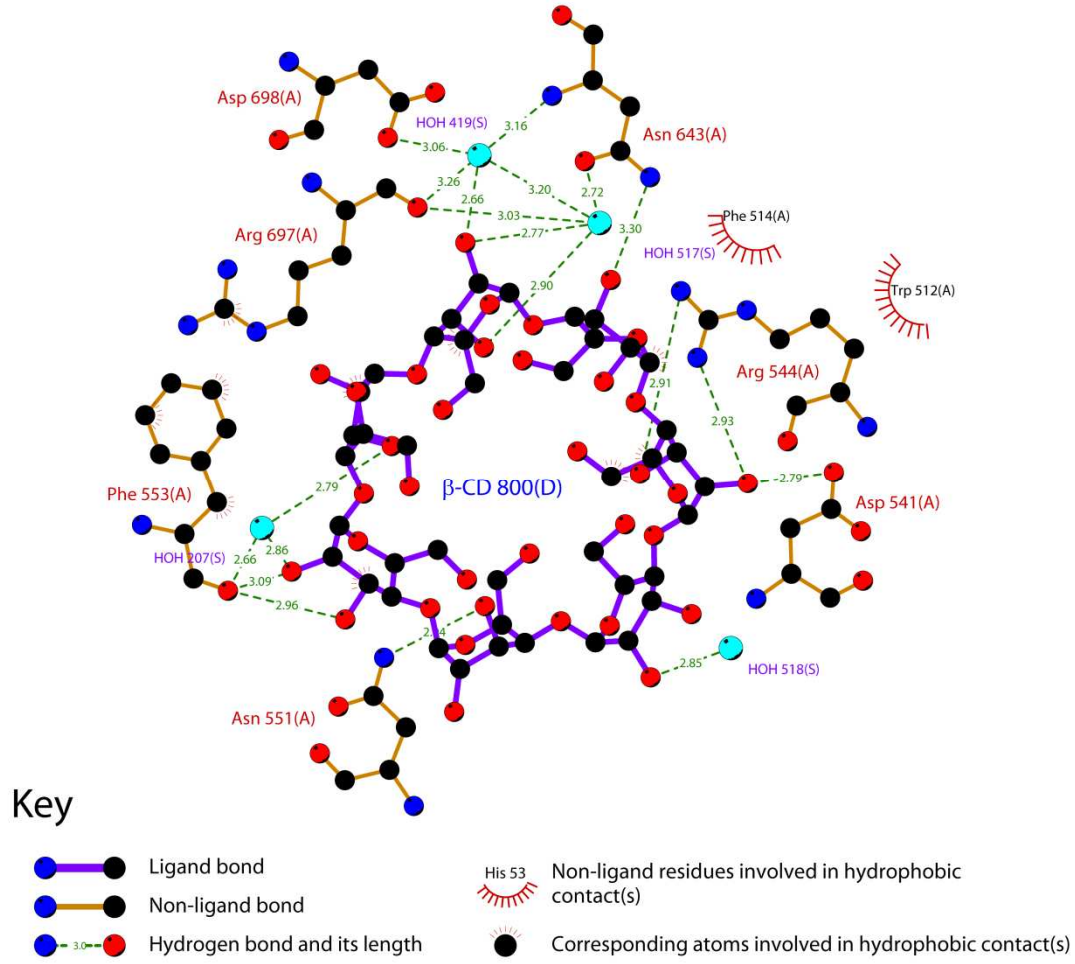

Figure 3.19. Schematic drawing of the LD residues interacting with β-CD. The figure was based on a cartoon generated by the program LIGPLOT (*112*). Both CDs have some less well-defined Glc residues (subsites 0' and –1') with weighted $2F_o–F_c$ less than 1.0σ.

Glycerol used in the crystallization buffer (LD:β-CD) and in the cryo-protectant was found in the active site of LD:β-CD (Figure 3.20). The binding of glycerol (Gol) in the active site of carbohydrate active enzymes during co-crystallization is a well known phenomenon (*113, 114*). Arg^{471} interacts with Gol^{302} in the active site of LD. Also the three catalytic residues interact with Gol^{302}, while the second glycerol molecule found at the active site (Gol^{303}) have hydrogen bonds directly to Asp^{473} Oδ1/Oδ2 and water mediated hydrogen bonds to Glu^{510} Oε1/Oε2. Moreover, Gol^{303} is at a distance of 4.2 Å of Tyr^{357}. Superimposition of LD:β-CD and the KpPUL:matotetraose (G4) complex (*31*) shows that the two Gol^{303} primary hydroxyl groups superimpose perfectly with O6

and O5 of the Glc residue at subsite −1 and that the secondary alcohol is found in close proximity to O4 of the same Glc residue. In addition, three water molecules in the LD structure are located at the sites of O1, O2 and O3 of the same glucose residue at subsite –1 of KpPUL (Figure 3.18A). Additional five glycerol molecules (Gol^{301} and Gol^{304}–Gol^{307}) were found in the LD:β-CD structure (Figure 3.16A). One (Gol^{306}) is buried in a part of Loop 2 and the rest were solvent exposed. Two were situated on the surface interacting directly or *via* water molecules with LD, whereas one was found in the groove formed at the interface of the CBM48 domain and the catalytic domain. The last glycerol molecule was in a solvent channel between the N-domain and the CBM48. Possibly because glycerol was not included in the crystallization conditions for LD:α-CD but only used as cryoprotectant, only one glycerol molecule was found in the LD:α-CD structure. The Gol molecule was buried in Loop 2 similarly to Gol^{306} found in the LD:β-CD complex.

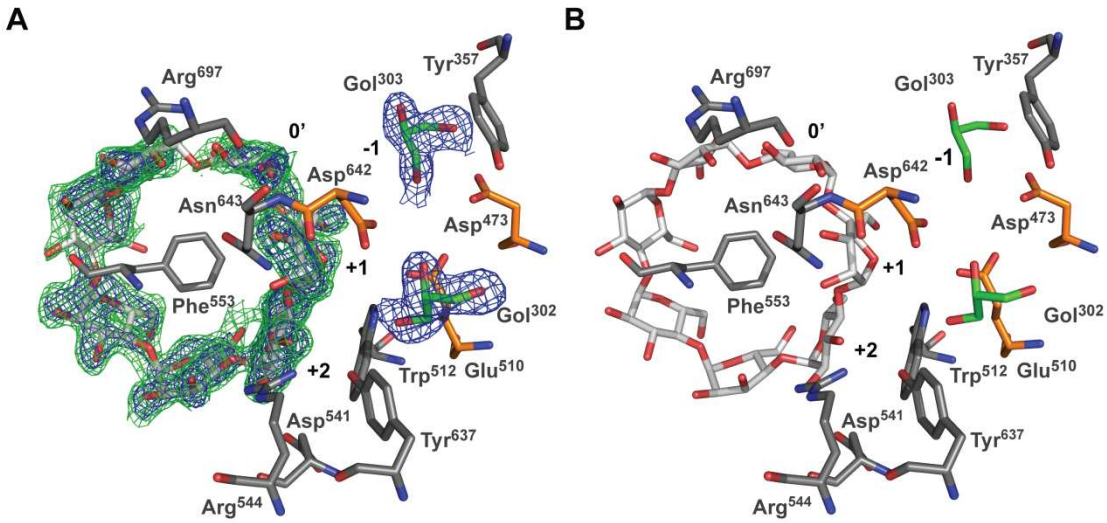

Figure 3.20. β-CD and glycerol bound in the active site of LD shown with (A) or without (B) the $2F_o–F_c$ maps. The $2F_o–F_c$ at 1.0σ and 0.6σ are shown as blue and green mesh, respectively. β-CD is coloured in light gray, glycerol in green, LD active site residues in dark gray. The catalytic residues, Asp^{473}, Glu^{510}, and Asp^{642} are shown in orange. The subsite numbers and residue numbers are black and gray, respectively.

4 Discussion

4.1 Limit Dextrinase

4.1.1 Cloning and Expression of LD

Previous attempts to produce recombinant LDs from plants resulted in extremely poor yields (*22, 23*) and very low specific activity highlighting (*24*) the difficulties in producing large multidomain recombinant plant proteins. Earlier attempts to produce barley LD thus resulted in full-length and truncated inactive forms (*41*). A new attempt was made to produce LD in *E. coli* due to the findings of several mutations in the clone used in the previous attempts, which was then corrected to wt-LD sequence. The selected production strain for the intracellular production of LD contained an extra plasmid harbouring the genes encoding the tRNA for the seven rare codons. However, expression of the new LD construct did not lead to the production of active full-length LD, which once again emphasises the challenge in producing large multidomain plant proteins in a bacterial expression system. The *P. pastoris* system has been proved to be an excellent host for production of plant proteins (*26, 99, 115*). This system also showed to be efficient in the heterologous production of barley LD. Optimization of a fed-batch protocol in a 5-L bioreactor thus resulted in 16 mg/L highly active recombinant LD secreted to the culture supernatant indicating accumulation of functional and stable recombinant LD under the applied culture conditions (Figure 3.1). Lowering the induction temperature to 22–25 °C has been reported to increase amounts of secreted heterologous protein (*116-118*). This was confirmed by pilot scale expression of LD at 22 °C resulting in more than 10 times higher yield than at 30 °C. This is assumed to be due to enhanced LD folding and/or reduced protease activity in the medium (*116, 119*), since LD was previously reported to be fully stable at 30 °C (*66*).

The functional recombinant barley LD achieved in excellent yields and outstanding quality enabled biochemical and structural characterization of this pivotal enzyme in cereal starch metabolism and in food processing, in particular in the brewing and malting industry (*120, 121*).

4.1.2 Characterisation of LD

4.1.2.1 Hydrolytic Activity

As indicated by the purification summary (Table 3.1) a low specific activity was observed in the β-CD-Sepharose eluate. The approximately 2-fold increase in activity in the gel filtration eluate is not believed to be solely due to removal of contaminant species as judged by the SDS-PAGE (Figure 3.2), but was probably due to residual β-CD, which was efficiently removed by gel filtration, resulting in a final specific activity of 14.2 U/mg or approximately twice the value measured for LD purified from barley malt (*47*). The high specific activity was also reflected by the kinetic constants $k_{cat,app}$= 78 s^{-1} and $K_{m,app}$= 0.16 mg/mL. Previously, K_m and k_{cat} values for barley malt LD hydrolysing pullulan at pH 5.0 and 40 °C were reported in the ranges 0.16–0.44 mg/mL and 33–60 s^{-1}, respectively (*37, 122*), and giving 2.4–3.5 fold lower catalytic efficiency

than the present recombinant LD. In comparison reported K_m and k_{cat} values of pullulanases from *Klebsiella planticola* and BaPUL were 0.09 mg/mL and 81 s^{-1}, and 0.24 mg/mL and 120 s^{-1}, respectively (*122*).

The deviation from the hyperbolic fit of the kinetic data at pullulan concentrations above 0.2 mg/mL (Figure 3.3) has not previously been described for barley LD. This behavior may reflect transglycosylation reactions even though the initial rate kinetics towards pullulan models an uncompetitive substrate inhibition. Transfer of fluorescently labeled maltotriose onto newly hydrolysed pullulan (*42*) provides evidence for barley LD catalysed transglycosylation and transglycosylation was also reported for rice LD using pullulan as substrate (*43*). Although the *in vivo* function of LD is mostly considered in starch debranching, the present findings motivate further kinetic and structural analysis to elucidate features that contribute to the transglycosylation activity and the suggested role in starch biosynthesis.

4.1.2.2 Transglycosylation

The transfer of α-maltosyl fluoride to maltose at lower LD concentrations (25 nM) resulted in the formation of only one conformation from α-maltosyl of each substituted product, with a specific position of the branch point, indicated by a single uniform spot on the TLC (data not shown). Based on previous results (*41*) it is assumed that the α-maltosyl fluoride is transferred to the non-reducing end of the acceptor. However, a 50% increase in LD concentration (37.5 nM) had a significant influence on the transglycosylation reaction pattern resulting in transfer of α-maltosyl fluoride to either the reducing or non-reducing end of the of the acceptor maltose. The formation of products with different α-1,6 branch points was indicated by the close migration of two spots on the TLC. The strong interaction at subsite +2 mediated by hydrophobic stacking and hydrogen bonds (see section 3.4.4 and 4.3.4 for detailed description of the substrate subsites) presumably contributes to the majority of the branch points being at the non-reducing end. Pullulanase from *Aerobactor aerogenes* has also been shown to transfer maltose to the reducing end of a maltose acceptor resulting in 14% of the products containing the α-1,6 linkage at the reducing glucose unit which results an isomaltose based structure (*40*). Since isomalto-oligosaccharides are believed to have prebiotic affect (*123, 124*) the oligosaccharide obtained from the LD catalysed transglycosylation with an isomaltose-like structure may also be a prebiotic candidate.

The activated G2F functions as a significantly better glycosyl donor than does the transglycosylation product (G2–α-1,6–G4), which allows accumulation of the transglycosylation product (Figure 3.4A). However, this was not the case using G3F as donor indicated by the much slower conversion to G4 and fast hydrolysis of the transglycosylation product (Figure 3.4B), which may be due to the formed transglycosylation product being a better glycosyl donor than G3F. This would explain the observed difference in the ability to function as an activated substrate donor between G2F and G3F.

Use of maltotetraose as acceptor can lead to four theoretical possible structures with one maltose substituted to either one of the four glucose residues. TLC data, however, indicates that only one of these products is formed by the appearance of a single spot for the G2–α-1,6–G4 product. This may suggest a preferred position of the G4 binding at the aglycone site. Structural analyses of this product will help elucidating the subsites of the LD active site. However, one might speculate based on the

protein:ligand interaction observed in the LD:β-CD and the KpPUL:G4 structures, that maltotetraose will bind at subsite +2 to 1' resulting in the formation of a α-1,6 bond at the second glucose residue from the reducing end. Furthermore, the results from the transglycosylation with different lengths of donor and acceptor clearly shows that longer sugar chains, both side- and main-chain, are preferred for hydrolysis. These results are in agreement with previous analysis of the hydrolytic specificity of LD towards branched oligosaccharides (*11*, *41*). Based on these preliminary result future experiments analysing the initial rate of transglycosylation will reveal more about the preferred length of donor and acceptor.

The inhibition of LD by 4-*O*-α-D-glucopyranosylmoranoline (G1M) indicates binding in the active site. G1M, a disaccharide derivative of the very potent glycosidase inhibitor 1-deoxynojirimycin (DNJ) comprises an endocyclic nitrogen insted of the oxygen pyranosidic atom (Figure 4.1A). The inhibition ability of G1M and other iminosugars is believed to be caused by mimicking both the conformation and the charge of the oxocarbonium ion intermediate (*125*), which involves binding of G1M at subsite –1 to –2 of the active site. Barley β-amylase crystals soaked with G1M refined to 1.8 Å confirmed the position of G1M (*Rejzek & Field, manuscript in prep*). However, the formation of transglycosylation products from the transfer of G2F to G1M suggests that G1M also binds at subsite +1 to +2 of LD. Based on the previous results with transfer of G2F to maltose, is most likely that the transfer of G2F to G1M occurs on the glucopyranose ring, which is assumed to be positioned at subsite +1.

The glucosidase inhibitor acarbose (Figure 4.1B) showed also to be an acceptor for transglycosylation resulting in both mono- and disubstitution. Crystal structures of acarbose in complex with various glycosidases, glycogen debranching enzyme TreX from *Sulfolobus solfatarius* (*126*), α-amylase from *Bacillus halmapalus* (*127*), and β-amylase from barley (*Rejzek & Field, manuscript in prep*), show that acarbose binds differently to the active site of all enzymes making it impossible to predict the mode of binding to LD. Isolation and structural analysis of the product is therefore needed in order to determine the position of the newly formed α-1,6 branch point.

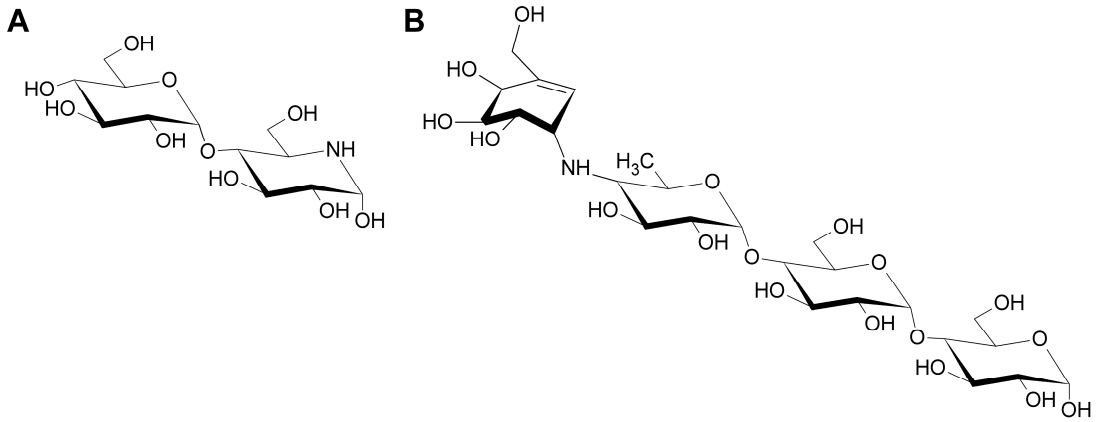

Figure 4.1. Structures of the glycoside hydrolases inhibitors G1M (4-*O*-α-D-glucopyranosylmoranoline (A) and acarbose (B).

The transglycosylation products from the transfer of G2 to G1M and acarbose by LD could be potential inhibitors with altered inhibitory activity towards glycoside hydrolases compared with the parent inhibitor (G1M or acarbose). Optimization of the transglycosylation reactions using G1M and acarbose as acceptors is, however, needed in order to increase the yield of the product. Changing the ratio of donor:acceptor may

prevent the polymerisation of maltose and thereby increase the yield of the preferred product. Doing so, one should be aware of the inhibitory affect of G1M. A solution could be to mutate the catalytic nucleophile to *e.g.* an alanine, which will change the LD from being a hydrolase to a potential α-glycosynthase (*128*). The mutation of the catalytic nucleophile is changing the enzyme from being a retaining to an inverting enzyme, since the reaction would require the use of β-maltosyl fluoride as donor (*128*). A LD nucleophile mutant would also be useful in increasing the yield of the transglycosylation product from the transfer of maltotriosyl to maltotetraose which is readily hydrolysed.

α- and β-CD are extremely good acceptors for transglycosylation reaction catalysed by LD presumably owing to the high affinity of α- and β-CD towards LD (Table 3.3). Binding of the CD to the active site does not seem to prevent the binding of α-maltosyl fluoride at subsite –1 and –2, which would then leave the CD in a favourable position for an attack of the glycosyl intermediate. Surprisingly the cleavage of the formed β-CD product does not seem to be inhibited by the relatively high β-CD concentration, resulting in only a minor product accumulation. However, MS data showed the masses corresponding to mono-, di,- tri- and to tetra-substituted β-CD. Structural analysis of the formed products will eventually reveal if the G2s are positioned on the CD ring and/or if a polymerisation occurs of the maltosyl-β-CD. Synthesis of multiple substituted products (dimaltosyl-β-CD and trimaltosyl-β-CD) by KpPUL catalysed transglycosylation has previously been shown (*44, 129*) suggesting that the β-CD ring indeed contains multiple substitutions.

The lower transfer rate as judged by comparison of the developed TLC plates from the G2 transglycosylation of α-CD and β-CD (data not shown) and the clear accumulation of G2–α-1,6–α-CD substituted products (Figure 3.5) indicates that the position of α-CD in the active site is not optimal for synthesis and in particular cleavage of the α-1,6 linkage. The restrain of the α-CD ring contribute to a presumed weaker binding at subsite 0'-1' compared with β-CD (see section 3.4.4 and 4.3.4) and an unfavourable position of the C6 hydroxyl group, which is essential for the formation of the α-1,6 linkage. It is believed as with β-CD that the LD catalysed transglycosylation of α-CD results in multiple substitutions of the ring (*44*).

The ability of cyclodextrins to form inclusion complexes in the cavities is well known (*130*). Furthermore, branched CDs which have a water solubility 50–100 times greater than that of unsubstituted CDs have also the potential to function as drug carriers for target delivery systems (*130*). Therefore multiple substituted CD obtained by LD catalysed transglycosylation reaction will not only have great potential in the application as drug carrier, but also as food ingredients (*131*).

4.1.2.3 Cyclodextrin Affinity

Comparison of the affinity of α-, β- and γ-CD to KpPUL showed strong binding of β-CD driven both by hydrogen bond formation and by hydrophobic contacts as indicated by a favourable entropic change upon β-CD binding (*101*). The affinity of β-CD for LD and the bacterial pullulanase is in the same range. Remarkably, however affinity of the KpPUL for α- and γ-CD (K_d = 100 and 102 μM, respectively) was 4 and 3 times lower than of the barley enzyme (Table 3.3), suggesting that the LD binding site differs significantly from the KpPUL active site, which allows optimized interaction with the ligands. The strong binding of α- and β-CD to LD is in part caused by

aromatic stacking in the active site cleft as described in section 3.4.4 and discussed further in section 4.3.4. β-CD is by far the preferred ligand, thus underscoring the resemblance between the conformations of β-CD and α-glucan helices present in starch (*7*).

4.2 Limit Dextrinase Inhibitor

Proteinaceous inhibitors of α-amylases are known to play an important role in plant defense against pathogens and pests and in the control of endogenous α-amylase activity (*50, 58, 132-134*). LDI is the sole example of an endogenous inhibitor of a debranching enzyme, which is believed to be relevant both for starch biosynthesis and degradation, and in brewing technology (*48, 66, 75*). Despite this importance the LD/LDI interaction, however, remains to be described in details. The established expression system for LDI, and expression of the target enzyme LD together forms the basis for thorough investigations of the LD/LDI complex formation.

4.2.1 Cloning and Expression of LDI

Several different LDI constructs has been expressed in different host systems such as *Lactococuccus lactis*, *E. coli*, and *P. pastoris* in previous attempts to produces LDI recombinantly (*135*). These, however, resulted in either no expression of LDI or more than 50-fold reduction in inhibitory activity compared with LDI isolated from barley kernels (*135*). The unsuccessful expression of active LDI using the intein based construct in *E coli* once again emphasises the challenge in producing LDI recombinantly. However, the use of *P. pastoris* resulted in the production of recombinant LDI with high inhibitory activity. The decrease in cell wet-weight during the methanol phase suggests that over-expression of LDI is toxic for the host which might be due to inhibition of yeast glycoside hydrolase(s). A well known disadvantage in the use of *P. pastoris* as host for heterologous expression of proteins is the presents of secreted proteases in the expression media (*136*). The activity of *P. pastoris* produced proteases is believed to cause the heterogeneous population of LDI, which lowers the yield of purified homogeneous LDI.

4.2.2 LD Inhibition by wt-LDI

Since it was shown previously that the cereal-type α-amylase inhibitors (CM-proteins) inhibit their target enzyme by binding to the catalytic site competitive inhibition was also assumed for LD by LDI (*51, 54, 55, 59, 60*). However, this was not observed for the LDI inhibition of LD (data not shown), as the Hanes-Woolf plot slopes obtained at 0 or 2 nM were not parallel. Instead a 33% deviation between the slopes was observed indicating that the mode of inhibition is only partially competitive, when using pullulan as substrate. This behaviour is in agreement with that of other cereal-type inhibitors when using larger and more complex substrates for analysis of enzyme activities (*56, 58*). In the case of RATI, the inhibition mode thus shifted from competitive when using *p*-nitrophenyl α-D-maltoside to complex inhibition, when larger

oligosaccharide α-maltosideheptaoside (DP7) or α-maltodextrin of DP27 were used as substrates(*58*). Data obtained for inhibition using these substrates agreed both with a partial competitive and a partial mixed type inhibition mechanism. Complete inhibition of PPA was also not achieved in the presence of any of the larger substrates (DP7 and DP27), even at 50–100-fold molar excess of RATI (*58*). Furthermore, the extent of inhibition changed significantly with substrate concentration (*56, 58*), which was explained by RATI binding to the substrate (*56*). When correcting the RATI concentration by subtracting the estimated amount of inhibitor bound to substrate (DP27), the inhibition was found to be competitive with K_i = 0.1 nM (*56*). It is possible the deviation from the 1:1 molar stoichiometry of LDI:LD observed in (Figure 3.10B) is due to the binding of LDI to pullulan (DP ~ 300).

As demonstrated in section 3.1.5 the kinetics of hydrolysis of pullulan by LD is modelled by Michaelis-Menten kinetics with substrate inhibition, which may be due to genuine substrate inhibition or an intrinsically high transglycosylation activity. Either way, it is highly likely that this high substrate affinity exerts a significant influence on the binding of LDI to LD. As a consequence the apparent K_i value (1.7 nM) obtained by fitting the competitive model to the data is expected to be higher than the actual K_i value. Deviation from the 1:1 molar ratio for obtaining complete inhibition seems to be shared by several plant inhibitors (*58, 60, 137*). Barley α-amylase/subtilisin inhibitor (BASI), a strong inhibitor of barley α-amylase 2 (K_i = 77 nM, K_D = 25 nM) belonging to the Kunitz inhibitor type forms 1:1 complex, as shown by the crystal structure of the complex (*138*). Still at a 1:1 molar inhibition was only approximately 60% using Blue Starch as substrate (*137*).

4.2.3 Homology Modelling of LDI

The N-terminal of the LDI model was found to be disordered and assumed to be very flexible. In the case of the wheat inhibitor 0.19 no electron density was present for residues 1–4 indicating multiple conformations and therefore highly flexible (*108*) and in the native structure of RATI the N-terminal was described as a “wagging tail” (*102*). Upon binding to the target enzyme TMA the N-terminal of the wheat homolog 0.28 became well defined (*55*). A similar observation was noted for the five flexible N-terminal residues of RATI, which in the complex with TMA adopt a 3_{10}-helical conformation that spans the substrate binding site of TMA (*59*). Assuming a similar mode of binding, the terminal part of LDI may be similarly ordered upon binding to LD. Furthermore, the open architecture of the active cleft of LD (*139*) compared with TMA seems to be able to accommodate the three extra N-terminal residues specific for LDI. N-terminal elongations or insertions of wheat inhibitor 0.28 either diminished or abolished the inhibition (*140*). For N-terminal 0.28 mutants, which retained inhibitory activity though decreased, a four-fold longer preincubation time was required to reach the maximum inhibition level, suggesting that the N-terminal might only play a role upon binding and is not crucial for stabilizing the inhibitor-enzyme complex (*140*). This is in agreement with the findings for the N-terminal truncated mutants of LDI, where the deletion of three and five residues only seems to have a modest effect on the $k_{on,}$ of complex formation.

The interaction with the catalytic residues and the importance of a free N-terminal α-amino group was apparent not only from the crystal structure of the TMA/RATI, but

also by mutational analysis of catalytic residues of α-amylase from *Bacillus subtilis* (*60*). Changing the catalytic acids of α-amylase to their corresponding amides resulted in a substantial loss in the inhibitor binding (*60*). One could speculate that the ε-amino group of Lys^{6} in LDI could play a similar role in the interaction with the catalytic residues as seen for the α-amino group of Ser^{1} (RATI) (*59*).This positively charged residue (Lys^{6}) is unique for the LDI inhibitor (Figure 3.13A).

The conserved structural arrangement surrounding Arg^{58} seems to be fundamental for the change from α-helix 2 to α-helix 3 as well as being important for the exposure of residue 56, a histidine in case of LDI, but either a tyrosine or a tryptophan in other inhibitors (Figure 3.13A). In the structure of TMA/RATI, the His^{56} equivalent, Tyr^{54} has hydrophobic interactions with Val^{2} (RATI), Trp^{56} and Trp^{57} in TMA (*59*). The equivalent Tyr^{53} in wheat inhibitor 0.28 was also seen to interact with residues in TMA (*55*). It is therefore likely that His^{56} is involved in the interaction between LD and LDI. The interaction could be caused by π-stacking of His^{56} to tyrosine and/or tryptophan residues ($Tyr3^{52}$ and Trp^{354} in LD), which are by superimposition of LD on to TMA found in similar positions as Trp^{56} and Trp^{57} (TMA). This π-stacking may be disrupted by protonation of the His^{56} side-chain and weaken binding to LD in agreement with SPR data at slightly acidic pH (Table 3.5).

The second binding segment of TMA/RATI comprises two flexible loops, L3 and L4, interacting with a protruding loop in TMA (residue 132–149). The lack of this loop in the LD results in a groove-like structure of the surface, thereby making the distance between LD and LDI too large for direct interaction when superimposing LD and LDI onto the TMA/RATI complex.

4.2.4 SPR Analysis of Binding of LDI and LDI Mutants to LD

SPR biosensors, when properly utilized, can be very powerful, sensitive biophysical tools for analysing the binding kinetics and energetics of the interaction between biomolecules, requiring small amounts of proteins. The experimental set up developed in the present study, resulted in high quality data as judged by the signal to noise ration and by the residual falling mostly within 5%. This study gives valuable insight on the driving force of interaction between LD and LDI. The high affinity of the LD/LDI complex was mainly due to a very low off-rate $k_{off} = 5 \times 10^{-5}$ s^{-1} whereas the $k_{on} = 1 \times 10^{6}$ M^{-1} s^{-1} (in 10 mM Mes/NaOH pH 6.0, 150 mM NaCl, 25 °C) was in the standard range for a typical protein-protein interaction (*103, 104*). The general dependency on ionic strength was determined at different NaCl concentrations (Table 3.4). An increase in ionic strength only affected the affinity to a minor extent primarily due less than 2-fold change in k_{on}. The k_{off}, however, was virtually insensitive to ionic strength, indicating that long-range electrostatic forces only play a minor role in the interaction between LD and LDI (*141*). This suggests that any formed salt bridges are likely to be shielded in the formed complex.

The optimum pH (pH 6.5) of the interaction is in good agreement with the physiological slightly acidic to neutral pH prevalent in the endosperm of the mature seed, which is shown to acidify during germination (*105, 106*), and the increase in K_D of 12–15 fold at both lower and higher pH values showed that K_D was dependent on pH. This is in agreement with the pH optimum for enzyme inhibition found for LDI *(62)*. K_D of LD/LDI interaction dependency on pH (Table 3.5), may reflect alteration of protein

surface charge patterns. Above the role of protonation of His^{56} was discussed and similarly introduction of negative charges or loss of positive charges (perhaps at Lys^{6}) can interfere with the hydrophobic interaction and decrease the stability of the complex.

The binding affinity of the LD and LDI varied with the temperature allowing calculation of the van't Hoff thermodynamic parameters. The favourable entropy obtained both in the linear and non-linear van't Hoff analysis suggests that formation of LD/LDI increases the area of buried apolar surface, supported also by lack of detectable binding at low ionic strength even when using 20-fold higher LD concentration (Table 3.4). Although the size of the determined heat capacity estimated from the non-linear van't Hoff analysis is remarkably large, the significant decrease in heat capacity is consistent with an increase in the area of buried hydrophobic surface (*142*). The thermodynamic analysis of the interaction between PPA and the wheat inhibitor 0.19 showed an increase in entropy, again suggesting that hydrophobic interactions plays a significant role in the binding *(51)*. This thermodynamic fingerprint with favourable enthalpy and entropy has been reported for several protein-protein interaction *(142)* and resembles that determined for the binding of *Streptomyces* subtilisin inhibitor to subtilisin from *Bacillus subtilis* with $\Delta G°$ = –57,9 kJ/mol, $\Delta H°$ of –19,8 kJ/mol and $T\Delta S°$ = 38 kJ/mol) (*143*). The heat capacity, however, calculated for the subtilisin/subtilisin inhibitor interaction is $\Delta Cp°$ = –1.02 kJ/(K·mol). Values of $\Delta Cp°$ for protein-protein interaction has be shown in the range of 0.8 to –3.2 kJ/(K·mol) (*142*) with an average value of –1.4 ± 0.8 kJ/(K·mol) placing the calculated $\Delta Cp°$ of the LD/LDI interaction on the borderline.

The literature reports that N-terminal residues of cereal-type inhibitors interact with the active site of target enzymes (*56, 59, 60, 140*). So far, however, only a few α-amylases have been investigated as targets and as their active site cleft is narrower than of debranching enzymes, their inhibition may be more sensitive to changes in the N-terminal structure of the inhibitor. Deletion from the LDI specific Thr^{1}–Glu^{3}, *i.e.* the N-terminus in other inhibitors, and Ser^{4}–Val^{5} hardly affected K_D. Elongation of the N-terminal sequence of LDI by a charged and a hydrophobic residue (EF-LDI) had no effect on k_{on}, but doubled k_{off} for the LD/LDI complex formation. This is presumably due to accommodation of these extra residues including a negative charge in the LD active site cleft. The finding suggests that the role of the LDI N-terminal segment in both formation and stability of the complex with LD is different from that observed previously for cereal type α-amylase inhibitors. Molecular recognition of branched substrates by debranching enzymes necessitates a wider active site cleft topology opened from both the glycone and aglycone sides of the cleft as compared to the deeper and narrower active site clefts of α-amylases. It is proposed that these differences in active site topology result in different molecular recognition where the affinity and the specificity of the interaction is not optimized to rely strongly on the flexible N-terminal part of the inhibitor as in the case of α-amylases as evident from the present data. The rationale to this difference will have to await the determination of the complex structure between LDI and LD. It is tempting to speculate that minimizing the dependence on this loop and increasing the proportion of buried apolar surface in the interaction may be thermodynamically sound due to the high entropic penalty of fixing this loop in one conformation of several possible which can be accommodated by the open cleft of debranching enzymes in contrast to the more deep and narrow clefts of α-amylases, where the loop may be evolved for optimal chemical and steric fit in the cleft of the target enzyme.

4.3 3D structure

4.3.1 The Overall Structure

The closest structural relative to LD is KpPUL (PDB code: 2FGZ). The two enzymes both belong to GH13 subfamily 13 (*6*) and have an overall sequence identity of 30.2% and a similarity of 45.6% (*144*). KpPUL could, despite this relatively large difference in primary structure, be used as template for molecular replacement. A substantial induced-fit motion was observed by the binding of substrate analogous (maltose, maltotriose, and maltotetraose) to KpPUL (*31*). The differences in geometries between β-CD and α-CD are not large enough to cause significant structural changes in the active site. Is was however, not possible to obtain crystals of LD in the absence of an inhibitor, which might be due to a more flexible and/or differently folded +2 subsite in the apo-protein, like it was observed for KpPUL.

The two LD molecules located around the crystallographic two-fold symmetry axis have active sites facing each other in the *C*2 crystals (Figure 4.2), while this is not the case in the $P2_12_12_1$ crystals. The N-terminal domain, which appears more flexible and has poorly defined loops, makes up one half of the molecular interface of the crystallographic dimer. A pore (diameter 51.9 Å) separates the active sites of the crystallographic dimer. A similar pore, but with a diameter of 65.6 Å was observed in KpPUL and speculated to be relevant for the binding of longer polysaccharide substrates (*31*), even though there has been no evidence of KpPUL forming dimers in solution. The presence of the extra N-terminal domain in KpPUL explains the larger pore diameter. LD has not been reported to form dimers in solution, however, size exclusion chromatography on a Hiload Superdex 200 26/60 column (GE Healthcare) results in a small LD fraction (less than 1% as judged from the chromatogram) eluting prior the main fraction at a position corresponding to a LD dimer. A similar dimeric arrangement of molecules has not been observed for the phylogenetic more distantly related BsPUL (GH13_14) and BaPUL (GH13_14). Both BsPUL and KpPUL have been reported to display activity towards glycogen (*145*, *146*), whereas LD is not hydrolyzing glycogen and have less than ~1% of the pullulan activity level towards amylopectin (*11*). The molecular interactions of the crystallographic dimers of the debranching enzyme PaISO (GH13_11) differ from the ones observed in KpPUL and LD. In contrast to LD, PaISO has a preference for larger and more complex polymers such as amylopectin and glycogen and their β-limit dextrins, but has no activity towards pullulan and only minor activity towards dextrins (*38*, *147*).

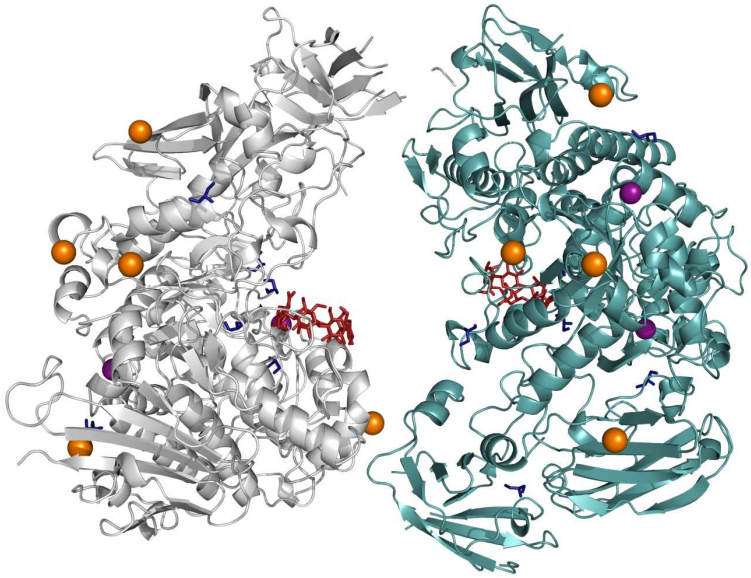

Figure 4.2. The crystallographic dimer of the LD:β-CD complex around the crystallographic 2-fold axis. The LD monomers are coloured in light gray and cyan. β-CD bound in the active site is shown in red and glycerol molecules are coloured blue. Calcium and iodine ions are shown as spheres and colored purple and orange, respectively.

4.3.2 The Carbohydrate Binding Module 48

CBM48 motifs originating from GH13_12, GH13_13 and GH13_14 members are all localized N-terminal to the catalytic $(\beta/\alpha)_8$-barrel (*30*). This is also the case in LD (Figure 3.16). Structure-based alignment of CBM48 with CBM20, that is known to bind onto raw starch (*148*), shows that the two tryptophans identified as key residues in the interaction with starch or the starch mimic, β-CD (*149*) are conserved in CBM48 of the glycogen binding domain (GBD) of the AMP-activated protein kinase from *Rattus norvegicus*. Furthermore, Trp^{33} and Trp^{100} of GBD are identified in the structure of the β-CD complex as critically involved in binding β-CD to GBD. These tryptophans, however, are both missing in CBM48s of KpPUL (*30*) and HvLD. In HvLD, Tyr^{212} corresponds to the second tryptophan, Trp^{100} in GBE, and is situated in a cleft and is not exposed on the surface as is the case of Trp^{100} in GBD. This indicates that if HvLD CBM48 is involved in carbohydrate binding, then the binding-mode and key residues differ from those interacting in GBE CBM48. So far functional roles in carbohydrate binding have not yet been confirmed experimentally for any pullulanase (*30*).

Despite a 6-fold molar excess of CDs in the LD-CD mix prior to the crystallization setup, neither α-CD nor β-CD were found to be bound at the CBM48 domain in the structure. This is in agreement with the failure to observe binding of raw starch to LD. Barley LD starch granule absorption experiments thus resulted in complete recovery of LD activity in the supernatant (*72*).

4.3.3 Ca^{2+}-Sites

The first Ca^{2+} site (Ca1, Figure 3.17A) is embedded in the enzyme and only accessible for solvent *via* two of the seven ligand sites (solvent exposed surface area is 1.1 $Å^2$) The ligands coordinating the Ca^{2+} are located in the long protruding Loop 2, which is an important part of the active site and the catalytic domain. The Asn^{701} ligand is positioned next to Tyr^{700}, which interacts with the glucose residue at subsite –2 (identified by superimposition of LD:β-CD and KpPUL:G4). By connecting Loop 2 with the core of the catalytic domain and thereby shaping a part of the active site, the Ca^{2+} site is likely to be functionally relevant despite an average Ca^{2+}-O distances of 2.6 Å (the mean Ca-O distance in proteins is 2.4 Å (*150*)).

The second Ca^{2+} (Figure 3.17B) is more solvent exposed (the solvent exposed surface area is 22 $Å^2$) and interacts with ligands from helices α1 and α2 of the $(α/β)_8$-barrel. The Ca^{2+} interacts with the protein through only main-chain atoms and the site does not resemble any of the known high affinity sites in α-amylses (*151*). The site has even longer average Ca^{2+}-O distances than site 1 (average length 2.7 Å) and therefore may be a crystallization artifact rather than a structural relevant site.

4.3.4 $(β/α)_8$-Barrel and Substrate Subsites

The $(β/α)_8$-like barrel of LD has no α-helix 5. This is also observed in several other α-1,6 acting enzymes, *e.g.* KpPUL (*31*), PaISO (*152*) and neopullulanase from *Bacillus stearothermophilus* (*153*). These findings suggest that the lack of α5 contributes to the α-1,6 specificity of these enzymes, whereas the more conserved β-strands in particular the 3, 4, 5 and 7 strands of the barrel and the loops immediately following these strands provides a scaffold for the residues involved in catalysis and substrate binding in both α-1,4 and α-1,6 acting enzymes. The lack of a fifth helix in the barrel result in a more spacious pocket at the reducing end of the substrate binding site, thus it becomes less discriminating towards branching in general, but even more important, it positions Trp^{512} for a perfect stacking with Glc at subsite +2 (see below). Despite a high structural similarity around the active site there are significant differences between LD and KpPUL especially in the loop replacing the fifth helix between β5 and β6. This loop, which contains residues Asp^{513}–Asn^{520} in LD corresponding to residues Asp^{709}–Ser^{713} in KpPUL, differs both in amino acid sequence and in structure. The longer loop in LD includes Phe^{514}. This residue seems to narrow the active site cleft around subsites +1 and +2 by 1–3 Å. The prolonged loop in LD may therefore contribute to the difference observed in substrate specificity between the two enzymes (*11, 40, 145*).

Met^{440}, which is positioned in a β-turn of the B-domain and is specific for LD seems to be essential for the substrate specificity. Superimposition of LD:β-CD onto KpPUL:G4 complex shows that Met^{440} clashes with the Glc residue at subsite –4 and that steric hindrance will reduce binding of substrates with a branched chain of G4 or longer. It is therefore reasonable to believe that the LDs preferred length of the branched-chains is no longer than three glucose units. In the KpPUL structure, this particular β-turn is stabilized by a disulfide bridge between Cys^{643} and Cys^{644} and by interaction between the main-chain carbonyl group of Cys^{643} and O4 of the Glc residue at subsite –3. The position of the main-chain carbonyl group of LD Ala^{439} is identical to that of the KpPUL Cys^{643} carbonyl, which suggests that Ala^{439} can be involved in

substrate interaction in LD. That interactions at subsite –3 is of importance for substrate chain-length preference is in agreement with the observed relative rate of hydrolysis by LD of 6^3-α-maltotriosylmaltotetraose, which is 2-fold higher than that of 6^3-α-maltosylmaltotetraose (*11*). At subsite –2, the sugar-aromatic stacking between Tyr^{700} and a Glc residue causes very well-defined binding. Furthermore, the distance between Oδ1 and Oδ2 of Asp^{698} and O2 and O3 of the Glc residue at this subsite is believed to be within 3–3.5 Å by superimposing KpPUL:G4 and LD and thereby likely to further improve binding at subsite –2.

The loop between β4 and α4 contains the presumed catalytic nucleophile, Asp^{473} and contributes together with Tyr^{357}, His^{404}, Arg^{471}, Glu^{510}, Asp^{642} and the main-chain carbonyl oxygen of Ala^{438} to the structure of subsite –1. The position of Gol^{303} and three water molecules (w^{68}, w^{115}, w^{224}) are mimicking a Glc residue at subsite –1 and gives credibility to the position of the proposed α-1,6 linkage cleavage site.

A conserved Leu found in the solely α-1,6 acting enzymes, Leu^{474} in LD, Leu^{678} in KpPUL, Leu^{376} in PaISO Leu^{623} in BaPUL and Leu^{407} in BsPUL, is positioned next to the catalytic nucleophile, where it obstructs the formation of a subsite +1' for α-1,4 linked glucose residues corresponding to subsite +1 in α-1,4 active enzymes and it neighbor upon Trp^{512} thereby aid defining subsite +2. This Leu is therefore believed to be a key residue in discriminating between α-1,4 and α-1,6 acting enzymes. The neopullulanases and amylopullulanases that both display dual (α-1,4 and α-1,6) activity have the shorter Val replacing the Leu in this position, thereby allow binding at subsite +1 (α-1,4 substrate binding).

Among the most striking differences found by comparison of the structures of LD and PaISO is the absent of Loop 2 and the difference in length of the loop between β8 and α8, which is 33 residues longer in LD as well as the significantly longer loop in PaISO between β7 and α7. Loop 2 and in particular the prolonged β8-α8 loop in LD makes the cleft around subsite –2 through –4 and 0' through –1' narrower, which may in part inhibit the binding of additional branched chains as found in glycogen and glycogen β-limit dextrins. However, the observed difference in activity towards amylopectin β-limit dextrins and amylopectin (*11*) is probably caused by the difference in the length of the sugar side-chain extending from subsite –2/–3, where Met^{440} prevents optimum binding due to steric hindrance (as described above). The side-chain of the solvent exposed Phe^{620} had no significant electron density, which indicates a high flexibility. Phe^{620} will, however, irrespective of flexibility narrow the cleft extending from subsite +2. This residue may play a role for the substrate specificity by limiting the binding of longer substrates.

4.3.5 Mechanism

As described in section 1.21 LD catalysed hydrolysis/transglycosylation takes place *via* a double displacement mechanism involving a oxocarbonium ion-like transition state. The interaction between Gol^{303} and His^{404} indicates that His^{404} can stabilize the charged oxocarbonium ion-like transition state as proposed. The position of His^{641} in a superimposition of LD:β-CD and the KpPUL:G4 complex indicate that the distances from ε2 of the imidazol side-chain to O2 and O3 of a glucose residue at subsite –1 are ~2.9 Å and thereby supports the proposed role of His^{641}.

LD is known to act as transferases at higher substrate concentration despite a highly solvent accessible active site (*11, 70*). A similar open active cleft is also observed in the *E. coli* glycogen branching enzyme (*154*). One explanation for the transferase activity, however, could be that at high substrate concentration simultaneous binding of sugar chains at subsite –1 though –2/–3 and at subsite 1' throgh +2 would preclude water from the active site prior to the nucleophilic attack and the formation of the covalent intermediate thereby preferentially allowing the transfer of one sugar chain to the other by a α-1,6-glucosidic linkage. This assumes that the affinity at the aglycone subsites is high enough to maintain high carbohydrate ligand occupancy. It is tempting to speculate that the affinities of these sites are crucial in modulating the transglycosylation *versus* hydrolysis.

5 Concluding Remarks and Perspectives

The present Ph.D. project has provided the first report on the successful production of functional and stable recombinant barley LD and its endogenous proteinaceous inhibitor, LDI. This enables studies of the molecular basis for the substrate specificity and transglycosylation activity of LD as well as the regulation of LD activity by LDI. The detailed SPR analysis of binding kinetics and energetics of the LD/LDI complex reveals binding in the subnanomolar range which was due to very slow dissociation. The van't Hoff parameters indicates that the binding was driven by both enthalpic and entropic contributions. Furthermore, electrostatic interactions seemed not to play a role as salt screening had essentially no effect. K_D, however, depended on pH, possibly due to charge disruption of hydrophobic interactions. Analysis of LDI variants suggests that the N-terminal segment has a different role compared with other cereal-type inhibitor enzyme complex formation (*61*). In addition, the preliminary results obtained in this Ph.D. project on the crystallization of the LD/LDI complex may contribute to the establishment of optimal crystallization conditions and eventually lead to determination the tertiary structure of the complex. The tertiary structure can be used to identify residues involved in the specificity and affinity of the complex formation, and based on these directions rational mutational analysis altering the sensitivity of LD to LDI can be made. Furthermore, the access to recombinant LDI also makes it possible for the first time to investigated the proposed role of barley thioredoxin in the regulation LDI inhibitor activity .

Moreover, the achieved efficient production of fully functional recombinant LD in excellent yield also enabled structural determination of LD in complex with the inhibitors α- and β-CD. This first structure of a plant limit dextrinase is used for gaining insight into the specificity determinants and the possible role in starch biosynthesis.

It is unknown if the proposed role of plant LD in the starch biosynthesis only involves the trimming of the newly synthesized branch points or if LD is also involved in the formation of new α-1,6 branch points. However, independent of the specific action of LD all evidence suggest that the morphology of the starch granular is highly dependent on the LD activity (*21, 155*). The access to recombinant LD makes it possible to gain new insights into starch metabolism in cereals and other plants.

Based on the data indicating that LD is involved both in starch biosynthesis and degradation it suggests here that LD is one of the key enzymes in production of tailor made starch for application in both the food biotechnology and in bioethanol production. Rational mutational analysis based on the 3D structure presented here can be made in order to alter the substrate specificity and thereby produce novel products to use in *e.g.* the food industry.

6 Reference List

1. Cantarel, B. L., Coutinho, P. M., Rancurel, C., Bernard, T., Lombard, V., and Henrissat, B. (2009) The carbohydrate-active enzymes database (CAZy): an expert resource for glycogenomics, *Nucleic Acids Res. 37 (Database issue)*, D233–D238.

2. Henrissat, B., and Davies, G. (1997) Structural and sequence-based classification of glycoside hydrolases, *Curr. Opin. Struct. Biol. 7*, 637–644.

3. Coutinho, P. M., Deleury, E., Davies, G. J., and Henrissat, B. (2003) An evolving hierarchical family classification for glycosyltransferases, *J. Mol. Biol. 328*, 307–317.

4. Coutinho, P. M., and Henrissat, B. (1999) Carbohydrate-active enzymes: an integrated database approach, in *Recent Advances in Carbohydrate Bioengineering* (Gilbert, H. J., Davies, G., Henrissat, B., and Svensson, B., Eds.), pp 3–12, The Royal Society of Chemistry, Cambridge.

5. Boraston, A. B., Bolam, D. N., Gilbert, H. J., and Davies, G. J. (2004) Carbohydrate-binding modules: fine-tuning polysaccharide recognition, *Biochem. J. 382*, 769–781.

6. Stam, M. R., Danchin, E. G. J., Rancurel, C., Coutinho, P. M., and Henrissat, B. (2006) Dividing the large glycoside hydrolase family 13 into subfamilies: towards improved functional annotations of α-amylase-related proteins, *Protein Eng. Des. Sel. 19*, 555–562.

7. Buléon, A., Colonna, P., Planchot, V., and Ball, S. (1998) Starch granules: structure and biosynthesis, *Int. Biol. Macromol. 23*, 85–112.

8. MacGregor, A. W. (1987) α-amylase, limit dextrinase, and α-glucosidase enzymes in barley and malt, *Crit. Rev. Biotechnol. 5*, 117–128.

9. Burton, R. A., Zhang, X. Q., Hrmova, M., and Fincher, G. B. (1999) A single limit dextrinase gene is expressed both in the developing endosperm and in germinated grains of barley, *Plant Physiol. 119*, 859–871.

10. Hardie, D. G. (1975) Control of carbohydrase formation by gibberellic acid in barley endosperm, *Phytochemistry 14*, 1719–1722.

11. Manners, D. J., and Yellowlees, D. (1971) Studies on carbohydrate metabolising enzymes. XXVI Limit dextrinase from germinated barley, *Starch/Stärke 23*, 228–234.

12. Kristensen, M., F. Lok, V. Planchot, I. Svendsen, R. Leah, B. Svensson. (1999) Isolation and characterization of the gene encoding the starch debranching

enzyme limit dextrinase from germinating barley, *Biochim. Biophys. Acta 1431*, 538–546.

13. Schroeder, S. W., and MacGregor, A. W. (1998) Synthesis of limit dextrinase in germinated barley kernels and aleurone tissues, *J. Am. Soc. Brew. Chem. 56*, 32–37.

14. Dinges, J. R., Colleoni, C., James, M. G., and Myers, A. M. (2003) Mutational analysis of the pullulanase-type debranching enzyme of maize indicates multiple functions in starch metabolism, *Plant Cell 15*, 666–680.

15. Delatte, T., Umhang, M., Trevisan, M., Eicke, S., Thorneycroft, D., Smith, S. M., and Zeeman, S. C. (2006) Evidence for distinct mechanisms of starch granule breakdown in plants, *J. Biol. Chem. 281*, 12050–12059.

16. Sissons, M. J., Lance, R. C. M., and Sparrow, D. H. B. (1993) Studies on limit dextrinase in barley. 3. Limit dextrinase in developing kernels, *J. Cereal Sci. 1993*, 19–24.

17. Martin, C., and Smith, A. M. (1995) Starch synthesis, *Plant Cell 7*, 971–985.

18. Smith, A. M. (2001) The biosynthesis of starch granules, *Biomacromolecules 2*, 335–341.

19. Streb, S., Delatte, T., Umhang, M., Eicke, S., Schorderet, M., Reinhardt, D., and Zeeman, S. C. (2008) Starch granule biosynthesis in *Arabidopsis* is abolished by removal of all debranching enzymes but restored by the subsequent removal of an endoamylase, *Plant Cell 20*, 3448–3466.

20. Fujita, N., Kubo, A., Suh, D. S., Wong, K. S., Jane, J. L., Ozawa, K., Takaiwa, F., Inaba, Y., and Nakamura, Y. (2003) Antisense inhibition of isoamylase alters the structure of amylopectin and the physicochemical properties of starch in rice endosperm, *Plant Cell Physiol. 44*, 607–618.

21. Fujita, N., Toyosawa, Y., Utsumi, Y., Higuchi, T., Hanashiro, I., Ikegami, A., Akuzawa, S., Yoshida, M., Mori, A., Inomata, K., Itoh, R., Miyao, A., Hirochika, H., Satoh, H., and Nakamura, Y. (2009) Characterization of pullulanase (PUL)-deficient mutants of rice (*Oryza sativa* L.) and the function of PUL on starch biosynthesis in the developing rice endosperm, *J. Exp. Bot. 60*, 1009–1023.

22. Wu, C., Colleoni, C., Myers, A. M., and James, M. G. (2002) Enzymatic properties and regulation of ZPU1, the maize pullulanase-type starch debranching enzyme, *Arch. Biochem. Biophys. 406*, 21–32.

23. Renz, A., Schikora, S., Schmid, R., Kossmann, J., and Beck, E. (1998) cDNA sequence and heterologous expression of monomeric spinach pullulanase:

multiple isomeric forms arise from the same polypeptide, *Biochem. J. 331* 937–945.

24. Repellin, A., Baga, M., and Chibbar, R. N. (2008) *In vitro* pullulanase activity of wheat (*Triticum aestivum* L.) limit-dextrinase type starch debranching enzyme is modulated by redox conditions, *J. Cereal Sci. 47*, 302–309.

25. Tibbot, B. K., Henson, C. A., and Skadsen, R. W. (1998) Expression of enzymatically active, recombinant barley α-glucosidase in yeast and immunological detection of α-glucosidase from seed tissue, *Plant Mol. Biol. 38*, 379–391.

26. Naested, H., Kramhøft, B., Lok, F., Bojsen, K., Yu, S., and Svensson, B. (2006) Production of enzymatically active recombinant full-length barley high pI α-glucosidase of glycoside family 31 by high cell-density fermentation of *Pichia pastoris* and affinity purification, *Protein Expr. Purif. 46*, 56–63.

27. Jespersen, H. M., MacGregor, E. A., Sierks, M. R., and Svensson, B. (1991) Comparison of the domain-level organization of starch hydrolases and related enzymes, *Biochem. J. 280* 51–55.

28. MacGregor, E. A., Janecek, S., and Svensson, B. (2001) Relationship of sequence and structure to specificity in the α-amylase family, *Biochim. Biophys. Acta 1546*, 1–20.

29. Matsuura, Y., Kusunoki, M., Harada, W., and Kakudo, M. (1984) Structure and possible catalytic residues of TAKA-amylase A, *J. Biochem. 95*, 697–702.

30. Machovič, M., and Janeček, Š. (2008) Domain evolution in the GH13 pullulanase subfamily with focus on the carbohydrate-binding module family 48, *Biologia 63*, 1053–1064.

31. Mikami, B., Iwamoto, H., Malle, D., Yoon, H. J., Demirkan-Sarikaya, E., Mezaki, Y., and Katsuya, Y. (2006) Crystal structure of pullulanase: evidence for parallel binding of oligosaccharides in the active site, *J. Mol. Biol. 359*, 690–707.

32. Turkenburg, J. P., Brzozowski, A. M., Svendsen, A., Borchert, T. V., Davies, G. J., and Wilson, K. S. (2009) Structure of a pullulanase from *Bacillus acidopullulyticus*, *Proteins 76*, 516–519.

33. Finn, R. D., Tate, J., Mistry, J., Coggill, P. C., Sammut, S. J., Hotz, H. R., Ceric, G., Forslund, K., Eddy, S. R., Sonnhammer, E. L. L., and Bateman, A. (2008) The Pfam protein families database, *Nucleic Acids Res. 36*, D281–D288.

34. Gouet, P., Courcelle, E., Stuart, D. I., and Metoz, F. (1999) ESPript: multiple sequence alignments in PostScript, *Bioinformatics 15*, 305–308.

35. Davies, G., and Henrissat, B. (1995) Structures and mechanisms of glycosyl hydrolases, *Structure 3*, 853–859.

36. Yamashita, M., Matsumoto, D., and Murooka, Y. (1997) Amino acid residues specific for the catalytic action towards α-1,6-glucosidic linkages in *Klebsiella pullulanase*, *J. Ferment. Bioeng. 84*, 283–290.

37. Greffe, L., Jensen, M. T., Bosso, C., Svensson, B., and Driguez, H. (2003) Chemoenzymatic synthesis of branched oligo- and polysaccharides as potential substrates for starch active enzymes, *ChemBioChem. 4*, 1307–1311.

38. Kainuma, K., Kobayashi, S., and Harada, T. (1978) Action of *Pseudomonas isoamylase* on various branched oligo- and poly-saccharides, *Carbohydr. Res. 61*, 345–357.

39. Abdullah, M., Catley, B. J., Lee, E. Y. C., Robyt, J., Wallenfels. K, and Whelan, W. J. (1966) Mechanism of carbohydrase action.11. Pullulanase an enzyme specific for hydrolysis of α-1,6-bonds in amylaceous oligo- and polysaccharides, *Cereal Chem. 43*, 111–118.

40. Abdullah, M., and French, D. (1970) Substrate specificity of pullulanase, *Arch. Biochem. Biophys. 137*, 483–493.

41. Jensen, M. T. (2004) Structure and function of barley limit dextrinase. Mutational analysis of barley α-amylase isozyme differences and interaction with branched oligosaccharides, in *Institute of Biochemistry and Molecular Biology*, p 171, University of Southern Denmark, DK-5230 Odense M.

42. McDougall, G. J., Ross, H. A., Swanston, J. S., and Davies, H. V. (2004) Limit dextrinase from germinating barley has endotransglycosylase activity, which explains its activation by maltodextrins, *Planta 218*, 542–551.

43. Yamasaki, Y., Nakashima, S., and Konno, H. (2008) Pullulanase from rice endosperm, *Acta Biochim. Pol. 55*, 507–510.

44. Yoshimura, Y., Kitahata, S., and Okada, S. (1988) Effects of temperature on 6-*O*-α-maltosyl cyclodextrin production from α-maltosyl fluoride and cyclodextrins *Agric. Biol. Chem. 52*, 1655–1659.

45. Kang, H. K., Cha, H., Yang, T. J., Park, J. T., Lee, S., Kim, Y. W., Auh, J. H., Okada, Y., Kim, J. W., Cha, J., Kim, C. H., and Park, K. H. (2008) Enzymatic synthesis of dimaltosyl-β-cyclodextrin via a transglycosylation reaction using TreX, a *Sulfolobus solfataricus* P2 debranching enzyme, *Biochem. Biophys. Res. Commun. 366*, 98–103.

46. Longstaff, M. A., and Bryce, J. H. (1993) Development of limit dextrinase in germinated barley (*Hordeum vulgare* L.) (evidence of proteolytic activation), *Plant Physiol. 101*, 881–889.

47. MacGregor, A. W., Macri, L. J., Schroeder, S. W., and Bazin, S. L. (1994) Limit dextrinase from malted barley: extraction, purification and characterization, *Cereal Chem. 71*, 610–617.

48. MacGregor, A. W., Macri, L. J., and Bazin, S. L. (1995) Limit dextrinase in barley and malt and its possible role in malting and brewing, in *Proceedings of the 25th Congress* (Wijngaarden, M. v., Ed.), pp 185–192, European Brewery Convention, Brussels, Belgium.

49. Wong, J. H., Iiao, I. A., Kobrehel, K., and Buchanan, B. B. (1995) Thioredoxin-dependent deinhibition of pullulanase of barley malt by inactivation of a specific inhibitor protein, *Plant Physiol. 108*, 67–67.

50. Franco, O. L., Rigden, D. J., Melo, F. R., and Grossi-de-Sa, M. F. (2002) Plant α-amylase inhibitors and their interaction with insect α-amylases - structure, function and potential for crop protection, *Eur. J. Biochem. 269*, 397–412.

51. Oneda, H., Lee, S., and Inouye, K. (2004) Inhibitory effect of 0.19 α-amylase inhibitor from wheat kernel on the activity of porcine pancreas α-amylase and its thermal stability, *J. Biochem. 135*, 421–427.

52. Svensson, B., Fukuda, K., Nielsen, P. K., and Bonsager, B. C. (2004) Proteinaceous α-amylase inhibitors, *Biochim. Biophys. Acta 1696*, 145–156.

53. Murzin, A. G., Brenner, S. E., Hubbard, T., and Chothia, C. (1995) SCOP - a structural classification of proteins database for the investigation of sequences and structures, *J. Mol. Biol. 247*, 536–540.

54. Franco, O. L., Rigden, D. J., Melo, F. R., Bloch, C., Silva, C. P., and Grossi-de-Sa, M. F. (2000) Activity of wheat α-amylase inhibitors towards bruchid α-amylases and structural explanation of observed specificities, *Eur. J. Biochem. 267*, 2166–2173.

55. Payan, F. (2004) Structural basis for the inhibition of mammalian and insect α-amylases by plant protein inhibitors, *Biochim. Biophys. Acta 1696*, 171–180.

56. Alam, N., Gourinath, S., Dey, S., Srinivasan, A., and Singh, T. P. (2001) Substrate-inhibitor interactions in the kinetics of α-amylase inhibition by Ragi α-amylase/trypsin inhibitor (RATI) and its various N-terminal fragments, *Biochemistry 40*, 4229–4233.

57. MacGregor, A. W., Donald, L. J., MacGregor, E. A., and Duckworth, H. W. (2003) Stoichiometry of the complex formed by barley limit dextrinase with its

endogenous inhibitor. Determination by electrospray time-of-flight mass spectrometry, *J. Cereal Sci. 37*, 357–362.

58. Maskos, K., Huber-Wunderlich, M., and Glockshuber, R. (1996) RBI, a one-domain α-amylase/trypsin inhibitor with completely independent binding sites, *FEBS Lett. 397*, 11–16.

59. Strobl, S., Maskos, K., Wiegand, G., Huber, R., Gomis-Rüth, F. X., and Glockshuber, R. (1998) A novel strategy for inhibition of α-amylases: yellow meal worm α-amylase in complex with the Ragi bifunctional inhibitor at 2.5 Å resolution, *Structure 6*, 911–921.

60. Takase, K. (1994) Site-directed mutagenesis reveals critical importance of the catalytic site in the binding of α-amylase by wheat proteinaceous inhibitor, *Biochemistry 33*, 7925–7930.

61. MacGregor, E. A., Bazin, S. L., Ens, E. W., Lahnstein, J., Macri, L. J., Shirley, N. J., and MacGregor, A. W. (2000) Structural models of limit dextrinase inhibitors from barley, *J. Cereal Sci. 31*, 79–90.

62. MacGregor, A. W., Macri, L. J., Schroeder, S. W., and Bazin, S. L. (1994) Purification and characterization of limit dextrinase inhibitors from barley, *J. Cereal Sci. 20*, 33–41.

63. McCafferty, C. A., Jenkinson, H. R., Brosnan, J. M., and Bryce, J. H. (2004) Limit dextrinase - does its malt activity relate to its activity during brewing, *J. Inst. Brew. 110*, 284–296.

64. Enevoldsen, B. S. (1978) Degradation of Starch by Amylases in Beer Brewing, *J. Jpn. Soc. Starch Sci. 25*, 89-99.

65. Enevoldsen, B. S. (1978) Degradation of starch by amylases in beer brewing, *J. Jpn. Soc. Starch Sci. 25*.

66. Sissons, M., Taylor, M., and Proudlove, M. (1995) Barley malt limit dextrinase - its extraction, heat-stability, and activity during malting and mashing, *J. Am. Soc. Brew. Chem. 53*, 104–110.

67. Yang, X., Westcott, S., Gong, X., Evans, E., Zhang, X.-Q., Lance, R. C. M., and Li, C. (2009) Amino acid substitutions of the limit dextrinase gene in barley are associated with enzyme thermostability, *Mol. Breeding 23*, 61–74.

68. MacWilliam, I. C., and Harris, G. (1959) The separation of limit dextrinase from R-enzyme and aspects of the activity of the separated enzymes, *Arch. Biochem. Biophys. 84*, 442–454.

69. Sambrook, J., and Russell, D. (2001) *Molecular cloning, a laboratory manual.*, 3 ed., Cold Spring Harbour Laboratory Press, Cold Spring Habour, New York.

70. Vester-Christensen, M. B., Abou Hachem, M., Naested, H., and Svensson, B. (2009) Secretory expression of functional barley limit dextrinase by *Pichia pastoris* using high cell-density fermentation, *Protein Expr. Purif. In press doi: 10.1016/j.pep.2009.08.016*.

71. Invitrogen. (2008) *Pichia* expression kit, a manual of methods for expression of recombinant proteins in *Pichia pastoris* Invitrogen manual K1710-01; www.Invitrogen.Com.

72. Kristensen, M., Planchot, V., Abe, J. I., and Svensson, B. (1998) Large-scale purification and characterization of barley limit dextrinase, a member of the α-amylase structural family, *Cereal Chem. 75*, 473–479.

73. Stratton, J., Chiruvolu, V., and Meager, M. (1998) High cell-density fermentation, in *Pichia protocols. Methods in molecular biology* (Higgings, D. R., and Cregg, J. M., Eds.), pp 107–120, Humana Press inc., Totowa, NJ.

74. Invitrogen. (2008) *Pichia* fermentation process guidelines; www.invitrogen.com.

75. Stahl, Y., Coates, S., Bryce, J. H., and Morris, P. C. (2004) Antisense downregulation of the barley limit dextrinase inhibitor modulates starch granule size distribution, starch composition and amylopectin structure, *Plant J. 39*, 599–611.

76. McCleary, B. V. (1992) Measurement of the content of limit dextrinase in cereal flours, *Carbohydr. Res. 227*, 257–268.

77. Fox, J. D., and Robyt, J. F. (1991) Miniaturizing of three carbohydrate analyses a microsample plate reader, *Anal. Biochem. 195*, 93–96.

78. de Melo, E. B., Gomes, A. D., and Carvalho, I. (2006) α- and β-Glucosidase inhibitors: chemical structure and biological activity, *Tetrahedron 62*, 10277–10302.

79. Oudjeriouat, N., Moreau, Y., Santimone, M., Svensson, B., Marchis-Mouren, G., and Desseaux, V. (2003) On the mechanism of α-amylase - acarbose and cyclodextrin inhibition of barley amylase isozymes, *Eur. J. Biochem. 270*, 3871–3879.

80. Myszka, D. G., He, X., Dembo, M., Morton, T. A., and Goldstein, B. (1998) Extending the range of rate constants available from BIACORE: Interpreting mass transport-influenced binding data, *Biophys. J. 75*, 583–594.

81. Candiano, G., Bruschi, M., Musante, M., Santucci, L., Ghiggeri, G. M., Carnemolla, B., Orecchia, P., Zardi, L., and Righetti, P. G. (2004) Blue silver: Avery sensitive colloidal Coomassie G-250 staining for proteome analysis, *Electrophoresis 25*, 1327−1333.

82. Gobom, J., Nordhoff, E., Mirgorodskaya, E., Ekman, R., and Roepstorff, P. (1999) Sample purification and preparation technique based on nano-scale reversed-phase columns for the sensitive analysis of complex peptide mixtures by matrix-assisted laser desorption/ionization mass spectrometry, *J. Mass Spectrom. 34*, 105−116.

83. Rist, W., Mayer, M. P., Andersen, J. S., Roepstorff, P., and Jorgensen, T. J. D. (2005) Rapid desalting of protein samples for on-line microflow electrospray ionization mass spectrometry, *Anal. Biochem. 342*, 160−162.

84. Barkholt, V., and Jensen, A. L. (1989) Amino-acid analysis - determination of cysteine plus half-cystine in proteins after hydrochloric-acid hydrolysis with a disulfide compound as additive, *Anal. Biochem. 177*, 318–322.

85. DeLano, W. L. (2002) The PyMOL Molecular Graphics System, 1.1 ed., DeLano Scientific, Palo Alto, CA, USA.

86. Wallner, B., and Elofsson, A. (2003) Can correct protein models be identified?, *Protein Sci. 12*, 1073−1086.

87. Leslie, A. G. W. (1992) *Joint CCP4 and ESF-EAMCB Newsletter on Protein Crystallography No. 26*.

88. **CCP4**. (1994) The CCP4 Suite: Programs for Protein Crystallography, *Acta Crystallogr. D Biol. Crystallogr. 50*, 760−763.

89. Potterton, E., Briggs, P., Turkenburg, M., and Dodson, E. (2003) A graphical user interface to the CCP4 program suite, *Acta Crystallogr. D Biol. Crystallogr. 59*, 1131−1137.

90. McCoy, A. J., Grosse-Kunstleve, R. W., Adams, P. D., Winn, M. D., Storoni, L. C., and Read, R. J. (2007) Phaser crystallographic software, *J. Appl. Crystallogr. 40*, 658−674.

91. Adams, P. D., Grosse-Kunstleve, R. W., Hung, L. W., Ioerger, T. R., McCoy, A. J., Moriarty, N. W., Read, R. J., Sacchettini, J. C., Sauter, N. K., and Terwilliger, T. C. (2002) PHENIX: building new software for automated crystallographic structure determination, *Acta Crystallogr. D Biol. Crystallogr. 58*, 1948−1954.

92. Painter, J., and Merritt, E. A. (2006) Optimal description of a protein structure in terms of multiple groups undergoing TLS motion, *Acta Crystallogr. D Biol. Crystallogr. 62*, 439−450.

93. Emsley, P., and Cowtan, K. (2004) Coot: model-building tools for molecular graphics, *Acta Crystallogr. D Biol. Crystallogr. 60*, 2126–2132.

94. Laskowski, R. A., Macarthur, M. W., Moss, D. S., and Thornton, J. M. (1993) Procheck - a program to check the stereochemical quality of protein structures, *J. Appl. Crystallogr. 26*, 283–291.

95. Davis, I. W., Leaver-Fay, A., Chen, V. B., Block, J. N., Kapral, G. J., Wang, X., Murray, L. W., Arendall, W. B., Snoeyink, J., Richardson, J. S., and Richardson, D. C. (2007) MolProbity: all-atom contacts and structure validation for proteins and nucleic acids, *Nucleic Acids Res. 35*, W375–W383.

96. Hutchinson, E. G., and Thornton, J. M. (1996) PROMOTIF - A program to identify and analyze structural motifs in proteins, *Protein Sci. 5*, 212–220.

97. Kristensen, M., Lok, F., Planchot, V., Svendsen, I., Leah, R., and Svensson, B. (1999) Isolation and characterization of the gene encoding the starch debranching enzyme limit dextrinase from germinating barley, *Biochim.Biophys.Acta 1431*, 538-546.

98. Hastie, T., Friedman, J., and Tibshirani, R. (2001) *The elements of statistical learning: Data mining, inference, and prediction*, Springer, New York, NY.

99. Baumann, M. J., Eklof, J. M., Michel, G., Kallas, A. M., Teeri, T. T., Czjzek, M., and Brumer, H. (2007) Structural evidence for the evolution of xyloglucanase activity from xyloglucan endo-transglycosylases: Biological implications for cell wall metabolism, *Plant Cell 19* 1947–1963.

100. Brumer, H., Sims, P. F. G., and Sinnott, M. L. (1999) Lignocellulose degradation by *Phanerochaete chrysosporium*: Purification and characterization of the main α-galactosidase, *Biochem. J. 339*, 43–53.

101. Iwamoto, H., Ohno, M., Ohmori, M., Hirose, J., Tanaka, A., Sakai, S., and Hiromi, K. (1994) Comparison of the binding of β-cyclodextrin and α-cyclodextrin and γ-cyclodextrin with pullulanase from *Klebsiella pneumoniae* as studied by equilibrium and kinetic fluorometry, *J. Biochem. 116*, 1264–1268.

102. Gourinath, S., Alam, N., Srinivasan, A., Betzel, C., and Singh, T. P. (1999) Structure of the bifunctional inhibitor of trypsin and α-amylase from ragi seeds at 2.2 Å resolution, *Acta Crystallogr. D Biol. Crystallogr. 56*, 287–293.

103. Koren, R., and Hammes, G. G. (1976) Kinetic study of protein-protein interactions, *Biochemistry 15*, 1165–1170.

104. Northrup, S. H., and Erickson, H. P. (1992) Kinetics of protein-protein association explained by Brownian dynamics computer-simulation, *Proc. Natl. Acad. Sci. U. S. A. 89*, 3338–3342.

105. Dominguez, F., and Cejudo, F. J. (1999) Patterns of starchy endosperm acidification and protease gene expression in wheat grains following germination, *Plant Physiol. 119*, 81–87.

106. Sinjorgo, K. M. C., Devries, M. A., Heistek, J. C., Vanzeijl, M. J., Vanderveen, S. W., and Douma, A. C. (1993) The effect of external pH on the gibberelic-acid response of barley aleurone, *J. Plant Physiol. 142*, 506–509.

107. Cristobal, S., Zemla, A., Fischer, D., Rychlewski, L., and Elofsson, A. (2001) A study of quality measures for protein threading models, *BMC Bioinformatics 2*, 5.

108. Oda, Y., Matsunaga, T., Fukuyama, K., Miyazaki, T., and Morimoto, T. (1997) Tertiary and quaternary structures of 0.19 α-amylase inhibitor from wheat kernel determined by X-ray analysis at 2.06 Å resolution, *Biochemistry 36*, 13503–13511.

109. Kadziola, A., Abe, J.-I., Svensson, B., and Haser, R. (1994) Crystal and molecular structure of barley α-amylase, *J. Mol. Biol. 239*, 104–121.

110. Jespersen, H. M., MacGregor, E. A., Henrissat, B., Sierks, M. R., and Svensson, B. (1993) Starch- and glycogen-debranching and branching enzymes: prediction of structural features of the catalytic $(\beta/\alpha)_8$-barrel domain and evolutionary relationship to other amylolytic enzymes, *J. Protein Chem. 12*, 791–805.

111. Davies, G. J., Wilson, K. S., and Henrissat, B. (1997) Nomenclature for sugar-binding subsites in glycosyl hydrolases, *Biochem. J. 321*, 557–559.

112. Wallace, A. C., Laskowski, R. A., and Thornton, J. M. (1995) LIGPLOT: A program to generate schematic diagrams of protein-ligand interactions, *Prot. Eng. 8*, 127–134.

113. Fushinobu, S., Hidaka, M., Honda, Y., Wakagi, T., Shoun, H., and Kitaoka, M. (2005) Structural basis for the specificity of the reducing end xylose-releasing exo-oligoxylanase from *Bacillus halodurans* C-125, *J. Biol. Chem. 280*, 17180–17186.

114. Hidaka, M., Kitaoka, M., Hayashi, K., Wakagi, T., Shoun, H., and Fushinobu, S. (2006) Structural dissection of the reaction mechanism of cellobiose phosphorylase, *Biochem. J. 398*, 37–43.

115. Haruhide, M., Bak-Jensen, K. S., Gottschalk, T. E., Motawia, M. S., Damager, I., Møller, B. L., and Svensson, B. (2001) Modulation of activity and substrate binding modes by mutation of single and double subsites+1/+2 and-5/-6 of barley α-amylase 1, *Eur. J. Biochem. 268*, 6545–6558.

116. Jahic, M., Wallberg, F., Bollok, M., Garcia, P., and Enfors, S. (2003) Temperature limited fed-batch technique for control of proteolysis in *Pichia pastoris* bioreactor cultures, *Microb. Cell Fact. 2*, 1–11.

117. Whittaker, M. M., and Whittaker, J. W. (2000) Expression of recombinant galactose oxidase by *Pichia pastoris*, *Protein Expr. Purif. 20*, 105–111.

118. Woo, J. H., Stavrou, Y. Y., Liu, S., and Neville, D. M. (2004) Increasing secretion of a bivalent anti-T-cell immunotoxin by *Pichia pastoris*, *Appl. Environ. Microbiol. 70*, 3370–3376.

119. Gasser, B., Saloheimo, M., Rinas, U., Dragosits, M., Rodríguez-Carmona, E., Baumann, K., Giuliani, M., Parrilli, E., Branduardi, P., Lang, C., Porro, D., Ferrer, P., Tutino, M., Mattanovich, D., and Villaverde, A. (2008) Protein folding and conformational stress in microbial cells producing recombinant proteins: A host comparative overview., *Microb. Cell Fact. 7*, 1–18.

120. MacGregor, A. W., Bazin, S. L., Macri, L. J., and Babb, J. V. (1999) Modelling the contribution of α-amylase, β-amylase and limit dextrinase to starch degradation during mashing, *J. Cereal Sci. 29*, 161–169.

121. Ross, H. A., Sungurtas, J., Ducreux, L., Swanston, J. S., Davies, H. V., and McDougall, G. J. (2003) Limit dextrinase in barley cultivars of differing malting quality: Activity, inhibitors and limit dextrin profiles, *J. Cereal Sci. 38*, 325–334.

122. Greffe, L., Jensen, M. T., Chang-Pi-Hin, F., Fruchard, S., O'Donohue, M. J., Svensson, B., and Driguez, H. (2002) Chemoenzymatic syntheses of linear and branched hemithiomaltodextrins as potential inhibitors for starch-debranching enzymes, *Chem. Eur. J. 8*, 5447–5455.

123. Crittenden, R. G., and Playne, M. J. (1996) Production, properties and applications of food-grade oligosaccharides, *Trends Food Sci. Technol. 7*, 353–361.

124. Kaneko, T., Kohmoto, T., Kikuchi, H., Shiota, M., Iino, H., and Mitsuoka, T. (1994) Effects of isomaltooligosaccharides with different degrees of polymerization on human fecal bifidobacteria, *Biosci. Biotechnol. Biochem. 58*, 2288–2290.

125. Lillelund, V. H., Jensen, H. H., Liang, X. F., and Bols, M. (2002) Recent developments of transition-state analogue glycosidase inhibitors of non-natural product origin, *Chem. Rev. 102*, 515–553.

126. Woo, E. J., Lee, S., Cha, H., Park, J. T., Yoon, S. M., Song, H. N., and Park, K. H. (2008) Structural insight into the bifunctional mechanism of the glycogen-

debranching enzyme TreX from the archaeon *Sulfolobus solfataricus, J. Biol. Chem. 283,* 28641–28648.

127. Davies, G. J., Brzozowski, A. M., Dauter, Z., Rasmussen, M. D., Borchert, T. V., and Wilson, K. S. (2005) Structure of a *Bacillus halmapalus* family 13 α-amylase, BHA, in complex with an acarbose-derived nonasaccharide at 2.1 A resolution, *Acta Crystallogr. D Biol. Crystallogr. 61*, 190–193.

128. Okuyama, M., Mori, H., Watanabe, K., Kimura, A., and Chiba, S. (2002) α-glucosidase mutant catalyzes "α-glycosynthase"-type reaction, *Biosci. Biotechnol. Biochem. 66*, 928–933.

129. Okada, Y., Koizumi, K., and Kitahata, S. (1994) Separation and characterization of five positional isomers of trimaltosyl-cyclomaltoheptaose (trimaltosyl-β-cyclodextrin), *Carbohydr. Res. 254*, 1–13.

130. Challa, R., Ahuja, A., Ali, J., and Khar, R. K. (2005) Cyclodextrins in drug delivery: An updated review, *AAPS PharmSciTech 6*, 329–357.

131. Szente, L., and Szejtli, J. (2004) Cyclodextrins as food ingredients, *Trends Food Sci. Tech. 15*, 137–142.

132. Bellincampi, D., Camardella, L., Delcour, J. A., Desseaux, V., D'Ovidio, R., Durand, A., Elliot, G., Gebruers, K., Giovane, A., Juge, N., Sorensen, J. F., Svensson, B., and Vairo, D. (2004) Potential physiological role of plant glycosidase inhibitors, *Biochim. Biophys. Acta 1696*, 265–274.

133. Mundy, J., Svendsen, I. B., and Hejgaard, J. (1983) Barley α-amylase-subtilisin inhibitor.1. Isolation and characterization, *Carlsberg Res. Commun. 48*, 81–90.

134. Sorensen, J. F., Kragh, K. M., Sibbesen, O., Delcour, J. A., Goesaert, H., Svensson, B., Tahir, T. A., Brufau, J., Perez-Vendrell, A. M., Bellincampi, D., D'Ovidio, R., Camardella, L., Giovane, A., Bonnin, E., and Juge, N. (2004) Potential role of glycosidase inhibitors in industrial biotechnological applications, *Biochim. Biophys. Acta 1696*, 275–287.

135. Bønsager, B. C. (2007) Proteome analysis of dissected barley seed tissues during germination and radicle elongation & heterologous expression of barley limit dextrinase inhibitor, in *Ph.D Thesis, Department of Chemistry, Carlsberg Laboratory & Enzyme and Protein Chemistry, BioCentrum-DTU*, p 98, Technical University of Denmark, DK-2800 Kgs. Lyngby.

136. De Schutter, K., Lin, Y. C., Tiels, P., Van Hecke, A., Glinka, S., Weber-Lehmann, J., Rouze, P., de Peer, Y. V., and Callewaert, N. (2009) Genome sequence of the recombinant protein production host *Pichia pastoris, Nat. Biotechnol. 27*, 561–566.

137. Bonsager, B. C., Nielsen, P. K., Abou Hachem, M., Fukuda, K., Praetorius-Ibba, M., and Svensson, B. (2005) Mutational analysis of target enzyme recognition of the β-trefoil fold barley α-amylase/subtilisin inhibitor, *J. Biol. Chem. 280*, 14855–14864.

138. Vallée, F., Kadziola, A., Bourne, Y., Juy, M., Rodenburg, K. W., Svensson, B., and Haser, R. (1998) Barley α-amylase bound to its endogenous protein inhibitor BASI: crystal structure of the complex at 1.9 angstrom resolution, *Structure 6*, 649–659.

139. Vester-Christensen, M. B., Abou Hachem, M., Svensson, B., and Henriksen, A. (2009) Crystal structure of barley limit dextrinase. A debranching enzyme involved in starch synthesis and breakdown, *J. Biol. Chem. To be submitted*.

140. Garcia-Maroto, F., Carbonero, P., and Garcia-Olmedo, F. (1991) Site-directed mutagenesis and expression in *Escherichia coli* of WMAI-1, a wheat monomeric inhibitor of insect α-amylase, *Plant Mol. Biol. 17*, 1005–1011.

141. Selzer, T., Albeck, S., and Schreiber, G. (2000) Rational design of faster associating and tighter binding protein complexes, *Nat. Struct. Biol. 7*, 537–541.

142. Stites, W. E. (1997) Protein-protein interactions: Interface structure, binding thermodynamics, and mutational analysis, *Chem. Rev. 97*, 1233–1250.

143. Takahashi, K., and Fukada, H. (1985) Calorimetric studies of the binding of *Streptomyces* subtilisin inhibitor to subtilisin of *Bacillus subtilis* strain N', *Biochemistry 24*, 297–300.

144. Needleman, S. B., and Wunsch, C. D. (1970) A general method applicable to search for similarities in amino acid sequence of two proteins, *J. Mol. Biol. 48*, 443–453.

145. Bender, H., and K., W. (1966) Pullulanase (an amylopectin and glycogen debranching enzyme) from *Aerobacter aerogenes*, *Methods Enzymol. 8*, 555–559.

146. Shim, J.-H., Park, J.-T., Hong, J.-S., Kim, K. W., Kim, M.-J., Auh, J.-H., Kim, Y.-W., Park, C.-S., Boos, W., Kim, J.-W., and Park, K.-H. (2009) Role of maltogenic amylase and pullulanase in maltodextrin and glycogen Metabolism of *Bacillus subtilis* 168, *J. Bacteriol. 191*, 4835–4844.

147. Nakamura, Y. (1996) Some properties of starch debranching enzymes and their possible role in amylopectin biosynthesis, *Plant Sci. 121*, 1–18.

148. Penninga, D., vanderVeen, B. A., Knegtel, R. M. A., vanHijum, S., Rozeboom, H. J., Kalk, K. H., Dijkstra, B. W., and Dijkhuizen, L. (1996) The raw starch binding domain of cyclodextrin glycosyltransferase from *Bacillus circulans* strain 251, *J. Biol. Chem. 271*, 32777–32784.

149. Sorimachi, K., Le Gal-Coëffet, M. F., Williamson, G., Archer, D. B., and Williamson, M. P. (1997) Solution structure of the granular starch binding domain of *Aspergillus niger* glucoamylase bound to β-cyclodextrin, *Structure 5*, 647–661.

150. Harding, M. M. (2001) Geometry of metal-ligand interactions in proteins, *Acta Crystallogr. D Biol. Crystallogr. 57*, 401–411.

151. Boel, E., Brady, L., Brzozowski, A. M., Derewenda, Z., Dodson, G. G., Jensen, V. J., Petersen, S. B., Swift, H., Thim, L., and Woldike, H. F. (1990) Calcium-binding in α-amylase - an X-ray-diffraction study at 2.1 Å resolution of two enzymes from *Aspergillus*, *Biochemistry 29*, 6244–6249.

152. Katsuya, Y., Mezaki, Y., Kubota, M., and Matsuura, Y. (1998) Three-dimensional structure of *Pseudomonas* isoamylase at 2.2 Å resolution, *J. Mol. Biol. 281*, 885–897.

153. Hondoh, H., Kuriki, T., and Matsuura, Y. (2003) Three-dimensional structure and substrate binding of *Bacillus stearothermophilus* neopullulanase, *J. Mol. Biol. 326*, 177–188.

154. Abad, M. C., Binderup, K., Rios-Steiner, J., Arni, R. K., Preiss, J., and Geiger, J. H. (2002) The X-ray crystallographic structure of *Escherichia coli* branching enzyme, *J. Biol. Chem. 277*, 42164–42170.

155. Dinges, J. R., Colleoni, C., Myers, A. M., and James, M. G. (2001) Molecular structure of three mutations at the maize sugary1 locus and their allele-specific phenotypic effects, *Plant Physiol. 125*, 1406–1418.

7 Appendix

7.1 Mass Spectra from Transglycosylation

7.1.1 Donor: α-Maltosyl Fluoride, Acceptor: Maltose

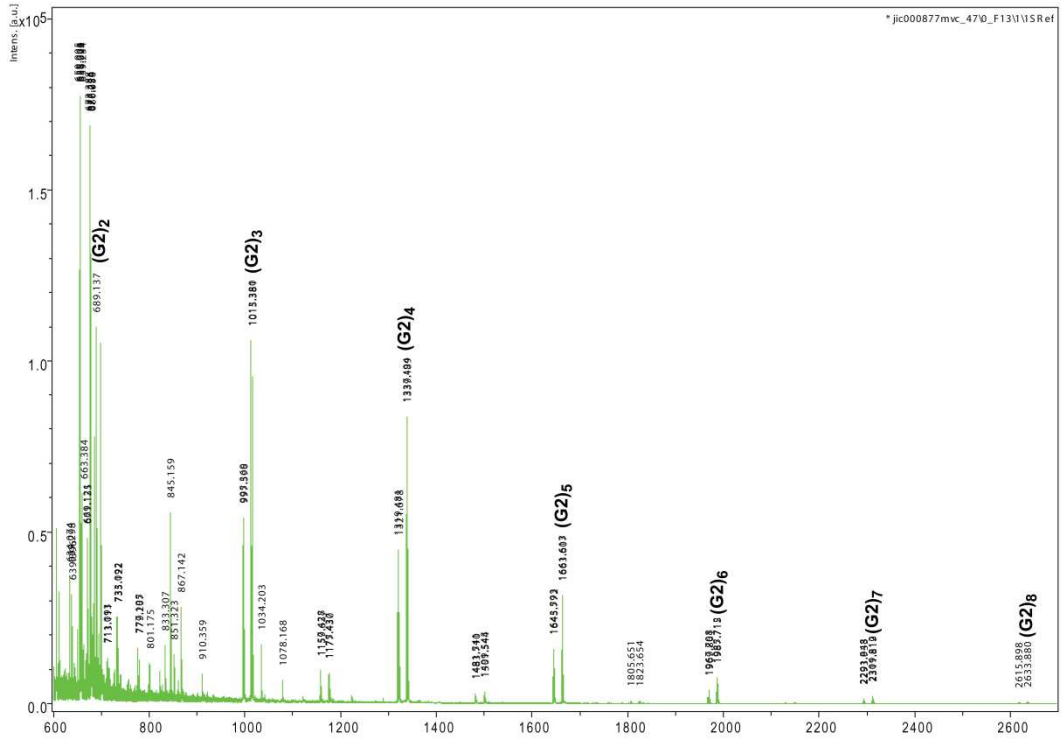

7.1.2 Donor: α-Maltosyl Fluoride, Acceptor: 4-*O*-α-D-glucopyranosylmoranoline

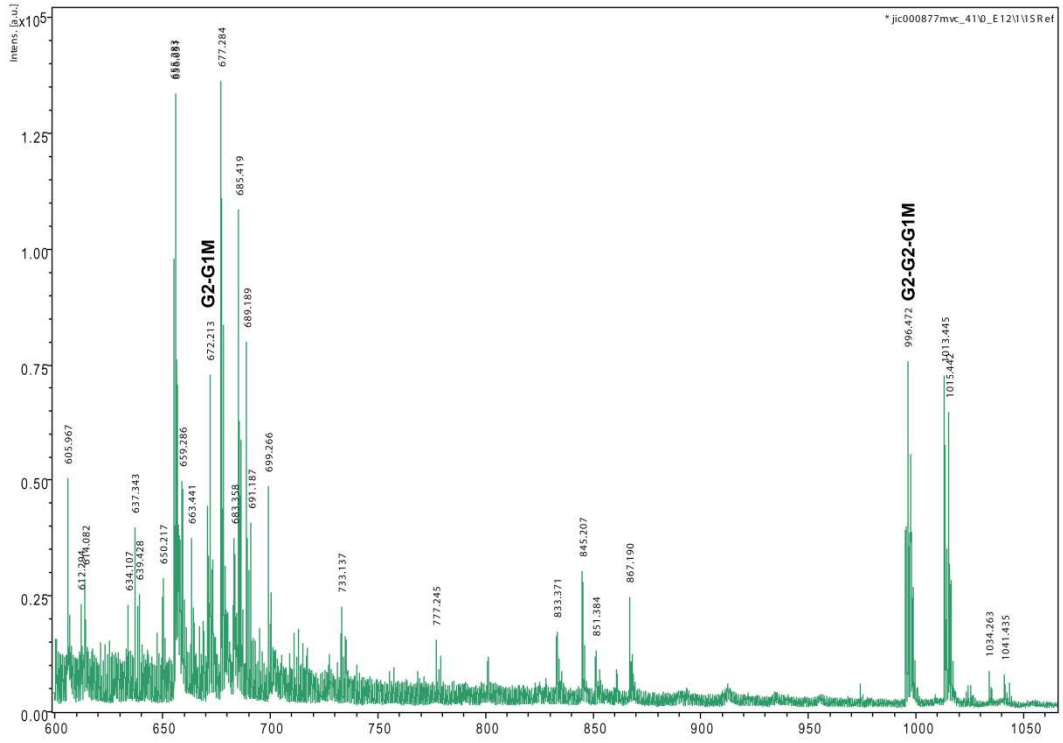

7.1.3 Donor: α-Maltosyl Fluoride, Acceptor: Acarbose

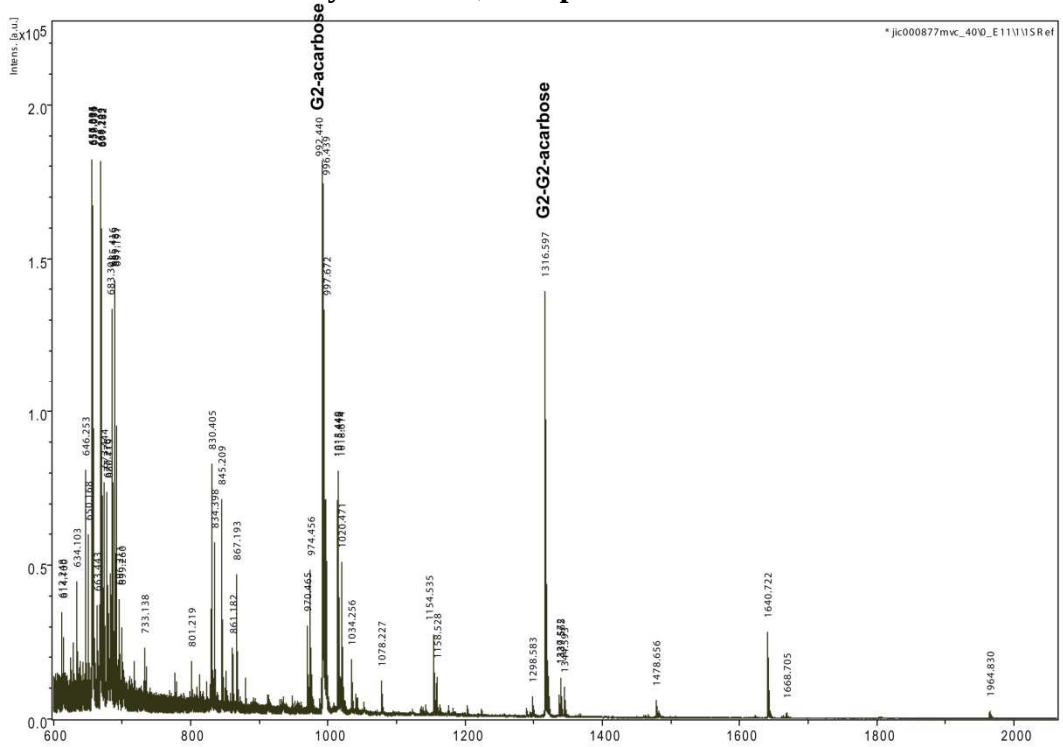

7.1.4 Donor: α-Maltosyl Fluoride, Acceptor: α-CD

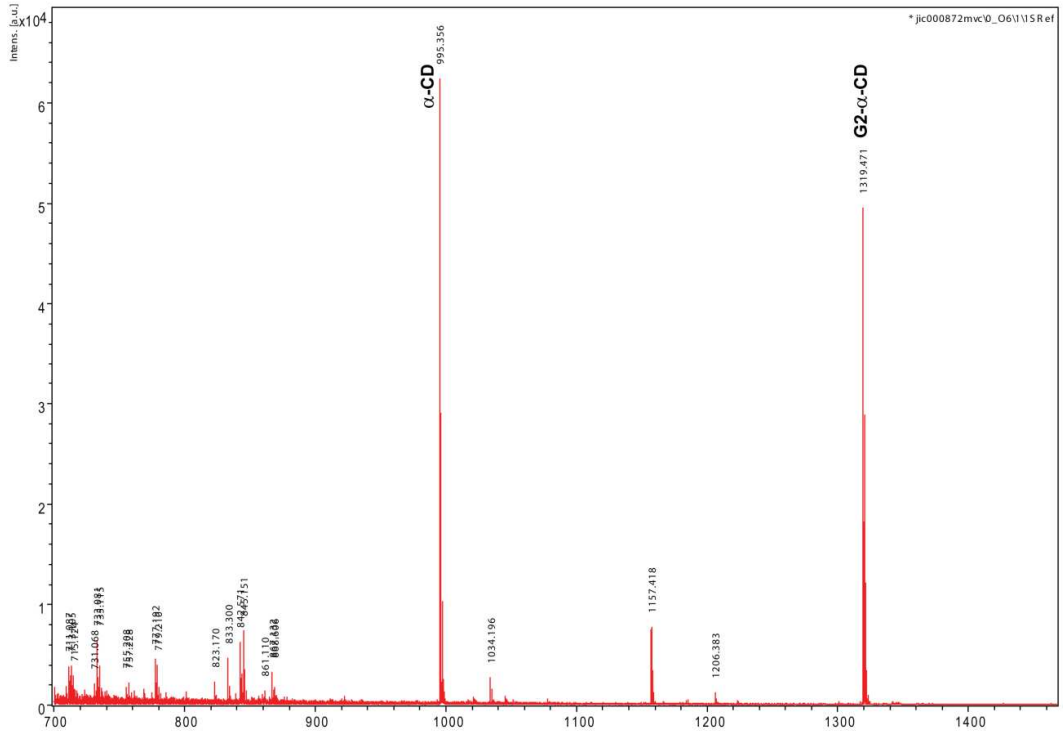

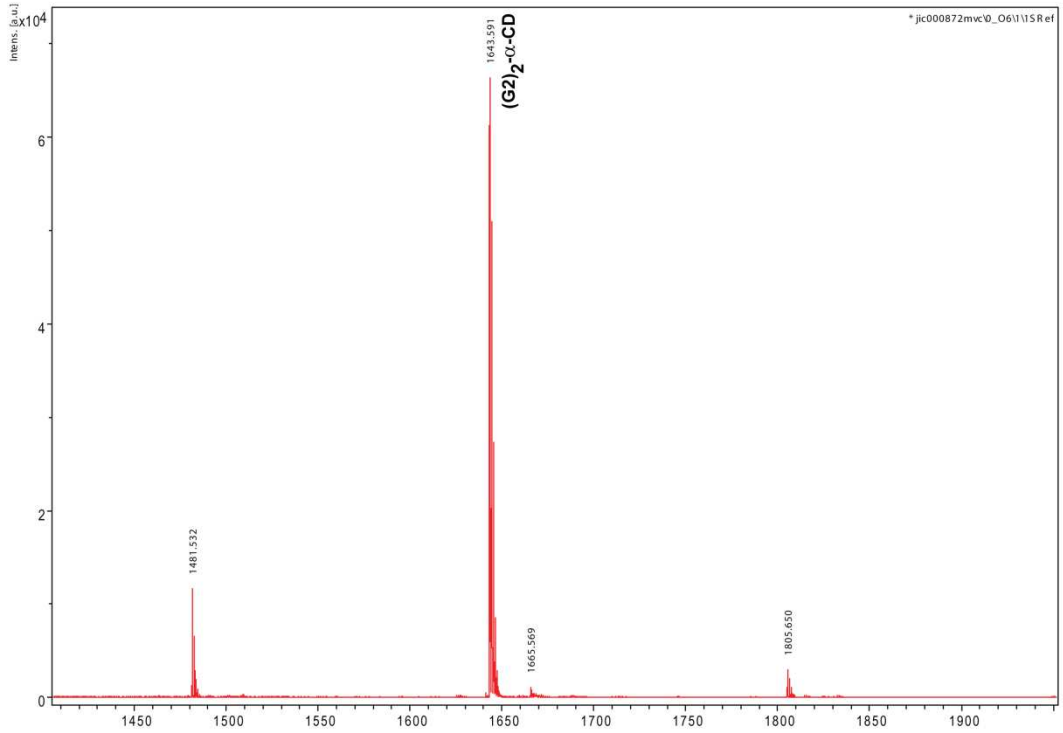

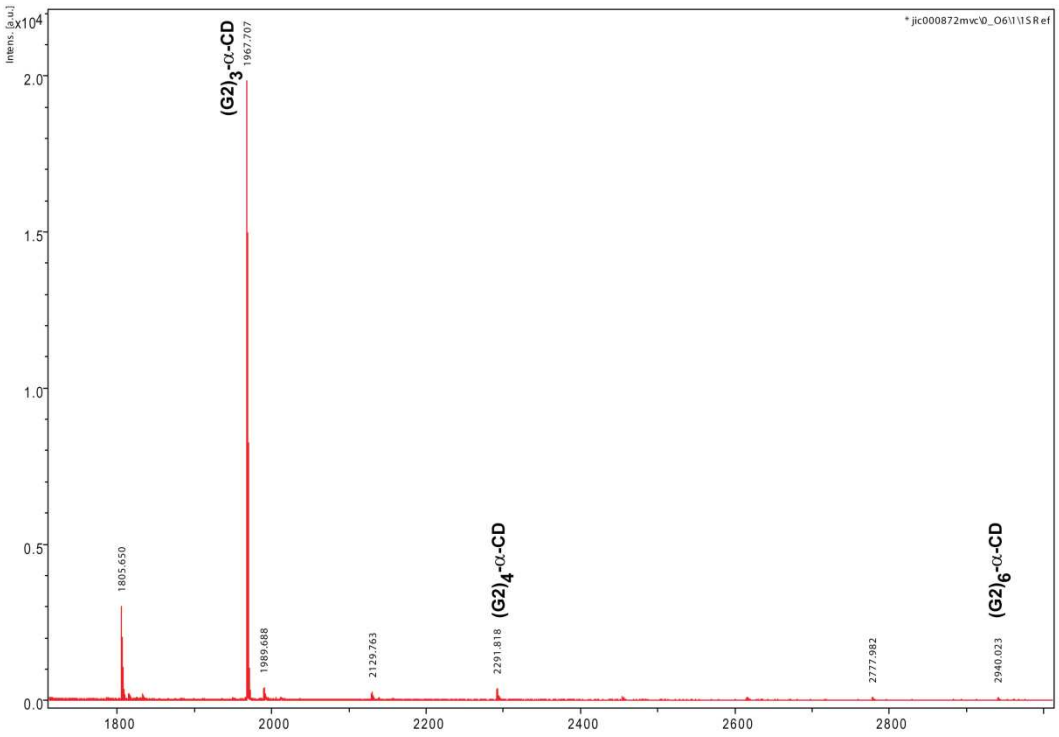
Intens. [a.u.]
x10^4
2.0
1.5
1.0
0.5
0.0
* jic000872mvc\0_O6\1\1SRef
(G2)3-α-CD
1967.707
1805.650
1989.688
2129.763
(G2)4-α-CD
2291.818
2777.982
(G2)6-α-CD
2940.023
1800
2000
2200
2400
2600
2800

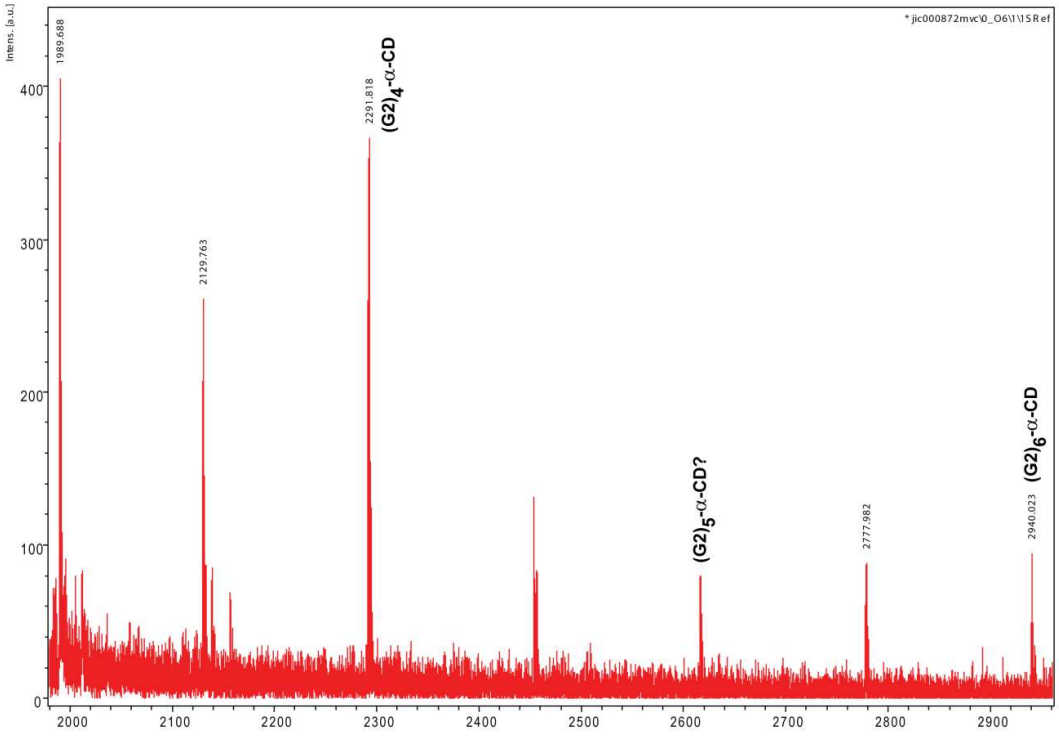
Intens. [a.u.]
400
300
200
100
0
* jic000872mvc\0_O6\1\1SRef
1989.688
2129.763
2291.818
(G2)4-α-CD
(G2)5-α-CD?
2777.982
2940.023
(G2)6-α-CD
2000
2100
2200
2300
2400
2500
2600
2700
2800
2900

7.2 LC-MS of ΔE^3LDI

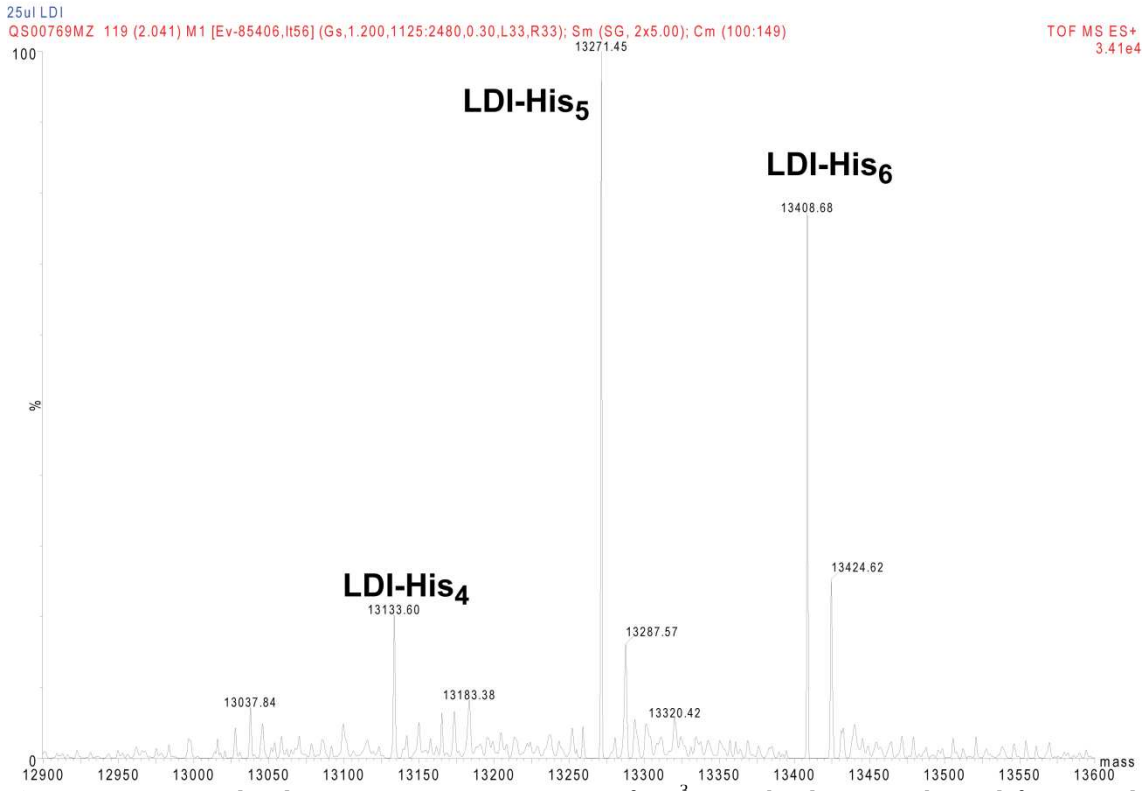

Figure 7.1. Deconvoluted ESI-QTOF Mass Spectrum of ΔE^3LDI. The data was obtained from 25 µl purified ΔE^3LDI.

7.3 Purification of LD/LDI Complex

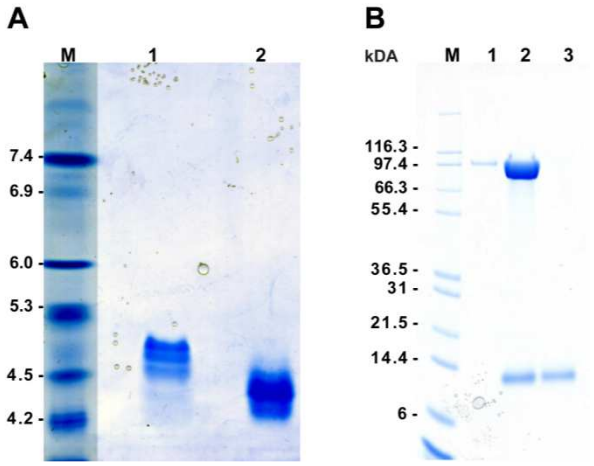

Figure 7.2. (A) Coomassie stained isoelectric focusing gel (pH 3–10). Lane 1, purified LD/LDI complex; lane 2, purified LD. (B) Coomassis stained SDS-PAGE gel from gel filtration purification of LD/LDI complex. Lane 1, middle fraction from first peak eluted which is believed to be dimerized LD; lane 2, middle fraction from LD/LDI peak; lane 3, middle fraction from LDI peak.

7.4 Oral Presentations

RSC Carbohydrate Group Meeting 2009, Norwich, UK. 15th to 16th of September 2009.
"Production and purification of recombinant barley limit dextrinase and its endogenous inhibitor and characterization of the protein-protein interaction" (selected from abstract).

Invited speaker at the COST 928 2nd Annual Meeting. Istanbul, Turkey. 15th to 17th of October 2008.
"Investigation of the interaction between recombinant barley limit dextrinase and its endogenous inhibitor."

2008 Plant Polysaccharide Workshop, Sigtuna, Sweden, 3rd to 5th of August 2008.
"Production and purification of recombinant barley limit dextrinase and its endogenous inhibitor" (selected from abstract).

7.5 Poster Presentations

"Interaction between recombinant barley limit dextrinase and the proteinaceous barley limit dextrinase inhibitor." **Vester-Christensen, M. B.**; Jensen, J.M.; Abou Hachem, M. and Svensson, B. 8th Carbohydrate Bioengineering Meeting, Ischia, Naples, Italy, 10th to 13th of May 2009.

"Production in *Pichia pastoris* and characterization of recombinant barley limit dextrinase." **Vester-Christensen, M. B.**; Næsted, H.; Abou Hachem, M. & Svensson, B. European Symposiun on Enzymes in Grain Processing, Norwich, UK, March 31st to April 2nd 2008.

"Production in *Pichia pastoris* and characterization of recombinant barley limit dextrinase." **Vester-Christensen, M. B.**; Næsted, H.; Abou Hachem, M. & Svensson, B. Annual Plant Biotech Denmark Meeting 29th to 30th of January 2008.

"Production of recombinant barley limit dextrinase." **Vester-Christensen, M. B.**; Naested, H.; Abou Hachem, M. & Svensson, B. 3th Symposium on the Alpha-Amylase Family, Smolenice Castle, Slovakia, 23rd to 27th of September 2007.

"Physico-chemical characterization of limit dextrinase from barley." **Vester-Christensen, M. B.**; Næsted, H. & Svensson, B. 7th Carbohydrate Bioengineering Meeting , Braunschweig, DE, 22nd to 25th of April 2007.

"Production of recombinant barley limit dextrinase." **Vester-Christensen, M. B.**; Næsted, H.; Abou Hachem, M. & Svensson, B. Annual Plant Biotech Denmark Meeting 23rd to 24th of January 2007.

7.6 Publications

The following publications are enclosed.

Vester-Christensen, M. B., Abou Hachem, M., Naested, H., and Svensson, B. (2009) Secretory expression of functional barley limit dextrinase by *Pichia pastoris* using high cell-density fermentation, *Protein Expr. Purif.*, doi: 10.1016/j.pep.2009.08.016. *In press*.

Vester-Christensen, M. B., Abou Hachem, M., Svensson, B., and Henriksen, A. (2009) Crystal structure of barley limit dextrinase. A debranching enzyme involved in starch synthesis and breakdown, to be submitted to J. Biol. Chem.

Vester-Christensen, M. B., Jensen, J. M. Abou Hachem, M., Svensson, B., N-terminal mutations of the high-affinity barley limit dextrinase inhibitor suggests a mode of action different from that of α-amylase inhibitors from the same family, to be submitted to Biochemistry.

Protein Expression and Purification xxx (2009) xxx–xxx

Contents lists available at ScienceDirect

Protein Expression and Purification

journal homepage: www.elsevier.com/locate/yprep

Secretory expression of functional barley limit dextrinase by *Pichia pastoris* using high cell-density fermentation

Malene Bech Vester-Christensen, Maher Abou Hachem, Henrik Naested, Birte Svensson *

Enzyme and Protein Chemistry, Department of Systems Biology, Søltofts Plads, Building 224, Technical University of Denmark, DK-2800 Kgs. Lyngby, Denmark

ARTICLE INFO

Article history:
Received 19 June 2009
and in revised form 17 August 2009
Available online xxxx

Keywords:
Barley limit dextrinase
High cell-density fermentation
Pichia pastoris
Pullulan hydrolysis
Cyclodextrin affinity

ABSTRACT

Heterologous production of large multidomain proteins from higher plants is often cumbersome. Barley limit dextrinase (LD), a 98 kDa multidomain starch and α-limit dextrin debranching enzyme, plays a major role in starch mobilization during seed germination and is possibly involved in starch biosynthesis by trimming of intermediate branched α-glucan structures. Highly active barley LD is obtained by secretory expression during high cell-density fermentation of *Pichia pastoris*. The LD encoding gene fragment without signal peptide was subcloned in-frame with the *Saccharomyces cerevisiae* α-factor secretion signal of the *P. pastoris* vector pPIC9K under control of the alcohol oxidase 1 promoter. Optimization of a fed-batch fermentation procedure enabled efficient production of LD in a 5-L bioreactor, which combined with affinity chromatography on β-cyclodextrin–Sepharose followed by Hiload Superdex 200 gel filtration yielded 34 mg homogenous LD (84% recovery). The identity of the recombinant LD was verified by N-terminal sequencing and by mass spectrometric peptide mapping. A molecular mass of 98 kDa was estimated by SDS–PAGE in excellent agreement with the theoretical value of 97419 Da. Kinetic constants of LD catalyzed pullulan hydrolysis were found to $K_{m,app}$ = 0.16 ± 0.02 mg/mL and $k_{cat,app}$ = 79 ± 10 s^{-1} by fitting the uncompetitive substrate inhibition Michaelis–Menten equation, which reflects significant substrate inhibition and/or transglycosylation. The resulting catalytic coefficient, $k_{cat,app}/K_{m,app}$ = 488 ± 23 mL/(mg s) is 3.5-fold higher than for barley malt LD. Surface plasmon resonance analysis showed α-, β-, and γ-cyclodextrin binding to LD with K_d of 27.2, 0.70, and 34.7 μM, respectively.

Introduction

Limit dextrinase (LD)[1] is a plant enzyme that is essential for starch debranching, e.g. during cereal seed germination. Starch is the major energy reserve in seeds and tubers and occurs as compact supramolecular granules composed of the polysaccharides amylose and amylopectin. Amylose is a linear α-1,4-glucan, whereas the more abundant amylopectin contains frequent α-1,6-glucosidic bonds connecting shorter linear α-1,4-linked branch chains of varying length to the α-1,4-glucan main chain [1]. In barley, starch granules are stored in the seed endosperm that consists of dead tissue and the concerted action of different amylolytic enzymes is required for its breakdown to metabolisable oligosaccharides, maltose, and glucose [1]. LD thus hydrolyzes α-1,6-glucosidic bonds in α-limit dextrins derived from amylopectin, but has low activity towards amylopectin itself [2]; α-amylase hydrolyzes α-1,4 glucans in an endo-fashion; β-amylase catalyzes release of maltose from non-reducing ends of the substrates and is unable to pass α-1,6-branch points; and the α-glucosidase primarily hydrolyzes maltooligosaccharides to glucose [3]. LD (EC. 3.2.1.41, pullulanase) is indeed the sole debranching enzyme in both seed and tuber starch mobilization [3,4]. LD shows high activity towards pullulan, a linear polysaccharide composed of α-1,6-linked maltotrioside repeats [2,3]. It is a large multidomain enzyme belonging to subfamily 13 of glycoside hydrolase family 13 (GH13_13) [5,6].

In barley a single gene encodes LD, which is induced in the germinating seed by the phytohormone gibberellic acid (GA_3) [4,7]. Transcripts of the LD gene can be detected in the aleurone layer already 12 h after the onset of germination, but LD activity does not increase until 2 days later and reaches a maximum at day 5 after onset of germination [7,8]. The level of LD activity in the starchy endosperm is low compared with the α-amylase activity. Furthermore, the release of LD from the aleurone to the endosperm appears to be slower than of α-amylase [8] and it was suggested therefore to occur as a consequence of cell wall degradation and

* Corresponding author. Fax: +45 4588 6307.
E-mail address: bis@bio.dtu.dk (B. Svensson).

[1] *Abbreviations used:* AICc, Aikaike information criteria; AmpR, ampicillin resistance; AOX, alcohol oxidase; CD, cyclodextrin; CWW, cell wet weight; GA_3, gibberellic acid; GH13, glycoside hydrolase family 13; HIS4, histidinol dehydrogenase; KanR, kanamycin resistance; LD, limit dextrinase; LDI, limit dextrinase inhibitor; MALDI-TOF-MS, matrix assisted laser desorption ionization time-of-flight mass spectrometry; MeOH, methanol; PAGE, polyacrylamide gel-electrophoresis; SDS, sodium dodecyl sulfate; SPR, surface plasmon resonance; SS, sum of squared residuals.

1046-5928/$ - see front matter © 2009 Elsevier Inc. All rights reserved.
doi:10.1016/j.pep.2009.08.016

not *via* a secretory pathway. The secretion of LD, however, has been a matter of debate since a putative leader sequence has been identified upstream the mature peptide, but was not predicted to be a signal peptide targeting to the ER [4,7].

In addition to an important role in starch degradation in germinating seeds, LD is shown in maize [9] and *Arabidopsis* [10] to participate in the breakdown of transitory starch in leaves. Furthermore, LD is present in developing grains and suggested to play a role in starch biosynthesis [7,8,11]. The hypothesis that the structure of amylopectin is the outcome of a balance between debranching and branching enzyme activities [12,13] gets support both from maize deficient in pullulanase-type debranching enzyme (i.e. LD), having affected starch granule morphology [9] and from a quadruple debranching enzyme deficient *Arabidopsis* mutant with abolished starch granule biosynthesis [14].

LD purified after extraction from germinating barley seeds occurs in a "bound", apparently inactive form, and in a free enzymatically active form. The ratio of bound to free form changed with time after the onset of germination [15]. The inactive LD form was proposed to consist of a complex with the endogenous limit dextrinase inhibitor (LDI) [16]. Extraction under reducing conditions led to fully active LD [15,17]. Whether the disappearance of LDI at germination is due to reduction by thioredoxin *h* [18] or degradation by a cysteine protease [15] remains to be uncovered.

In addition to the roles in starch biosynthesis and degradation LD is central in beer production by catalyzing oligosaccharide debranching during malting and mashing [19]. However, even though barley malt LD has been known since the fifties [20] insight is lacking on the precise role of LD and its interplay with LDI in biological and industrial processes as well as on the structure/function relationships and the molecular basis for substrate specificity and formation of the LDI-LD complex. In the past recombinant production of LD from maize [21], spinach [22], and wheat [23] resulted in very poor yields, which emphasized the challenge of producing plant proteins in *Escherichia coli*. A similar situation was found for barley α-glucosidase [24], in which case, however, a breakthrough was obtained by high cell-density fermentation of the host *Pichia pastoris* resulting in good yields of very pure and five times more catalytically efficient α-glucosidase than the enzyme purified from malt [25].

The aim of the present work is to produce functional, recombinant LD in amounts sufficient for thorough analysis of stability, enzymatic properties including LDI interaction, and structure determination by X-ray crystallography. To this end an expression system was developed using *P. pastoris* as host and high cell-density fermentation in a bioreactor, which resulted in excellent yield of homogenous recombinant LD with higher activity than the enzyme purified from barley malt [26,27].

Materials and methods

Construction of LD expression plasmid

LD cDNA (GenBank Accession No. AF022725) [4] was used as template in PCR with forward primer 5′-AA**GCGGCCGC**TGCGTTCA TGCCGGA-3′ and reverse primer 5′-AA**GCGGCCGC**TTAACACCGAG GTTCGACAAAGACT-3′ involving preheating at 94 °C (2 min), 30 cycles at 94 °C (15 s), 55 °C (30 s), and 72 °C (3 min), followed by a final elongation (7 min). The resulting PCR product (2678 bp) encoding the mature LD lacking the putative leader sequence (amino acid residues 22–905 according to Accession No. AAD04189, NCBI Protein database) with flanking NotI restriction sites introduced by the primers (in bold) was digested, gel-purified and cloned into the NotI site of the pPIC9K vector (Invitrogen, USA) to obtain in-frame cloning with the α-mating-factor secretion signal from *Saccharomyces cerevisiae* (Fig. 1A). *E. coli*, XL10-Gold (Stratagene, USA) was transformed with the resulting pPICK9/LD (Fig. 1B) and isolated plasmids from single colony transformants, selected on LB-agar plates containing 100 μg/mL ampicillin, were analyzed for correct orientation of the inserted gene using the XbaI restriction site present in both vector and insert. The sequence of the final construct was verified by sequencing using forward primers 5′-TACTATTGCCAGCATTGCTGC-3′, 5′-TGCAATTACCCGGCGTGC TG-3′, 5′-GAATATCGTCAGATGGTCCA-3′, and 5′-TGATGTTATCAG TGTGAAGA-3′; and reverse primers 5′-CGGTTTTCCCACTCTCTTG G-3′, 5′-TTAACCTATCAACCATGAAA-3′, 5′-AACACCCCAATTGTTTG TTT-3′, and 5′-GCAAATGGCATTCTGACATCC-3′ covering the LD mature protein encoding region. Small scale plasmid preparation, restriction enzyme digestion, ligation, and transformation followed standard molecular biology protocols [28].

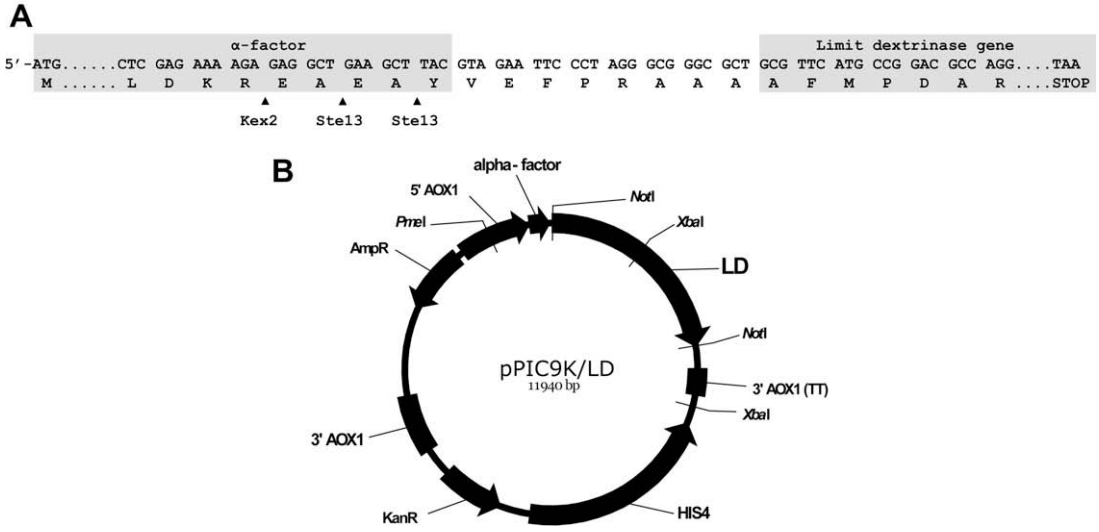

Fig. 1. Design of pPIC9K/LD plasmid. (A) Schematic representation of the construction of LD gene cloned in-frame with α-factor secretion signal. The linker in between α-factor and the LD gene is a part of the multiple cloning site. (B) The LD encoding expression plasmid used for *P. pastoris* transformation.

Please cite this article in press as: M.B. Vester-Christensen et al., Secretory expression of functional barley limit dextrinase by *Pichia pastoris* using high cell-density fermentation, Protein Expr. Purif. (2009), doi:10.1016/j.pep.2009.08.016

Transformation of P. pastoris and selection for expression and LD secretion

Prior to transformation, pPICK9K/LD (20 μg) was linearized with PmeI followed by purification (Strataclean; Stratagene, USA), precipitation, and redissolving in sterile Milli-Q water. Electrocompetent *P. pastoris* strain GS115 (Invitrogen, USA) was transformed with the linearized plasmid by electroporation using a Micropulser (Bio-Rad, USA). Transformants were isolated by prototrophic growth on minimal medium lacking histidine and supplemented with 1% sorbitol (RDB plates: 1 M sorbitol, 2% dextrose, 1.34% yeast nitrogen base without amino acids (YNB), 1.64 μM biotin, 270 μM L-glutamic acid, 335 μM L-methionine, 342 μM L-lysine, 381 μM L-leucine, 381 μM L-isoleucine) [29]. Plates were incubated at 30 °C for 2–4 days.

Transformants secreting LD were selected by colony blotting using antibodies against LD from barley malt [30]. Single colonies of His^+ transformants were picked from the initial RDB plates, transferred to YPD plates, grown for 2 days and then replicated to nitrocellulose membranes (Hybond ECL, 0.45 μm, Amersham Biosciences, Germany) placed on minimal medium plates containing 0.5% methanol (MM plates: 1.34% YNB, 1.64 μM biotin, 0.5% methanol) followed by incubation at 30 °C for 2 days. Secreted LD was detected by immunoblotting using anti-LD primary antibody [30], and goat anti-rabbit alkaline phosphatase conjugated secondary antibody (Dako, Denmark). The membrane was rinsed with Milli-Q water to remove cells before blocking in TBST with BSA (25 mM Tris–HCl, pH 7.5, 150 mM NaCl, 0.2% v/v Tween 20, 1% BSA) for 30 min. The primary antibody was diluted 1:3000 in TBST and the antigen–antibody interaction was carried out at room temperature for 30 min. The membrane was washed (3 × 10 min) with TBST before probing with secondary antibody diluted 1:2000 in TBST (30 min). After washing (3 × 10 min) with TBST the immunoblot was developed using nitroblue tetrazolium (NBT)/bromo chloro indolyl phosphate (BCIP) colorimetric method (100 mM Tris–HCl, pH 9.5, 100 mM NaCl, 5 mM $MgCl_2$, 0.33 mg/mL NBT, 0.17 mg/mL BCIP) and the reaction was stopped by change to Milli-Q water. LD from barley malt served as positive and *P. pastoris* strain GS115 transformed with the empty vector pPIC9K as negative control.

Pilot scale expression

Twelve His^+ transformants selected by colony immunoblotting were tested for expression in 50 mL culture using buffered complex medium following the supplier's guidelines for Mut^+ phenotype [29]. LD activity was monitored after 96 h using the Limit-Dextrizyme assay (see below; Megazyme, Ireland). The culture medium was changed by adding 60 volumes of 100 mM Na acetate, pH 5.5, followed by 10-fold concentration (Centricon, 30 kDa cut-off; Millipore, Ireland) prior to testing. Due to low LD activity in shake flask cultures, a 5 h assay reaction time was applied to ensure detection of secretory expression of active LD. The effect of induction temperature was analyzed by comparing LD activity in cell-free extract of cultures grown in minimal medium at either 30 or 22 °C for 72 h. The transformant selected for large scale bioreactor production was shown to release LD activity in minimal medium after induction at 22 °C for 72 h.

High cell-density fermentation

The bioreactor fermentation has three stages; (i) a glycerol batch phase generating biomass; (ii) a glycerol feed phase, with glycerol being delivered at growth limiting rate for continued biomass generation and derepression of the alcohol oxidase promoter AOX1; and (iii) a methanol feed phase for induction of expression with increasing methanol feed to a maximum level at 11 g/(L h). Methanol induction was maintained for 89 h.

The fermentation procedure guidelines for methanol feeding of the Mut^+ phenotype [31] were optimized and the fermentation was carried out in a 5-L Biostat B (B. Braun Biotech International, Germany) bioreactor equipped with an additional feed pump, gas mixer, dissolved oxygen tension polarographic electrode, and water cooler [31,32]. The 2 L starting basal salt medium containing PMT1 [32] trace salts was inoculated with 150 mL culture (OD_{600} = 16) propagated overnight at 30 °C in buffered complex medium (BMGY: 1% w/v yeast extract, 2% w/v peptone, 0.1 M KH_2PO_4, pH 6.0, 1.34% w/v YNB, 1.64 μM biotin, 1% v/v glycerol) [29]. The temperature was maintained at 29 °C by water cooling during glycerol batch and fed-batch phases. Prior to induction, the temperature was decreased to 22 °C and kept throughout the methanol feed phase. Solutions of 50% glycerol and 100% methanol both containing PTM1 trace salts were used for as carbon source during glycerol feed phase and methanol feed phase, respectively. Continuous addition of 28% aqueous ammonia served to maintain the pH at 5.5 and as a nitrogen source.

Purification of LD

Cells were harvested after 5 days of fermentation (centrifugation, 12,000*g*, 4 °C, 30 min), and the supernatant (2.5 L) was kept at 4 °C after adding sodium azide (final concentration 0.02% w/v). LD was purified by a two-step procedure involving affinity chromatography using β-cyclodextrin (β-CD) conjugated to Sepharose followed by gel filtration (Hiload Superdex 200 26/60). The culture supernatant was split in two and ammonium sulfate was added to a final concentration of 1 M to secure binding of LD to β-CD–Sepharose [30], followed by centrifugation (12,000*g*, 4 °C, 30 min) and filtration (0.45 μm, GE Water & Process Technologies, USA), and pumped (30 mL/h) onto β-CD–Sepharose (20 mL bed volume in XK 16/10 column; GE Healthcare, Sweden) equilibrated in 10 mM Na acetate, pH 5.5, 500 mM NaCl, 5 mM $CaCl_2$. After wash with equilibration buffer (four column volumes; 60 mL/h), bound LD was eluted with 10 mM Na acetate, pH 5.5, 5 mM $CaCl_2$, 7 mM β-CD at the same flow rate. Fractions (960 μL) were collected in tubes containing 40 μL 1 M HEPES, pH 7.0, 125 mM $CaCl_2$, 0.125% Triton X-100 and aliquots were analyzed by SDS–PAGE. Fractions with LD activity (see below for assay) were pooled and concentrated to 18 mL (Centricon; 30 kDa cut-off, Millipore, Ireland) after 2 mL were removed and dialyzed (Spectra/por dialysis membrane MWCO 12–14 kDa; Spectrum Laboratories, USA) 2 × 12 h against 2 × 3 L 50 mM MES, pH 6.6, 250 mM NaCl and assayed for activity. Subsequently 4 × 4 mL portions from the concentrated β-CD pool (approximately 2.5 mg/mL LD) were chromatographed on a Hiload Superdex 200 26/60 column (GE Healthcare, Sweden) equilibrated with 50 mM MES, pH 6.6, 250 mM NaCl and eluted (30 mL/h) with the same buffer. Collected fractions (4 mL) were analyzed by SDS–PAGE and LD-containing fractions were pooled, concentrated (Centricon, 30 kDa cut-off; Millipore, Ireland), assayed for activity, and stored at 4 °C. An ÄKTAexplorer (GE Healthcare, Sweden) interfaced by UNICORN 5.0 control software (GE Healthcare, Sweden) was used for both chromatographic procedures.

Enzyme activity

LD activity during pilot expression, fermentation, and purification was assayed with Limit-Dextrizyme tablets (Megazyme, Ireland) in 0.1 M Na acetate, pH 5.5, 0.005% Triton X-100. LD (5–10 nM) diluted in assay buffer (0.5 mL) was preheated (5 min) on a 40 °C water bath before adding the Azurine-crosslinked-pullulan substrate tablet. The reaction was stopped after 10 min by adding

Please cite this article in press as: M.B. Vester-Christensen et al., Secretory expression of functional barley limit dextrinase by *Pichia pastoris* using high cell-density fermentation, Protein Expr. Purif. (2009), doi:10.1016/j.pep.2009.08.016

5 mL 1% w/v Tris and vigorously whirl-mixing. After 10 min incubation at R.T., the tubes were whirl-mixed and 2 mL were transferred to Eppendorf tubes and centrifuged (14,000*g*, 10 min). The absorbance of the supernatant was measured at 590 nm. One activity Unit is defined as the amount of enzyme that releases one micromole of glucose reducing-sugar equivalents per min from pullulan under the defined assay conditions [33].

Kinetic constants of LD was determined from initial rates of hydrolysis at 12 different concentrations (0.02–1 mg/mL) of pullulan (Megazyme, Ireland) by 3.6 nM LD in 20 mM Na acetate, pH 5.5, 5 mM $CaCl_2$, 0.005% Triton X-100 (starting assay volume: 1.1 mL) at 37 °C. Aliquots (200 μL) were removed at 3 min intervals during 0–15 min, stopped by mixing with 500 μL freshly prepared developing buffer (0.4 M Na carbonate, pH 10.7, 2.5 mM $CuSO_4$, 2.5 mM 4,4′-dicarboxy-1,2′-biquinoline, 6 mM L-serine) and 300 μL Milli-Q water [34] and the absorbance was measured after 30 min at 80 °C in microtiter plates (300 μL, in duplicates) at A_{540}. The release of reducing sugar was quantified using a maltose standard curve. V_{max} and K_m were determined by fitting either the Michaelis–Menten equation (Eq. (1)) or the equation for uncompetitive substrate inhibition (Eq. (2)) to the initial rates. $K_{i,s}$ is the dissociation constant for the inhibitory substrate–enzyme–substrate ternary complex.

$$V = \frac{V_{max}}{1 + \frac{K_m}{[S]}} \tag{1}$$

$$V_{i,sub} = \frac{V_{max}}{1 + \frac{K_m}{[S]} + \frac{[S]}{K_{i,s}}} \tag{2}$$

The fitting and plotting were performed using the Enzyme Kinetics Module 1.0 of the program Sigmaplot 9.01 (Systat Software, Germany).

Cyclodextrin affinity

Affinity of LD for α-, β- and γ-cyclodextrin (CD) was determined using surface plasmon resonance (SPR) (BIAcore® T100; GE Healthcare, Sweden). LD was immobilized in the presence of 1 mM β-CD on a CM5 sensor chip (GE Healthcare, Sweden) using random amine coupling (2800–3200 response units, RU). Sensorgrams (RU *vs.* time) of binding of α-, β- and γ-CD in the range of 2.5–160 μM (17 concentrations), 0.125–40 μM (14 concentrations), and 4–160 μM (16 concentrations), respectively, were obtained at 25 °C using 3 min association and 2 min dissociation. CDs were dissolved in 20 mM Na acetate, pH 5.5, 100 mM NaCl, 0.005% surfactant P-20, which was also used as running buffer. K_d (Eq. (3)) was calculated by steady-state affinity fitting (BIAcore evaluation software 1.1) to the equilibrium response *R* of CD at a given concentration after subtracting the reference flow cell signal; R_{max} is the response at saturation of the ligand on the chip.

$$R = \frac{R_{max} \cdot [CD]}{[CD] + K_d} \tag{3}$$

Protein assays

LD concentration was either quantified by Bradford Coomassie Plus kit (Pierce) with BSA as standard or spectrophotometrically at 280 nm using a molar extinction coefficient of $1.52 \times 10^5\ M^{-1}\ cm^{-1}$ determined experimentally on the basis of LD concentration calculated by aid of amino acid analysis. A lower theoretical value of $130{,}680\ M^{-1}\ cm^{-1}$ (www.expasy.org/tools/protparam.html) probably reflects influence of the protein structure on spectral properties of tyrosine and tryptophan residues.

SDS–PAGE, isoelectric focusing, and immunoblotting

Protein purity was assessed by SDS–PAGE using NuPAGE® Novex Bis-Tris 4–12% gels (Invitrogen) in 1% MES buffered polyacrylamide minigel Novex system with reducing agent added in the sample preparation and anti-oxidant in the buffer system according to the manufacturers' recommendations and Coomassie Brilliant Blue G-250 staining [35].

Isoelectric focusing (IEF) was performed using the PhastSystem (Pharmacia, Sweden), pH 4–6 PhastGels (GE Healthcare, Sweden) with low pI calibration kit (GE Healthcare, UK) and Silver Kit staining (Pharmacia, Sweden). Immunoblotting was carried out using the Novex gel system with the XCell SureLock Mini-Cell according to the supplier's manual (Invitrogen). LD was detected using polyclonal rabbit antibody raised against LD purified from barley malt [30] in combination with goat anti-rabbit alkaline phosphatase conjugated antibody (Dako, Denmark).

Mass spectrometry, amino acid analysis, and protein sequencing

In-gel trypsin digestion of spots cut out from protein bands of SDS–PAGE gels and micropurification on Poros 20 R2 home-made nanocolumns (Perseptive, Biosystems, USA) were done as described [36]. Peptides were eluted with 1 μL matrix solution (5 g/L α-cyano-hydroxycinnamic acid in 70% [v/v] CH_3CN and 0.1% [w/v] trifluoroacetate) directly onto the MALDI target and analyzed using an Ultraflex II MALDI-TOF-TOF mass spectrometer (Bruker-Daltonics, Germany) in positive ion reflector mode. Spectra were analyzed using FlexAnalysis software (Bruker-Daltonics, Germany) and calibrated by trypsin autolysis products (*m*/*z* 842.51 and *m*/*z* 2211.10). Peptide mass data were searched against the NCBI non-redundant database using Biotools software (Bruker-Daltonics) and the Mascot server (http://www.matrixscience.com).

Amino acid analysis was performed after 24 h hydrolysis as described [37]. Protein sequencing was carried out by automated N-terminal Edman degradation in a Procise 494 sequenator according to the manufacturer's recommendations (Applied Biosystems Foster City, USA). Highly pure Milli-Q water (18 MΩ) was used throughout.

Results

Cloning and selection of LD secreting transformants

The gene fragment encoding LD without the previously proposed putative transit peptide [4] was cloned downstream of the *P. pastoris* AOX1 promoter in pPIC9K in-frame with the N-terminal α-factor secretion signal to achieve secretion of recombinant LD by *P. pastoris*. The cloning resulted in an N-terminal tripeptide (ATQ) deletion of mature LD compared to our earlier published gene sequence [4]. The same triptide sequence was lacking in approximately 50% of the LD molecules purified from germinating seeds [30] and in the gene sequence determined by others [7]. The linearized construct (Fig. 1B) was inserted into the genome by homologous recombination resulting in stable integration as judged from the maintained *P. pastoris* GS115 Mut^+ His^+ phenotype. Successful secretory expression was documented by strong colony immunoblotting response for 20 transformants out of 50 selected randomly and significant variation in production level was judged from intensity differences (not shown). This corroborated the variations in LD activity (2.4–36.8 mU/mL) observed in a pilot scale secretory expression of the selected transformants. No LD activity was produced by strain GS115 transformed with empty pPIC9K and based on the results one transformant, LD26, was selected for further analysis. Remarkably, after 72 h induction no measurable LD activ-

Please cite this article in press as: M.B. Vester-Christensen et al., Secretory expression of functional barley limit dextrinase by *Pichia pastoris* using high cell-density fermentation, Protein Expr. Purif. (2009), doi:10.1016/j.pep.2009.08.016

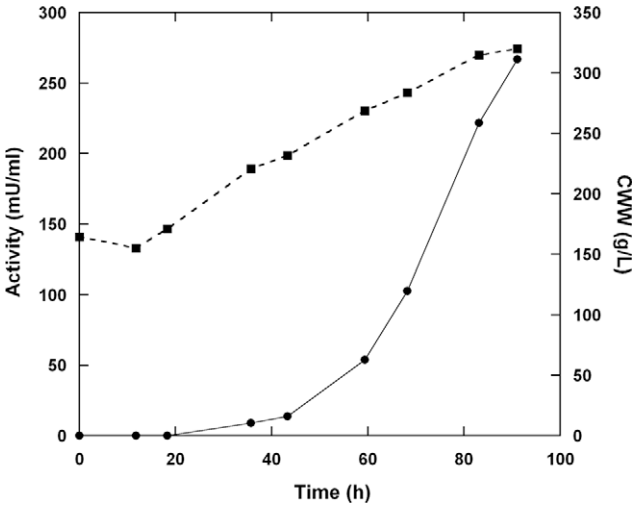

Fig. 2. Progress of secreted LD activity (●) and CWW (cell wet weight) (■) during fermentation from the start of the methanol induction.

ity was detected in minimal medium at 30 °C from LD26, whereas induction at 22 °C for 72 h gave a 10-fold activity increase compared to the highest activity measured after 96 h induction at 30 °C.

Fermentation and secretory expression in 5-L bioreactor

Very low LD yields in shake flask cultures motivated implementation of fed-batch high cell-density fermentation. Cell wet weight (CWW) and LD activity were monitored throughout the different stages of this fermentation. The initial batch phase (30 h) resulted in CWW of 114 mg/mL. The culture was then switched to fed-batch mode with 15 g/(L h) glycerol feed for 6 h leading to CWW of 164 mg/mL. This was followed by initiation of induction by a methanol feed of 1 g/(L h) for 2 h to allow adaptation to methanol metabolism. The methanol flow was successively increased to reach the maximum of 11 g/(L h) after 12 h. LD activity in the medium and CWW increased with time (Fig. 2). The culture was terminated at 125 h (89 h induction) as the reactor headspace became limiting. The CWW was 315 g/L and the 2.5 L cell-free supernatant contained about 16 mg/L active LD as calculated from the specific activity of purified recombinant LD.

Purification and characterization of recombinant LD

LD purification was monitored by activity assay and SDS–PAGE (Table 1 and Fig. 3A). Less than 1% of the total activity in the culture supernatant appeared in the flow-through after application to β-CD–Sepharose in 1 M ammonium sulfate and the affinity chromatography resulted in high yield of very pure LD (Fig. 3A, lane 2). Precipitation of eluted LD observed in preliminary experiments was prevented by immediate adjustment of the eluate to pH 6.7 (see Materials and methods). Gel filtration further increased the LD purity and removed β-CD (Table 1 and Fig. 3A, lane 3). Immunoblotting of pooled LD-containing fractions showed a predominant band corresponding to an apparent molecular mass of 98 kDa (Fig. 3B, lane 2) in excellent agreement with both the theoretical value of 97,419 Da and the migration of barley malt LD (Fig. 3B, lane 1). A trace component of slightly lower molecular mass visible in SDS–PAGE possibly represented a cleavage product of secreted LD. The purification procedure resulted in 34 mg recombinant LD with specific activity of 14.2 U/mg corresponding to 11-fold purification and 84% recovery from the culture supernatant (Table 1).

The identity of recombinant LD was verified by peptide mapping using MALDI-TOF-MS (data not shown). A search against the NCBI non-redundant database resulted in mono-isotopic mass

Table 1
Purification of LD from 2.5 L *P. pastoris* culture supernatant.

	Total protein (mg)	Total activity (U)	Recovery (%)	Specific activity (U/mg)	Purification (fold)
Supernatant	456.9	573.3	100.0	1.3	1.0
β-CD–Sepharose	82.7	551.7	96.2	6.7	5.2
Sephadex G200	33.6	477.3	83.3	14.2	11.0

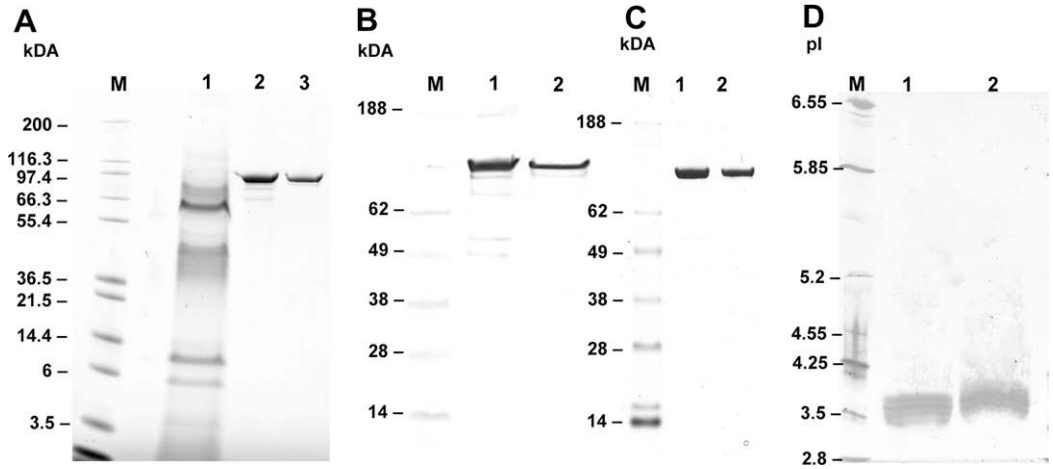

Fig. 3. (A) Coomassie stained SDS–PAGE. Lane 1, culture supernatant (~3.5 μg total protein); lane 2, pool of β-CD–Sepharose eluate (~2.5 μg total protein); lane 3, pool of Hiload Superdex 200 eluate (~0.8 μg total protein). (B) Immunoblotting using barley LD specific antibody. Lane 1, LD purified from barley malt (~70 ng); lane 2, purified recombinant LD (~40 ng). (C) Coomassie stained SDS–PAGE. Lane 1, LD purified from barley malt (~1 μg); lane 2, purified recombinant LD (~1 μg). (D) Isoelectric focusing of LD (pH 4–6 PhastGels). Lane 1, LD purified from barley malt (~0.8 μg); lane 2, purified recombinant LD (~0.8 μg).

Please cite this article in press as: M.B. Vester-Christensen et al., Secretory expression of functional barley limit dextrinase by *Pichia pastoris* using high cell-density fermentation, Protein Expr. Purif. (2009), doi:10.1016/j.pep.2009.08.016

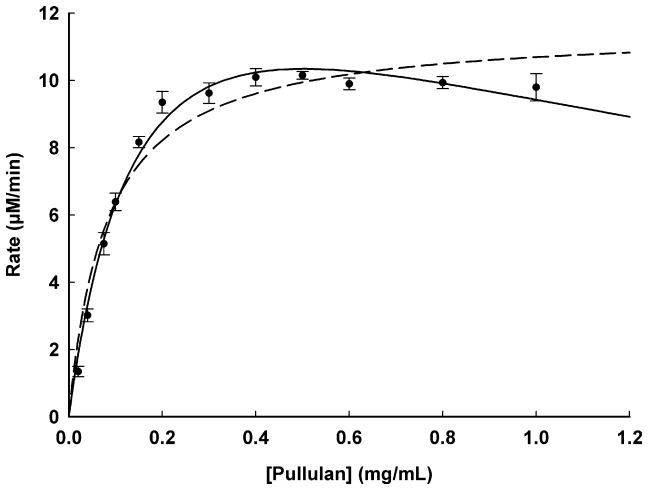

Fig. 4. Apparent initial rate of release of reducing sugar as a function of pullulan concentration. Solid line, fit of Michaelis–Menten expression with uncompetitive substrate inhibition. Dashed line, classical Michaelis–Menten plot. Error bars indicate SD for triplicate measurements.

peaks with 27% sequence coverage of the LD protein sequence. Tryptic peptides comprising the four putative N-glycosylated positions were not identified, owing to size incompatibility with the present mass spectrometric analysis for two of them. However, the migration of LD in SDS–PAGE analysis as a single sharp band corresponding to the expected molecular mass is not supportive of significant glycosylation. Three different processed forms of LD can be predicted depending on the protease cleavage site, Kex2 or any of the two Ste13 sites, used (Fig. 1A). Using the NotI site for the cloning will therefore normally, in the processed protein, result in a 9–13 amino acids N-terminal extension that originates from the expression plasmid (Fig. 1A). N-terminal sequencing of LD revealed an alternative processed form of the secreted enzyme (AAFMPDAR, Fig. 1A) presumably due to cleavage by one or more proteases produced by *P. pastoris*.

Isoelectric focusing of the recombinant LD and LD purified from barley malt showed a similar migration pattern with pI of ≈4.1 (Fig. 3D). A number of closely migrating bands appear in a broader smeared zone indicating slight charge heterogeneity in both enzyme preparations.

Fitting the Michaelis–Menten equation to initial rates of LD catalyzed hydrolysis of pullulan revealed deviation of the hyperbolic fit from experimental data, in particular at substrate concentrations above 0.2 mg/mL (Fig. 4). Noticeably, however, fitting the Michaelis–Menten expression for uncompetitive substrate inhibition matched the data very clearly (Fig. 4). This is supported using standard statistical tools for model selection such as the corrected Akaike information criterion (AICc) [38] and the sum of squared residuals (SS) (tools included in the Sigmaplot 9.01 software). The Michaelis–Menten expression for uncompetitive substrate inhibition yields an AICc = −43.4 and SS = 8.3, while the regular Michaelis–Menten equation has values of AICc = −14.3 and SS = 20.1. Such deviation from the Michaelis–Menten model observed for other glycoside hydrolases, has previously been attributed to an increased transglycosylation rate at higher substrate concentrations rather than to substrate inhibition [39,40]. For LD this is in agreement with the K_m value for pullulan being significantly higher when fitting the equation for uncompetitive substrate inhibition as compared to fitting the regular Michaelis–Menten equation (Table 2).

Table 3
LD affinity towards cyclodextrins determined by SPR.

Analyte	K_d (μM)	Relative K_d[a]
α-CD	27.2 ± 0.9	39
β-CD	0.7 ± 0.1	1
γ-CD	34.7 ± 0.2	50

Measurements were performed at 25 °C in 20 mM Na acetate, pH 5.5, 100 mM NaCl, 0.005% P-20. K_d is based on independent duplicate runs, each run having three data points at each concentration.
[a] K_d values normalized to β-CD.

The previously reported binding of cyclodextrins to debranching enzymes [41] is here confirmed and analyzed for the recombinant LD using surface plasmon resonance. The approximately 100-fold difference in molecular mass between the chip-immobilized LD and the three CD analytes poises high demands on sensitivity. The developed experimental set up, however, resulted in highly reproducible sensorgrams for all three CDs with R_{max} values of 16–25 RU. Fitting of a one binding site model to the SPR data of β-CD revealed a submicromolar K_d, whereas α- and γ-CD had 40–50 times weaker affinity (Table 3).

Discussion

The functional recombinant barley LD achieved in excellent yields and outstanding quality enables future biochemical and structural characterization of this pivotal enzyme in cereal starch metabolism and in food processing, in particular in the brewing and malting industry [42,43]. Previous attempts to produce recombinant LDs from plants resulted in extremely poor yields [21,22] and very low specific activity [23] highlighting the difficulties in producing large multidomain recombinant plant proteins. Earlier attempts to produce barley LD thus resulted in full-length and truncated inactive forms [44]. Here heterologous production of barley LD was successfully conducted in *P. pastoris*. Optimization of a fed-batch protocol in a 5-L bioreactor thus resulted in 16 mg/L highly active recombinant LD secreted to the culture supernatant indicating accumulation of functional and stable recombinant LD under the applied culture conditions (Fig. 2). Lowering the induction temperature to 22–25 °C has been reported to increase amounts of secreted heterologous protein [45–47]. This was confirmed by pilot scale expression of LD at 22 °C resulting in more than 10 times higher yield than at 30 °C. We assume this is due to enhanced LD folding and/or reduced protease activity in the medium [45,48], since LD was previously reported to be fully stable at 30 °C [49].

Comparison of the affinity of α-, β- and γ-CD for pullulanase from *Klebsiella pneumoniae* showed strong binding of β-CD driven both by hydrogen bond formation and by hydrophobic contacts as indicated by a favorable entropic change upon β-CD binding

Table 2
Apparent kinetic constants of LD on pullulan obtained by nonlinear least-squares curve fitting.

Classical Michaelis–Menten			Uncompetitive substrate inhibition			
$K_{m,app}$ (mg/mL)	$k_{cat,app}$ (s^{-1})	$(k_{cat}/K_m)_{app}$ (mL/(mg s))	$K_{m,app}$ (mg/mL)	$k_{cat,app}$ (s^{-1})	$K_{i,s,app}$ (mg/mL)	$(k_{cat}/K_m)_{app}$ (mL/(mg s))
0.081 ± 0.003	61 ± 13	753	0.16 ± 0.02	78 ± 10	1.5 ± 0.4	488

Values are based on independent triplicate measurements.

Please cite this article in press as: M.B. Vester-Christensen et al., Secretory expression of functional barley limit dextrinase by *Pichia pastoris* using high cell-density fermentation, Protein Expr. Purif. (2009), doi:10.1016/j.pep.2009.08.016

[41]. The affinity of β-CD for LD and the bacterial pullulanase is in the same range. Remarkably, however affinity of the bacterial pullulanase for α- and γ-CD (K_d = 100 and 102 μM, respectively) was four and three times lower than of the barley enzyme (Table 3), suggesting that the LD binding site possesses a higher level of plasticity allowing generally optimization of the ligand interactions. β-CD is by far the preferred ligand, thus underscoring the resemblance between the conformations of β-CD and α-glucan helices present in starch [1]. The strong binding of β-CD to LD is most likely caused by aromatic stacking in the active site cleft as supported by the reported K_i value of 40 μM [4]. An enhanced β-CD–Sepharose binding in 1 M ammonium sulfate, secured very high recovery of LD from the culture supernatant. A lower specific activity of LD in the β-CD–Sepharose eluate was probably due to residual β-CD, which was efficiently removed by gel filtration, resulting in a final specific activity of 14.2 U/mg or approximately twice the value measured for LD purified from barley malt [50]. The high specific activity was also reflected by the kinetic constants $k_{cat,app}$ = 78 $s^{-1}$and $K_{m,app}$ = 0.16 mg/mL. Previously, K_m and k_{cat} values for barley malt LD hydrolyzing pullulan at pH 5.0 and 40 °C were reported in the ranges 0.16–0.44 mg/mL and 33–60 s^{-1}, respectively [26,27], and giving 2.4–3.5-fold lower catalytic efficiency than the present recombinant LD. In comparison reported K_m and k_{cat} values of pullulanases from *Klebsiella planticola* and *Bacillus acidopullulyticus* were 0.09 mg/mL and 81 s^{-1}, and 0.24 mg/mL and 120 s^{-1}, respectively [27].

The deviation from the hyperbolic fit of the kinetic data at pullulan concentrations above 0.2 mg/mL (Fig. 4) has not previously been described for barley LD. This behavior may reflect transglycosylation reactions even though the initial rate kinetics towards pullulan models an uncompetitive substrate inhibition. Transfer of fluorescently labeled maltotriose onto newly hydrolyzed pullulan [51] provides evidence for barley LD catalyzed transglycosylation and transglycosylation was also reported for rice LD using pullulan as substrate [52]. Although the *in vivo* function of LD is mostly considered in starch debranching, the present findings motivate further kinetic and structural analysis to elucidate features that contribute to the transglycosylation activity and the suggested role in starch biosynthesis.

The successful production of functional and stable recombinant LD enables studies of the molecular basis for the substrate specificity and transglycosylation as well as the regulation of LD activity by the endogenous proteinaceous inhibitor LDI. Overall the access to recombinant LD makes it possible to gain new insights into starch metabolism in cereals and other plants.

Acknowledgments

The expert technical assistance of Karina Jansen, Morten Ejby and Anne Blicher is gratefully acknowledged. Martin J. Baumann is thanked for fruitful discussions of the transglycosylation activity of carbohydrases. This work is supported by a Ph.D. scholarship from DTU to MBVC, the Danish Natural Science Research Council, the Centre for Advanced Food Studies, and the Carlsberg Foundation.

References

[1] A. Buléon, P. Colonna, V. Planchot, S. Ball, Starch granules: structure and biosynthesis, Int. J. Biol. Macromol. 23 (1998) 85–112.
[2] D.J. Manners, D. Yellowlees, Studies on carbohydrate metabolising enzymes. Part XXVI. Limit dextrinase from germinated barley, Starch/Stärke 23 (1971) 228–234.
[3] A.W. MacGregor, α-amylase limit dextrinase, and α-glucosidase enzymes in barley and malt, Crit. Rev. Biotechnol. 5 (1987) 117–128.
[4] M. Kristensen, F. Lok, V. Planchot, I. Svendsen, R. Leah, B. Svensson, Isolation and characterization of the gene encoding the starch debranching enzyme limit dextrinase from germinating barley, Biochim. Biophys. Acta 1431 (1999) 538–546.
[5] P.M. Coutinho, B. Henrissat, Carbohydrate-active enzymes server. Available from: <www.Cazy.Org/>.
[6] M.R. Stam, E.G.J. Danchin, C. Rancurel, P.M. Coutinho, B. Henrissat, Dividing the large glycoside hydrolase family 13 into subfamilies: towards improved functional annotations of alpha-amylase-related proteins, Protein Eng. Des. Sel. 19 (2006) 555–562.
[7] R.A. Burton, X.Q. Zhang, M. Hrmova, G.B. Fincher, A single limit dextrinase gene is expressed both in the developing endosperm and in germinated grains of barley, Plant Physiol. 119 (1999) 859–871.
[8] S.W. Schroeder, A.W. MacGregor, Synthesis of limit dextrinase in germinated barley kernels and aleurone tissues, J. Am. Soc. Brew. Chem. 56 (1998) 32–37.
[9] J.R. Dinges, C. Colleoni, M.G. James, A.M. Myers, Mutational analysis of the pullulanase-type debranching enzyme of maize indicates multiple functions in starch metabolism, Plant Cell 15 (2003) 666–680.
[10] T. Delatte, M. Umhang, M. Trevisan, S. Eicke, D. Thorneycroft, S.M. Smith, S.C. Zeeman, Evidence for distinct mechanisms of starch granule breakdown in plants, J. Biol. Chem. 281 (2006) 12050–12059.
[11] M.J. Sissons, R.C.M. Lance, D.H.B. Sparrow, Studies on limit dextrinase in barley. 3. Limit dextrinase in developing kernels, J. Cereal Sci. 17 (1993) 19–24.
[12] C. Martin, A.M. Smith, Starch synthesis, Plant Cell 7 (1995) 971–985.
[13] A.M. Smith, The biosynthesis of starch granules, Biomacromolecules 2 (2001) 335–341.
[14] S. Streb, T. Delatte, M. Umhang, S. Eicke, M. Schorderet, D. Reinhardt, S.C. Zeeman, Starch granule biosynthesis in *Arabidopsis* is abolished by removal of all debranching enzymes but restored by the subsequent removal of an endoamylase, Plant Cell 20 (2008) 3448–3466.
[15] M.A. Longstaff, J.H. Bryce, Development of limit dextrinase in germinated barley (*Hordeum vulgare* L.) (evidence of proteolytic activation), Plant Physiol. 101 (1993) 881–889.
[16] L.J. Macri, A.W. MacGregor, S.W. Schroeder, S.L. Bazin, Detection of a limit dextrinase inhibitor in barley, J. Cereal Sci. 18 (1993) 103–106.
[17] A.W. MacGregor, L.J. Macri, S.W. Schroeder, S.L. Bazin, Purification and characterization of limit dextrinase inhibitors from barley, J. Cereal Sci. 20 (1994) 33–41.
[18] J.H. Wong, I.A. Iiao, K. Kobrehel, B.B. Buchanan, Thioredoxin-dependent deinhibition of pullulanase of barley malt by inactivation of a specific inhibitor protein, Plant Physiol. 108 (1995) 67.
[19] C.A. McCafferty, H.R. Jenkinson, J.M. Brosnan, J.H. Bryce, Limit dextrinase—does its malt activity relate to its activity during brewing, J. Inst. Brew. 110 (2004) 284–296.
[20] I.C. MacWilliam, G. Harris, The separation of limit dextrinase from R-enzyme and aspects of the activity of the separated enzymes, Arch. Biochem. Biophys. 84 (1959) 442–454.
[21] C.Y. Wu, C. Colleoni, A.M. Myers, M.G. James, Enzymatic properties and regulation of ZPU1, the maize pullulanase-type starch debranching enzyme, Arch. Biochem. Biophys. 406 (2002) 21–32.
[22] A. Renz, S. Schikora, R. Schmid, J. Kossmann, E. Beck, CDNA sequence and heterologous expression of monomeric spinach pullulanase: multiple isomeric forms arise from the same polypeptide, Biochem. J. 331 (1998) 937–945.
[23] A. Repellin, M. Baga, R.N. Chibbar, *In vitro* pullulanase activity of wheat (*Triticum aestivum* L.) limit-dextrinase type starch debranching enzyme is modulated by redox conditions, J. Cereal Sci. 47 (2008) 302–309.
[24] B.K. Tibbot, C.A. Henson, R.W. Skadsen, Expression of enzymatically active, recombinant barley alpha-glucosidase in yeast and immunological detection of alpha-glucosidase from seed tissue, Plant Mol. Biol. 38 (1998) 379–391.
[25] H. Naested, B. Kramhoft, F. Lok, K. Bojsen, S.K. Yu, B. Svensson, Production of enzymatically active recombinant full-length barley high pI alpha-glucosidase of glycoside family 31 by high cell-density fermentation of *Pichia pastoris* and affinity purification, Protein Expr. Purif. 46 (2006) 56–63.
[26] L. Greffe, M.T. Jensen, C. Bosso, B. Svensson, H. Driguez, Chemoenzymatic synthesis of branched oligo- and polysaccharides as potential substrates for starch active enzymes, Chembiochem 4 (2003) 1307–1311.
[27] L. Greffe, M.T. Jensen, F. Chang-Pi-Hin, S. Fruchard, M.J. O'Donohue, B. Svensson, H. Driguez, Chemoenzymatic syntheses of linear and branched hemithiomaltodextrins as potential inhibitors for starch-debranching enzymes, Chem. Eur. J. 8 (2002) 5447–5455.
[28] J. Sambrook, D. Russell, Molecular Cloning, a Laboratory Manual, Cold Spring Harbour Laboratory Press, Cold Spring Harbour, New York, 2001.
[29] Invitrogen, *Pichia* expression kit, a manual of methods for expression of recombinant proteins in *Pichia pastoris* Invitrogen manual K1710-01, 2008. Available from: <www.Invitrogen.Com/>.
[30] M. Kristensen, V. Planchot, J.I. Abe, B. Svensson, Large-scale purification and characterization of barley limit dextrinase, a member of the α-amylase structural family, Cereal Chem. 75 (1998) 473–479.
[31] J. Stratton, V. Chiruvolu, M. Meager, High cell-density fermentation, in: D.R. Higgings, J.M. Cregg (Eds.), *Pichia* Protocols. Methods in Molecular Biology, Humana Press, Inc., Totowa, NJ, 1998, pp. 107–120.
[32] Invitrogen, *Pichia* fermentation process guidelines, 2008. Available from: <www.Invitrogen.Com/>.
[33] B.V. McCleary, Measurement of the content of limit dextrinase in cereal flours, Carbohydr. Res. 227 (1992) 257–268.
[34] J.D. Fox, J.F. Robyt, Miniaturizing of 3 carbohydrate analyses a microsample plate reader, Anal. Biochem. 195 (1991) 93–96.

Please cite this article in press as: M.B. Vester-Christensen et al., Secretory expression of functional barley limit dextrinase by *Pichia pastoris* using high cell-density fermentation, Protein Expr. Purif. (2009), doi:10.1016/j.pep.2009.08.016

[35] G. Candiano, M. Bruschi, M. Musante, L. Santucci, G.M. Ghiggeri, B. Carnemolla, P. Orecchia, L. Zardi, P.G. Righetti, Blue silver: a very sensitive colloidal Coomassie G-250 staining for proteome analysis, Electrophoresis 25 (2004) 1327–1333.
[36] J. Gobom, E. Nordhoff, E. Mirgorodskaya, R. Ekman, P. Roepstorff, Sample purification and preparation technique based on nano-scale reversed-phase columns for the sensitive analysis of complex peptide mixtures by matrix-assisted laser desorption/ionization mass spectrometry, J. Mass Spectrom. 34 (1999) 105–116.
[37] V. Barkholt, A.L. Jensen, Amino-acid analysis—determination of cysteine plus half-cystine in proteins after hydrochloric-acid hydrolysis with a disulfide compound as additive, Anal. Biochem. 177 (1989) 318–322.
[38] T. Hastie, J. Friedman, R. Tibshirani, The Elements of Statistical Learning: Data Mining, Inference, and Prediction, Springer, New York, NY, 2001.
[39] M.J. Baumann, J.M. Eklof, G. Michel, A.M. Kallas, T.T. Teeri, M. Czjzek, H. Brumer, Structural evidence for the evolution of xyloglucanase activity from xyloglucan endo-transglycosylases: biological implications for cell wall metabolism, Plant Cell 19 (2007) 1947–1963.
[40] H. Brumer, P.F.G. Sims, M.L. Sinnott, Lignocellulose degradation by *Phanerochaete chrysosporium*: purification and characterization of the main α-galactosidase, Biochem. J. 339 (1999) 43–53.
[41] H. Iwamoto, M. Ohno, M. Ohmori, J. Hirose, A. Tanaka, S. Sakai, K. Hiromi, Comparison of the binding of β-cyclodextrin and α-cyclodextrin and γ-cyclodextrin with pullulanase from *Klebsiella pneumoniae* as studied by equilibrium and kinetic fluorometry, J. Biochem. 116 (1994) 1264–1268.
[42] A.W. MacGregor, S.L. Bazin, L.J. Macri, J.V. Babb, Modelling the contribution of alpha-amylase, beta-amylase and limit dextrinase to starch degradation during mashing, J. Cereal Sci. 29 (1999) 161–169.
[43] H.A. Ross, J. Sungurtas, L. Ducreux, J.S. Swanston, H.V. Davies, G.J. McDougall, Limit dextrinase in barley cultivars of differing malting quality: activity, inhibitors and limit dextrin profiles, J. Cereal Sci. 38 (2003) 325–334.
[44] M.T. Jensen, Structure and function of barley limit dextrinase. Mutational analysis of barley α-amylase isozyme differences and interaction with branched oligosaccharides, Institute of Biochemistry and Molecular Biology, University of Southern Denmark, DK-5230 Odense M, 2004, p. 171.
[45] M. Jahic, F. Wallberg, M. Bollok, P. Garcia, S. Enfors, Temperature limited fed-batch technique for control of proteolysis in *Pichia pastoris* bioreactor cultures, Microb. Cell Fact. 2 (2003) 1–11.
[46] M.M. Whittaker, J.W. Whittaker, Expression of recombinant galactose oxidase by *Pichia pastoris*, Protein Expr. Purif. 20 (2000) 105–111.
[47] J.H. Woo, Y.Y. Liu, S. Stavrou, D.M. Neville, Increasing secretion of a bivalent anti-T-cell immunotoxin by *Pichia pastoris*, Appl. Environ. Microbiol. 70 (2004) 3370–3376.
[48] B. Gasser, M. Saloheimo, U. Rinas, M. Dragosits, E. Rodríguez-Carmona, K. Baumann, M. Giuliani, E. Parrilli, P. Branduardi, C. Lang, D. Porro, P. Ferrer, M. Tutino, D. Mattanovich, A. Villaverde, Protein folding and conformational stress in microbial cells producing recombinant proteins: a host comparative overview, Microb. Cell Fact. 7 (2008) 1–18.
[49] M. Sissons, M. Taylor, M. Proudlove, Barley malt limit dextrinase—its extraction, heat-stability, and activity during malting and mashing, J. Am. Soc. Brew. Chem. 53 (1995) 104–110.
[50] A.W. MacGregor, L.J. Macri, S.W. Schroeder, S.L. Bazin, Limit dextrinase from malted barley: extraction, purification and characterization, Cereal Chem. 71 (1994) 610–617.
[51] G.J. McDougall, H.A. Ross, J.S. Swanston, H.V. Davies, Limit dextrinase from germinating barley has endotransglycosylase activity, which explains its activation by maltodextrins, Planta 218 (2004) 542–551.
[52] Y. Yamasaki, S. Nakashima, H. Konno, Pullulanase from rice endosperm, Acta Biochim. Pol. 55 (2008) 507–510.

Please cite this article in press as: M.B. Vester-Christensen et al., Secretory expression of functional barley limit dextrinase by *Pichia pastoris* using high cell-density fermentation, Protein Expr. Purif. (2009), doi:10.1016/j.pep.2009.08.016

CRYSTAL STRUCTURE OF BARLEY LIMIT DEXTRINASE. A DEBRANCHING ENZYME INVOLVED IN STARCH BIOSYNTHESIS AND BREAK DOWN

Malene Bech Vester-Christensen[1,2], Maher Abou Hachem[1], Birte Svensson[1*], and Anette Henriksen[2*]

From Enzyme and Protein Chemistry[1], Department of Systems Biology, Søltofts Plads, Building 224, Technical University of Denmark, DK-2800 Kgs. Lyngby, Denmark and the Protein Chemistry Group[2], Carlsberg Laboratory, Carlsberg Research Center, Gamle Carlsberg Vej 10, DK-2500 Valby, Denmark

Running head: Crystal structure of barley limit dextrinase

Address correspondence to: Anette Henriksen, Protein Chemistry Group, Carlsberg Laboratory, Carlsberg Research Center, Gamle Carlsberg Vej 10, DK-2500 Valby, Denmark. Phone + 45 33 27 52 22; E-mail: anette@crc.dk and Birte Svensson, Enzyme and Protein Chemistry, Department of Systems Biology, Søltofts Plads, Building 224, Technical University of Denmark, DK-2800 Kgs. Lyngby, Denmark. Phone +45 4525 2740; Fax +45 4588 6307; E-mail bis@bio.dtu.dk

Barley limit dextrinase (HvLD)[1] catalyses hydrolysis of α-1,6-glucosidic linkages from the amylopectin component of starch, an activity that plays a role in starch degradation during germination and presumable also in starch biosynthesis during grain filling. The crystal structures of HvLD in complex with the competitive inhibitors α- and β-cyclodextrin (CD) are solved and refined to 2.5 Å and 2.1 Å, respectively. HvLD belongs to glycoside hydrolase family 13 (subfamily 13) and is composed of four domains; an eight β-strand N-terminal domain; a putative carbohydrate binding module (CBM48), a catalytic $(\beta/\alpha)_8$-like barrel domain lacking α-helix 5; and a C-terminal two-sheet β-sandwich motif domain. The CDs as expected are accommodated at the carbohydrate main-chain binding-site occupying aglycone subsites +1 and +2. A glycerol and three water molecules mimic a glucose residue at subsite –1, thereby identifying residues involved in substrate binding. The spaciousness of Met[440], a unique residue at its position amongst the α-1,6 acting enzymes would clash with any glucose residue at subsite –4. The observed steric hindrance is proposed to affect substrate specificity. A part of an extended loop (residues Asp[513]–Asn[520]) between β5 and β6 of the catalytic domain differs from microbial pullulanases in sequence and structure and seems to contribute both to the observed substrate specificity and to higher affinity of HvLD towards α-CD compared to pullulanases. Novel insight into specificity determinants and a possible role in starch biosynthesis is illuminated by this first structure of a plant limit dextrinase.

Starch is the most prominent carbohydrate in the human diet and the major carbohydrate reserve in cereal seeds where it is found as compact supramolecular granules. Starch is also a very important industrial raw material. Barley seed starch is composed of about 70% amylopectin, an α-glucan containing α-1,6 glucosidally linked branch points, and 30% amylose, a linear α-1,4-glucan (reviewed in (1)). In addition to starch synthases and branching enzymes, successful biosynthesis of amylopectin in plants involves two types of α-1,6 debranching enzymes, the limit dextrinases (LDs, EC 3.2.1.41) or pullulanases and the isoamylases (EC 3.2.1.68) (2,3).

LD is found in developing grains in accordance with a role in starch biosynthesis (4-6). Maize mutants lacking pullulanase-type debranching enzyme, *i.e.* LD, exhibit changes in starch granule morphology (7). Moreover, starch granule biosynthesis is abolished in quadruple *Arabidopsis* knock-outs deficient in three isoamylase isozymes and the single LD isozyme (8). This further supports the hypothesis that the amylopectin structure is the result of the action of debranching and branching enzyme activities (9-11). Debranching in starch degradation during germination, however, depend solely on LD that has high activity towards α-1,6 glucosidic linkages in limit dextrins derived from amylopectin (12), but the enzyme display

remarkably low activity on amylopectin itself (13).

LD is highly activity towards pullulan, a linear polysaccharide composed of α-1,6-linked maltotriose repeats (12,13). LD therefore has been classified with the pullulanases that are large multidomain enzymes of either glycoside hydrolase family 13 subfamily 12 (firmicutes), subfamily 13 (bacteria and eukaryota) or subfamily 14 (bacteria) (14,15). Several plant pullulanase – also referred to as LD - encoding genes have being identified, but the vast majority of characterized pullulanases are microbial. The lack of an LD structure stems for its low natural abundance and lack of efficient heterologous expression systems. Previous attempts to produce maize (16), spinach (17), and wheat (18) LD recombinantly resulted in very low yields. However, our recently established expression in *Pichia pastoris* provides > 20 mg functional HvLD (19). The kinetics of pullulan hydrolysis showed deviation from the Michaelis-Menten model at relatively low substrate concentrations and initial hydrolysis rates were modeled by including a substrate inhibition term to give $K_{m,app}$ = 0.16 mg/ml and $k_{cat,app}$ = 78 s^{-1}. This behaviour may also reflect a high intrinsic transglycosylation activity or a combination of this and substrate inhibition (19). This kinetic seems to be unique for LD and may have biologically significance through the proposed role of LD in amylopectin biosynthesis. Recombinant HvLD has up to 3.5-fold higher catalytic efficiency than LD purified from germinating barley seeds (12,19,20). Surface plasmon resonance (SPR) and activity assays (21) showed β-cyclodextrin (CD) to bind strongly (K_d of 0.7 µM), while α- and γ-CD had 40–50 times weaker affinity for HvLD (19). The affinity of β-CD for HvLD and *Klebsiella pneumoniae* pullulanase (KpPUL) was in the same range, whereas KpPUL had 4 and 3 times lower affinity for α- and γ-CD, respectively (22) The significantly higher affinity with β-CD was suggested to reflect its resemblance with the conformation of α-glucan helices in starch (1,19).

Several α-1,6 glucoside hydrolases, *i.e.* pullulanases and LDs (EC 3.2.1.41), isoamylases (EC 3.2.1.68), neopullulanases (EC 3.2.1.135), the latter having a α-1,4 activity as the main activity, share a similar domain organisation, although the number of domains can vary. Hence, pullulanases possess an N-terminal part varying in length and which can be composed of several structural domains including carbohydrate binding modules (CBMs) preceding the catalytic $(\beta/\alpha)_8$-like barrel domain. In LDs and pullulanases a loop protrudes between β-strand 2 and α-helix 2 and is often referred to as Loop 2 (23). Furthermore, a long loop connects β-strand 3 and α-helix 3 (by convention called B-domain (23,24)), despite the fact that this is not a truly independent domain. The catalytic domain is followed by a C-terminal two-sheet β-sandwich fold described first in TAKA-amylase A, an α-amylase from *Aspergillus oryzae* (25).

LDs and isoamylases have one annotated CBM namely CBM48 (26), whereas 3D structures of KpPUL and *Bacillus acidopullulyticus* pullulanase (BaPUL) (27,28) show both CBM41 and CBM48 situated N-terminally to the catalytic domain. Based on multiple sequence alignment of GH13 family members and using Pfam domain prediction (23,29), the catalytic domain of LD was proposed to be preceded by an N-terminal part including a sequence of unknown function and a CBM48 module (26).

Besides the biologically important roles in starch biosynthesis and degradation, HvLD catalyzed hydrolysis of branched maltooligosaccharides in malting and mashing is central for beer production (30). Although HvLD was studied since the fifties (31) insight is lacking both on the precise biological role of HvLD and on the molecular basis for its substrate specificity also in industrial processes.

The crystal structures of HvLD in complex with the inhibitors α- and β-CD are described and represent the first LD crystal structures. The two LD/ligand complexed structures provide novel insight on the carbohydrate LD interactions at the substrate main-chain aglycone binding subsites +1 and +2. The protein carbohydrate recognition and residues involved in specificity are discussed including structures of other α-1,6 acting enzymes.

EXPERIMENTAL PROCEDURES

Crystallization and Data Collection. HvLD showing $K_{m,app}$ = 0.16 mg/ml and $k_{cat,app}$ = 78 s^{-1} toward pullulan and a single band on SDS-PAGE was obtained using *Pichia pastoris* as host and concentrated to 9 mg/ml for the initial crystallization screens (19). Initially, crystallization using the hanging-drop, vapor-diffusion method was explored with Crystal Screen™, Crystal Screen™ 2, and PEG/Ion™ Screen (Hampton Research, Aliso Viejo, CA) at 22 °C. The HvLD solution contained β-CD in a 1:10 molar ratio. Crystals obtained from different condition in the PEG/Ion Screen all showed the same crystal morphology, *i.e.*, bundles of very thin needles. These were used for micro-seeding in later screens.

Prior to crystallization, HvLD (20 mg/ml; 50 mM MES, pH 6.6, 250 mM NaCl) was incubated on ice with α- or β-CD in 6-fold molar excess and final HvLD concentration of 13.3 mg/ml. The crystallization drop was placed on cover slips mixing 1.5 µl HvLD-CD with 1 or 2 µl reservoir solution. Additive Screen I–III (Hampton Research) was used to optimize crystallization conditions. Based on the additive screen cysteine (0.2 µl, 0.1 M) was added to the drop to a final concentration of 5–7 mM. HvLD:β-CD co-crystals were obtained using a reservoir solution of 22% (w/v) PEG 3350, 5% (v/v) glycerol, 0.3 M NaI and streak seeding the drops, or a reservoir solution of 30% (w/v) PEG 3350, 10% (v/v) glycerol, 0.3 M NaI without seeding. HvLD:α-CD co-crystals were obtained using a reservoir solution of 30% (w/v) PEG 3350, 0.3 M NaI without seeding. In all cases, crystals appeared within one week. HvLD:β-CD crystals grown in 22% (w/v) PEG and 5% (v/v) glycerol were cryo-protected using a 1:1 mix of reservoir solution and PEG 400. HvLD:α-CD crystals were cryo-protected using a 1:1 mix of reservoir solution and 30% (w/v) PEG 3350, 10% (v/v) glycerol, 0.3 M NaI. All crystals used for data collection were mounted on Mesh Litholoops (loop size 0.2 mm and mesh size 40 µm; Molecular Dimensions, Newmarket, UK) and flash-frozen in a steam of nitrogen. Crystal mounting in conventional cryo-loops gave rise to excessive mosaicity in the diffraction data.

X-ray diffraction data of HvLD:β-CD crystals were collected at the ESRF, Grenoble, France at the micro focus beamline ID23-2 at a wavelength of 0.873 Å. X-ray diffraction data of HvLD:α-CD were collected at MAX-lab II, Lund University, Sweden at beamline I911-5 at a wavelength 0.91 Å.

Phasing, Model Building, Refinement and Structural Analysis. The data were integrated in Mosflm (32) scaled using the program Scala from the CCP4i Suite (33,34), and the resultant structure factors were used for molecular replacement using Phaser (35) based on residues 177–1070 from KpPUL (PDB code: 2FGZ). The initial HvLD:β-CD model was build using Phenix.autobuild from the molecular replacement (MR) phases and included 95% of the HvLD amino acid residues. Several rounds of model building and refinement were needed for both HvLD:β-CD and HvLD:α-CD using Phenix.refine (36) with simulated annealing and translation/libration/screw (TLS) refinement (15 segments) activated (37) and COOT 0.5.2 (38) for molecular visualization, validation and rebuilding. The HvLD:β-CD structure was used as model for MR to solve the structure of HvLD:α-CD. In addition to the COOT validation functions, final analysis of model geometry optimization were done in PROCHECK (39) and Molprobity (40). The structure of HvLD was compared with KpPUL, (apo, PDB code: 2FGZ; G4, 2FHF), *Bacillus subtilis* str. 168 (BsPUL) (2E8Y), and BaPUL (2WAN), as well as isoamylase from *Pseudomonas amyloderamosa* (PaISO) (1BF2) and *E. coli* glycogen branching enzyme (1M7X) using the program Pymol 1.1 which was also used for rendering the structural figures (41). The protein secondary structure motifs were obtained from PDBsum which are computed using PROMOTIF v.3.0 (42). The final round of phenix.refine included all reflections, while all other refinement rounds had 5% randomly chosen reflections kept aside as test set.

RESULTS

Crystallization, Structure Determination and Model Quality. While initial crystallization

trials of HvLD failed to produce crystals within three months, the PEG/Ion Screen ultimately resulted in protein crystals within a year. HvLD was found to crystallize as bundles of very thin needles under different conditions, which all contained either iodine or thiocyanate. The crystal morphology did not depend on protein or precipitant concentration, but addition of cysteine resulted in thicker separate, single crystal needles. Crystals obtained from seeded drops were very homogenous and measured 0.002 × 0.002 × 0.006 mm^3, while crystals obtained without seeding were slightly bigger and of highly variable quality. The seeded needles diffracted to 2.6 Å and belonged to space group $P2_12_12_1$, with one molecule in the unit cell and cell dimensions of a = 85.0 Å, b = 93.8 Å and c = 114.7 Å. The non-seeded crystals of HvLD:β-CD and HvLD:α-CD were of space group *C*2 and diffracted to 2.1 Å and 2.5 Å, respectively, with one molecule in the unit cell and solvent contents of 43.7% (HvLD:β-CD) and 47.2% (HvLD:α-CD). Cell dimensions are given in Table 1 that summarizes data collection statistics.

The final structures show overall good electron density. However, the first two amino acids and residues 22–28, 40–49, and 102–109 in the N-domain had low level or no sigmaA weighted $2F_o$-F_c electron density and were not included in the models. In addition to the three loops in the N-domain, loop 806–810 in the C-domain had less than 1σ $2F_o$-F_c electron density for both side- and main-chain atoms. Two calcium ions, iodide (9 in HvLD:α-CD; 5 in HvLD:β-CD), glycerol (one in HvLD:α-CD; 7 in HvLD:β-CD) and water molecules (223 in HvLD:α-CD; 604 in HvLD:β-CD) are modeled and the resulting R_{cryst} and R_{free} from the refinement are 16.3% and 20.0% for the HvLD:β-CD and 17.7% and 22.6% for the HvLD:α-CD structure, respectively (Table 1). R_{cryst} dropped to 15.7% and 17.3%, respectively, in the final refinement cycle that included all reflections. The HvLD moieties of the two cyclodextrin complexes are virtually identical with an r.m.s.d. of 0.7 Å for all C^{α} atoms. Due to the higher resolution of the HvLD:β-CD, this complex is used to describe the overall structure.

The geometry of the models is good with approximately 89% of the residues in the most favored region of the Ramachandran plot and only one residue (Phe^{566}) in a disallowed region. Phe^{566} is in a turn in the loop between β-strand 6 and α-helix 6 of the $(\beta/\alpha)_8$-like barrel. The unfavorable φ and ψ angles in this tight turn could be caused by the bi-dentate salt bridge between the spatially adjacent Glu^{568} and Arg^{875}, and the multiple hydrogen bonds emanating from Gln^{559}: Gln^{559} Nε2 - Glu^{568} O, Gln^{559} Nε2 - Thr^{563} O, Gln^{559} Oε1 - Gln^{574} Nε2 and Gln^{559} Oε1 - Asn^{570} N. In addition, the aliphatic part of the Arg^{581} side-chain contributes to hydrophobic interactions with the side-chain of Phe^{566}. Three residues Ala^{439}, Ala^{515} and Asn^{643} were found in the generously allowed region of the Ramachandran plot. Ala^{439} is in the center of a loop located in between two α-helices in the B-domain part of the catalytic domain (23). The β-turn in the loop is sustained by the hydrogen bond between the main-chain Ala^{439} N and the main-chain Asn^{436} O. Ala^{515} is borderline to an additional allowed region in the φ/ψ plot and placed in the loop region, which also contains the general acid, Glu^{510} and Trp^{512} (at subsite +2, see below for detailed description). The exact position of this loop exposes Phe^{514} towards subsite +2. It is influenced by hydrogen bonds between Asp^{513} Oδ1 - Asn^{525} Nδ2, Asp^{513} Oδ2 - Ala N, Glu^{516} Oε1 - Ser^{437} Oγ, Glu^{516} Oε2 -Asn^{442} Nδd and the salt bridge Glu^{516} Oε2 - Arg^{427} Nη1. The strained φ and ψ angles of Asn^{643}, which is positioned next to the third acid in the catalytic site, is due to the Asn^{643} N - Arg^{697} O hydrogen bond, but also the direct interactions of the side-chain with the β-CD glucose residue at subsite +1 could have an effect.

Overall Structure. The final model of HvLD in complex with β-CD is shown in Figure 1. The domain boarders, indicated by sequence alignment with structurally related proteins (23), are slightly displaced relative to those seen from the HvLD structure. The structure comprises four structural domains; the N-domain (reidues 3–124) of unknown function, a carbohydrate binding module (125–230) assigned to CBM48 of which a few members have been demonstrated to bind to glycogen

(26), the catalytic domain (231–774), and the C-domain (775–885) of unknown function. The N-domain consists of 8 β-strands arranged primarily in an anti-parallel fashion and 4 α-helices: the CBM48 contains 9 strands and 2 α-helices; while the catalytic domain has 33 α-helices and 12 β-strands. The core of this domain forms a $(\beta/\alpha)_8$-like barrel (Suppl. material Table S2) resembling the corresponding domain in α-amylases (25,43) except that HvLD has no helix α5, but a loop connecting β5 and β6 which carries Trp^{512} and embeds subsite +2. As observed in the KpPUL structure (27) and previously described as Loop 2 (23,27,44), a long loop protrudes from the barrel scaffold following the second β-strand, which includes Tyr^{357} and forms part substrate binding subsite –1 (see below for detailed description of the active site). The loop referred to as the B-domain extends from β3. It makes part of the active site cleft contributing to accommodate the oligosaccharide substrate branch chain as identified by superimposition of HvLD:β-CD with the KpPUL:maltotetraose (G4) complex. Finally, the C-domain comprises a β-sandwich fold, in which each of the two sheets in the sandwich contains 4 β-strands flanked by 4 short α-helices.

Two Ca^{2+} binding sites were found in both HvLD:α-CD and HvLD:β-CD (Fig. 2). The first site is located in Loop 2 close to subsite –1 and Tyr^{357} and is identical to one of the five Ca^{2+} binding sites identified in KpPUL (27). It shows pentagonal bipyramidal geometry, with Ca^{2+} ligated by the side-chain oxygen atoms of Asp^{351} (Oδ1) and Asn^{701} (Oδ1), the main-chain carbonyl oxygens of Gln^{348} and Tyr^{353} and three water molecules (Fig. 2A). The average Ca^{2+}-O distance is 2.6 Å. The second HvLD Ca^{2+} site has an octahedral geometry. The Ca^{2+} ligands are the side-chain oxygen of Ser^{297} Oγ, main-chain carbonyl oxygens of Gly^{393}, Leu^{301} and Ser^{297}, and two water molecules. This site is located in the catalytic domain and connects the loops extending from the C-terminal ends of β-strand 2 (Loop 2) and 3 (B-domain) (Fig. 2B*)*. The average Ca^{2+}-O distance is 2.7 Å. One negatively charged residue contributes to metal binding in site 1, while no negative charge contributes to metal binding in site 2.

The Active Site of HvLD and Cyclodextrin Binding. The active site is defined by the positions of the catalytic residues, *i.e.* the catalytic nucleophile Asp^{473}, the general acid/base catalyst Glu^{510} and the third catalytic site acid Asp^{642} (Fig. 1 and Fig. 3B-D) as confirmed by sequence alignment (24,44,45). The α- and β-CDs are bound at this site (Fig. 3B). Designation of the substrate-binding subsite numbering is in accord with previous definitions (27,46). Subsites at the reducing end of the substrate are defined by positive numbers and subsites at the non-reducing end have negative numbers, all starting from the point of hydrolysis (46). The active site of HvLD is composed of two binding sites; the first (the branch binding site) is defined by subsites –1 and –2 and the second (the main-chain site) comprises subsites +2 through 0' (Fig. 3A). Due to different structural restraints imposed by the cyclic six- and seven-membered oligo-glucoside rings, α- and β-CD bind differently to HvLD (Fig. 3B) and β-CD (K_d = 0.7 μM) has 40-fold higher affinity for HvLD than α-CD (K_d = 27.2 μM) (19).

Several amino acid residues of HvLD are involved in binding of β-CD (Fig. 3D and Fig. 4). The majority of β-CD-protein interactions occur at subsite +2. Asp^{541} Oδ2 is in hydrogen bond contact with Glc O2, Arg^{544} Nη2 interact with Glc O2, and Nη1 interacts with Glc O3 (Fig. 4). The position of Arg^{544} is further stabilized by a hydrogen bond between Arg^{544} Nη1 and the hydroxyl group of Tyr^{637} (Fig. 3C, D). Finally, the indole ring of Trp^{512} stacks with the Glc at subsite +2 (Fig. 3C, D and Fig. 4). The Trp^{512} Nε1 interacts with the general acid/base Glu^{510} Oε2, stabilizing the position of this pivotal residue. At subsite +1, Asn^{643} Nδ2 interacts with O3 of Glc. Furthermore, Asn^{643} Oδ1 interacts *via* a water molecule with O2 and O3 of Glc at subsite 0' (Fig. 3B; Fig. 4). In addition, van der Waals interactions between Arg^{697} and Glc at subsite 0' are observed. Binding at this site could be stabilized by water mediated contacts to Arg^{697} O and Asp^{698} Oδ1. Finally, the aromatic ring of Phe^{553} is immersed in the central cavity of the β-CD molecule having van der Waals interactions or possibly weak aromatic hydrogen bonds (C(-H)..O distance = 3.3 Å–

3.9 Å) to O4 of several Glc units of β-CD (Fig. 3D). The Phe^{553} Cζ is situated in the plane defined by the β-CD Glc residues, with an approximate inclination between this plane and the plane of the Phe^{553} aromatic ring of 20°. Furthermore, the Phe^{553} O interacts *via* a water molecule with O3 of Glc of β-CD opposite subsite –1 (Fig. 4). This interaction is not present in HvLD:α-CD. Comparing the α-CD and the β-CD HvLD complexes we suggest that the 40-fold weaker binding of α-CD (19) to be due to lack of interaction between Arg^{697} and two Glc residues both directly or *via* water mediated contact (Fig. 3B), lack of interaction of Asn^{643} Nδ2 and an O3 as well as a missing water mediated interaction between Asn^{643} Oδ1 and O2 and O3 atoms at subsite 0', the absence of a hydrogen bond between Asn^{551} and the Glc residue at subsite +4 (Fig. 4) and a less favorable interaction with Phe^{553}. The α-CD plane is ~1 Å below the Phe^{553} Cζ atom and the inclination between the aromatic ring plane and the α-CD Glc residues is close to 45°, which might give rise to loss of the hydrogen bond character of the interaction. Both CDs have some less well-defined Glc residues (at subsites 0' and –1') with weighted $2F_o–F_c$ less than 1.0σ. Despite the fact that these Glc residues are within interaction range of HvLD (Fig. 3C) they cannot be major contributors to the binding.

Glycerol from the crystallization buffer (HvLD:β-CD) and the cryo-protectant was found in the active site of HvLD:β-CD (Fig.3D). Co-crystallized glycerol (Gol) bound in the active site of carbohydrate active enzymes is a well known phenomenon (47,48). Arg^{471} interacts with Gol^{302} in the active site of HvLD as do the three catalytic residues, while the second glycerol molecule found at the active site (Gol^{303}) are in direct hydrogen bond contact with the catalytic nucleophile Asp^{473} Oδ1/Oδ2 and *via* water mediated hydrogen bonds with Glu^{510} Oε1/Oε2. Moreover, Gol^{303} is at a distance of 4.2 Å of Tyr^{357} (Fig. 3C, D). Superimposition of HvLD:β-CD and KpPUL:G4 (27) shows that the two Gol^{303} primary hydroxyl groups superimpose perfectly with O6 and O5 of Glc at subsite –1 and that the secondary alcohol group is in close proximity to O4 of the same Glc residue. In addition, three water molecules in the HvLD structure are located at the positions corresponding to O1, O2 and O3 of the same Glc residue at subsite –1 of KpPUL (Fig. 3A). Additional five glycerol molecules (Gol^{301}, Gol^{304}–Gol^{307}) were found in HvLD:β-CD (Fig. 1). One (Gol^{306}) is buried in a part of Loop 2 while the rest are solvent exposed. Two were situated on the surface interacting directly or *via* water molecules with HvLD, whereas one was found in the groove formed at the interface of the CBM48 domain and the catalytic domain. The last glycerol molecule was in a solvent channel between the N-domain and the CBM48. Possibly because glycerol was not included in crystallization conditions for HvLD:α-CD but only used as cryoprotectant only one Gol molecule was found in the HvLD:α-CD structure, which was buried in Loop 2 similar to Gol^{306} in HvLD:β-CD.

DISCUSSION

The Overall Structure. The closest structural relative to HvLD is KpPUL (PDB code: 2FGZ). Both enzymes belong to GH13 subfamily 13 (15) and have an overall sequence identity of 30.2% and a similarity of 45.6% (49). KpPUL served, despite this large difference in primary structure, as template for molecular replacement to solve the structure of HvLD. Important induced-fit movement was observed by binding substrate analogues (maltose, maltotriose and maltotetraose) to KpPUL (27). The different geometries between β-CD and α-CD were not large enough to result in significant conformational differences at the active site. However, HvLD crystal were not obtained in the absence of cyclodextrin inhibitors, possibly due to a more flexible and/or differently folded +2 subsite in the apo-protein, as observed for KpPUL (27).

The two HvLD molecules located around the crystallographic two-fold symmetry axis have active sites facing each other in *C*2 (Suppl. material Fig. 1S), while this is not the case in $P2_12_12_1$ crystals. The N-terminal domain that appears flexible and has poorly defined loops, makes up one half of the molecular interface of the crystallographic dimer. A pore (diameter 52 Å) separates the

active sites in the crystallographic dimer. A similar pore, but with a diameter of 66 Å was found in KpPUL and speculated to be relevant for the binding of polysaccharide substrates (27), even though there is no evidence that KpPUL dimerises in solution. The presence of an extra N-terminal domain in KpPUL can explain the larger pore diameter. The presence of similar pores leading to the substrate binding site in the crystal structures of KpPUL and HvLD may suggest a functional importance of the pore. A similar dimeric molecular organization, however, was not observed for the phylogenetically more distant BsPUL and BaPUL both belonging to GH13 subfamily 14. BsPUL and KpPUL both degraded glycogen (50,51), in contrast to HvLD that cannot hydrolyze glycogen and has less <1% of the activity level towards pullulan towards amylopectin (13). The molecular interactions of crystallographic dimers for the debranching PaISO (GH13 subfamily 11) differ from those observed in KpPUL and HvLD. PaISO shows a preference for larger more complex polymers such as amylopectin and glycogen and their β-limit dextrins, but has no activity towards pullulan and low activity towards dextrins (52,53).

Carbohydrate Binding Module 48. CBM48 motifs from GH13_12, GH13_13 and GH13_14 members are all localized N-terminal to the catalytic $(\beta/\alpha)_8$-barrel (26). This is also the case in HvLD (Fig. 1). Structure-based alignment of CBM48 with CBM20, that is known to bind onto raw starch (54), shows that two tryptophans identified as key residues in the interaction with starch or the starch mimic β-CD (55), are conserved in CBM48 - or the glycogen binding domain (GBD) of AMP-activated protein kinase from *Rattus norvegicus*. Furthermore, Trp^{33} and Trp^{100} of GBD are identified in the structure of the β-CD complex as critically involved in binding β-CD to GBD. These tryptophans, however, are both missing in CBM48s of KpPUL (26) and HvLD. In HvLD, Tyr^{212} corresponds to the second tryptophan, Trp^{100} in GBE, and is situated in a cleft and is not exposed on the surface as is the case of Trp^{100} in GBD. This indicates that if HvLD CBM48 is involved in carbohydrate binding, then the binding-mode and key residues differ from those interacting in GBE CBM48. So far functional roles in carbohydrate binding have not yet been confirmed experimentally for any pullulanase (26).

Despite the 6-fold molar excess of CDs present in the HvLD-CD mix used for crystallization, neither α-CD nor β-CD were found to be bound to the CBM48 domain in the HvLD structure, which is in agreement with the observed failure of HvLD to bind onto raw barley starch granules (21).

Ca^{2+} Binding Sites. The Ca1 site (Fig. 2A) is buried in the enzyme (solvent exposed surface area is 1.1 $Å^2$) and only accessible for solvent *via* two of the seven ligands. All protein ligands coordinating the Ca^{2+} except Asp^{701} are from the long protruding Loop 2 that is an important part of the catalytic domain and contributes to the active site. Asn^{701} however, is situated next to Tyr^{700} that interacts with Glc bound at subsite –2 (identified by superimposition of HvLD:β-CD and KpPUL:G4). By connecting Loop 2 with the core of the catalytic domain and thereby shaping a part of the active site, Ca1 is likely to be functionally relevant despite an average Ca^{2+}-O distance of 2.6 Å compared to a mean Ca-O distance in proteins of 2.4 Å (56).

The Ca2 site is more accessible (solvent exposed surface area is 22 $Å^2$) and interacts with ligands from helices α1 and α2 of the $(\beta/\alpha)_8$-barrel. The Ca^{2+} interacts with the protein through only main-chain atoms and this site does not resemble any of the known high affinity sites in α-amylases (57). The site has even longer average Ca^{2+}-O distances than site 1 (average length 2.7 Å) and therefore may be a crystallization artifact rather than a structural relevant site.

$(\beta/\alpha)_8$-Barrel and Substrate Binding Subsites. The $(\beta/\alpha)_8$-like barrel of HvLD has no α-helix 5. This is also observed in several other α-1,6 acting enzymes, *e.g*. KpPUL (27), PaISO (58) and neopullulanase from *Bacillus stearothermophilus* (59). These findings suggest that the lack of α5 contributes to the α-1,6 specificity, whereas the more conserved barrel β-strands 3, 4, 5 and 7 strands and the loops immediately following these strands provide a scaffold for the residues involved in catalysis and substrate binding in both α-1,4 and α-1,6 acting enzymes. Due to the missing

fifth helix the barrel domain has a spacious pocket where the reducing end of the substrate is accommodated and the enzyme becomes less discriminating towards branching in general. Even more important, Trp^{512} gets in position for excellent stacking with Glc at subsite +2 (see below). Despite high structural similarity around the active site there are distinct differences between HvLD and KpPUL especially in the loop replacing between β5 and β6, which is Asp^{513}–Asn^{520} in HvLD and Asp^{709}–Ser^{713} in KpPUL, which differ in both sequence and in conformation. The longer loop in HvLD includes Phe^{514} and seems to narrow the active site cleft near subsites +1 and +2 by 1–3 Å. This loop may therefore contribute to the substrate specificity difference observed between HvLD and KpPUL (13,50,60).

In addition Met^{440} located in a β-turn of B-domain is specific for HvLD and seems essential for its substrate specificity. Superimposition of HvLD:β-CD onto KpPUL:G4 thus shows that Met^{440} clashs with Glc at subsite –4 and this steric hindrance may prevent binding of substrates with a branch chain of four Glc or longer. It is reasonable to believe that HvLD has preference for branches no longer than three Glc units. In KpPUL this particular β-turn is stabilized by a Cys^{643} – Cys^{644} disulfide and by interaction between main-chain Cys^{643} O and O4 of the Glc residue at subsite –3. The position of the main-chain carbonyl group of HvLD Ala^{439} is identical to that of the KpPUL Cys^{643}, suggesting that Ala^{439} may interact with substrate in HvLD. That subsite –3 is involved in substrate chain-length preference agrees with the relative rate of hydrolysis by HvLD of 6^3-α-maltotriosylmaltotetraose, being 2-fold higher than of 6^3-α-maltosylmaltotetraose (13). At subsite –2, stacking between Tyr^{700} and a Glc residue results in very well-defined binding. Furthermore, the distance from Asp^{698} Oδ1 and Oδ2 to O2 and O3 of the Glc residue at this subsite is suggested to be within 3–3.5 Å by superimposing KpPUL:G4 and HvLD and thereby likely to strengthen binding at subsite –2.

The loop between β4 and α4 contains the catalytic nucleophile in GH13 identified as Asp^{473} in HvLD by sequence alignment (24). It contributes together with Tyr^{357}, His^{404}, Arg^{471}, Glu^{510}, Asp^{642} and main-chain Ala^{438} O to form subsite –1. The Gol^{303} and three water molecules (w^{68}, w^{115}, w^{224}), mimicking a Glc at subsite –1, give credibility to the position of the proposed α-1,6 linkage cleavage site.

A conserved Leu^{474} in HvLD found in strictly α-1,6 specific hydrolases, *i.e.* Leu^{678} in KpPUL, Leu^{376} in PaISO, Leu^{623} in BaPUL and Leu^{407} in BsPUL, adjacent to the catalytic nucleophile, obstructs formation of a subsite +1' for a α-1,4 linked Glc residue, corresponding to subsite +1 in α-1,4 active enzymes. This leucine neighbors Trp^{512} thereby aid defining subsite +2 and is proposed to be a key residue in discriminating α-1,4 from α-1,6 acting enzymes. Neopullulanases and amylopullulanases both displaying dual (α-1,4 and α-1,6) activity have the shorter Val rather than Leu at this position, which allows binding at subsite +1 (α-1,4 substrate binding).

Among the most striking differences found by comparison of HvLD and PaISO structures is the presence of Loop 2 and the 33 residues longer loop between β8 and α8 in HvLD as well as the significantly longer loop in PaISO between β7 and α7. Loop 2 and in particular the long β8-α8 loop makes the cleft around subsites –2 through –4 and 0' to –1' narrower in HvLD, which may disfavor binding of additional branched chains as found in glycogen and glycogen β-limit dextrins. However, the observed difference in activity towards amylopectin β-limit dextrins and amylopectin (13) is probably, in part, caused by the difference in the length of the branch-chain extending from subsite –2/–3, where Met^{440} prevents optimum binding due to steric hindrance (as described above). Finally, the side-chain of the solvent exposed Phe^{620} showed no significant electron density, which indicates a high flexibility. Phe^{620} will, however, irrespective of this flexibility narrows the cleft extending from subsite +2 and may therefore be important for substrate specificity by restricting binding of longer substrates.

Mechanism. HvLD catalyzes hydrolysis of α-1,6 glycosidic bonds *via* general acid catalysis that requires a catalytic nucleophile (Asp^{473}) and a catalytic acid/base proton donor (Glu^{510}). Cleavage of the α-1,6 linkage results in

retention of the anomeric configuration *via* a double displacement mechanism, characteristic of the GH13 family (24). The two-step reaction involves nucleophilic attack from deprotonated Asp^{473} forming a covalent β-glycosyl intermediate and simultaneously protonation of the leaving aglycone by Glu^{510}. The oxocarbonium ion-like transition state is believed to be stabilized by side-chains from several conserved amino acids in the active site, especially His^{404} and His^{641} (45,61). The deprotonated Glu^{510} acts as base by activating the acceptor being either water or the primary alcohol at C6 in the Glc residue in the intermediate, which results in overall retention of the α configuration in either hydrolysis (Fig. 5A) or transglycosylation forming a new α-1,6 glycosidic bond (Fig. 5B).

The interaction between Gol^{303} and His^{404} suggests that His^{404} stabilizes the charged oxocarbonium ion-like transition state. The position of His^{641} in a superimposition of HvLD:β-CD and the KpPUL:G4 complex indicates that the distances from ε2 of the imidazole side-chain to O2 and O3 of a Glc unit at subsite –1 are ~2.9 Å which supports His^{641} to play a role in transition state stabilization.

HvLD is known to act as a transferase at higher substrate concentration resulting in substantial transglycosylation despite a highly solvent accessible active site (13,19). A similar open active cleft is observed in *E. coli* glycogen branching enzyme (62). One explanation for the transferase activity, however, could be that at high substrate concentration simultaneous binding of carbohydrate chains at subsites –1 through –2/–3 and at subsite 1' through +2 excludes water from the active site prior to the nucleophilic attack and formation of the covalent intermediate thereby preferentially allowing the transfer of a carbohydrate chain to the other by formation of an α-1,6-glucosidic linkage. This assumes that the affinity at the aglycone subsites is high enough to maintain high carbohydrate ligand occupancy. It is tempting to speculate that the affinities of these sites are crucial in modulating the transglycosylation *versus* hydrolysis.

It is unknown if the proposed role of plant LD in starch biosynthesis only involves trimming of newly synthesized branch points, or if LD is involved also in the formation of new α-1,6 branch points. However, independent of the specific action of LD, evidence suggests that the morphology of the starch granule is highly dependent on the LD activity (7,8). This suggests LD as a key enzyme in production of tailor made starch for applications in food biotechnology and in bioethanol production. Rational mutational analysis based on the present HvLD 3D structure can be made to alter substrate specificity enabling formation of novel α-glucans *e.g.* for the food industry.

Acknowledgement. Access to synchrotron beam time was made possible by support from DANSCATT. We would like to acknowledge the beamline scientists Elspeth Gordon at the ESFR ID23-2 beamline and Marjolein Thunnissen at the MAX-lab II I911-5 beamline for assistance during data collection and in particular Dr. Valerie Pye, Carlsberg Laboratory for the actual data collection at ESFR ID23-2. This work is supported by the Danish Natural Science Research Council, the Centre for Advanced Food Studies and the Carlsberg Foundation. MBVC held a Ph.D. scholarship from DTU.

REFERENCES

1. Buléon, A., Colonna, P., Planchot, V., and Ball, S. (1998) *Int. Biol. Macromol.* **23**, 85–112
2. Fujita, N., Kubo, A., Suh, D. S., Wong, K. S., Jane, J. L., Ozawa, K., Takaiwa, F., Inaba, Y., and Nakamura, Y. (2003) *Plant Cell Physiol.* **44**, 607–618
3. Fujita, N., Toyosawa, Y., Utsumi, Y., Higuchi, T., Hanashiro, I., Ikegami, A., Akuzawa, S., Yoshida, M., Mori, A., Inomata, K., Itoh, R., Miyao, A., Hirochika, H., Satoh, H., and Nakamura, Y. (2009) *J. Exp. Bot.* **60**, 1009–1023
4. Burton, R. A., Zhang, X. Q., Hrmova, M., and Fincher, G. B. (1999) *Plant Physiol.* **119**, 859–871
5. Schroeder, S. W., and MacGregor, A. W. (1998) *J. Am. Soc. Brew. Chem.* **56**, 32–37
6. Sissons, M. J., Lance, R. C. M., and Sparrow, D. H. B. (1993) *J. Cereal Sci.* **1993**, 19–24
7. Dinges, J. R., Colleoni, C., James, M. G., and Myers, A. M. (2003) *Plant Cell* **15**, 666–680
8. Streb, S., Delatte, T., Umhang, M., Eicke, S., Schorderet, M., Reinhardt, D., and Zeeman, S. C. (2008) *Plant Cell* **20**, 3448–3466
9. Ball, S., Guan, H.-P., James, M., Myers, A., Keeling, P., Mouille, G., Buléon, A., Colonna, P., and Preiss, J. (1996) *Cell* **86**, 349–352
10. Martin, C., and Smith, A. M. (1995) *Plant Cell* **7**, 971–985
11. Smith, A. M. (2001) *Biomacromolecules* **2**, 335–341
12. Greffe, L., Jensen, M. T., Bosso, C., Svensson, B., and Driguez, H. (2003) *ChemBioChem.* **4**, 1307–1311
13. Manners, D. J., and Yellowlees, D. (1971) *Starch/Stärke* **23**, 228–234
14. Cantarel, B. L., Coutinho, P. M., Rancurel, C., Bernard, T., Lombard, V., and Henrissat, B. (2009) *Nucleic Acids Res.* **37 (Database issue)**, D233–D238
15. Stam, M. R., Danchin, E. G. J., Rancurel, C., Coutinho, P. M., and Henrissat, B. (2006) *Protein Eng. Des. Sel.* **19**, 555–562
16. Wu, C., Colleoni, C., Myers, A. M., and James, M. G. (2002) *Arch. Biochem. Biophys.* **406**, 21–32
17. Renz, A., Schikora, S., Schmid, R., Kossmann, J., and Beck, E. (1998) *Biochem. J.* **331** 937–945
18. Repellin, A., Baga, M., and Chibbar, R. N. (2008) *J. Cereal Sci.* **47**, 302–309
19. Vester-Christensen, M. B., Abou Hachem, M., Naested, H., and Svensson, B. (2009) *Protein Expr. Purif. In press* **doi: 10.1016/j.pep.2009.08.016**
20. Greffe, L., Jensen, M. T., Chang-Pi-Hin, F., Fruchard, S., O'Donohue, M. J., Svensson, B., and Driguez, H. (2002) *Chem. Eur. J.* **8**, 5447–5455
21. Kristensen, M., Planchot, V., Abe, J. I., and Svensson, B. (1998) *Cereal Chem.* **75**, 473–479
22. Iwamoto, H., Ohno, M., Ohmori, M., Hirose, J., Tanaka, A., Sakai, S., and Hiromi, K. (1994) *J. Biochem.* **116**, 1264–1268
23. Jespersen, H. M., MacGregor, E. A., Sierks, M. R., and Svensson, B. (1991) *Biochem. J.* **280** 51–55

24. MacGregor, E. A., Janecek, S., and Svensson, B. (2001) *Biochim. Biophys. Acta* **1546**, 1–20
25. Matsuura, Y., Kusunoki, M., Harada, W., and Kakudo, M. (1984) *J. Biochem.* **95**, 697–702
26. Machovič, M., and Janeček, Š. (2008) *Biologia* **63**, 1053–1064
27. Mikami, B., Iwamoto, H., Malle, D., Yoon, H. J., Demirkan-Sarikaya, E., Mezaki, Y., and Katsuya, Y. (2006) *J. Mol. Biol.* **359**, 690–707
28. Turkenburg, J. P., Brzozowski, A. M., Svendsen, A., Borchert, T. V., Davies, G. J., and Wilson, K. S. (2009) *Proteins* **76**, 516–519
29. Finn, R. D., Tate, J., Mistry, J., Coggill, P. C., Sammut, S. J., Hotz, H. R., Ceric, G., Forslund, K., Eddy, S. R., Sonnhammer, E. L. L., and Bateman, A. (2008) *Nucleic Acids Res.* **36**, D281–D288
30. McCafferty, C. A., Jenkinson, H. R., Brosnan, J. M., and Bryce, J. H. (2004) *J. Inst. Brew.* **110**, 284–296
31. MacWilliam, I. C., and Harris, G. (1959) *Arch. Biochem. Biophys.* **84**, 442–454
32. Leslie, A. G. W. (1992) *Joint CCP4 and ESF-EAMCB Newsletter on Protein Crystallography* **No. 26**
33. **CCP4**. (1994) *Acta Crystallogr. D Biol. Crystallogr.* **50**, 760–763
34. Potterton, E., Briggs, P., Turkenburg, M., and Dodson, E. (2003) *Acta Crystallogr. D Biol. Crystallogr.* **59**, 1131–1137
35. McCoy, A. J., Grosse-Kunstleve, R. W., Adams, P. D., Winn, M. D., Storoni, L. C., and Read, R. J. (2007) *J. Appl. Crystallogr.* **40**, 658–674
36. Adams, P. D., Grosse-Kunstleve, R. W., Hung, L. W., Ioerger, T. R., McCoy, A. J., Moriarty, N. W., Read, R. J., Sacchettini, J. C., Sauter, N. K., and Terwilliger, T. C. (2002) *Acta Crystallogr. D Biol. Crystallogr.* **58**, 1948–1954
37. Painter, J., and Merritt, E. A. (2006) *Acta Crystallogr. D Biol. Crystallogr.* **62**, 439–450
38. Emsley, P., and Cowtan, K. (2004) *Acta Crystallogr. D Biol. Crystallogr.* **60**, 2126–2132
39. Laskowski, R. A., Macarthur, M. W., Moss, D. S., and Thornton, J. M. (1993) *J. Appl. Crystallogr.* **26**, 283–291
40. Davis, I. W., Leaver-Fay, A., Chen, V. B., Block, J. N., Kapral, G. J., Wang, X., Murray, L. W., Arendall, W. B., Snoeyink, J., Richardson, J. S., and Richardson, D. C. (2007) *Nucleic Acids Res.* **35**, W375–W383
41. DeLano, W. L. (2002) The PyMOL Molecular Graphics System. 1.1 Ed., DeLano Scientific, Palo Alto, CA, USA.
42. Hutchinson, E. G., and Thornton, J. M. (1996) *Protein Sci.* **5**, 212–220
43. Kadziola, A., Abe, J.-I., Svensson, B., and Haser, R. (1994) *J. Mol. Biol.* **239**, 104–121
44. Jespersen, H. M., MacGregor, E. A., Henrissat, B., Sierks, M. R., and Svensson, B. (1993) *J. Protein Chem.* **12**, 791–805
45. Kristensen, M., F. Lok, V. Planchot, I. Svendsen, R. Leah, B. Svensson. (1999) *Biochim. Biophys. Acta* **1431**, 538–546
46. Davies, G. J., Wilson, K. S., and Henrissat, B. (1997) *Biochem. J.* **321**, 557–559
47. Fushinobu, S., Hidaka, M., Honda, Y., Wakagi, T., Shoun, H., and Kitaoka, M. (2005) *J. Biol. Chem.* **280**, 17180–17186

48. Hidaka, M., Kitaoka, M., Hayashi, K., Wakagi, T., Shoun, H., and Fushinobu, S. (2006) *Biochem. J.* **398**, 37–43
49. Needleman, S. B., and Wunsch, C. D. (1970) *J. Mol. Biol.* **48**, 443–453
50. Bender, H., and K., W. (1966) *Methods Enzymol.* **8**, 555–559
51. Shim, J.-H., Park, J.-T., Hong, J.-S., Kim, K. W., Kim, M.-J., Auh, J.-H., Kim, Y.-W., Park, C.-S., Boos, W., Kim, J.-W., and Park, K.-H. (2009) *J. Bacteriol.* **191**, 4835–4844
52. Kainuma, K., Kobayashi, S., and Harada, T. (1978) *Carbohydr. Res.* **61**, 345–357
53. Nakamura, Y. (1996) *Plant Sci.* **121**, 1–18
54. Penninga, D., vanderVeen, B. A., Knegtel, R. M. A., vanHijum, S., Rozeboom, H. J., Kalk, K. H., Dijkstra, B. W., and Dijkhuizen, L. (1996) *J. Biol. Chem.* **271**, 32777–32784
55. Sorimachi, K., Le Gal-Coëffet, M. F., Williamson, G., Archer, D. B., and Williamson, M. P. (1997) *Structure* **5**, 647–661
56. Harding, M. M. (2001) *Acta Crystallogr. D Biol. Crystallogr.* **57**, 401–411
57. Boel, E., Brady, L., Brzozowski, A. M., Derewenda, Z., Dodson, G. G., Jensen, V. J., Petersen, S. B., Swift, H., Thim, L., and Woldike, H. F. (1990) *Biochemistry* **29**, 6244–6249
58. Katsuya, Y., Mezaki, Y., Kubota, M., and Matsuura, Y. (1998) *J. Mol. Biol.* **281**, 885–897
59. Hondoh, H., Kuriki, T., and Matsuura, Y. (2003) *J. Mol. Biol.* **326**, 177–188
60. Abdullah, M., and French, D. (1970) *Arch. Biochem. Biophys.* **137**, 483–493
61. Yamashita, M., Matsumoto, D., and Murooka, Y. (1997) *J. Ferment. Bioeng.* **84**, 283–290
62. Abad, M. C., Binderup, K., Rios-Steiner, J., Arni, R. K., Preiss, J., and Geiger, J. H. (2002) *J. Biol. Chem.* **277**, 42164–42170
63. Wallace, A. C., Laskowski, R. A., and Thornton, J. M. (1995) *Prot. Eng.* **8**, 127–134

FOOTNOTES

*to whom all correspondence should be addressed: E-mail: bis@bio.dtu.dk, Phone: +45 4525 2740, Fax: +45 4588 6307, E-mail:anette@crc.dk, Phone: +45 3327 5222, Fax: +45 3327 4708

[1]The abbreviations used are: BaPUL, pullulanase from *Bacillus acidopullulyticus*; BsPUL, pullulanase from *Bacillus subtilis* str. 168; CBM, carbohydrate binding module; CD, cyclodextrin; G4, maltotetraose; GBD, glycogen binding domain; Glc, glucose, Gol, glycerol; HvLD, limit dextrinase; KpPUL, pullulanase from *Klebsiella pneumoniae*; MR, molecular replacement, PaISO, isoamylase from *Pseudomonas amyloderamosa*; PEG, polyethylene glycol; SPR, surface plasmon resonance; TLS, translation/libration/screw.

FIGURE LEGENDS

Fig. 1. Overall structure of HvLD. *A.* overall structure of HvLD:β-CD and the same structure rotated 90°. N-domain in red, CBM48 in yellow, catalytic domain in light gray and C-domain in light cyan. Ca^{2+} in purple, I^{+} in orange, glycerol in blue and β-CD in green. The catalytic residues, Asp^{473}, Glu^{510}, and Asp^{642} are shown in dark gray. *B.* topology diagram of LD. α-helices are shown as cylinders in dark gray and labeled a, β-strands are shown as arrows in light gray and labeled b.

Fig. 2. The two Ca^{2+} binding sites in HvLD. *A*. The first Ca^{2+} binding site (Ca1) has pentagonal bipyramidal geometry. *B.* The second HvLD Ca^{2+} site (Ca2) displays an octahedral geometry. The Ca^{2+} is shown in gray, water molecules in dark gray and ligand side-chains in light gray with residue numbers in black. Polar interactions are shown with dashed lines. Ca^{2+} The distance between the Ca^{2+} and the ligand atom is shown by a black label.

Fig. 3. Substrate binding site of HvLD. *A.* Superimposition of HvLD:β-CD on KpPUL:maltotetraose (G4) complex. Glycerol 303 is colored green, and water molecules in the active site of HvLD in red The glycerol and water $2F_o–F_c$ maps at 1.0 σ are shown as a grey mesh. The G4 molecules of the KpPUL:G4 complex are drawn in blue (representing the carbohydrate main-chain) and light blue (representing the carbohydrate branch chain). *B.* Superimposition of HvLD:β-CD on HvLD:α-CD. β-CD and α-CD are colored in light gray and cyan, respectively, *C*. β-CD and glycerol bound in the active site of HvLD shown with or *D*. without the $2F_o–F_c$ maps. The $2F_o–F_c$ at 1.0σ and 0.6σ are shown as blue and green mesh, respectively. *A, B, C* and *D*, β-CD is colored in light gray, glycerol in green and HvLD active site residues in dark gray. The catalytic residues, Asp^{473}, Glu^{510}, and Asp^{642} are shown in orange. The subsite numbers and residue numbers are black and gray, respectively

Fig. 4. Schematic drawing of the LD residues interacting with β-CD. The figure was based on a cartoon generated by the program LIGPLOT (63). Both CDs have some less well-defined Glc residues (at subsites 0' and –1') with weighted $2F_o–F_c$ less than 1.0σ.

Fig 5. The mechanism of HvLD catalysed α-1,6 hydrolysis with retention of the α-anomeric configuration. *A*, The reaction can result in hydrolysis or *B*, in formation of a new glucosidic bond (transglycosylation).

TABLES

Table 1. Data collection and refinement statistics

	HvLD·β-CD	HvLD·α-CD
Protein Data Bank Code		
Data collection		
Space group	*C*2	*C*2
Cell dimensions		
a, *b*, *c* (Å)	175.0, 82.4, 59.4	174.8, 85.6, 61.1
α, β, γ (°)	90.0, 96.1, 90.0	90.0, 96.8, 90.0
Molecules/asymmetric unit	1	1
Wavelength	0.873	0.910
Resolution (Å)	41.2–2.10	33.5–2.50
R_{sym} (%)	12.8 (45.8)[a]	9.3 (42.6)
Mean(I)/σ(mean(I))	11.4 (4.2)[a]	13.1 (2.3)
Completeness (%)	99.6 (99.2)[a]	97.0 (87)
Unique reflections	47764 (7091)[a]	12135 (3528)
Redundancy	4.3 (4.3)[a]	3.7 (3.1)
Wilson B-factor[b] (Å^2)	15.6	50.1
Refinement		
Resolution (Å)	41.2–2.10	33.5–2.5
Used reflections	48242	30653
R_{cryst}/R_{free} (%)	16.4/20.4	17.7/22.6
Final R_{cryst}	15.7	17.3
No. protein atoms	6709	6714
No. calcium ions	2	2
No. iodide atoms	5	9
No. of glycerol	7	1
No. of cyclodextrin	1	1
No. of waters	604	223
Mean *B*-factor (Å^2)	12.2	35.1
R.m.s.d. values from ideal		
Bond lengths (Å)	0.003	0.003
Bond angles (°)	0.742	0.658
Ramachandran plot[c]		
Most favorable (%)	89.0	88.4
Additional allowed (%)	10.5	11.2
Generously allowed (%)	0.4	0.3
Disallowed (%)	0.1	0.1

[a]Highest resolution bin. [b]From Truncate (33). [c]Calculated with Procheck (39).

FIGURES

Figure 1

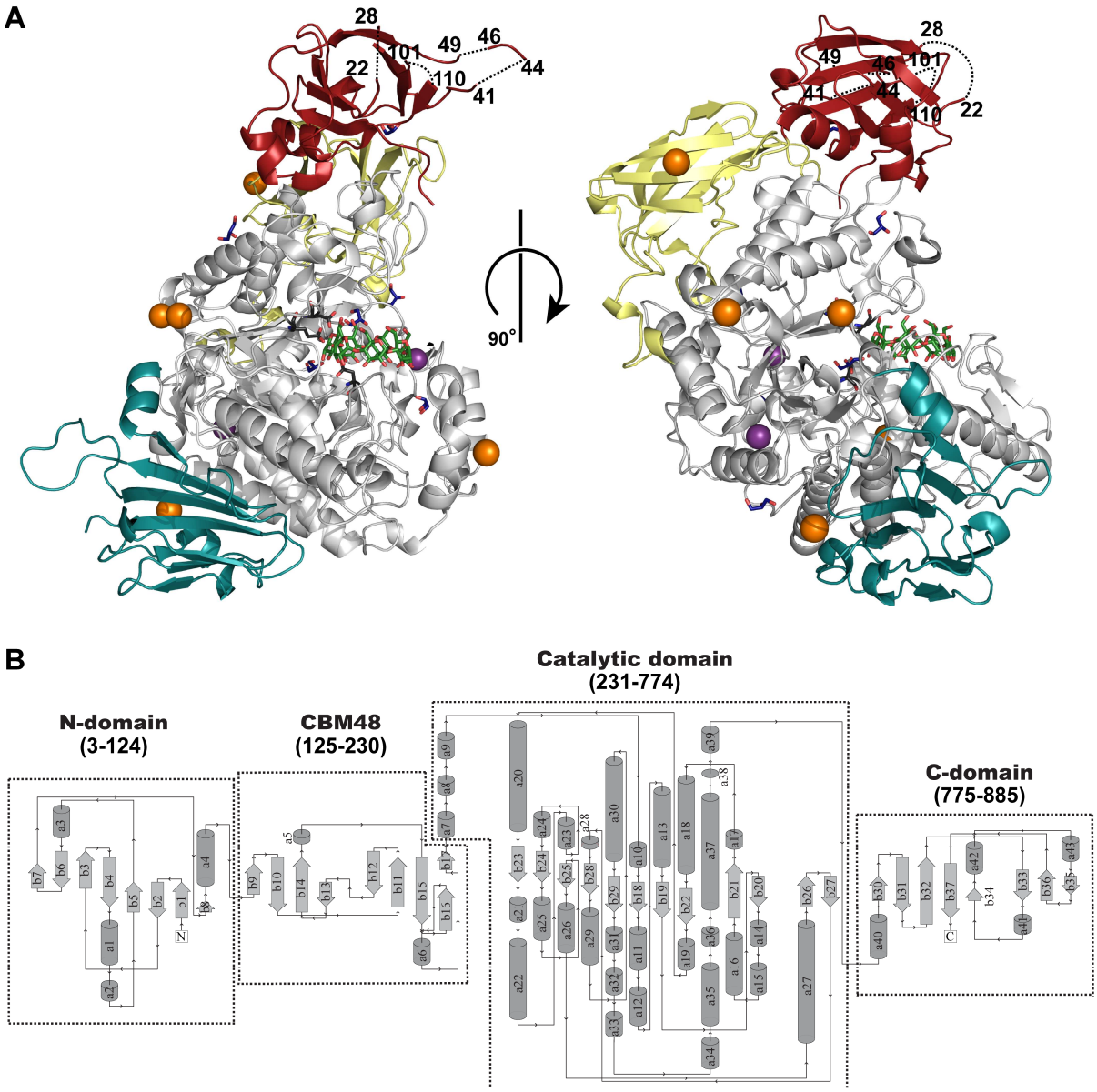

Figure 2

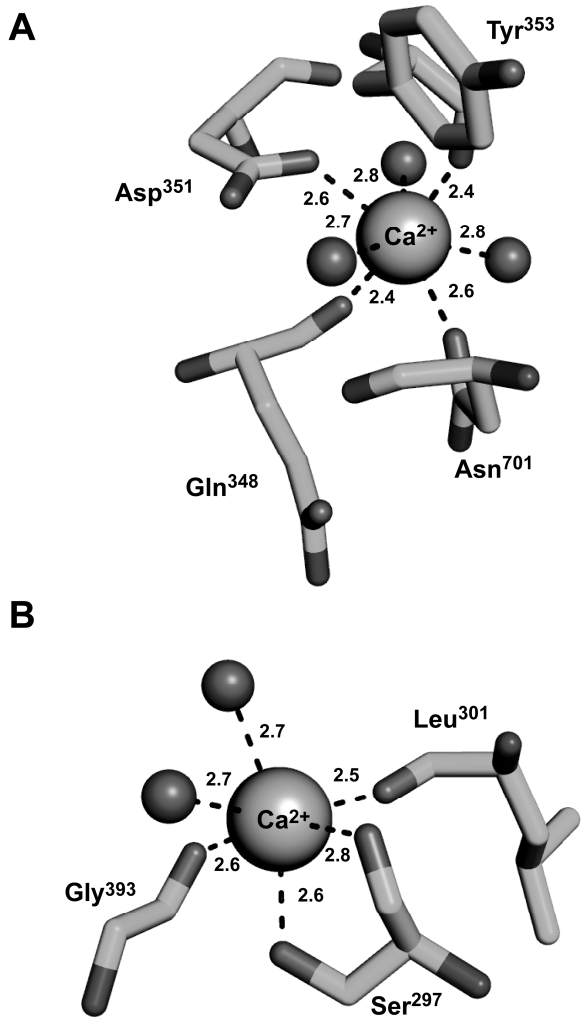
A
Tyr353
Asp351
2.8
2.6
2.4
2.7
Ca2+
2.8
2.4
2.6
Gln348
Asn701
B
2.7
Leu301
2.7
2.5
Ca2+
2.6
2.8
Gly393
2.6
Ser297

Figure 3

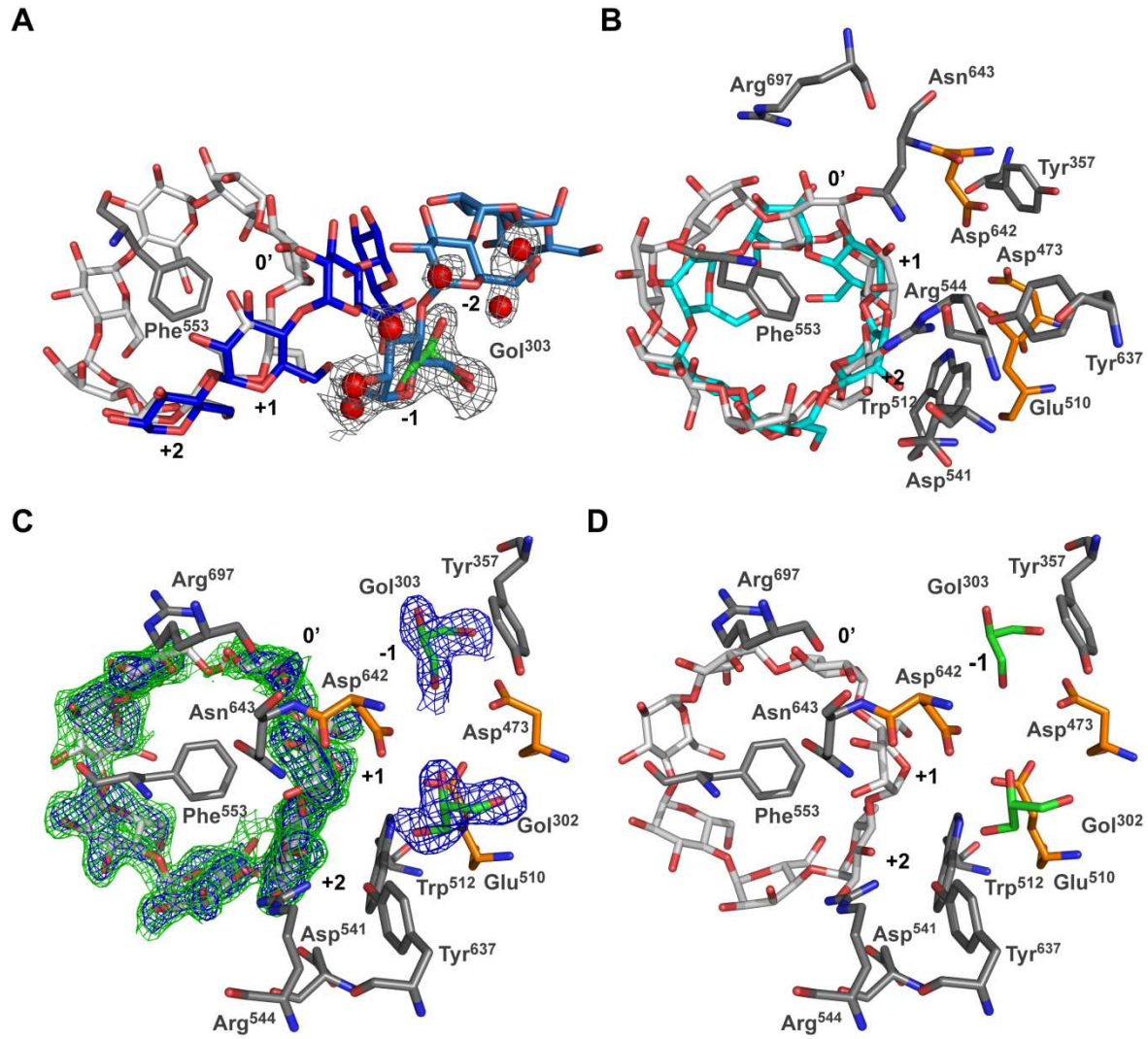
A
0'
Phe553
+1
+2
-2
-1
Gol303
B
Arg697
Asn643
Tyr357
0'
Asp642
Asp473
+1
Arg544
Phe553
Tyr637
+2
Trp512
Glu510
Asp541
C
Arg697
Gol303
Tyr357
0'
-1
Asp642
Asn643
Asp473
+1
Phe553
Gol302
+2
Trp512
Glu510
Asp541
Tyr637
Arg544
D
Arg697
Gol303
Tyr357
0'
Asp642
-1
Asn643
Asp473
+1
Phe553
Gol302
+2
Trp512
Glu510
Asp541
Tyr637
Arg544

Figure 4

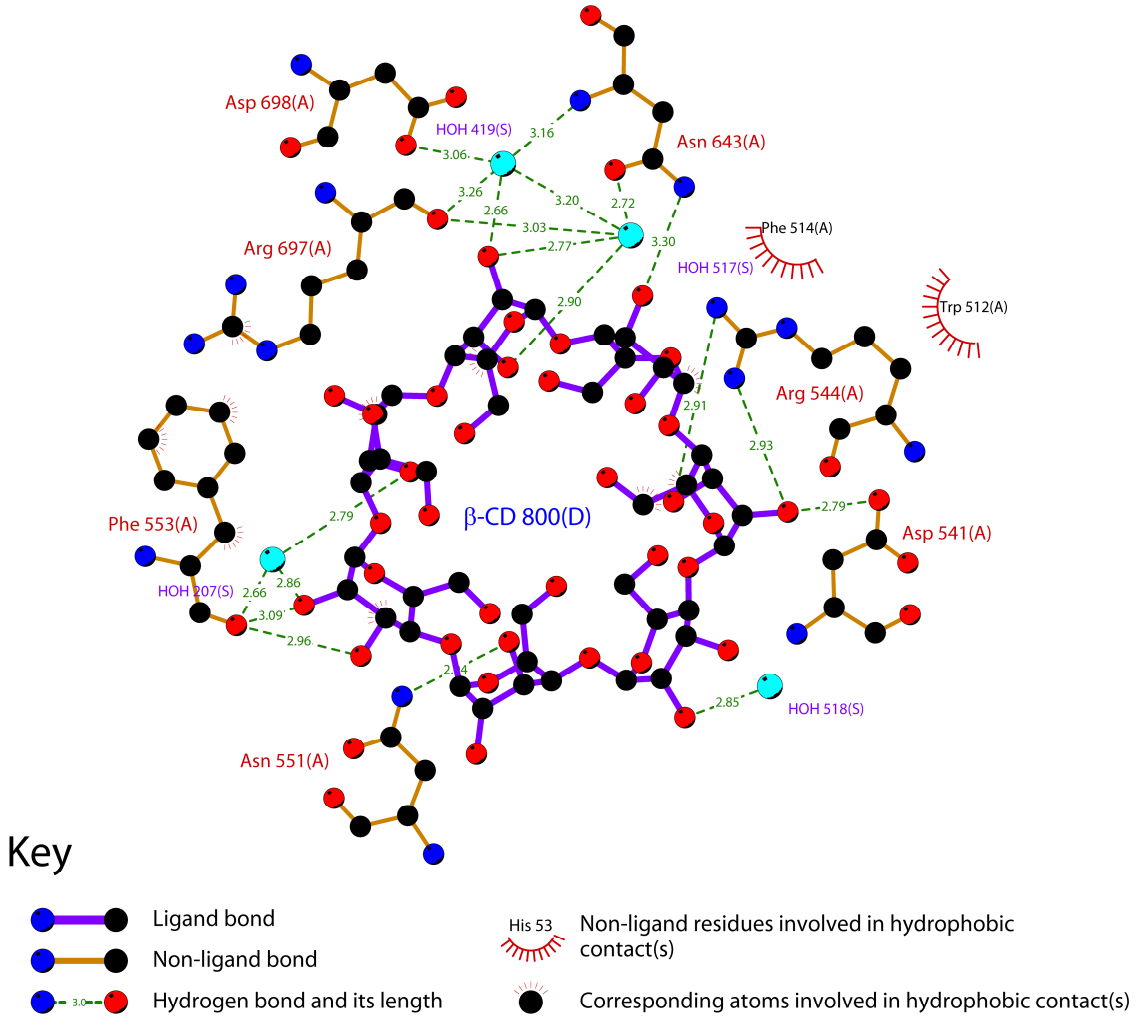
Asp 698(A)
HOH 419(S)
3.16
3.06
Asn 643(A)
3.26
2.66
3.20
2.72
3.03
2.77
3.30
Phe 514(A)
HOH 517(S)
Arg 697(A)
2.90
Trp 512(A)
Arg 544(A)
2.91
2.93
β-CD 800(D)
2.79
2.79
Phe 553(A)
Asp 541(A)
HOH 207(S)
2.66
2.86
3.09
2.96
2.85
HOH 518(S)
Asn 551(A)
Key
Ligand bond
Non-ligand bond
3.0
Hydrogen bond and its length
His 53
Non-ligand residues involved in hydrophobic contact(s)
Corresponding atoms involved in hydrophobic contact(s)

Figure 5

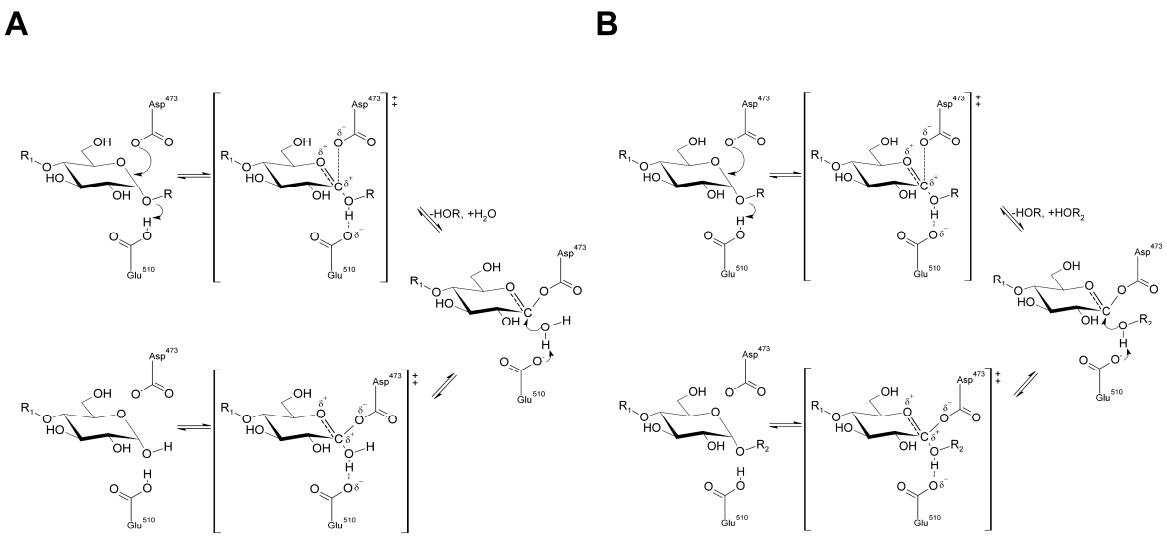

SUPPLEMENTAL DATA

FIGURE LEGENDS

Fig. 1S. The crystallographic dimer of HvLD:β-CD around the crystallographic two-fold axis. The HvLD monomers are colored in light gray and cyan. β-CD bound in the active site is shown in red and glycerol molecules are colored blue. Ca^{2+} and I^{+} ions are shown as spheres and colored purple and orange, respectively.

TABLES

Table S2. Secondary structure elements of the $(\beta/\alpha)_8$ barrel

Structure element of the (β/α)-barrel	Sequence
β1 (b18)	256-TIYEL-259
α1 (a13)	288-AGMEHLRKLSDA-299
β2 (b19)	303-HVHL-306
α2 (a18)	377-SRIIEYRQMVQALNR-391
β3 (b22)	395-RVVMDV-400
α3 (a20)	448-FMVDRLIVDDLLNWAVN-464
β4 (b23)	469-GFRF-472
α4 (a22)	480-KRTMMRAKSLQ-491
β5 (b24)	506-YLYG-509
α5	absent in structure
β6 (b25)	537-GSFN-540
α6 (a27)	577-EADTRRSLATYADQIQIGL-595
β7 (b28)	634-TIN-636
α7 (a30)	660-VDERCRINHLASMMAL-675
β8 (b29)	680-IPFFH-684
α8 (a37)	748-KGHILAALDSFVDILKIR-765

Numbers in parenthesis refers to the position of the structural elements in the topology diagram in Fig. 1B.

FIGURES

Figure 1S

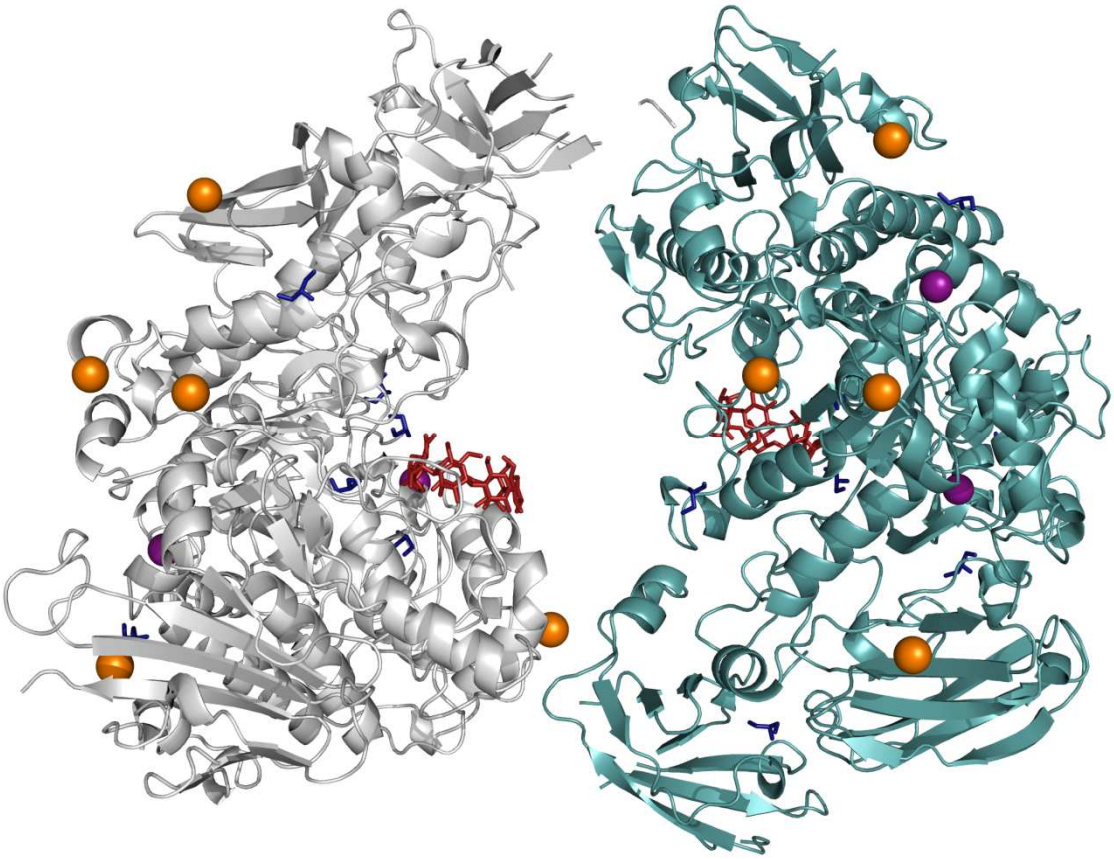

N-terminal mutations of the high-affinity barley limit dextrinase inhibitor suggests a mode of action different from that of α-amylase inhibitors from the same family

*Malene B. Vester-Christensen, Johanne M. Jensen, Maher Abou Hachem and Birte Svensson**

Enzyme and Protein Chemistry, Department of Systems Biology, Søltofts Plads, Building 224, Technical University of Denmark, DK-2800 Kgs. Lyngby, Denmark

RECEIVED DATE (to be automatically inserted after your manuscript is accepted if required according to the journal that you are submitting your paper to)

TITLE RUNNING HEAD Binding of limit dextrinase to its endogenous inhibitor

[†]This work was supported by the Danish Natural Science Research Council, the Carlsberg Foundation, the Danish Centre for Advanced Food Studies (LMC), and a Ph. D. scholarship from the Technical University of Denmark (to MBVC)

*To whom correspondence should be addressed: Phone: + 45 4525 2740; Fax: +45 4588 6307; E-mail: bis@bio.dtu.dk

Abbreviations: CFHI, bifunctional corn Hageman factor inhibitor; CWW, cell wet weight; GH13_13, glycoside hydrolase family 13 subfamily 13; LD, limit dextrinase; LDI, limit dextrinase inhibitor; Ni-NTA, nickel-nitrilotriacetic acid; PAGE, polyacrylamide gel-electrophoresis; PPA, porcine pancreatic α-amylase; RATI, ragi α-amylase/trypsin inhibitor; RU, response unit; SDS, sodium dodecyl sulfate; SPR, surface plasmon resonance; TFA, trifluoroacetic acid; TMA, α-amylase from the larvae of *Tenebrio molitor*

The barley limit dextrinase (LD) hydrolyses α-1,6-glucosidic linkages in limit dextrins and amylopectin during starch degradation in germinating seeds. LD forms an inactive complex with the endogenous limit dextrinase inhibitor (LDI) belonging to the CM-protein - or cereal-type inhibitor – family. Mode of inhibition and a possible role of the LDI N-terminal sequence for binding are examined. Recombinant production of LDI was established in *Pichia pastoris* and kinetics and energetics for recombinant wild-type LD binding wild-type and N-terminal sequence LDI variants were determined by aid of surface plasmon resonance (SPR). Fitting a 1:1 binding model to SPR data showed a high-affinity of $K_D = 40 \pm 3 \times 10^{-12}$ M with association and dissociation rate constants $k_{on} \sim 1 \times 10^6$ M^{-1} s^{-1} and $k_{off} \sim 5 \times 10^{-5}$ s^{-1} at pH 6.0, 150 mM NaCl and 25 °C. K_D depended on pH as k_{off} increased 10-fold with pH being raised from the optimum for binding at pH 6.5 to pH 10, while k_{on} was essentially unaffected. k_{off} and k_{on} changed only by factor of 2 in the range 75 mM – 1 M NaCl, thus electrostatic forces seemed not important for LD/LDI stability. van't Hoff thermodynamic parameters, $\Delta H° = -27$ kJ mol^{-1}, $T\Delta S° = 30$ kJ mol^{-1} yielding a binding free energy $\Delta G° = -57$ kJ mol^{-1}, calculated from K_D (10–35 °C) indicated that LD/LDI formation was both entropically and enthalpically favorable. N-terminal extended or truncated LDI sequence variants had K_D marginally altered suggesting that wild-type LDI N-terminal sequence is not essential for LD binding.

Barley limit dextrinase (LD) is a large multidomain enzyme belonging to subfamily 13 of glycoside hydrolase family 13 (GH13_13) (*1, 2*). LD catalyses hydrolysis of α-1,6-glucosidic linkages in limit dextrins, pullulan - a linear polysaccharide composed of α-1,6-linked maltotrioside repeats - and amylopectin and the concerted action of LD, α-glucosidase, α- and β-amylase results in degradation of endosperm starch to maltose and glucose during the seed germination (*3*). The high activity of LD in oligosaccharide debranching in malt and during mashing contributes to the yield of fermentable sugars, hence making LD important in beer production (*4*). LD occurs in extracts of germinating barley seeds on a "bound", inactive and a free, enzymatically active form, respectively (*5*). Inactive LD was proposed to exist in complex with an endogenous limit dextrinase inhibitor (LDI); extraction under reducing conditions resulted in full LD activity (*5, 6*). The amount of free LD increases with time after the onset of germination, coinciding with disappearance of LDI (*5, 7*). The important factor behind the loss of LDI, remains to be identified, however both LDI disulfide reduction by thioredoxin *h* (*8*) and proteolytic degradation (*5*) have been proposed

LDI belongs to the CM-protein family of small 110–160 amino acid residues long proteins found in chloroform/methanol extracts of cereal flour. Inhibitors of this family also referred to as cereal-type inhibitors (*9*) include α-amylase and protease inhibitors primarily acting on different exogenous enzymes (*9*) and they were proposed to be part of the plant defense against pest and pathogens (*9*). CM-proteins occur in different states of oligomerisation (monomer, dimer or tetrameri) (*10*) and the monomer structure has a common four-helical bundle simple up-and-down topology referred to as the bifunctional inhibitor/lipid-transfer protein/seed storage 2S albumin fold (SCOP: Structural Classification of Proteins (*11*)). Certain family members of high sequence identity (up 98%) still have distinct target enzyme specificity (*12*) and the structural variation responsible for this difference residing in a flexible loop connecting α-helices 3 and 4

and in the C-terminal region, makes prediction of interactions between inhibitors and enzymes challenging in the absence of a three-dimensional structure of the complex (*12, 13*). Loops near the enzyme catalytic site are also important for inhibitor complex formation (*12*). Cereal-type inhibitors formed 1:1 complexes with target enzymes (*13-19*), and acted as α- competitive inhibitors of amylase catalyzed *p*-nitrophenyl α-D-maltoside hydrolysis with K_i of 11–57 nM, depending on inhibitor and enzyme (*14, 16, 17*).

The Ser^{1} α-amino group of the α-amylase/trypsin bifunctional inhibitor from ragi (RATI) interacts *via* hydrogen bonds and electrostatic interactions directly with carboxyl groups of Asp^{185} and Asp^{287} from the catalytic site of α-amylase of larvae of *Tenebrio molitor* (TMA), as shown by X-ray crystallography. Furthermore, Val^{2} (RATI) with Trp^{56}, Trp^{57} and Tyr^{60} (TMA) had important hydrophobic interactions (*18*).

LDI of 114 amino acid residues included four disulfide bonds and one free thiol group - possibly Cys^{59} (*20*). Two LDI forms of identical amino acid sequence and inhibitory activity were purified in very small amounts from mature barley seeds and showed different p*I* of 6.7 and 7.2 due to glutathionylation and cysteinylation, respectively, at Cys^{59} (*20, 21*). Although binding of LDI to LD was found by mass spectrometric determination result in a 1:1 (*15, 20, 21*), detailed analysis was lacking on affinity and mechanism of binding. Modeling the LDI structure using RATI of 46% sequence identity as template proposed the fold to be shared with the CM-proteins (*13, 20, 22, 23*). CM-family trypsin inhibitors share a loop sequence assumed to account for trypsin inhibition is lacking in LDI (*15*). LDI was suggested to bind to the active site of LD (*20*) in the same way as RATI interacts with TMA (*18*). This implies that the N-terminus of LDI is critical in complex formation with LD (*20*). It was suggested that LDI Ser^{4} and Val^{5} interact with LD and that the LDI tripeptide Thr^{1}–Glu^{3} determines the specificity for LD and lack of inhibitory activity towards α-amylases (*20*). LDI purified from barley seeds showed some

variation in the the C-terminus, that makes it less likely that the C-terminal sequence participates in binding to LD (*15, 21*). LDI is found as highly specific for LD and does not inhibit the debranching pullulanase from *Aerobacter aerogenes* and isoamylase from *Pseudomonas amyloderamosa* (*6*).

One reason for detailed insights into the LD/LDI system being missing has been difficulties with purification of LD and LDI from their natural sources. Very recently, however, we produced fully functional recombinant LD in excellent yields using *Pichia pastoris*, enabling determination of the structure (*24, 25*). Here is described successful expression also of LDI in *P. pastoris* allowing inhibition of studies of the LD catalyzed hydrolysis of pullulan as well as mutational analysis of the impact of the N-terminal sequence on the inhibitory potential using surface plasmon resonance (SPR).

MATERIALS AND METHODS

Materials. Restriction enzymes were from New England Biolabs (Ipswich, MA); T4 ligase (The LigaFast Rapid DNA Ligation System) was from Promega (Madison, WI); Expand High Fidelity Polymerase was from Roche Applied Science (Mannheim, Germany). Oligonucleotides were from Eurofins MWG Operon (Ebersberg, Germany). pPICZαA expression vector and *Pichia pastoris* expression strain X33 were from Invitrogen (Carlsbad, CA). Pullulan and Limit-Dextrizyme tablets were from Megazyme (Bray, Ireland). Recombinant LD was produced as previously described (*24*).

C*loning and Site-Directed Mutagenesis of LDI*. Frozen barley seeds (cultivar Morex) were dehusked and homogenized in a mortar cooled in liquid nitrogen. RNA was extracted (RNeasy Plant Mini kit; Qiagen, Düsseldorf, Germany) and RT-PCR was done (One-Step RT-PCR Kit, Qiagen) using 5'-GAGAGA**CATATG**ACCCTGGAGAGCGTCAAGGACG-3' (forward) and

5’-**GGATCC**CCTTATCCCGGCTCCTGGACGGACGA-3’ (reverse) primers. The cDNA was cloned into pCR 2.1-TOPO (Invitrogen) using the *Nde*I and *Bam*HI sites (in bold) and the resulting plasmid was used for transformation of *Escherichia coli* TOP10 competent cells (Invitrogen). cDNA corresponding to amino acid residues 25–138 (accession No, ABB88573, NCBI Protein database) encoding a protein sequence identical to the previously published (*20*, *26*), was used as template for PCR amplification of the expression construct using 5’-AAAAAAAAA**GAATTC**ACCCTGGAGAGCG-3’ (forward) and 5’-TGATTAACT**GGTACC**TTA*ATGATGATGATGATGATG*TCCCGGCTCCTG-3’ (reverse) primers in a hot-start PCR at 94 °C (3 min), 3 cycles at 94 °C (30 s), 50 °C (30 s), and 72 °C (45 s), followed by 22 cycles at 94 °C (30 s), 58 °C (30 s), and 72 °C (45 s) and a final elongation (7 min). The PCR product encoding the LDI gene and a C-terminal hexa-histidine tag (in italic) was cloned in-frame with the *Saccharomyces cerevisiae* α-factor secretion signal of the pPICZα A *P. pastoris* vector using *EcoR*I and *Kpn*I sites (in bold). The *EcoR*I site resulted in a Glu-Phe N-terminal extension of the wild-type (**EF**TLESVKDECQ; denoted EF-LDI).) and site-directed mutagenesis (QuikChange® Lightning Site-Directed Mutagenesis Kit, Stratagene, La Jolla, CA) using 5’-GAGAAAAGAGAGGCTGAAGCTACCCTGGAGAGCGTCAAGGACGA-3’ (forward) and 5’-TCGTCCTTGACGCTCTCCAGGGTAGCTTCAGCCTCTCTTTTCTC-3’ (reverse) primers resulted in the native N-terminus (TLESVKDECQ; denoted wt-LDI). N-terminal truncation of TLESV (denoted ΔV^5LDI) was obtained (QuikChange® Lightning Site-Directed Mutagenesis Kit) using 5’-GAGAAAAGAGAGGCTGAAGCTAAGGACGAGTGCCAACCAGGGGT-3’ (forward) and 5’-ACCCCTGGTTGGCACTCGTCCTTAGCTTCAGCCTCTCTTTTCTC-3’ (reverse) primers (Figure 1). Correct wt-LDI and the predicted variants assumed processing at the second Ste13 site of *S. cerevisiae* α-factor secretion signal in pPICZαA (*27*). Small scale plasmid preparation,

restriction enzyme digestion, ligation, and transformation followed standard molecular biology protocols (*28*).

Expression and Purification of Wild-Type and Mutant LDI. Expression plasmids were linearized by *Pme*I, transformed into *P. pastoris* strain X33 by electroporation and selected on YPDS plates supplemented with 100 µg/mL zeocin (Invitrogen). Six clones of each construct were tested for production of LDI in culture flasks (100 mL BMGY media) (EasySelect™ *Pichia* Expression Kit, Invitrogen (*27*)). The cultures were induced after 24 h growth in BMGY medium at 30 °C by transferring to BMMY medium (*27*) at 17 °C. After 72 h methanol induction, cells were removed by centrifugation (12,000*g*, 4 ˚C, 30 min) and LDI production was verified by SDS-PAGE and LD inhibition by measuring residual activity of LD (10 nM) after addition of culture supernatant (30 µL) using Limit-Dextrizyme tablets in 0.1 M Na acetate pH 5.5, 0.005% Triton X-100. To produce high amounts of LDI, selected wt-LDI and EF-LDI clones were cultured in a 5-L Biostat B bioreactor (B. Braun Biotech International, Melsungen Germany) equipped with additional feed pump, gas mixer, dissolved oxygen tension polarographic electrode, and water cooler according to the guidelines for methanol feeding Mut^+ phenotype (*29, 30*). Cells (OD_{600} = 22) grown in shake flask (300 mL) overnight at 30 °C in BMGY were harvested by centrifugation (1,500*g*, 20 ˚C, 5 min), resuspended in fresh BMGY (80 mL), and used for inoculating the starting basal salt medium (3 L) containing PMT1 trace salts (*29*). Temperature was maintained at 28 °C by water cooling during glycerol batch (~20 h) and fed-batch (30 mL h^{-1} 50% (w/v) glycerol; ~7 h) phases, adjusted to 17 °C prior to induction and maintained during the methanol feed (22–28 h). The methanol flow was successively increased from 1 g L^{-1} h^{-1} to reach the maximum of 11 g L^{-1} h^{-1} after 8 h.. Aqueous ammonia (28%) was added to maintain pH 5.5 and serve as nitrogen source.

The below detailed protocol ensured good yields of LDI. Cells were subsequently removed by centrifugation (12,000*g*, 4 °C, 30 min), the supernatant (3.2 L) was added sodium azide (to 0.02% (w/v)). Imidazole and NaCl were added to culture supernatants to 10 mM and 500 mM, respectively, and pH was adjusted to 7.4 by addition of K_2HPO_4(s), followed by centrifugation (12,000*g*, 4 °C, 30 min) and filtration (0.45 µm) before application onto the Ni-NTA column (Ge Healthcare, Uppsala, Sweden) (120 mL h^{-1}) equilibrated with 20 mM Na phosphate, pH 7.4, 10 mM imidazole, 500 mM NaCl. After washing with equilibration buffer (60 mL h^{-1}) LDI was eluted (60 mL h^{-1}) by a two-step linear imidazole gradient of equilibration buffer mixed with 20 mM Na phosphate pH 7.4, 500 mM imidazole, 500 mM NaCl (0–10%, 10 mL; 10–100%, 300 mL). LDI containing fractions (5 mL) were identified by SDS-PAGE, and combined in two pools (2 × 50 mL), each concentrated (Centricon; 3 kDa cut-off, Millipore, Cork, Ireland) to 15 mL and dialyzed (Spectra/por dialysis membrane, cut-off 6–8 kDa; Spectrum Laboratories, Rancho Dominguez, CA) against 2 × 5 L 5 mM Bicine/NaOH pH 8.5 and 1 × 5 L 10 mM Bicine/NaOH pH 8.5, centrifuged (12,000g, 4 ˚C, 30 min) and for anion exchange chromatography loaded (2 × 15 mL) onto a MonoQ 10/100 GL column (GE Healthcare) and washed (150 mL h^{-1}; 150 mL) with the above buffer. Protein was eluted by a five-step linear salt and pH gradient of buffers A: 10 mM Bicine/NaOH pH 8.5 and B: 10 mM Hepes/NaOH pH 7.0, 250 mM NaCl (0–12.5%, 24 mL; 12.5–25%, 160 mL; 25–30%, 8 mL; 30–38%, 15 mL; 38–100%, 80 mL). LDI eluting as a single peak identified by the chromatogram and SDS-PAGE of collected fractions (4 mL) were pooled, concentrated and buffer changed to 10 mM Bicine/NaOH pH 8.5, 100 mM NaCl (Centricon, 3 kDa cut-off; Millipore).

The ΔV^5LDI variant was produced essentially as described above in shake flask culture (500 mL) using 48 h induction. The supernatant was adjusted to pH 7.4, 10 mM imidazole, 500 mM NaCl and purified on Ni-NTA column (1 mL; as above), and buffer changed to 10 mM

Bicine/NaOH pH 8.5 (Microcon, 3 kDa cut-off; Millipore). ΔV^5LDI (770 µg mL^{-1}) gave a single band in SDS-PAGE as well as a single N-terminal sequence and was used for SPR analysis without further purification.

An ÄKTAexplorer (GE Healtcare) interfaced by UNICORN 5.0 control software (GE Healtcare) was used for all chromatographic procedures.

Protein Characterization. SDS-PAGE (NuPAGE® Novex Bis-Tris 4–12%) was performed as recommended by the manufacturer (Invitrogen). Protein concentration was estimated (Bradford Coomassie Plus kit; Pierce, Rockford, IL) using BSA as standard and by A_{280} using ε of 3.9×10^5 M^{-1} cm^{-1}, obtained by aid of amino acid analysis of LDI after 24 h acid hydrolysis (*31*). Automated N-terminal sequence analysis (Procise 494 sequenator; Applied Biosystems, Foster City, CA) was performed according to the manufacturer's recommendations.

LD inhibition. wt-LDI (0.1–0.2 µM, 300 µL; 10 mM Bicine/NaOH pH 8.5, 0.1 M NaCl) was preincubated with LD (52 nM, 1200 µL; 100 mM Na acetate pH 5.5, 5 mM $CaCl_2$, 0.005% Triton X-100) for 15 min at 25 °C and 110 µL was added to 990 µL pullulan (DP ~ 300) at 8 different concentrations (0.025–0.3 mg mL^{-1}) in 100 mM Na acetate pH 5.5, 5 mM $CaCl_2$, 0.005% Triton X-100 at 37 ˚C to final concentrations of LDI and LD of 2 or 4 nM and 4.2 nM, respectively. Aliquots (200 µL) were removed at 3 min intervals during 0–15 min, stopped by mixing with 500 µL freshly prepared developing buffer (0.4 M Na carbonate pH 10.7, 2.5 mM $CuSO_4$, 2.5 mM 4,4'-dicarboxy-1,2'-biquinoline, 6 mM L-serine) and 300 µL Milli-Q water (*32*) and the absorbance was measured after 30 min at 80 ºC in microtiter plates (300 µL, in duplicates) at A_{540}. The release of reducing sugar was quantified using a maltose standard curve.

K_i for inhibition of LD was determined from initial rates of pullulan hydrolysis with or without LDI added by fitting the model for tight competitive inhibition (eq. 1) to the data (Enzyme Kinetics Module 1.0 of Sigmaplot 9.01; Systat Software, Chicago, IL). K_{app} is the apparent

inhibition constant when dissociation of the enzyme-inhibitor complex is affected by substrate addition.

(eq. 1) $$v_i = \left(\frac{v_0}{2 \cdot [\mathrm{E}]} \right) \cdot \left(([\mathrm{E}] - [\mathrm{I}] - K_{ap}) - \sqrt{([\mathrm{E}] - [\mathrm{I}] - K_{app})^2 + 4 \cdot [\mathrm{E}] \cdot K_{app}} \right),$$

where $K_{app} = K_i \cdot \left(1 + \frac{[\mathrm{S}]}{K_m} \right)$

To determine the molar ratio for 100% inhibition, pullulan and LD concentrations were kept constant at 0.17 mg/mL and 4 nM, respectively, and the LDI concentration varied between 0 and 20 nM in the assay, yielding LDI:LD molar ratios 0–5. The assay was carried out as above.

Surface Plasmon Resonance. The LD/LDI interaction was analyzed by SPR (BIAcore® T100; GE Healthcare). Immobilization of LDI wild-type and variants on BIAcore CM5 sensor chips was performed by amine coupling according to the manufacturer's protocol using 10 μg mL^{-1} LDI in 5 mM Na acetate buffer pH 4 resulting in 200–400 response units (RU) bound in sample cells. Reference cells were treated by the same procedure without LDI. Sensorgrams (RU *vs.* time) of LD (0.1–80 nM) binding using 4 and 15 min association and dissociation times, respectively, were recorded. Regeneration was performed by 2 × 60 s injections of 10 mM glycine/HCl pH 1.5 at 30 μL min^{-1}. Standard condition for binding kinetics was 25 °C, flow rate 30 μL min^{-1} and seven LD concentrations (0.1–4 nM) in running buffer 10 mM Mes/NaOH pH 6.0, 150 mM NaCl, 0.005% P-20 surfactant. The mass transfer rate constant, k_t was obtained from binding kinetics for the LD/LDI interaction at 30 μL min^{-1} and 60 μL min^{-1} at 25 °C to evaluate possible mass transfer limitations.

Effects of ionic strength and pH on the kinetics was determined as above at 75 mM – 1 M NaCl in the above running buffer and by using different running buffers all containing NaCl (150 mM),; pH 5.0–5.5, 10 mM Na acetate; pH 6.0–6.5, 10 mM Mes/NaOH; pH 7.0–7.5 10 mM

Hepes/NaOH; pH 8.0–9.0, 10 mM Bicine/NaOH; pH 9.5–10.0, glycine/NaOH, respectively. Temperature dependence was measured at nine temperatures (10–45 °C) using standard running buffer and five LD concentrations (0.4–8 nM). Two independent data sets were collected for all conditions. All concentrations were analyzed in duplicates, except for 0.4 nM LD that was analyzed in quadruplicates and served as a control to assess the response level changes during the course of the experiment. Sensorgrams from reference cells were subtracted from sample cell sensorgrams to account for refractive index changes due to minor solvent differences and for possible nonspecific LD binding to the cell surface. The reference cell subtracted sensorgrams were corrected by subtraction of averaged blank sensorgrams (buffer injected) to account for drift specific for the sample cell. Double corrected sensorgrams from the different binding experiments were analyzed using BIAcore T100 Evaluation Software version 1.1. A 1:1 binding model (eq. 2) (*33*) also accounting for possible mass-transport limitations was fitted globally using non-linear regression to sensorgrams generated for each set of ligand concentrations to determine the association rate constant, k_{on} (M^{-1} s^{-1}) and dissociation rate constant, k_{off} (s^{-1})

(eq. 2) $$LD_0 \xrightarrow{k_t} LD + LDI \underset{k_{off}}{\overset{k_{on}}{\rightleftharpoons}} LD/LDI$$

where LD_0 and LD are the concentrations in the bulk and at the chip surface, respectively, and k_t is the mass transfer rate constant (RU M^{-1} m s^{-1}). The quality of the fits was judged by the residual plots given by the BIAcore T100 Evaluation Software.

The equilibrium dissociation constant K_D (M) is also determined from eq. 3.

(eq. 3) $$K_D = k_{off}/k_{on}$$

The van't Hoff thermodynamic parameters at 25 °C and standard conditions were calculated from non-linear (eq. 4) and linear van't Hoff (eq. 5) (BIAcore T100 Evaluation Software version 1.1) equations using kinetic data of the temperature dependence between 10–35 °C.

(eq. 4) $$\mathrm{RT}\ln K_{\mathrm{D}} = \Delta H^{\circ}_{\mathrm{T}_0} - T\Delta S^{\circ}_{\mathrm{T}_0} + \Delta C^{\circ}_{\mathrm{p}}(T - T_0) - T\Delta C^{\circ}_{\mathrm{p}} \ln\left(\frac{T}{T_0}\right)$$

(eq. 5) $$\Delta G^{\circ} = \mathrm{RT}\ln K_{\mathrm{D}},\ \Delta G^{\circ} = \Delta H^{\circ} - T\Delta S^{\circ}$$

Where $\Delta G°$, $\Delta H°$ and $\Delta S°$ are the standard free energy, enthalpy, and entropy change, respectively. T is the absolute temperature (K), T_0 is the reference temperature (298.15 K for standard conditions), $\Delta Cp°$ is heat capacity change under standard conditions, R = 8.314 J K^{-1} mol^{-1} is the gas constant and K_D is the equilibrium dissociation constant (3).

Sequence Alignment and LDI Model Prediction. Multiple sequence alignment included LDI with four structure-determined inhibitors LDI, RATI, bifunctional corn Hageman factor inhibitor (CHFI), the dimeric and the monomeric wheat inhibitors 0.19 and 0.28 (ClustalW2 server; http://www.ebi.ac.uk/Tools/clustalw2/index.html). The pairwise alignment algorithms EMBOSS Needle was used for global alignment of LDI with RATI, CHFI, 0.19 and 0.28. LDI has previously been modeled (*20*), however, the homology modeling programs have evolved dramatically in the recent years (*34*), therefore RATI (PDB code: 1B1U) was used as template in LDI homology modeling using the default parameters of the HHpred server (Homology detection & structure prediction by HMM-HMM comparison, http://toolkit.tuebingen.mpg.de/hhpred#). The quality of the obtained LDI model was analyzed using the ProQ - protein quality prediction server (http://www.sbc.su.se/~bjornw/ProQ/ProQ.cgi) (*35*).

RESULTS

Expression and Purification of LDI and LDI-mutants. Fed-batch high cell-density fermentation resulted in ~ 6 mg/L inhibitory active wt-LDI or EF-LDI in the cell free extract (3.2 L) as assessed by SDS-PAGE. The amount of LDI increased in the medium during the methanol phase despite a small decrease in CWW towards the end of the fermentation. EF-LDI and wt-LDI cultures were terminated after 22 h and 28 h induction at CWW of 170 g L and 120 g L, respectively. Both EF-LDI and wt-LDI eluted from Ni-NTA as two overlapping peaks, the first of which contained full-length and some lower molecular weight LDI fragments as shown by SDS-PAGE. Fractions were combined in two pools based on purity judged from SDS-PAGE and purified by anion exchange chromatography (supplemental material Figure 1). N-terminal sequencing showed partial truncation of the EF-LDI resulting in protein (ΔE^3LDI) lacking the N-terminal pentapeptide, *i.e.* the N-terminal tripeptide (TLE) compared to wt-LDI, presumably caused by proteases present in the culture medium (*36*). This N-terminus corresponded to that of RATI (*23*) (see Figure 4) and ΔE^3LDI is central for elucidating the functional role of the LDI N-terminal sequence in the interaction with LD. Anion exchange chromatography resulted in highly pure wt-LDI with native N-terminus (supplemental material Figure 1).

TheΔV^5LDI variant was obtained in a yield of 1.5 mg and N-terminal sequencing showed an unexpected EAEAKDECQ sequence in which EAEA (Figure 1) originates from the α-factor secretion signal, reflecting that the Kex2 site was used for processing rather than the Ste13 site (*27*).

Kinetics of LDI Inhibition of LD. Rates of hydrolysis of pullulan by LD at different [LDI] enabled calculation of the K_i of LDI to 1.7 nM ± 0.1 by fitting the model for tight competitive inhibition (See Methods, eq. 1) (Figure 2A). The high standard deviation at inhibition by 4 nM LDI is due to low residual LD activity. Fifty percent inhibition of LD was obtained at a 1.1:1

(4.4 nM:4 nM) LDI:LD ratio and >90% inhibition was seen at a molar ratio of 2:1 (8 nM:4nM) (Figure 2B). At LDI:LD of 5:1 (20 nM:4nM) 100% inhibition was obtained.

Validity of the Binding Kinetics Model. SPR analysis of the formation of the LD/LDI complex was performed by LD binding to LDI on the sensorchip. This approach has two advantages i) enhanced signal by binding the 10-fold larger LD to LDI on the chip and ii) signal robustness and longer chip life-time as LDI exhibits superior stability to LD, and tolerates repeated cycles of regeneration at pH 1.5. Thus signal recovery after 27 cycles was 73%. Rather low immobilization levels were used to minimize possible mass transfer limitation and essentially the same rate constants were obtained at flow rates of 30 μL min^{-1} and 60 μL min^{-1}. Furthermore, a mass transfer constant, $k_t > 10^9$ in all runs indicated the binding kinetics to be largely unaffected by mass-transport from bulk to chip. The signal magnitude did not permit [LD] < 0.1 nM (~ 2.5 × K_D) corresponding to 4–5 RU, and 8 nM was the upper limit as higher [LD] significantly reduced fit quality from a 1:1 model, probably due to chip heterogeneity implying less accessible sites or sites with lower affinity due conformational changes to be occupied after saturation of native high affinity LDI sites. The specificity of the binding was attested by < 5% non-specific LD binding with the reference cell.

Determination of Binding Rate Constants. The rate constants k_{on} and k_{off} were determined using a 1:1 binding model fitted globally to sensorgrams for each set of ligand concentrations. Representative data and excellent fits with 0.1–4 nM LD at standard conditions at pH 6.0 (Figure 3A) (and the corresponding residuals (Figure 3B)) and suboptimal conditions at pH 10.0 (Figure 3C) (and the corresponding residuals (Figure 3D)) show no systematic deviations of the residuals which are < 5%. The very high affinity in the subnanomolar range (see Tables 1–4 below) stemmed from slow k_{off} combined while k_{on} values are typical for protein-protein interactions (*37*, *38*). The fit quality was slightly inferior for data at pH 10, but still acceptable. The

deviations at the transition between association and dissociation phases may be caused by aggregation of LD at the chip surface at this pH.

Effect of Ionic Strength, pH and Temperature on the Binding Kinetics. No LD/LDI complex formation was detected by SPR at low ionic strength even applying 80 nM LD. However, addition of 300 NaCl at LD (0.1–4 nM) gave the lowest K_D = 27.2 ± 1.3 pM (Table 1), corresponded to the highest k_{on} and the lowest k_{off}, that in fact varied only modestly in the 75 mM – 1 M concentration range of NaCl.

The LD/LDI complex formation showed a noticeable maximum affinity at pH 6.5 with K_D = 27.2 ± 0.2 pM (Table 2), and K_D increasing 12–15 fold at lower and higher values, respectively in the range pH 5.0–10.0. The effect was most important on k_{off}, which from pH 5.0 decreased 5-fold to the minimum at pH 6.5 and then increased 10-fold from pH 6.5 to 10.0.

The rates of formation and dissociation of the LD/LDI complex was determined at 9 different temperatures in the range 10–45 °C (Table 3) using five LD concentrations (0.4–8 nM). The highest affinity was found at low temperatures (10–20 °C), and K_D increased 6.5-fold by increasing temperature to 45 °C mainly due to 16-fold increase in k_{off}. The remarkable increase in k_{off} above 35 °C, however, may reflect conformational changes of one or both proteins at the higher temperatures. The ~2 fold discrepancy between K_D values obtained at standard conditions (25 °C) in the temperature dependence analysis (Table 3) and in the ionic strength and pH studies (Table 1 and Table 2) primarily stems from k_{on} being approximately 2-fold lower in the temperature study. This may be caused by a small variation in the LD concentration due to an altered sample preparation procedure.

Thermodynamic Analysis of the LD/LDI Complex Formation. Despite the above K_D variation the energetics of the interaction at the reference temperature T = 298.15 K was extrapolated using the van't Hoff equation that describes the correlation between temperature

and the natural logarithm of K_D, and which allows calculation of the interaction using either the non-linear (eq. 4) or the linear van't Hoff equation (eq. 5). To diminish possible effects of conformational change and/or instability of the proteins at higher temperature the calculations included data measured at 10–35 °C. The use of the non-linear van't Hoff equation was justified by the curvature of the data in the measured range (Figure 5A). The LD/LDI complexation was driven by a large favorable free energy change $\Delta G°$ of –57 kJ mol^{-1} which resulted in a significant decrease in heat capacity ($\Delta Cp°$ = –3.2 kJ K^{-1} mol^{-1}. The binding was moreover characterized by favorable entropy term and enthalpy contributions of $T\Delta S°$ = 30 kJ mol^{-1} (corresponding to ~53% of the total free energy) and $\Delta H°$ = –27 kJ mol^{-1}, respectively. If the linear van't Hoff equation was applied (Figure 5B) the calculated contribution of the enthalpic and entropic components to the total free energy of binding were more and less favorable, respectively, with $T\Delta S°$ = 39 kJ mol^{-1} and $\Delta H°$ = –18 kJ mol^{-1}, the latter thus decreasing from 47% to 31% of the $\Delta G°$ of –57 kJ mol^{-1}.

Effect of the N-terminal Sequence on Binding Kinetics. Different variants of the LDI N-terminal sequence disclosed that it did not represent a structural element strictly required for the interaction between LD and LDI, as essentially retained K_D values were obtained for wt-, and truncated or extended LDI variants (Table 4). k_{on} seemed slightly reduced for truncated LDI forms whereas k_{off} for the elongated EF-LDI was doubled compared to wt-LDI.

Sequence Alignment and LDI Modeling. Multiple sequence alignment of LDI and RATI, CHFI, wheat inhibitors 0.19 and 0.28 showed largest sequence diversity in loops, in particular loop 3 (L3) between α-helices 3 and 4, and at the C-terminal region (Figure 4A). Pairwise alignment of LDI with the other inhibitors showed sequence identity/similarity of 48.4%/57.8%, 46.9%/53.1%, 25.8%/37.1%, and 21.7%/34.1%, respectively, and based on the higher identity

(and similarity) as well as the functional similarity to RATI, LDI was homology modeled using the RATI structure as template.

The quality of the obtained LDI model was getting a predicted LGscore of 2.035, *i.e.* in the category of "fairly good models" (*39*). The LDI model (Figure 4B) folds in a globular simple up-and-down four-helix motif with two short anti-parallel β-strands (Val^{69}–Thr^{71} and Gly^{74}–Val^{79}) typical of CM-proteins (*13*, *20*, *22*, *23*). The helices (α1−α4) are linked by loops (LDI numbering) L1 (Gly^{33}–Pro^{39}), L2 (Val^{53}–Pro^{54}), and L3 (Gly^{68}–Pro^{88}), of which the latter appeare to be very flexible. Thus no electron density was seen in wheat inhibitor 0.19 for Gly^{69}–Thr^{77} (*40*). LDI has a 8–13 residues shorter C-terminal tail (L4, Thr^{101}–Gly^{114}) following α4 compared to the other inhibitors (Figure 4A). Eight of the 9 LDI cysteine residues form disulfide bonds; Cys^{9}–Cys^{57}, Cys^{23}–Cys^{46}; Cys^{32}–Cys^{87}; and Cys^{47}–Cys^{105}, while Cys^{59} is free (*20*). Finally, the N-terminus of RATI is flexible (*23*) causing an unstructured N-terminus of the LDI model, where residues 1–3 (TLE) are not defined.

Noticeably, the structural arrangement around LDI Arg^{58} is conserved among CM-proteins. Non-polar parts of the Arg^{58} side chain contribute to the hydrophobic core in LDI and the guanidinium group hydrogen bonds to main-chain carbonyl oxygens of Leu^{50} and Val^{53} in α-helix 2 and L2, respectively. Furthermore, a hydrogen bonding pattern is observed between Arg^{58} Nη1, the Ser^{108} main chain carbonyl oxygen, and Asp^{55} Oδ1 and Oδ2 and between Arg^{58} Nη2 and the Val^{53} main-chain carbonyl oxygen and Asp^{55} Oδ1 resembling hydrogen bond patterns in crystal structures of RATI, CHFI and wheat inhibitor 0.19. No electron density was found for Leu^{118}–Glu^{122} in the structure of RATI in complex with TMA (*18*) and residues Tyr^{120}–Val^{123} of wheat inhibitor 0.28 in complex with TMA (*13*) suggesting that the C-terminus is very flexible also in the enzyme inhibitor complex.

DISCUSSION

Proteinaceous inhibitors of α-amylases are known to play an important role in plant defense against pathogens and pests and in the control of endogenous α-amylase activity (*9, 16, 41-43*). LDI is the sole example of an endogenous inhibitor of a debranching amylolytic enzyme, and its target enzyme LD plays a pivotal role at the interface of starch biosynthesis and degradation as well as in malting and brewing (*7, 26, 44*). Despite this importance, the LD/LDI interaction remains to be described in details. The established expression system for LDI, and newly reported expression of LD (*24*) enable discerning the kinetics and energetics of the LD/LDI complex formation. The achievement of the production of recombinant LDI in excellent yield and of high functional quality should be recognized in the light of CM-proteins being notoriously cumbersome to produce recombinantly. For this large protein family heterologous expression of recombinant functional protein is only reported of CFHI (*22*), wheat inhibitor 0.28 (*45*) and BIII from rye (*46*).

LD Inhibition by wt-LDI. Cereal-type α-amylase inhibitors act as competitive inhibitors by direct interaction with catalytic residues in target enzymes - all of glycoside hydrolase family 13 and the same mode of interaction was assumed for LD/LDI (*12, 13, 17-19*). However, the present LDI inhibition data did not confirmed this (data not shown) as the Hanes-Woolf plot slopes for LD hydrolysis of pullulan at 0 or 2 nM LDI were not parallel, but deviated by 33% indicating a partially competitive inhibition. This behavior resembles that of other cereal-type inhibitors when acting on complex, large substrates (*14, 16*). Thus RATI inhibition of PPA shifted from competitive, when using *p*-nitrophenyl α-D-maltoside to a partial competitive and partial mixed type inhibition mode when using either *p*-nitrophenyl α-D-maltoheptaoside or a maltodextrin of DP27 as substrate (*16*). Moreover, complete inhibition was not achieved using these larger substrates even at 50–100-fold molar excess of RATI over PPA (*16*). RATI was

found to bind to the substrate thus the extent of apparent inhibition depended on the substrate concentration (*14, 16*). Correcting [RATI] for the amount bound to the maltodextrin revealed a inhibition to be competitive with K_i = 0.1 nM (*14*). The LD/LDI deviation from 1:1 stoichiometry observed in Figure 2B may stem from LDI binding to pullulan. Recently, we showed that the kinetics of LD catalyzed hydrolysis of pullulan is modeled by Michaelis-Menten kinetics with substrate inhibition (*24*), which may be due to genuine substrate inhibition or to high transglycosylation activity or both. As a consequence the apparent K_i of 1.7 nM found in the present study by fitting the competitive model to the data is probably higher than the actual K_i value.

Homology Modeling of LDI. The N-terminal segment (Thr^1–Glu^8) of the modeled LDI was disordered and assumed to be very flexible. Similarly, residues 1–4 of wheat inhibitor 0.19 were not seen in the electron density (*40*) and in the native structure of RATI, the N-terminal segment was described as a "wagging tail" (*23*). In both the wheat inhibitor 0.28 and in RATI, this part became well defined adopting a 3_{10}-helix conformation in complex with TMA (*13, 18*). Compared to TMA LD has an open architecture of the active site cleft (*25*) that readily accommodates the Thr^1-Glu^3 extension characteristic of wt-LDI (Figure 4) whereas previously engineered N-terminal elongations or insertions of wheat inhibitor 0.28 diminished or completely abolished its activity (*45*). For N-terminal 0.28 mutants, which retained inhibitory activity though decreased, a four-fold longer preincubation time was required to reach the maximum inhibition level, suggesting that the N-terminal might only play a role upon binding and is not crucial for stabilizing the inhibitor-enzyme complex (*45*).

The structural arrangement surrounding the conserved Arg^{58} seems to be fundamental for the loop connecting α-helix 2 and α-helix 3 as well as being important for the exposure of residue 56, a histidine in LDI, but tyrosine or tryptophan in the other inhibitors (Figure 4A). In the

structure of TMA/RATI this Tyr^{54} has hydrophobic interactions with Val^{2} in RATI, and TMA Trp^{56} and Trp^{57} (*18*). Also Tyr^{53} in wheat inhibitor 0.28 is interacting with residues in TMA (*13*). On this basis His^{56} of LDI is suggested to be involved in the interaction with LDI, possibly by stacking of His^{56} onto Tyr^{352} and Trp^{354} in LD, which superimpose with Trp^{56} and Trp^{57} in TMA. This π-stacking may be disrupted by protonation of the His^{56} side-chain and weaken binding to LD in agreement with SPR data at slightly acidic pH (Table 2).

The second binding area in the TMA/RATI complex involves two flexible loops in RATI, L3 and L4 that interact with a protruding loop (residues 132–149) of TMA. LD lacks this TMA loop resulting in a groove on the surface, making the distance between LD and LDI too large for direct interaction when superimposing the structure of LD and LDI-model onto the TMA/RATI complex.

SPR Analysis of Binding of LDI and LDI Mutants to LD. SPR is a sensitive and powerful biophysical technique for analyzing kinetics and energetics of macromolecular interactions. Despite the advantage of high sensitivity and rapid analysis provided by SPR a set off in the absolute values of the binding constant, by *e.g.* mass transport limitation has to be taken into consideration (*47-49*). In the present study SPR provides novel insight into the binding forces involved in the LD/LDI interaction and the unusually high affinity was mainly due to a very low off-rate, $k_{off} = 5 \times 10^{-5}$ s^{-1}, of the LD/LDI complex, whereas $k_{on} = 1 \times 10^{6}$ M^{-1} s^{-1} was in the typical range for protein-protein interactions (*37, 38*).

The stability of the LD/LDI complex was not very sensitive to variation in ionic strength affecting affinity < 2-fold due to change in k_{on}, while k_{off} was virtually insensitive to change in ionic strength. This indicates that long-range electrostatic forces have a minor role in the LD/LDI interaction (*50*) and any salt bridges formed in the complex are likely to be shielded from solvent.

The optimum pH of the interaction is in good agreement with the physiological slightly acidic to neutral pH prevalent in the endosperm of the mature seed, which is shown to acidify during germination (*51, 52*), and it corresponds also to the pH optimum found for LD inhibition by LDI (*21*). K_D of LD/LDI interaction depended on pH, which may reflect alteration of protein surface charge patterns. Above the role of protonation of His^{56} was discussed and similarly introduction of negative charges or loss of positive charges (perhaps at Lys^{6}) can interfere with the hydrophobic interaction and decrease the stability of the complex.

The binding affinity of the LD and LDI varied with the temperature allowing calculation of the van't Hoff thermodynamic parameters. The favorable entropy obtained both in the linear and non-linear van't Hoff analysis suggests that formation of LD/LDI increases the area of buried apolar surface, supported also by lack of detectable binding at low ionic strength even when using 20-fold higher LD concentration (Table 1). Moreover, the significant decrease in heat capacity is also consistence with an increase in the burial of hydrophobic surface (*53*). The thermodynamic analysis of the interaction between PPA and the wheat inhibitor 0.19 showed an increase in entropy, again suggesting that hydrophobic interactions play a significant role in the binding (*17*). The contribution to the binding free energy of both enthaphic and entropic components has also been reported for other protein-protein interaction (*53*) here just to mention one namely the binding of *Streptomyces* subtilisin inhibitor to subtilisin of *Bacillus subtilis* with thermodynamic values of the change in binding free energy, enthalpy and entropy ($\Delta G°$ = –57,9 kJ mol^{-1}, $\Delta H°$ of –19,8 kJ $mol^{-1}$and $T\Delta S°$ = 38 kJ mol^{-1}) (*54*) similar to the one reported for LD/LDI in this study. The heat capacity, however, calculated for the subtilisin/subtilisin inhibitor interaction is $\Delta Cp°$ = –1.02 kJ K^{-1} mol^{-1}. Values of $\Delta Cp°$ for protein-protein interaction has be shown in the range of 0.8 to –3.2 kJ K^{-1} mol^{-1} (*53*) with an average value of –1.4 ± 0.8 kJ K^{-1} mol^{-1} placing the calculated $\Delta Cp°$ of the LD/LDI interaction on the borderline.

The literature reports that N-terminal residues of cereal-type inhibitors interact with the active site of target enzymes (*14, 18, 19, 45*). So far, however, only a few α-amylases have been investigated as targets and as their active site cleft is narrower than of debranching enzymes, their inhibition may be more sensitive to changes in the N-terminal structure of the inhibitor. Deletion from the LDI specific Thr^{1}–Glu^{3}, *i.e.* the N-terminus in other inhibitors, and Ser^{4} and Val^{5} hardly affected K_D. Elongation of the N-terminal sequence of LDI by a charged and a hydrophobic residue had no effect on k_{on}, but doubled k_{off}, for the LD/LDI complex formation, presumably due to accommodation of an extra charge in the LD active site cleft. The finding suggests that the role of the LDI N-terminal segment in both formation and stability of the complex with LD is different from that observed previously for cereal type α-amylase inhibitors.

CONCLUSION

Detailed SPR analysis of binding kinetics and energetics of the LD/LDI complex reveals binding in the subnanomolar range due to very slow dissociation and that the binding was driven by both enthalpic and entropic contributions. Electrostatic interactions seemed not to play a role as salt screening had essentially no effect. K_D, however, depended on pH, possibly due to charge disruption of hydrophobic interactions. Analysis of LDI variants suggests that the N-terminal segment has a different role compared with other cereal-type inhibitor enzyme complex formation (*20*).

ACKNOWLEDGMENT

Morten Ejby Hansen and Karina Jansen are acknowledged for excellent technical assistance and Anne Blicher for amino acid and N-terminal sequence analyses. Birgit Bønsager is greatfully thanked for providing the in-house cDNA clone of LDI.

REFERENCES

1. Cantarel, B. L., Coutinho, P. M., Rancurel, C., Bernard, T., Lombard, V., and Henrissat, B. (2009) The carbohydrate-active enzymes database (CAZy): an expert resource for glycogenomics, *Nucleic Acids Res. 37 (Database issue)*, D233–D238.
2. Stam, M. R., Danchin, E. G. J., Rancurel, C., Coutinho, P. M., and Henrissat, B. (2006) Dividing the large glycoside hydrolase family 13 into subfamilies: towards improved functional annotations of α-amylase-related proteins, *Protein Eng. Des. Sel. 19*, 555–562.
3. MacGregor, A. W. (1987) α-amylase, limit dextrinase, and α-glucosidase enzymes in barley and malt, *Crit. Rev. Biotechnol. 5*, 117–128.
4. McCafferty, C. A., Jenkinson, H. R., Brosnan, J. M., and Bryce, J. H. (2004) Limit dextrinase - does its malt activity relate to its activity during brewing, *J. Inst. Brew. 110*, 284–296.
5. Longstaff, M. A., and Bryce, J. H. (1993) Development of limit dextrinase in germinated barley (*Hordeum vulgare* L.) (evidence of proteolytic activation), *Plant Physiol. 101*, 881–889.
6. MacGregor, A. W., Macri, L. J., Schroeder, S. W., and Bazin, S. L. (1994) Limit dextrinase from malted barley: extraction, purification and characterization, *Cereal Chem. 71*, 610–617.
7. MacGregor, A. W., Macri, L. J., and Bazin, S. L. (1995) Limit dextrinase in barley and malt and its possible role in malting and brewing, in *Proceedings of the 25th Congress* (Wijngaarden, M. v., Ed.), pp 185–192, European Brewery Convention, Brussels, Belgium.
8. Wong, J. H., Iiao, I. A., Kobrehel, K., and Buchanan, B. B. (1995) Thioredoxin-dependent deinhibition of pullulanase of barley malt by inactivation of a specific inhibitor protein, *Plant Physiol. 108*, 67–67.
9. Franco, O. L., Rigden, D. J., Melo, F. R., and Grossi-de-Sa, M. F. (2002) Plant α-amylase inhibitors and their interaction with insect α-amylases - structure, function and potential for crop protection, *Eur. J. Biochem. 269*, 397–412.
10. Svensson, B., Fukuda, K., Nielsen, P. K., and Bonsager, B. C. (2004) Proteinaceous α-amylase inhibitors, *Biochim. Biophys. Acta 1696*, 145–156.
11. Murzin, A. G., Brenner, S. E., Hubbard, T., and Chothia, C. (1995) SCOP - a structural classification of proteins database for the investigation of sequences and structures, *J. Mol. Biol. 247*, 536–540.
12. Franco, O. L., Rigden, D. J., Melo, F. R., Bloch, C., Silva, C. P., and Grossi-de-Sa, M. F. (2000) Activity of wheat α-amylase inhibitors towards bruchid α-amylases and structural explanation of observed specificities, *Eur. J. Biochem. 267*, 2166–2173.
13. Payan, F. (2004) Structural basis for the inhibition of mammalian and insect α-amylases by plant protein inhibitors, *Biochim. Biophys. Acta 1696*, 171–180.
14. Alam, N., Gourinath, S., Dey, S., Srinivasan, A., and Singh, T. P. (2001) Substrate-inhibitor interactions in the kinetics of α-amylase inhibition by Ragi α-amylase/trypsin inhibitor (RATI) and its various N-terminal fragments, *Biochemistry 40*, 4229–4233.
15. MacGregor, A. W., Donald, L. J., MacGregor, E. A., and Duckworth, H. W. (2003) Stoichiometry of the complex formed by barley limit dextrinase with its endogenous inhibitor. Determination by electrospray time-of-flight mass spectrometry, *J. Cereal Sci. 37*, 357–362.

16. Maskos, K., Huber-Wunderlich, M., and Glockshuber, R. (1996) RBI, a one-domain α-amylase/trypsin inhibitor with completely independent binding sites, *FEBS Lett. 397*, 11–16.
17. Oneda, H., Lee, S., and Inouye, K. (2004) Inhibitory effect of 0.19 α-amylase inhibitor from wheat kernel on the activity of porcine pancreas α-amylase and its thermal stability, *J. Biochem. 135*, 421–427.
18. Strobl, S., Maskos, K., Wiegand, G., Huber, R., Gomis-Rüth, F. X., and Glockshuber, R. (1998) A novel strategy for inhibition of α-amylases: yellow meal worm α-amylase in complex with the Ragi bifunctional inhibitor at 2.5 Å resolution, *Structure 6*, 911–921.
19. Takase, K. (1994) Site-directed mutagenesis reveals critical importance of the catalytic site in the binding of α-amylase by wheat proteinaceous inhibitor, *Biochemistry 33*, 7925–7930.
20. MacGregor, E. A., Bazin, S. L., Ens, E. W., Lahnstein, J., Macri, L. J., Shirley, N. J., and MacGregor, A. W. (2000) Structural models of limit dextrinase inhibitors from barley, *J. Cereal Sci. 31*, 79–90.
21. MacGregor, A. W., Macri, L. J., Schroeder, S. W., and Bazin, S. L. (1994) Purification and characterization of limit dextrinase inhibitors from barley, *J. Cereal Sci. 20*, 33–41.
22. Behnke, C. A., Yee, V. C., Le Trong, I., Pedersen, L. C., Stenkamp, R. E., Kim, S. S., Reeck, G. R., and Teller, D. C. (1998) Structural determinants of the bifunctional corn Hageman factor inhibitor: X-ray crystal structure at 1.95 angstrom resolution, *Biochemistry 37*, 15277–15288.
23. Gourinath, S., Alam, N., Srinivasan, A., Betzel, C., and Singh, T. P. (1999) Structure of the bifunctional inhibitor of trypsin and α-amylase from ragi seeds at 2.2 Å resolution, *Acta Crystallogr. D Biol. Crystallogr. 56*, 287–293.
24. Vester-Christensen, M. B., Abou Hachem, M., Naested, H., and Svensson, B. (2009) Secretory expression of functional barley limit dextrinase by *Pichia pastoris* using high cell-density fermentation, *Protein Expr. Purif. In press doi: 10.1016/j.pep.2009.08.016*.
25. Vester-Christensen, M. B., Abou Hachem, M., Svensson, B., and Henriksen, A. (2009) Crystal structure of barley limit dextrinase. A debranching enzyme involved in starch synthesis and breakdown, *J. Biol. Chem. To be submitted*.
26. Stahl, Y., Coates, S., Bryce, J. H., and Morris, P. C. (2004) Antisense downregulation of the barley limit dextrinase inhibitor modulates starch granule size distribution, starch composition and amylopectin structure, *Plant J. 39*, 599–611.
27. Invitrogen. (2008) *Pichia* expression kit, a manual of methods for expression of recombinant proteins in *Pichia pastoris* Invitrogen manual K1710-01; www.Invitrogen.Com.
28. Sambrook, J., and Russell, D. (2001) *Molecular cloning, a laboratory manual.*, 3 ed., Cold Spring Harbour Laboratory Press, Cold Spring Habour, New York.
29. Invitrogen. (2008) *Pichia* fermentation process guidelines; www.invitrogen.com.
30. Stratton, J., Chiruvolu, V., and Meager, M. (1998) High cell-density fermentation, in *Pichia protocols. Methods in molecular biology* (Higgings, D. R., and Cregg, J. M., Eds.), pp 107–120, Humana Press inc., Totowa, NJ.
31. Barkholt, V., and Jensen, A. L. (1989) Amino-acid analysis - determination of cysteine plus half-cystine in proteins after hydrochloric-acid hydrolysis with a disulfide compound as additive, *Anal. Biochem. 177*, 318–322.
32. Fox, J. D., and Robyt, J. F. (1991) Miniaturizing of three carbohydrate analyses a microsample plate reader, *Anal. Biochem. 195*, 93–96.

33. Myszka, D. G., He, X., Dembo, M., Morton, T. A., and Goldstein, B. (1998) Extending the range of rate constants available from BIACORE: Interpreting mass transport-influenced binding data, *Biophys. J. 75*, 583–594.
34. Battey, J. N. D., Kopp, J., Bordoli, L., Read, R. J., Clarke, N. D., and Schwede, T. (2007) Automated server predictions in CASP7, *Proteins 69*, 68–82.
35. Wallner, B., and Elofsson, A. (2003) Can correct protein models be identified?, *Protein Sci. 12*, 1073–1086.
36. De Schutter, K., Lin, Y. C., Tiels, P., Van Hecke, A., Glinka, S., Weber-Lehmann, J., Rouze, P., de Peer, Y. V., and Callewaert, N. (2009) Genome sequence of the recombinant protein production host *Pichia pastoris*, *Nat. Biotechnol. 27*, 561–566.
37. Koren, R., and Hammes, G. G. (1976) Kinetic study of protein-protein interactions, *Biochemistry 15*, 1165–1170.
38. Northrup, S. H., and Erickson, H. P. (1992) Kinetics of protein-protein association explained by Brownian dynamics computer-simulation, *Proc. Natl. Acad. Sci. U. S. A. 89*, 3338–3342.
39. Cristobal, S., Zemla, A., Fischer, D., Rychlewski, L., and Elofsson, A. (2001) A study of quality measures for protein threading models, *BMC Bioinformatics 2*, 5.
40. Oda, Y., Matsunaga, T., Fukuyama, K., Miyazaki, T., and Morimoto, T. (1997) Tertiary and quaternary structures of 0.19 α-amylase inhibitor from wheat kernel determined by X-ray analysis at 2.06 Å resolution, *Biochemistry 36*, 13503–13511.
41. Bellincampi, D., Camardella, L., Delcour, J. A., Desseaux, V., D'Ovidio, R., Durand, A., Elliot, G., Gebruers, K., Giovane, A., Juge, N., Sorensen, J. F., Svensson, B., and Vairo, D. (2004) Potential physiological role of plant glycosidase inhibitors, *Biochim. Biophys. Acta 1696*, 265–274.
42. Mundy, J., Svendsen, I. B., and Hejgaard, J. (1983) Barley α-amylase-subtilisin inhibitor.1. Isolation and characterization, *Carlsberg Res. Commun. 48*, 81–90.
43. Sorensen, J. F., Kragh, K. M., Sibbesen, O., Delcour, J. A., Goesaert, H., Svensson, B., Tahir, T. A., Brufau, J., Perez-Vendrell, A. M., Bellincampi, D., D'Ovidio, R., Camardella, L., Giovane, A., Bonnin, E., and Juge, N. (2004) Potential role of glycosidase inhibitors in industrial biotechnological applications, *Biochim. Biophys. Acta 1696*, 275–287.
44. Sissons, M., Taylor, M., and Proudlove, M. (1995) Barley malt limit dextrinase - its extraction, heat-stability, and activity during malting and mashing, *J. Am. Soc. Brew. Chem. 53*, 104–110.
45. Garcia-Maroto, F., Carbonero, P., and Garcia-Olmedo, F. (1991) Site-directed mutagenesis and expression in *Escherichia coli* of WMAI-1, a wheat monomeric inhibitor of insect α-amylase, *Plant Mol. Biol. 17*, 1005–1011.
46. Dias, S. C., Franco, O. L., Magalhaes, C. P., de Oliveira-Neto, O. B., Laumann, R. A., Figueira, E. L. Z., Melo, F. R., and Grossi-de-Sa, M. F. (2005) Molecular cloning and expression of an α-amylase inhibitor from rye with potential for controlling insect pests, *Protein Journal 24*, 113–123.
47. Rich, R. L., and Myszka, D. G. (2000) Advances in surface plasmon resonance biosensor analysis, *Curr. Opin. Biotechnol. 11*, 54–61.
48. Schuck, P. (1997) Use of surface plasmon resonance to probe the equilibrium and dynamic aspects of interactions between biological macromolecules, *Annu. Rev. Biophys. Biomolec. Struct. 26*, 541–566.

49. Schuck, P., and Minton, A. P. (1996) Analysis of mass transport-limited binding kinetics in evanescent wave biosensors, *Anal. Biochem. 240*, 262–272.
50. Selzer, T., Albeck, S., and Schreiber, G. (2000) Rational design of faster associating and tighter binding protein complexes, *Nat. Struct. Biol. 7*, 537–541.
51. Dominguez, F., and Cejudo, F. J. (1999) Patterns of starchy endosperm acidification and protease gene expression in wheat grains following germination, *Plant Physiol. 119*, 81–87.
52. Sinjorgo, K. M. C., Devries, M. A., Heistek, J. C., Vanzeijl, M. J., Vanderveen, S. W., and Douma, A. C. (1993) The effect of external pH on the gibberelic-acid response of barley aleurone, *J. Plant Physiol. 142*, 506–509.
53. Stites, W. E. (1997) Protein-protein interactions: Interface structure, binding thermodynamics, and mutational analysis, *Chem. Rev. 97*, 1233–1250.
54. Takahashi, K., and Fukada, H. (1985) Calorimetric studies of the binding of *Streptomyces* subtilisin inhibitor to subtilisin of *Bacillus subtilis* strain N', *Biochemistry 24*, 297–300.

Table 1. Effect of ionic strength on binding and dissociation rates of LD/LDI[a]

NaCl (mM)	$k_{on} \times 10^5$ (M^{-1} s^{-1})	$k_{off} \times 10^{-5}$ (s^{-1})	K_D (pM)
0	No binding detected		
75	9.0 ± 0.0	3.4 ± 1.5	37.3 ± 17.0
150	15.4 ± 0.2	6.4 ± 0.2	42.0 ± 2.0
300	17.3 ± 0.3	4.7 ± 0.1	27.2 ± 1.3
1 M	9.4 ± 0.1	7.0 ± 0.1	74.1 ± 1.0

[a]Measurements were performed at 25 °C in 10 mM Mes/NaOH pH 6.0, 0.005% P-20. Seven LD concentrations in the ranges 0.1–4 nM and 1–80 nM were used for 75 mM – 1 M and 0 mM NaCl, respectively. K_D is based on independent duplicate experiments.

Table 2. pH dependence of binding and dissociation rates of LD/LDI[a]

pH	$k_{on} \times 10^5$ (M^{-1} s^{-1})	$k_{off} \times 10^{-5}$ (s^{-1})	K_D (pM)
5.0	6.1 ± 0.6	25.9 ± 3.2	425 ± 119
5.5	9.7 ± 0.1	8.6 ± 0.1	89.3 ± 0.1
6.0	14.2 ± 0.4	5.3 ± 0.1	37.3 ± 1.9
6.5	18.6 ± 0.2	5.1 ± 0.0	27.5 ± 0.2
7.0	18.1 ± 1.6	6.2 ± 0.2	34.5 ± 1.8
7.5	16.4 ± 0.0	8.1 ± 0.3	49.3 ± 1.7
8.0	16.7 ± 0.1	12.3 ± 0.0	73.8 ± 0.4
8.5	16.0 ± 0.12	21.8 ± 0.1	136.2 ± 2.2
9.0	12.4 ± 1.1	27.0 ± 0.5	219.2 ± 22.6
9.5	13.8 ± 0.3	31.3 ± 1.8	227.3 ± 18.0
10.0	14.5 ± 1.7	49.9 ± 4.4	345.1 ± 9.0

[a]Measurements were performed at 25 °C in appropriate buffers (see Materials & Methods), containing 150 mM NaCl and 0.005% P-20. Seven LD concentrations (0.1–4 nM) were used. K_D is based on independent duplicate experiments.

Table 3. Temperature dependence of binding and dissociation rate constants of the LD/LDI[a]

Temp. (°C)	$k_{on} \times 10^5$ (M^{-1} s^{-1})	$k_{off} \times 10^{-5}$ (s^{-1})	K_D (pM)
10	5.6 ± 0.0	4.9 ± 0.3	88.0 ± 6.0
15	6.5 ± 0.0	5.7 ± 0.2	88.2 ± 3.1
20	7.6 ± 0.0	6.6 ± 0.2	86.2 ± 2.1
25	8.8 ± 0.1	8.3 ± 0.1	94.5 ± 0.5
30	10.1 ± 0.1	11.5 ± 0.2	114.5 ± 3.0
35	11.2 ± 0.0	19.7 ± 0.0	176.7 ± 0.4
37	11.6 ± 0.1	26.1 ± 0.3	225.1 ± 0.2
40	12.5 ± 0.1	39.6 ± 0.3	317.1 ± 3.6
45	13.9 ± 1.7	79.9 ± 5.1	580.5 ± 106.8

[a]Measurements were performed at different temperatures in 10 mM Mes/NaOH pH 6.0, 150 mM NaCl, 0.005% P-20. Five LD concentrations (0.4–8 nM) were used. K_D is based on independent duplicate experiments.

Table 4. Effect of the LDI N-terminal sequence on binding and dissociation rate of complex formation with LD[a]

Inhibitor	$k_{on} \times 10^5$ (M^{-1} s^{-1})	$k_{off} \times 10^{-5}$ (s^{-1})	K_D (pM)
wt-LDI	14.8 ± 0.1	5.9 ± 0.7	40 ± 3
ΔV^5LDI	10.0 ± 0.0	5.7 ± 0.2	55 ± 2
ΔE^3LDI	9.1 ± 0.1	6.6 ± 0.1	72 ± 3
EF-LDI	13.5	11.3	84*

[a]Measurements were performed at 25 °C in 10 mM Mes/NaOH pH 6.0, 150 mM NaCl, 0.005% P-20. Seven LD concentrations in the range 0.1–8 nM were used. K_D is based on independent triplicate experiments. * Based on a single experiment.

Figure 1. N-terminal sequences of wild-type and LDI variants (see Material & Methods and Results sections for further description).

Figure 2. Inhibition of LD by wt-LDI. (A) Fit of Michaelis-Menten equation for tight competitive inhibition. No inhibitor (●), 2 nM LDI (○), 4 nM LDI (▼). Error bars indicate SD for duplicate measurements. (B) wt-LDI inhibition level (%) *vs*. LDI:LD (molar ratio); the curve is drawn though the experimental points. Error bars indicate SD for triplicate measurements.

Figure 3. Representative fits of a 1:1 binding model (gray line) to the SPR data (black line) and residuals. The LD concentration range is 0.1–4 nM. (A) Binding data at standard conditions, 10 mM Mes/NaOH pH 6.0, 150 mM NaCl, 0.005% surfactant P-20, 25 °C and (B) the corresponding residuals. (C) Binding data at suboptimum conditions, 10 mM Bicine/NaOH pH 10.0, 150 mM NaCl, 0.005% surfactant P-20, 25 °C and (D) the corresponding residuals.

Figure 4. (A) Multiple sequence alignment of the five inhibitors LDI, RATI, CHFI, and dimeric and monomeric wheat inhibitors, 0.19 and 0.28. Secondary structures of the modeled LDI structure is shown above the alignment and also indicated on the sequences by α-helices as dark gray and β-strands as light gray shading. (B) Homology model of LDI showing a helical bundle with a simple up-and-down topology. The α-helices and β-strands are shown in red and blue, respectively. The 4 disulfide bonds and Cys^{59} are shown as yellow sticks and His^{56} is colored gray.

Figure 5. van't Hoff plots of the fitting of the non-linear (A) or linear (B) function to the data.

	wt-LDI	TLESVKDECQ
	EF-LDI	EFTLESVKDECQ
	ΔE^{3}LDI	SVKDECQ
Expected	ΔV^{5}LDI	KDECQ
Actual	ΔV^{5}LDI	EAEAKDECQ

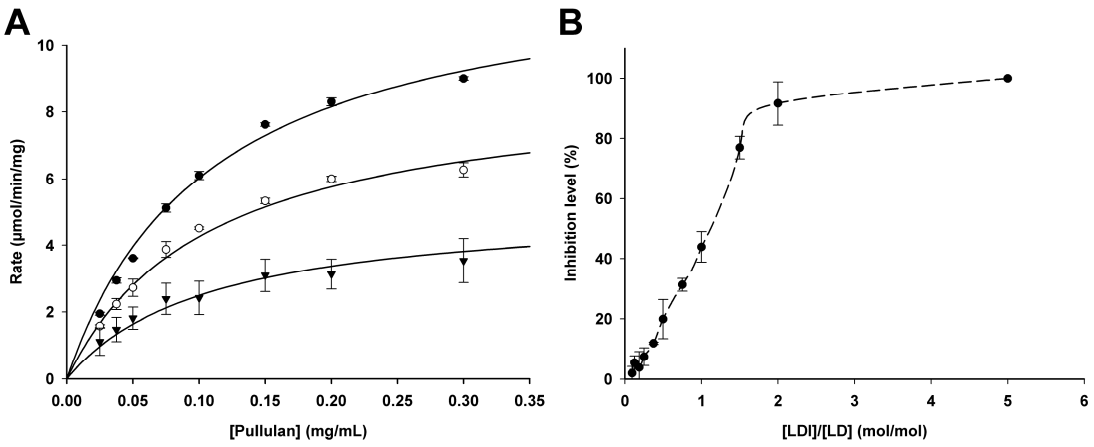
A
Rate (µmol/min/mg)
[Pullulan] (mg/mL)
B
Inhibition level (%)
[LDI]/[LD] (mol/mol)

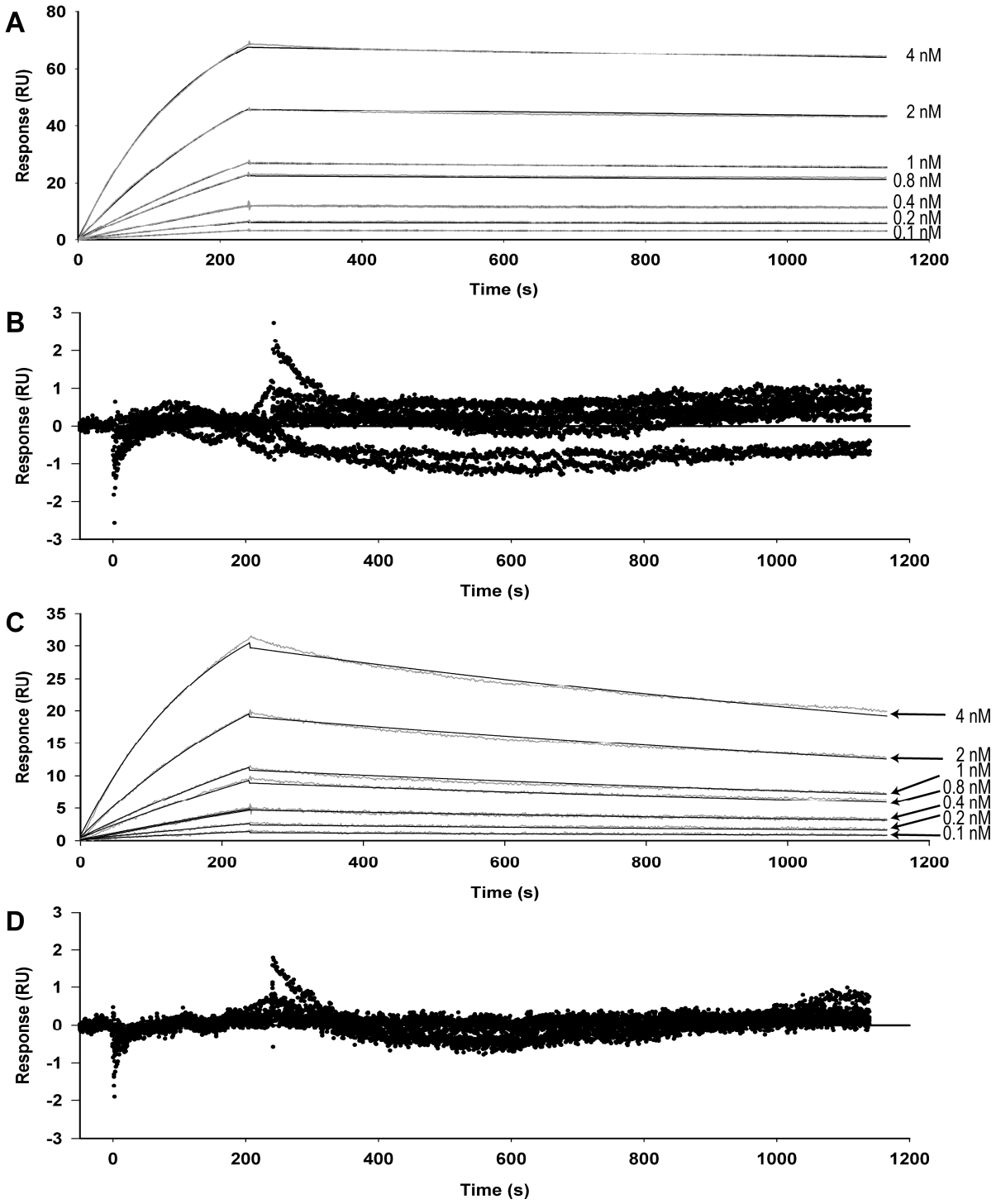
A
Response (RU)
Time (s)
4 nM
2 nM
1 nM
0.8 nM
0.4 nM
0.2 nM
0.1 nM
B
Response (RU)
Time (s)
C
Responce (RU)
Time (s)
4 nM
2 nM
1 nM
0.8 nM
0.4 nM
0.2 nM
0.1 nM
D
Response (RU)
Time (s)

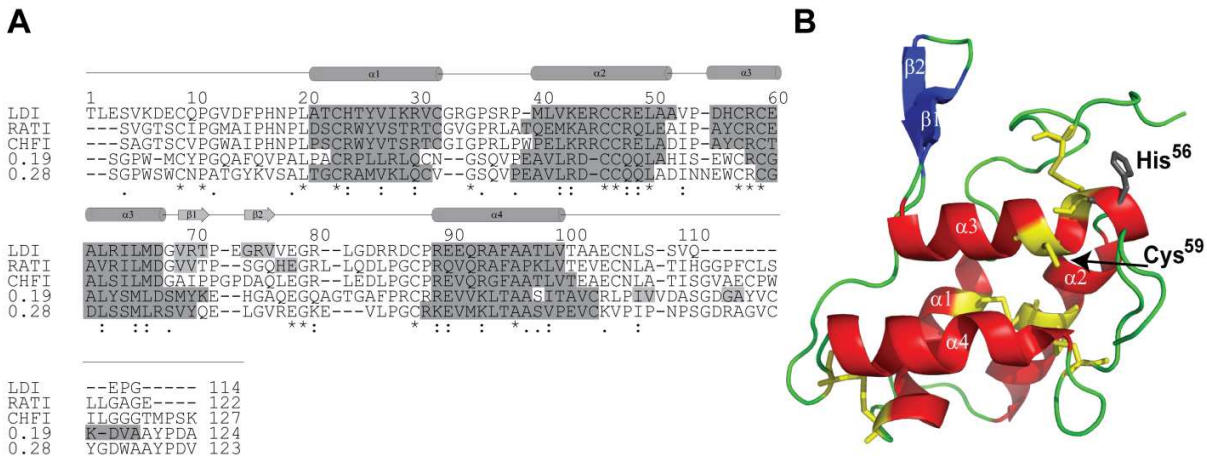
A
B
α1
α2
α3
β1
β2
α4
1 10 20 30 40 50 60
LDI TLESVKDECQPGVDFPHNPLATCHTYVIKRVCGRGPSRP-MLVKERCCRELAAVP-DHCRCE
RATI ---SVGTSCIPGMAIPHNPLDSCRWYVSTRTCGVGPRLATQEMKARCCRQLEAIP-AYCRCE
CHFI ---SAGTSCVPGWAIPHNPLPSCRWYVTSRTCGIGPRLPWPELKRRCCRELADIP-AYCRCT
0.19 --SGPW-MCYPGQAFQVPALPACRPLLRLQCN--GSQVPEAVLRD-CCQQLAHIS-EWCRCG
0.28 --SGPWSWCNPATGYKVSALTGCRAMVKLQCV--GSQVPEAVLRD-CCQQLADINNEWCRCG
70 80 90 100 110
LDI ALRILMDGVRTP-EGRVVEGR--LGDRRDCPREEQRAFAATLVTAAECNLS-SVQ-------
RATI AVRILMDGVVTP--SGQHEGRL-LQDLPGCPRQVQRAFAPKLVTEVECNLA-TIHGGPFCLS
CHFI ALSILMDGAIPPGPDAQLEGR--LEDLPGCPREVQRGFAATLVTEAECNLA-TISGVAECPW
0.19 ALYSMLDSMYKE--HGAQEGQAGTGAFPRCRREVVKLTAASITAVCRLPIVVDASGDGAYVC
0.28 DLSSMLRSVYQE--LGVREGKE---VLPGCRKEVMKLTAASVPEVCKVPIP-NPSGDRAGVC
LDI --EPG----- 114
RATI LLGAGE---- 122
CHFI ILGGGTMPSK 127
0.19 K-DVAAYPDA 124
0.28 YGDWAAYPDV 123
β2
β1
His56
Cys59
α3
α2
α1
α4

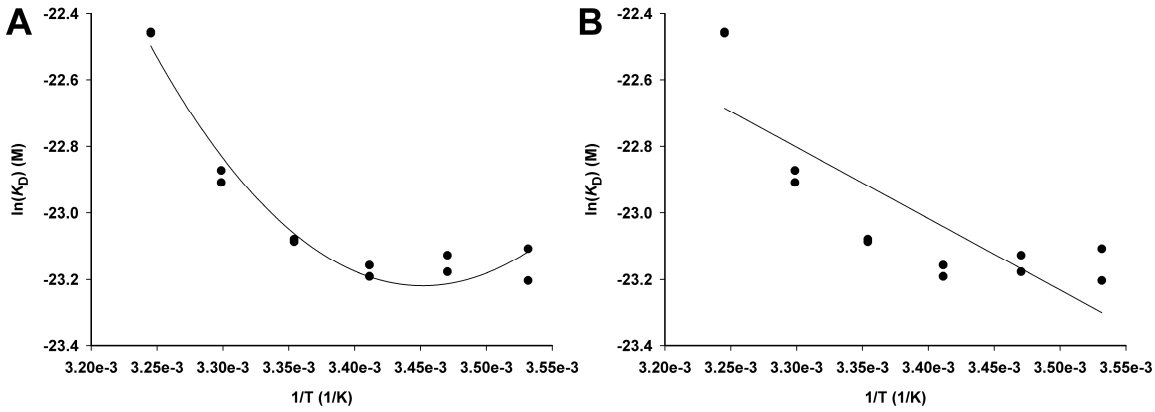
A
B
-22.4
-22.6
-22.8
-23.0
-23.2
-23.4
ln(K_D) (M)
3.20e-3
3.25e-3
3.30e-3
3.35e-3
3.40e-3
3.45e-3
3.50e-3
3.55e-3
1/T (1/K)

SUPPLEMENTAL MATERIAL

Figure S1. Coomassie stained SDS-PAGE of the purification of wt-LDI (A) Lane 1, culture supernatant. (B) Concentrated pools from Ni-NTA elution. Lane 1, pool 2; lane 2 pool 1. (C) Concentrated pools from anion exchange chromatography. Lane 1–6. Fractions from the anion exchange chromatography of wt-LDI were pooled according to the peaks of the chromatogram. Pool 4 was used for all the analysis; lane 7, pool from anion exchange chromatography of the first Ni-NTA pool. Expected size of the produced product is 13.5 kDa.